

**Different Architectural Polymers used in
Drug/Gene Delivery**

**A thesis submitted to Cardiff University in
candidature for the Degree of Doctor of
Philosophy**

A.H.L. Renuka Nilmini

UMI Number: U585225

All rights reserved

INFORMATION TO ALL USERS

The quality of this reproduction is dependent upon the quality of the copy submitted.

In the unlikely event that the author did not send a complete manuscript and there are missing pages, these will be noted. Also, if material had to be removed, a note will indicate the deletion.



UMI U585225

Published by ProQuest LLC 2013. Copyright in the Dissertation held by the Author.
Microform Edition © ProQuest LLC.

All rights reserved. This work is protected against
unauthorized copying under Title 17, United States Code.



ProQuest LLC
789 East Eisenhower Parkway
P.O. Box 1346
Ann Arbor, MI 48106-1346

**Dedicated to my mother
and the rest of my family without whom none of
this would have been even possible**

Acknowledgements

This project is collaboration in the truest sense, and could not exist without the support and input of more people than I can name on one written page. I would like to thank the following people who played an important role in the process.

First of all I would like to thank the Chairman and the Director of Rubber Research Institute of Sri Lanka, who granted me leave to embark on this project. Also I would like to thank School of Chemistry, Cardiff University for financial support of my studies.

It is difficult to overstate my gratitude to my supervisor, Dr. Peter C. Griffiths and I am deeply indebted to him for allowing me to join his team, for his expertise, advice, kindness and most of all for his patience. Throughout my thesis-writing period, he provided encouragement, sound advice, good teaching, good company, and lots of good ideas. I wish to thank him for who is as an enthusiastic, sagacious, honest minded individual with broad interests who provides steady support in the most difficult times. His trust and honesty, his efforts in understanding a student's personality and tailoring his approach accordingly translated for me into, although away from home country, a very pleasurable 3 years stay at Cardiff.

Thanks to Professor Paolo Ferruti (University of Milan), Professor Ruth Duncan, Dr Cameron Alexander (University of Nottingham) and Dr Lorella Izzo (University of Salerno) for their helpful scientific discussions and polymer materials.

I would like to thank Dr Alison Paul for her valuable advices given me not only on study matter but also on general matters during this period.

Many thanks go to Dr Emma Carter and Dr Damien Murphy for their invaluable support and basic instructions given me on operating the electron spin resonance spectrophotometer.

I would like to thank my colleagues, former and current who helped me direct and indirect, Marie, Paola, Zeena, Gemma, Craig, Abdul who have given me support and long-lasting friendship. The staff at RRISL especially Dr Champa wellappilli who helped me find this opportunity.

I would like to thank administrative and technical staff members of the school who have been kind enough to advice and help in their respective roles.

Special thanks go to my parents, being most inspiring and brilliant teachers in life, for being also greatest friends, an infinite source of admiration. My parents have always put education as a first priority in my life, and raised me to set high goals for myself. They taught me to value honesty, courage, and humility above all other virtues.

Last, but not least, I would like to give a special thanks to my husband- Upul and sons Janindu and Akindu for their love, patience, sacrifice, and understanding. Their presence at my side is a source of inspiration.

I do genuinely appeal to the graciousness of those whom I have failed to name above to magnanimously forgive the oversight and continue to maintain the interaction.

Summary

Synthetic polycations have shown promise as gene delivery vehicles but suffer from unacceptable toxicity and low transfection efficiency. In this thesis novel architectures are being explored to increase transfection efficiency, including hydrophobically modified poly(ethylene imine) (PEI), copolymers with thermoresponsive characters and bioresponsive polymers designed to promote cytosolic delivery.

The physical properties of weak polyelectrolytes may be tailored via hydrophobic modification to exhibit useful properties under appropriate pH and ionic strength conditions as a sequence of the often inherently competing effects of electrostatics and hydrophobicity. Pulsed-gradient spin-echo NMR (PGSE-NMR), electron paramagnetic resonance (EPR), and small-angle neutron scattering (SANS) have been used to examine the solution conformation and aggregation behavior of a series of hydrophobically modified hyperbranched PEI polymers in aqueous solution, and their interaction with sodium dodecylsulfate (SDS). According to PGSE-NMR, branched PEI_{2K} is monodispersed compared to PEI_{25K}, PEI_{50K} and PEI_{750K} samples. Analysis of the SANS data showed that the propensity to form highly elliptical or rod-like aggregates at higher pHs, reflecting both the changes in protonation behavior induced by the hydrophobic modification and a hydrophobic interaction, but that these structures were disrupted with decreasing pH (increasing charge).

The physicochemical characterization of a family of copolymers comprising a core of the cationic polymer PEI with differing thermoresponsive poly (N-isopropylacrylamide) (PNIPAM) grafts has been carried out using PGSE-NMR and SANS. Copolymers with longer chain PNIPAM grafts displayed clear evidence for the collapse of grafts with increasing temperature and the associated emergence of an attractive interpolymer interaction. These aspects depend on the number of PNIPAM grafts attached to the PEI core. Even though a collapse in the smaller PNIPAM grafts is observed for the third polymer, could not observe any interpolymer interaction. These facts provide further insight into the association behavior of these copolymers, which is fundamental to developing a full understanding of how they interact with nucleic acids.

Bioresponsive polymers designed to promote cytosolic delivery of macromolecular drugs (including proteins and genes) are so far unsuccessful to exhibit their potential in clinical applications. The physicochemical properties of poly(amidoamine) (PAA) ISA23.HCl have been studied as a model polymer, in order to understand the mechanism of endosomal escape of polymers with biologically relevant surfaces over the pH range the polymer would encounter during membrane trafficking. Previous work has demonstrated that ISA23.HCl interacted very strongly with the anionic surface of small globular micelles (SDS), but weak interaction with biologically relevant phospholipid –lyso-PC. This surprising conclusion is elaborated in this thesis for a series of simple membrane mimics studied via EPR using spin-probes dissolved into vesicles and a spin-labelled polymer. Vesicles have been prepared from mixtures of the three most common lipids found in membranes – 1,2-dipalmitoyl-sn-glycero-3-phosphocholine (DPPC), 1,2-dipalmitoyl-sn-glycero-3-[phosphor-L-serine] (sodium salt) (DPPS) and 1,2-dipalmitoyl-sn-glycero-3-phosphoethanolamine (DPPE) – in ratios that reflect the composition of plasma, endosomal and lysosomal membranes. The spectrum arising from the nitroxide spin-probe present in the lipid bilayer provided a measure of the dynamics and polarity of the bilayer. The nitroxide spin-

label covalently attached to the polymer gave a complementary measure of the polymer flexibility in the presence of the vesicles. No interaction between the polymer and vesicle surface was detected for any of these membrane mimics, across the entire pH range studied (pH 7.4 to 4.0).

1.7 This thesis context	31
 Chapter 2 Techniques	
2.1 Pulsed-gradient Spin-Echo NMR (PGSE-NMR)	39
2.1.1 Introduction	39
2.1.1.1. NMR diffusion measurements in retrospect	39
2.1.2 Diffusion	40
2.1.3 Self-diffusion	40
2.1.4 Basic principles	41
2.1.4.1 Relaxation process	42
2.1.4.2 Measuring diffusion with magnetic field gradients	43
2.1.4.3 The nuclear spin-echo (SE) method	44
2.1.4.4 Three-pulse sequences: the stimulated echo method	46
2.2 Electron Paramagnetic Resonance (EPR)	48
2.2.1 Introduction	48
2.2.2 Theory	48
2.2.2.1 The Zeeman effect	49
2.2.2.2 Spin-probes	52
2.2.3 EPR spectral parameters	53
2.2.3.1 The g factor	53
2.2.3.2 Hyperfine interactions	53
2.2.3.2.1 Hyperfine coupling constant as a probe solvent polarity	55
2.2.3.3 Rotational correlation time	57
2.3 Small Angle Neutron Scattering (SANS)	58
2.3.1 Introduction	58
2.3.2 Neutron production	58
2.3.3 Detailed instrumentation at ISIS	60
2.3.4 The scattering vector, Q	61
2.3.5 Scattering intensities	62
2.3.6 Contrast variation	63
2.3.7 Form factor, P(Q)	64
2.3.7.1 Sphere model	64
2.3.7.2 Rod model	64

2.3.7.3 Polyelectrolyte model	65
2.3.7.4 Solid ellipsoid model	65
2.3.8 Structure factor, $S(Q)$	66
2.4 Surface tension	
2.4.1 Introduction	67
2.4.2 Measurement of surface tension	69
2.4.2.1 Maximum bubble pressure method	69
 Chapter 3 Derivatizing weak polyelectrolytes and implication for their use in drug delivery – solution properties	
 3.1 Introduction	72
3.2 Materials and methods	74
3.3 Results	
3.3.1 Self-diffusion studies of different molecular weight PEI samples	75
3.3.1.1 Analysis of self-diffusion coefficient using a stretched exponential analysis	76
3.3.1.2 Analysis of self-diffusion coefficient using and Inverse Laplace Transformation	81
3.3.2 The effect of hydrophobe on polymer surface activity and aggregation	
3.3.2.1 Solution conformation – Effect of pH	83
3.3.2.2 16-DSE solubilised in possible hydrophobic moieties of different PEI	87
3.3.3 Internal structure of BPEI/SDS complexes	
3.3.3.1 SANS results	91
3.3.3.2 Impact of SDS solubilized spin probe on different PEI samples	94
3.4 Discussion	95
3.5 Conclusion	97
3.6 References	98

Chapter 4 Physicochemical characterization of thermoresponsive poly(N-isopropylacrylamide)-poly(ethylene imine) copolymers

4.1 Introduction	99
4.2 Materials and methods	101
4.3 Results	
4.3.1 PGSE-NMR	103
4.3.1.1 Self-diffusion studies of PNIPAM	103
4.3.1.2 Self diffusion studies of PEI-PNIPAM copolymers	107
4.3.1.2.1 Comparison of raw attenuation data of parent polymer (PEI 25K) and copolymers (PEI-PNIPAM)	107
4.3.1.2.2. Comparison of Self-diffusion coefficient and size of copolymers	108
4.3.2 SANS	114
4.3.2.1 SANS of copolymers	114
4.3.2.2 Modeling SANS data from copolymers	121
4.4 Discussion	126
4.5 Conclusions	129
4.6 References	130

Chapter 5 Studies on the mechanism of interaction of a bioresponsive endosomolytic polyamidoamine with interfaces – phospholipid-rich micelle and vesicle surfaces

5.1 Introduction	132
5.2 Material and methods	
5.2.1 Materials	134
5.2.2 Sample Preparation	
5.2.2.1 Micellar Solutions	134
5.2.2.2 Vesicle preparation	135
5.2.2.3 Hydrophobically modified PEI	136
5.2.2.4 Hydrophobically modified ISA23-TEMPO	136
5.2.3 Electron Paramagnetic Resonance	136
5.2.3.1 Polarity determination	137
5.3 Results	
5.3.1 Sodium dodecyl sulphate (SDS) as model surface	139

5.3.1.1 Raw EPR spectra of ISA23.HCl with 16-DSE and 5-DSE as spin probes.	139
5.3.2 Lyso PC as model system	146
5.3.2.1 Interaction of lyso-PC with BPEI _{25K} and hydrophobically modified PEI	147
5.3.2.2 Interaction of Lyso PC with ISA23-TEMPO	151
5.3.2.3 Interaction of SDS/Lyso PC mixed system with 10wt% hydrophobically modified ISA23-TEMPO	152
5.3.3 SDS/DHPC mixed micelles as model system	154
5.3.3.1 SDS/DHPC mixed micelles with spin probe polymer	154
5.3.3.2 SDS/DHPC mixed micelles with spin-labelled polymer	157
5.3.4 Membrane mimics as model surface	158
5.3.4.1 EPR studies of ISA23.HCl with model membranes (plasma, endosomal and Lysosoaml) using 5-DSE as spin probes.	159
5.3.4.2 EPR studies of ISA23-TEMPO with model membranes (plasma, endosomal and Lysosoaml)	163
5.3.5 Living cell as model surface	167
5.4 Discussion	167
5.5 Conclusions	168
5.6 References	170
 Chapter 6 ‘Future work’	
6.1 General Introduction	172
6.2 Definition of the effect of polymer stereochemistry on the physicochemical behavior of polymer therapeutics	
6.2.1 Introduction	172
6.2.2 Materials and methods	174
6.2.3 Results	175
6.2.3.1 Surface tension	175
6.2.3.2 SANS and EPR	177
 6.3 Physicochemical characterization of dendronised PEG based polymers	

6.3.1 Introduction	181
6.3.2 Materials and method	183
6.3.3 Results	185
6.4 Physicochemical characterization of dendronised pluronics polymer	
6.4.1 Introduction	187
6.4.2 Materials and methods	188
6.4.3 Results	189
6.5 Physicochemical characterization of ‘ion sensitive’ isothermal polymers	
6.5.1 Introduction	192
6.5.2 Materials and methods	192
6.5.3 Results	193
6.6 References	197

Abbreviations

DIVEMA	Divinylethermaleic anhydride
HIV	Human immunodeficiency virus
SCID	Severe combined immunodeficiency
HSV	Herpes simplex virus
AAV	Adeno-associated virus
PEG	Polymer poly(ethylene glycol)
EGF	Epidermal growth factor
FR	Folate receptor
FGF	Fibroblast growth factor
GAGs	Glycosaminoglycans
CPP	Cell penetrating peptides
DOTAP	1,2-dioleyl-3-trimethylammonium-propane
PLL	Poly(L-lysine)
DOPE	1,2-dioleyl-sn-glycerol-3-phosphoethanolamine
PMMA	Poly(methacrylic acid)
NPCs	Nuclear pore complexes
NLS	Nuclear localization sequence
PbAE	Poly(β-amino ester)
PCL	Poly-(ϵ-caprolactone)
SDM	Sulfadimethoxine
ADR	Adriamycin
His	Histidine
PHEA	Poly(2-hydroxyethyl aspartamide)
PVD	Poly(vinylpyrrolidone-co-dimethyl maleic anhydride)

DOX	Doxorubicin
PE	Phosphatidylethanolamine
CHMS	Cholesteryl hemisuccinate
PNIPAM	Poly(N-isopropylacrylamide)
LCST	Lower critical solution temperature
DMAEMA	2-(N,N-dimethylamino) ethylmethacrylate
PGSE-NMR	Pulsed-gradient spin-echo NMR
SE	Spin-echo
RF	Radiofrequency
EPR	Electron Paramagnetic Resonance
DPPH	1,1-Diphenyl-2-picryl-hydrazyl
EZI	Electron Zeeman interaction
ν_B	Bohr magneton.
g_e	Gyromagnetic ratio
τ_c	Rotational correlation time
ILL	Institute Max von Laue-Paul Langevine
\underline{K}_0	Incident wave vector
\underline{K}_s	Scattered wave vector
Q	Wave vector
P(Q)	Form factor
S(Q)	Structure factor
M_w	Molecular weight
ρ	Scattering length density
γ	Surface tension
PEI	Poly(ethylene imine)

SANS	Small-angle neutron scattering
TNBS	2,4,6-trinitrobenzenesulphonic acid
D_s	Self-diffusion coefficient
PEAAc	Poly(ethylacrylic acid)
PAA	Poly(amidoamine)
EPR	Enhanced permeability and retention effect
16-DSE	16-doxyl stearic acid methyl ester
5-DSE	5-doxyl stearic acid methyl ester
SDS	Sodium dodecylsulfate
CMC	Critical micelle concentration
<i>lyso</i> -PC	1-palmitoyl-2-hydroxy- <i>sn</i> -glycero-3-phosphocholine
DPPC	1,2-dipalmitoyl- <i>sn</i> -glycero-3-phosphocholine
DPPS	1,2-dipalmitoyl- <i>sn</i> -glycero-3-[phosphor-L-serine] (sodium salt)
DPPE	1,2-dipalmitoyl- <i>sn</i> -glycero-3-phosphoethanolamine
DHPC	1,2-diheptanoyl- <i>sn</i> -phosphatidylcholine
PCS	Photon correlation spectroscopy
CAC	Critical aggregation concentration

List of figures

Chapter 1 General Introduction

- Figure 1.1 Schematic representation of polymer therapeutics
- Figure 1.2 Barriers to gene delivery
- Figure 1.3 Major hurdles in drug/gene delivery
- Figure 1.4 Schematic representation of the different hurdles encountered by a gene delivery system to enter and traffic into a tumor cell
- Figure 1.5 Endo-lysosomal escape
- Figure 1.6 Hypothesis of endosomal escape of lipoplexes and polyplexes gene delivery systems
- Figure 1.7 Cytosolic transport and nuclear import.
- Figure 1.8 Schematic representation of nuclear entry mechanism through nuclear pore complexes.
- Figure 1.9 Schematic of thermoresponsive polymer response with temperature
- Figure 1.10 Schematic illustrations of stimuli-responsive antisense reagent comprising oligonucleotide and PNIPAM

Chapter 2 Techniques

- Figure 2.1 The Stejskal-Tanner PFGSE experiment
- Figure 2.2 The stimulated echo-sequence
- Figure 2.3 Electron spin levels in a magnetic field
- Figure 2.4 Schematic for a SANS experiment
- Figure 2.5 Schematic diagram of the fixed-geometry instrument LOQ at the ISIS facility, Didcot, UK
- Figure 2.6 The theory behind, and the mathematical derivation of the scattering wave vector (Q).
- Figure 2.7 unbalanced forces between a liquid-air interface and in the interior of the liquid
- Figure 2.8 The schematic illustration of the changing pressure inside the bubble with bubble life time

Chapter 3 Derivatizing weak polyelectrolytes & implications for their use in drug delivery - Solution properties

- Figure 3.1 Concentration dependence of the self-diffusion coefficient of PEI 2K g/mol
- Figure 3.2 Concentration dependence of the self-diffusion coefficient of PEI 25K g/mol
- Figure 3.3 Concentration dependence of the self-diffusion coefficient of PEI 50K g/mol
- Figure 3.4 Concentration dependence of the self-diffusion coefficient of PEI 750K g/mol
- Figure 3.5 Self-diffusion coefficient distributions for the four BPEI samples
- Figure 3.6 Panel (a) The effects of hydrophobic modification on the SANS from BPEI_{25K} in a 5wt% pH 10 aqueous solution; Panel (b) The effects of hydrophobic modification on the SANS from BPEI_{25K} in a 5wt% pH 4 aqueous solution
- Figure 3.7 Effect of pH on the EPR spectrum of 16-DSE solubilised in BPEI_{25K} at pH 3
- Figure 3.8 Effect of pH on the EPR spectrum of 16-DSE solubilised in HM_{1%}BPEI_{25K} at pH 3
- Figure 3.9 Effect of pH on the EPR spectrum of 16-DSE solubilised in HM_{10%}BPEI_{25K} at pH 3
- Figure 3.10 (a) Contrast variation SANS study of BPEI_{25K} ($C_{\text{polymer}}=5.0\text{wt } \%$) in the presence of 25mM SDS (b) Contrast variation SANS study of BPEI_{25K} ($C_{\text{polymer}}=5.0\text{wt } \%$) in the presence of 25mM SDS
- Figure 3.11; EPR spectra of 16-DSE solubilized in PEI/SDS solutions at ambient pH and with $C_{\text{polymer}}=1.0\text{wt } \%$

Chapter 4 Physicochemical characterization of thermoresponsive poly(N-isopropylacrylamide)-poly(ethylene imine) copolymers

- Figure 4.1 Typical attenuation functions and fits to a stretched exponential for 1wt% PNIPAM 20 K g/mol with different temperatures

- Figure 4.2 Temperature dependence of the self-diffusion coefficient of PNIPAM 20 K g/mol
- Figure 4.3 Typical attenuation functions and fits to a stretched exponential for polymer solutions with concentrations $C_{\text{polymer}}=4.5\text{wt\%}$ in D_2O
- Figure 4.4 Temperature dependence of the self-diffusion coefficient (filled circles) and associated hydrodynamic radius (open circles) of copolymer PEI(25)-g-PNIPAM(34)₄ at a concentration $C_{\text{polymer}}=4.5\text{wt\%}$
- Figure 4.5 Temperature dependence of the self-diffusion coefficient (filled circles) and associated hydrodynamic radius (open circles) of copolymer PEI(25)-g-PNIPAM(34)_{1.8} at a concentration $C_{\text{polymer}}=4.5\text{wt\%}$
- Figure 4.6 Temperature dependence of the self-diffusion coefficient (filled circles) and associated hydrodynamic radius (open circles) of copolymer PEI(25)-g-PNIPAM(18)_{3.4} at a concentration $C_{\text{polymer}}=4.5\text{wt\%}$
- Figure 4.7 Temperature dependence of the hydrodynamic radius of homopolymers PEI 25 K g/mol ($C_{\text{polymer}}=1\text{wt\%}$) (O) and PNIPAM 20K g/mol ($C_{\text{polymer}}=1\text{wt\%}$) (\square).
- Figure 4.8 Fit (solid line) to an ellipsoidal scatterer model to the small-angle neutron scattering from PEI 25 K g/mol in a 5wt% aqueous solution at pH 7
- Figure 4.9 Typical small-angle neutron scattering from PEI(25)-g-PNIPAM(18)_{3.4} in D_2O ; $[\text{polymer}]=4.5\text{wt\%}$
- Figure 4.10 SANS and fits as described in the text for 4.5wt% PEI(25)-g-PNIPAM(34)₄ as a function of temperature
- Figure 4.11 SANS and fits as described in the text for 2.5wt% PEI(25)-g-PNIPAM(34)_{1.8} as a function of temperature
- Figure 4.12 SANS from 2.5wt% PEI(25)-g-PNIPAM(34)₄ as a function of temperature
- Figure 4.13 SANS and represent fit as described in the text for 2.5wt% PEI(25)-g-PNIPAM(18)_{3.4} as a function of temperature
- Figure 4.14 SANS from 2wt% PNIPAM homopolymer 20K g/mol as a function of temperature

Chapter 5 Studies on the mechanism of interaction of a bioresponsive endosomolytic polyamidoamine with interfaces – phospholipid-rich micelle and vesicle surfaces

- Figure 5.1 The effect of pH on the EPR spectrum of 16-DSE solubilised in 25mM SDS
- Figure 5.2 The effect of pH on the EPR spectrum of 5-DSE solubilised in 25mM SDS
- Figure 5.3 pH dependence of the polarity index of 16-DSE solubilised into SDS solutions
- Figure 5.4 pH dependence of the polarity index of 5 DSE solubilised into SDS solutions
- Figure 5.5 pH dependence of the polarity index of a tempo spin-label grafted to ISA23-TEMPO
- Figure 5.6 The effect of pH on the EPR spectrum of 16-DSE solubilised 25mM lyso-PC
- Figure 5.7 The effect of pH on the EPR spectrum of 16-DSE solubilised 25mM lyso-PC presence of 25K g/mol PEI (a), presence of 1wt% hydrophobically modified PEI (b), presence of 10wt% hydrophobically modified PEI (c) at pH 7.2 (black); pH 5.5 (red); and pH 4 (green).
- Figure 5.8 The effect of pH on the EPR spectrum of 16-DSE solubilised 25mM lyso-PC presence (black) of 25K g/mol PEI and presence (green) of 1wt% hydrophobically modified PEI at pH 7 (a), pH 5.5 (b) and pH 4 (c).
- Figure 5.9 The effect of pH on the EPR spectrum of 16-DSE solubilised 25mM lyso-PC presence (black) of 25K g/mol PEI and presence (green) of 10wt% hydrophobically modified PEI at pH 7 (a), pH 5.5 (b) and pH 4 (c).
- Figure 5.10 The pH dependence of the polarity index of 0.2wt% ISA23-TEMPO
- Figure 5.11 pH dependence of the polarity index of a 10wt% HM ISA23-TEMPO (filled circles) and ISA23-TEMPO (open circles) in the presence of mixed micelles of SDS/lyso-PC (25mM) at pH 5.
- Figure 5.12 Solution composition dependence of the polarity index of 16-DSE solubilised into mixed micelles of SDS/DHPC (25mM)
- Figure 5.13 pH dependence of the polarity index of a ISA23-TEMPO in the presence of mixed micelles of SDS/DHPC (25mM)

- Figure 5.14** The effect of pH on the EPR spectrum of 5-DSE solubilised in model plasma membrane (green) and presence (black) of 0.2wt% ISA23.HCl at pH 7.2 (a); pH 5.5 (b) and pH 4.0 (c)
- Figure 5.15** The effect of pH on the EPR spectrum of 5-DSE solubilised in model endosomal membrane (green) and presence (black) of 0.2wt% ISA23.HCl at pH 7.2 (a); pH 5.5 (b) and pH 4.0 (c)
- Figure 5.16** The effect of pH on the EPR spectrum of 16-DSE solubilised in model plasma membrane (green) and presence (black) of 0.2wt% ISA23.HCl at pH 7.2 (a); pH 5.5 (b) and pH 4.0 (c)
- Figure 5.17** The effect of pH on the EPR spectrum of 16-DSE solubilised in model endosomal membrane (green) and presence (black) of 0.2wt% ISA23.HCl at pH 7.2 (a); pH 5.5 (b) and pH 4.0 (c)
- Figure 5.18** The effect of pH on the EPR spectrum of 16-DSE solubilised in model lysosomal membrane (green) and presence (black) of 0.2wt% ISA23.HCl at pH 7.2 (a); pH 5.5 (b) and pH 4.0 (c)
- Figure 5.19** The effect of pH on the EPR spectrum of 0.2wt% ISA23-TEMPO (black) and presence (green) of model plasma membrane at pH 7.2 (a); pH 5.5 (b) and pH 4.0 (c)

List of tables

Chapter 1 : Introduction

1.1 Strength and weaknesses of currently used vectors

Chapter 2: Techniques

2.1 Field for resonance, B_{res} , for a $g=2$ signal at selected microwave frequencies

Chapter 4: Physicochemical characterization of thermoresponsive poly(N-isopropylacrylamide)-poly(ethylene imine) copolymers

4.1 Molecular Characterization of the PEI-PNIPAM Copolymers and their analogues

4.2 Parameters derived from fits of SANS

4.3 Parameters derived from fits of SANS

4.4 Parameters derived from fits of SANS

Chapter 5: Studies on the mechanism of interaction of a bioresponsive endosomolytic polyamidoamine with interfaces – phospholipid-rich micelle and vesicle surfaces

5.1 Phospholipid composition of model membranes (percentage in molar terms)

Chapter 6: Future work

6.1 Characterization of syndio and atactic PMA

6.2 Molecular weight and polydispersity of polymers

6.3 Parameters derived from SANS and PGSE-NMR

6.4 Molecular characterization of different generation of Pluronics

6.5 Characterization of P6 and P7

6.6 Parameters derived from SANS and PGSE-NMR

1.0 General Introduction

1.1 Background

Delivering drugs to target sites in the body at the right time and in the right dose remains a formidable challenge. This is especially important with bio-macromolecular drugs such as DNA, RNA, short interfering RNA and therapeutic proteins. Historically, there have been three different approaches applied to delivery of those macromolecules.

The first approach consists of the use of naked DNA. Direct injection of free DNA to the tumour site has been shown to produce high levels of gene expression and the simplicity of this approach led to its use in a number of experimental protocols^{1,2}. This strategy appears to be limited to tissues that are easily accessible by direct injection such as the muscles³ and is unsuitable for systemic delivery as these complex biopolymers are readily deactivated by enzymes such as DNases and proteases outside their normal biological environment and hence require carrier vehicle or protective agent when administered as a drug. Accordingly the design and development of effective vehicles that are both safe and efficient has proved a major challenge.

The second approach involves using genetically altered viruses. For example, thus far viral vectors have been the most widely used, but viruses have limitations such as toxicity and immunogenicity. So delivery vehicles in turn must be able to transport the drug across biological barriers to the target site without causing an unwanted response. The human immune system, for example, has evolved to produce more than 10^8 different antibodies and more than 10^{12} different T-cells receptors to destroy foreign material. This means any drug delivery vehicle must evade interaction with a large number of biopolymers in order to be non-immunogenic.

The third approach for delivery systems concerns non-viral vectors, which are mainly of a cationic nature: cationic polymers and cationic lipids.

Generally non-viral vector systems are made of variety of organic and inorganic materials including non-biodegradable and biodegradable polymers, liposomes⁴, micelles⁵⁻⁷, quantum dots⁸, polymeric nanoparticles⁹⁻¹¹, gold nanoparticles^{12,13} and magnetic particles. The type of carrier system needed for a specific application is decided by therapeutic goal, type of payload, material safety profile and route of administration.

The need for materials that can carry one type of biopolymer (the therapeutic) while avoiding interactions with others (plasma proteins, antibodies, non-target-cell membranes) is fueling the development of ever more sophisticated carrier systems. Of particular interest are active or “smart” carrier vehicles, which display one set of properties under one set of conditions but can change their properties in response to a biological stimulus. For DNA and protein delivery, these properties must include an ability to form stable complexes or conjugates in order to protect the therapeutics from enzymes while overcoming barriers such as cell membranes and, in the case of DNA delivery, the nuclear envelope, combined with the ability to release the biotherapeutic at the target site. Polymers that can vary their architecture from a “closed” to an “open” conformation are perhaps the ideal systems for the contrasting requirements of protection and release. For example, as the polymer and drug cargo travel into different sub-cellular organelles within the body, they can experience a variety of environments. A physical or chemical change in the solvent surrounding the polymer may alter the intermolecular bonding between polymer and solvent, which may change the affinity of the polymer for the drug. Increased intermolecular bonding with the solvent in the case of certain polymers results in a chain-extended conformation with lower affinity for the drug, enabling drug release, whereas increased intramolecular bonds characteristic of a chain-collapsed polymer may form a tighter complex with the drug. As a consequence, polymers can be designed to respond via

conformational changes to stimuli in the biological environment, typically by harnessing physiological parameters that are locally regulated, such as temperature and pH, to maintain drug binding in the bloodstream but to effect release intracellularly.

1.2 Classification of polymer therapeutics

The term “polymer therapeutics” has been adopted to encompass several families of construct all using water-soluble polymers as components for design; polymeric drugs, polymer drug conjugates, polymer protein conjugates, polymeric micelles to which drug is covalently bound (figure 1.1), and those multi-component polyplexes being developed as non-viral vectors¹⁴⁻¹⁶. Irrespective of the sub-classification of these materials a number of characteristic chemical features are necessary attributes of all polymers for therapeutic application.

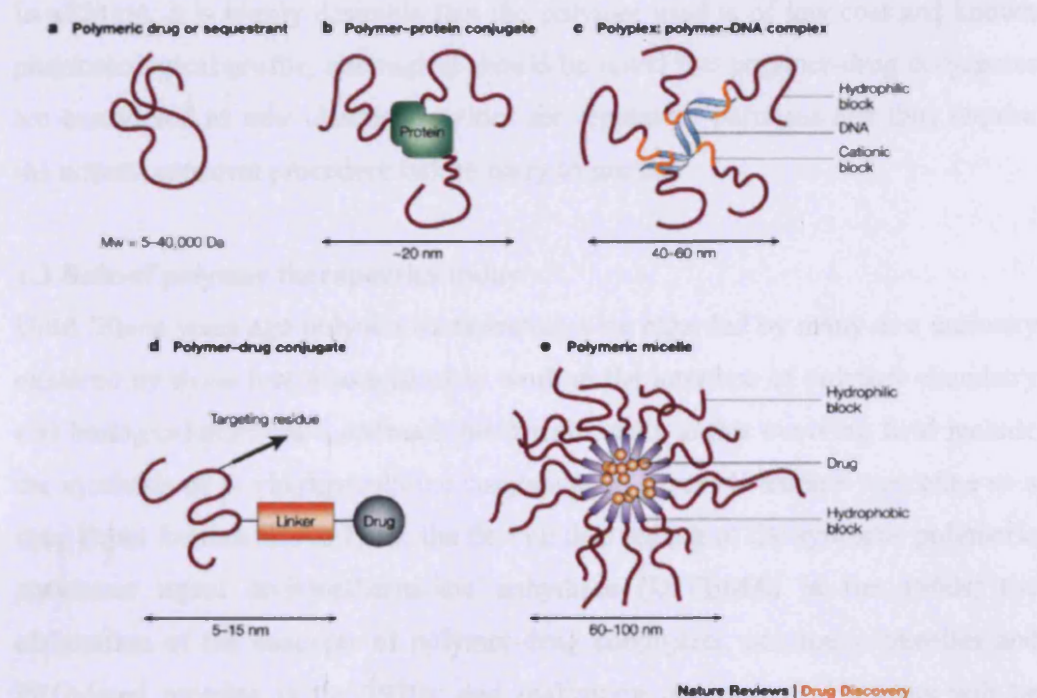


Figure 1.1; Schematic representation of polymer therapeutics¹⁴

The detailed chemistries of the polymers used in a therapeutic formulation can vary widely, but the basic requirements include:

1. Aqueous solubility
2. Biocompatibility or biodegradability
3. Functionality for conjugation of a drug, or for complex formation with a biomacromolecule
4. Able to carry and protect the payload from degradation
5. It must be able to:
 - target the appropriate cell type
 - avoid the accumulation in the liver
 - ideally introduce the payload into the cytosol via interaction with endosomal membrane or the plasma membrane
 - release the therapeutic agent at the target site

In addition, it is highly desirable that the polymer used is of low cost and known pharmacological profile, although it should be noted that polymer-drug conjugates are considered as new chemical entities for regulatory purposes and thus require the normal approval procedure before entry to market.

1.3 Role of polymer therapeutics today

Until fifteen years ago polymer therapeutics were regarded by many as a curiosity explored by those few who wished to work at the interface of polymer chemistry and biological sciences. Landmark historical events in this evolving field include the synthesis of N-vinylpyrrolidone conjugates of glycyl-L-leucine-mescaline as a drug depot formulation in 1955; the first clinical testing of the synthetic polymeric anticancer agent divinylethermaleic anhydride (DIVEMA) in the 1960s; the elaboration of the concepts of polymer-drug conjugates, polymeric micelles and PEGylated proteins in the 1970s; and realization that non-viral vectors will be essential in gene therapy¹⁴.

A water-soluble polymer is crucial for systemic administration. The linear or branched polymer chain can function as a bioactive (a polymeric drug) or, alternatively, and most usually, as an inert structural component of a conjugate, a polymeric micelle or a non viral-vector. The polymer-drug and polymer-protein conjugates that have been clinically tested typically have a tripartite structure; the polymer, a linker and the bioactive moiety. However, much more elaborate multicomponent compositions now exist, with additional features for cell-specific targeting, to regulate intracellular trafficking and nuclear localization, and to allow the incorporation of drug combinations. Modern polymer chemistry is producing increasingly intricate polymer structures, including multivalent polymers, branched polymers, graft polymers, dendrimers, dendronized polymers, block copolymers, stars and hybrid glycol- and peptide derivatives¹⁴. These will undoubtedly lead to the development of the polymer therapeutics of the future.

1.4 Gene therapy

Gene therapy can be defined as a transfer of genetic information into specific cells, for treatment of human disease¹⁷. The results could be substantial - diseases once considered incurable may be treated or even prevented, for instance, with DNA vaccines that inoculate against infectious diseases. Advances in molecular biology and genomic research have given a genetic identity to numerous diseases (e.g. sickle cell anaemia, HIV, Parkinson's disease, Huntington's disease, Alzheimer's disease) for which gene therapy may provide a possible prescription¹⁸⁻²¹. It is not difficult to envisage the treatment of genetic diseases such as haemophilia, muscular dystrophy or cystic fibrosis through replacement of faulty genes within the affected cells. Gene therapies are also being developed for cardiovascular²², neurological^{18,23,24} and infectious diseases²⁵, wound healing²⁶ and cancer²⁷⁻²⁹ by delivering genes to augment naturally occurring proteins to alter the expression of existing genes, or to produce cytotoxic proteins or prodrug-activating enzymes – for example, to kill tumour cells or inhibit proliferation of endothelial cells to prevent expression of viral genes can result in immune responses, which has led to the concept of DNA vaccines.

The broad potential of gene therapy has led to extensive efforts during the past 15 years. The first clinical trial for gene therapy, for the treatment of severe combined immunodeficiency (SCID), was initiated in 1990³⁰. However, it was not until April 2000 that Cavazzana-Calvo et al.³¹ reported the first clinical success with gene therapy, specifically the treatment of two infants with γ c-SCID. Also in that year, Kay et al.³² reported positive data, including increased circulating levels of factor IX, in a haemophilia clinical trial and Khuri et al.³³ reported the successful completion of a Phase II clinical trial using a combination of gene therapy and traditional chemotherapy to treat recurrent squamous-cell carcinoma of the head and neck. Considering that 863 gene-therapy clinical trials have been approved worldwide since 1989, the small number of successes is disappointing.

The essential requirement in gene therapy is identification of a therapeutic gene and transfer of that gene, often specifically to target cells, with high efficiency. In cancer therapy, short term gene expression is normally used but in chronic conditions requires long term gene expression. Almost all applications need tightly regulated gene expression levels. Finally, one must obviously accomplish each of these tasks in a way that is safe for the patient. Both toxicity/pathogenicity of the delivery vehicle and immune responses to the treatment must be considered.

1.4.1 Methods of gene delivery

The promise of gene therapy has yet to be fulfilled due to challenges associated with cell targeting specificity, gene transfer efficiency, gene expression regulation, and vector safety. Many viruses including retrovirus, adenovirus, herpes simplex virus (HSV) and adeno-associated virus (AAV) (table 1.1) have been modified to eliminate their toxicity and maintain their high capacity for gene transfer³⁴. Using either genetically engineered viruses or viruses with removed of their genetic material and replaced with therapeutic agents, some of the earliest clinical trials showed promising results. At that time many believed that viral vectors were poised to achieve the goal of gene therapy^{31,35,36}. It was not long after these initial reports of successful clinical implementation, however, that the severe side effects

possible with viral-based gene therapy were made strikingly evident. The concern that viral vectors could induce cancer via insertional mutagenesis-random transgenic insertion into the host chromosome disrupting the normal expression of a critical gene that ordinarily regulates cell growth and division-was realized when three clinical trial participants developed leukaemia-like complications post retroviral-based gene therapy^{37,38}. Moreover, the viral vectors themselves can initiate an immunogenic response which, in at least one reported incident, has led to a fatal outcome³⁹.

Although these safety issues do not disqualify the use of viruses as gene vectors, these drive the need to find out safer, less pathogenic and immunogenic gene delivery alternatives including lipid-based vectors, chemically modified viruses, inorganic materials, and polymer-based gene delivery systems. In addition to the potential safety benefits, such non-viral systems offer greater structural and chemical versatility for manipulating physicochemical properties, vector stability upon storage and reconstitution, and a larger gene capacity compared to their viral counterparts. Basically non-viral delivery systems include physical and chemical methods. For the physical approach, naked DNA is delivered directly to the cytoplasm by-passing the intracellular vesicles such as endosome and the lysosome, thus degradation by the lysosomal enzymes can be avoided. Physical techniques for gene delivery include direct injection^{1,2}, electroporation, the gene gun, laser irradiation, sonoporation and magnetofection. The chemical approach for non-viral gene delivery usually involves cationic vehicles such as lipids/liposomes and polymers.

Vector	Greatest advantages	Greatest disadvantages
Retrovirus	Ex vivo stable transduction of blood cells	Low efficiency in vivo; risk of insertional mutagenesis
Adenovirus	High short-term expression in vivo (in liver)	Immunogenicity and inflammatory responses
Adeno-associated virus (viral vectors in general)	Long-term expression in vivo High efficiency on particle basis	Small genome No repeated administration because of immunogenicity
Naked DNA	Simple (eg. For vaccination)	Low efficiency
Physically enhanced delivery of DNA	High expression in vivo	Limited localized area device required
Complex-based gene transfer (lipoplexes, polyplexes)	High expression ex vivo; expression in vivo (localized and systemic)	Short-term expression; toxicity of cationic carriers
Non viral vectors in general	High flexibility	Low efficiency on particle basis

Table 1.1; Strength and weaknesses of currently used vectors³⁵.

1.4.2 Gene packaging

Polyplexes should protect DNA from nucleases, as it sterically blocks the access of nucleolytic enzymes. The life-time of unprotected DNA is several minutes, but polyplex bound DNA is stable for up-to hours⁴⁰.

Generally any synthetic gene delivery system should be able to;

- 1) Neutralize the negatively charged phosphate backbone of DNA to prevent charge repulsion against the anionic cell surface. This process is entropically driven⁴¹ and polyplexes form spontaneously upon mixing of cationic polymers with plasmid DNA.
- 2) Condense the bulky structure of DNA to appropriate length scales for cellular internalization. The resulting particles are typically toroidal or spherical in structure^{42,43} with diameters ranging from 30 to several hundred nanometres
- 3) Protect the DNA from both extracellular and intracellular nuclease degradation.

In order to meet these requirements, there are three packaging strategies: electrostatic interaction, encapsulation and adsorption (figure 1.2).

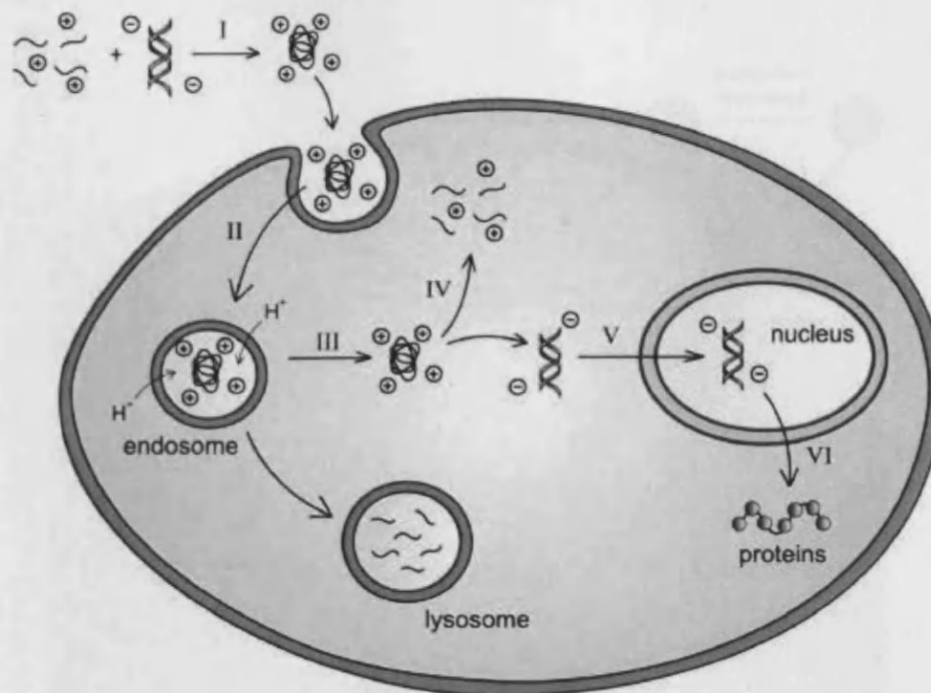
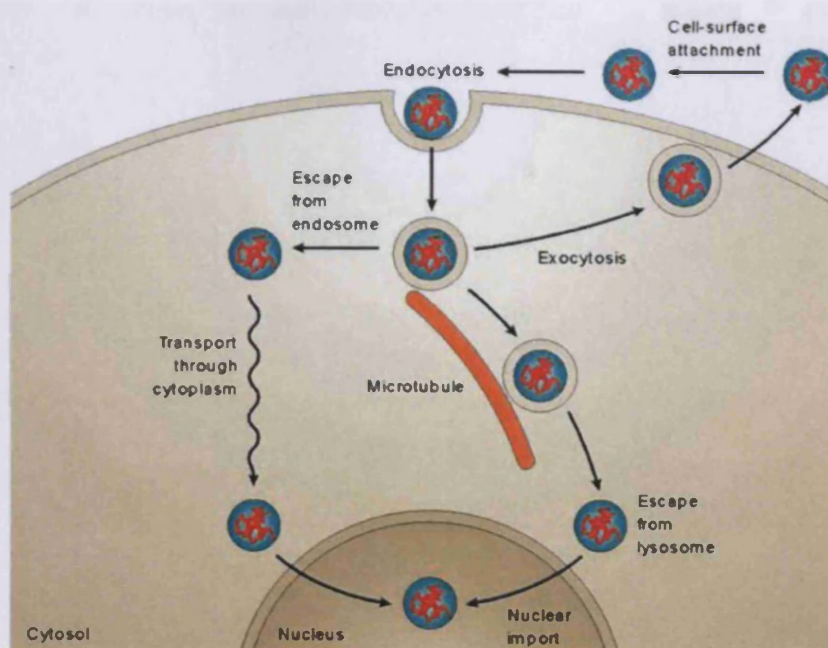


Figure 1.2 ; Barriers to gene delivery-(i) package therapeutic genes; (ii) gain entry into cells; (iii) escape the endo-lysosomal pathway; (iv) effect DNA/vector release; (v) traffic through the cytoplasm and into the nucleus; (vi) enable gene expression; and (vii) remain biocompatible⁴⁴

1.4.3 Principle hurdles for gene delivery

For successful gene delivery, treatment needs to be administered systematically and therefore targeted to the desired site of action. Hence polymer mediated gene delivery systems have to survive in the blood stream without being degraded or captured by cellular defence mechanisms⁴⁵⁻⁴⁸. Once at the target site, they have to extravasate into the tissue and bind specifically to the target cells. After their cellular internalization, intracellular barriers (endosomal escape, cytoplasm trafficking, nucleus entry) are additional hurdles (figure 1.3), in which each of the listed steps can be a major bottle neck for the efficiency of such a gene delivery system^{49,50}.



Copyright © 2005 Nature Publishing Group
Nature Reviews | Drug Discovery

Figure 1.3; Major hurdles in drug/gene delivery⁵¹

1.4.4 Cellular entry

On a cellular level, the first obstacle encountered by the polymer/DNA complex, or “polyplex”, is the plasma membrane. To gain entry into cell, passive diffusion is typically not afforded to polyplexes due to size restrictions of transmembrane pores and channels and low partition coefficients into lipid bilayers. The pathway followed by the cationic vectors, from the exterior of the cell to the nucleus is still not clear. However, electron and fluorescence microscopy studies have shown that lipoplexes and polyplexes can be detected in intracellular vesicles beneath the cell membrane, suggesting that they enter cells by endocytosis⁵². As such endocytic uptake occurs by at least four known pathways: clathrin-mediated endocytosis via coated pits (adsorptive or receptor mediated), lipid-raft mediated endocytosis (caveolae-mediated or not), phagocytosis, macro-pinocytosis^{53,54}(figure 1.4).

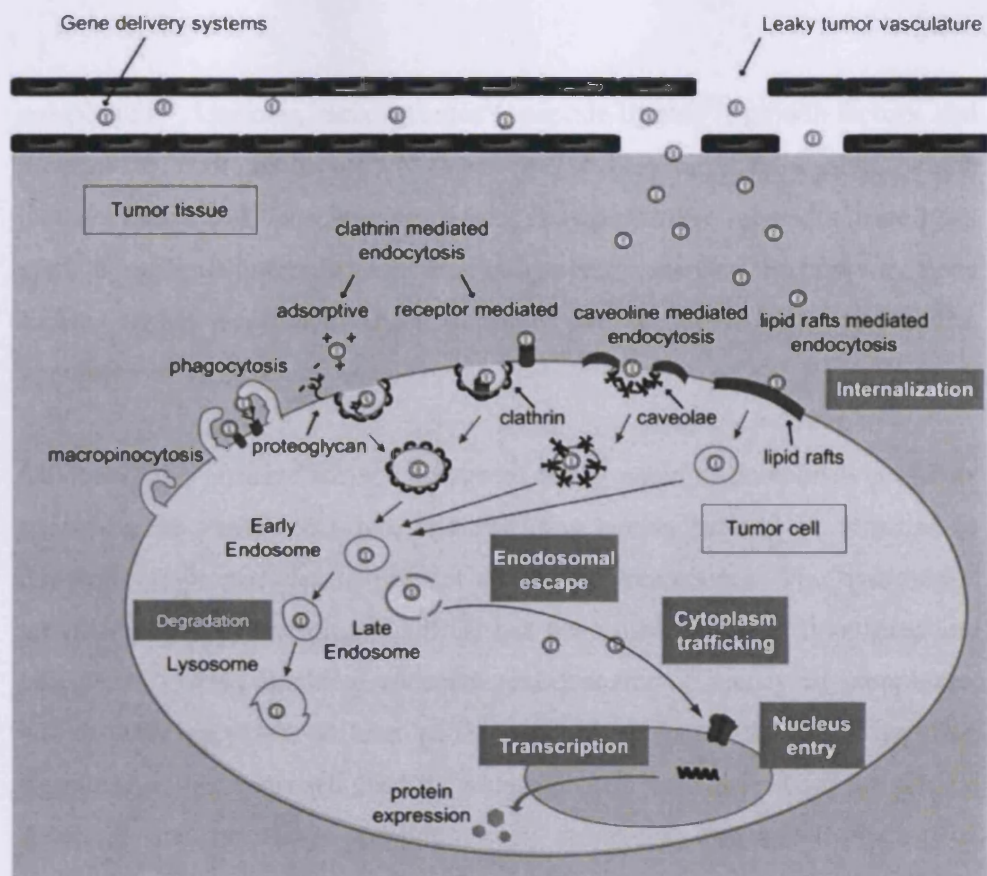


Figure 1.4; Schematic representation of the different hurdles encountered by a gene delivery system in order to enter and traffic into a tumor cell⁵⁵.

In terms of polymer-mediated gene delivery, all share a common uptake mode of enclosing the internalized polyplexes within transport vesicles derived from the plasma membrane.

1.4.4.1 Targeted uptake

1.4.4.1.1 Receptor-mediated targeting and endocytosis.

Especially for in vivo therapy it is necessary to direct gene delivery vehicles to specific cell types in order to avoid unwanted effects in non-target cells. Targeting can be achieved actively by incorporating structures which facilitate the exclusive uptake of the vector in certain tissues or cell types. Targeting ligands that have been evaluated for this purpose include small chemical

compounds⁵⁶, vitamins, carbohydrates⁵⁷, peptide ligands⁵⁸, growth factors, and proteins^{59,60,61} or antibodies⁶²⁻⁶⁴. Vectors that bear targeting ligands, which induce endocytosis upon binding to their cognate surface receptors, have been used to mediate internalization in a cell-specific manner. In this way gene expression has significantly been improved (10- to 1000- fold) compared to ligand-free complexes.

Obviously the positive surface charge of many nonviral complexes prohibits specific gene transfer in vivo, and shielding agents have to be attached to nonviral vector particles to prevent unspecific interactions. The hydrophilic polymer poly(ethylene glycol) (PEG) has been used to shield lipoplexes and polyplexes⁶¹. PEG-shielding reduced gene transfer efficiency of complexes, but the efficiency was at least partly restored by incorporation of targeting ligands. Another approach used the serum protein transferrin both for surface shielding and targeting. Applying such strategies, systemic targeting of tumours was demonstrated using folic acid receptors, transferrin receptor^{60,65,66}, or epidermal growth factor (EGF) receptor⁶¹ as target, providing first proof-of-concept that systemic targeting is possible, at least with nonviral shielded vectors.

Targeting of liposomes with phospholipid-anchored folate conjugate is an attractive approach to deliver chemotherapeutic agents to folate receptor (FR) expressing tumors. The use of polyethylene glycol-coated liposomes with folate attached to the outer end of a small fraction of phospholipid-anchored PEG molecules appears to be the most appropriate way to combine long-circulating properties critical for liposome deposition in tumors and binding of liposomes to FR on tumor cells⁶⁷.

Growth factor receptors such as epidermal growth factor (EGF) of fibroblast growth factor (FGF) receptors are attractive targets in cancer gene therapy since they are highly overexpressed in a variety of cancer tissues, including lung,

head, neck, bladder, liver and breast cancers (EGF-receptor)⁶⁸. These receptors bind to their target specifically and with high affinity, whereby upon bonding the receptors dimerize and are internalized together with their bound target.

EGF coupled PEI has been shown 300-fold increase of gene expression compared to the unmodified polymer⁶⁹. Similar observations were made when EGF-poly(L-lysine), EGF-PEI⁷⁰ or FGF-PLL⁷¹ conjugates were employed.

1.4.4.2 Non-specific uptake

1.4.4.2.1 Ionic interaction with membrane-bound proteoglycans and endocytosis

Cellular entry can also occur in the absence of targeting ligands. Some polyplexes are able to induce cellular uptake through charge mediated interactions with proteoglycans which are present on the cell surface⁷². Proteoglycans are composed of a membrane-associated core protein from which a chain of sulphated or carboxylated glycosaminoglycans (GAGs) extend into the extracellular space⁷³. These highly anionic GAG units determine much of the interactions between the cell surface and extracellular macromolecules and are responsible for the overall negative charge of the plasma membrane⁷⁴. Although the exact mechanism by which these membrane-bound molecules mediate cellular internalization remains unclear, they are believed to play a central role in the endocytic uptake of many non-targeted, positively-charged gene delivery systems⁷⁵.

1.4.4.2.2 Lipophilic interaction with phospholipid membrane and endocytosis

An alternative opportunity for cellular uptake relies on the interaction between vector-bound lipophilic residues and the phospholipid layers that comprise the cellular membrane⁷⁶. Thomas and Klibanov demonstrated the potential ability of long, lipophilic alkyl chains (i.e., dodecane, hexadecane) to increase endocytosis through interactions with the cell membrane resulting in increased

transfection efficiencies⁷⁷. Moreover, their results revealed that the position of lipophilic substitution (i.e., primary vs. tertiary amines of PEI) can have profound effects on the extent of this interaction and thus transfection efficiencies⁷⁷.

1.4.4.2.3. Cell penetrating peptide-mediated uptake

In past, cell penetrating peptides (CPP) have been extensively investigated for their ability to facilitate membrane translocation. Originally derived from viral proteins, these peptides are typically 5-40 amino acids in length, positively charged and amphipathic in nature. By virtue of their net positive charge, some CPPs have served as both the DNA-binding and cell penetrating component^{78,79}. Although the mechanism by which CPPs facilitate cellular uptake remains controversial, the prevailing hypotheses of CPP-mediated uptake include;

- 1) formation of peptide-lined pores within the membrane
- 2) direct penetration through the membrane and into the cytoplasm
- 3) transient uptake into a membrane-bound micellar structure that inverts to release the CPP and its genetic cargo inside the cytosol
- 4) the induction of endocytosis⁸⁰.

However, the predominant route of entry of cationic gene delivery systems seems to be by non-specific adsorptive endocytosis followed by the clathrin-coated pit mechanism as negatively charged glycoproteins, proteoglycans and glycerophosphates, present on the cell membrane, are able to interact with the positively charged systems⁷². Using specific inhibitors of different endocytosis pathways, Rejman et al.⁸¹ conclude that lipoplex 1,2-dioleoyl-3-trimethylammonium-propane (DOTAP/DNA) uptake can be preceded only by clathrin-mediated endocytosis, while polyplexes (PEI/DNA) can be taken in by two mechanisms, one involving caveole and the other clathrin-coated pits. However, the internalization pathway seems to be dependent on the system used and cells to transfect⁸² carrier systems containing a specific targeting

moiety, which are specifically recognised by a cell surface receptor, could enter cells via both adsorptive endocytosis and receptor-mediated endocytosis⁸³.

Macropinocytosis can also mediate the uptake of cationic carriers because of its ability to internalize large structures such as bacteria. Phagocytosis of lipoplexes and polyplexes, even in cell lines that are not professional phagocytes, has also been shown^{84,85}.

The relative contribution of each pathway in the internalization of synthetic vectors is poorly defined, given the large variety of carriers⁸⁶. Therefore, factors such as cell membrane composition or surface charge and the size⁸⁷ of complexes may influence the balance in favour of either one or the other pathway.

1.4.5 Endo-lysosomal escape

If cellular entry is gained by endocytosis, subsequent intracellular routing of vesicle-bound polyplexes can include recycling back to the cell surface, sorting to acidic, degradative vesicles (e.g., lysosome, phagosome), or delivery to an intracellular organelle (e.g., Golgi apparatus, endoplasmic reticulum)⁸⁶. The intracellular itinerary that the endocytic vesicles follow depends upon the pathway by which they were internalized. At present, clathrin mediated endocytosis is the most common pathway and has served as the route for which synthetic gene delivery systems have been designed. However, the emerging evidence suggesting that the uptake pathway, and thus intracellular routing and transfection efficiency, is dependent upon cell line, polyplex type and the conditions under which the polyplex is formulated^{81,88}. Within the clathrin-mediated endocytic pathway, polyplexes can be sequestered within endosomal vesicles and shuttled through the endo-lysosomal pathway. Release from these vesicles is paramount to avoiding enzymatic degradation within the lysosomal compartment (figure 1.5).

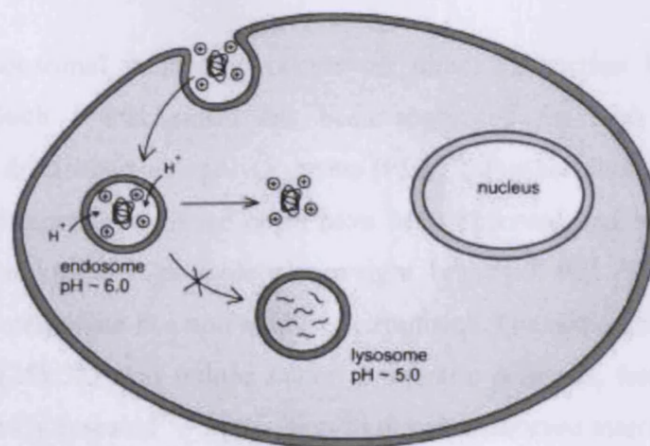


Figure 1.5; Endo-lysosomal escape⁴⁴

These vesicles rapidly acidify to pH 5-6 due to ATPase proton-pump enzyme in the vesicle membrane. Polyplexes can subsequently be trafficked into lysosomes, which further acidify to pH~4.5 and contain various degradative enzymes. It is believed that much of the DNA becomes trapped in these vesicles and is degraded. Only DNA that escapes into the cytoplasm can go on to reach the nucleus.

Several strategies have been used to overcome this barrier. Concurrently treating cells at the time of transfection with chloroquine, which is known to accumulate in the acidic vesicles and buffer their pH, results in improved gene delivery with some polymers⁸⁹. Although this technique is easy to use in vitro studies, it is impractical for in vivo gene delivery. Some researchers have conjugated whole, inactivated adenovirus particles to poly(L-lysine) (PLL), which improved gene transfection efficiency by up to 2,000-fold⁹⁰⁻⁹³. This enhancement was due to virus mediated endosomal escape, but the virion might also provide functionality for addressing subsequent intracellular barriers. This approach is also impractical owing to the increased difficulty of preparing the vector and safety concerns especially immunogenicity of the virus.

The mechanisms involved in endosomal release of DNA by cationic polymer-based vectors are unclear. Two hypotheses have been suggested to explain this escape. The first one is based on a idea that a physical disruption of the negatively

charged endosomal membrane occurs on direct interaction with the cationic polymer. Such a mechanism has been suggested for both polyamidoamine (PAMAM) dendrimers and poly(L-lysine (PLL)⁹⁴. Further, in electron microscopy studies, endosomal membrane holes have been observed and were related to the direct interaction of high molecular weight branched PEI (800 kDa) with the endosomal membrane in a non-acidic environment. The authors suggested that low MW PEIs (25kDa) also induce minor membrane damages, but that these holes may be quickly resealed⁹⁵. In addition to direct membrane interaction, the release of polyplexes may also be attributed to the extension of the polymer network as a result of the increasing electrostatic repulsion of charged groups during acidification⁹⁶. The second hypothesis used to explain endosomal disruption by cationic polymers with ionisable amine groups has been termed the “proton sponge” hypothesis (figure 1.6)^{97,98}. Endosomal membranes possesses an ATPase enzyme that actively transports protons from the cytosol from the cytosol into the vesicle resulting in acidification of the compartment⁹⁹

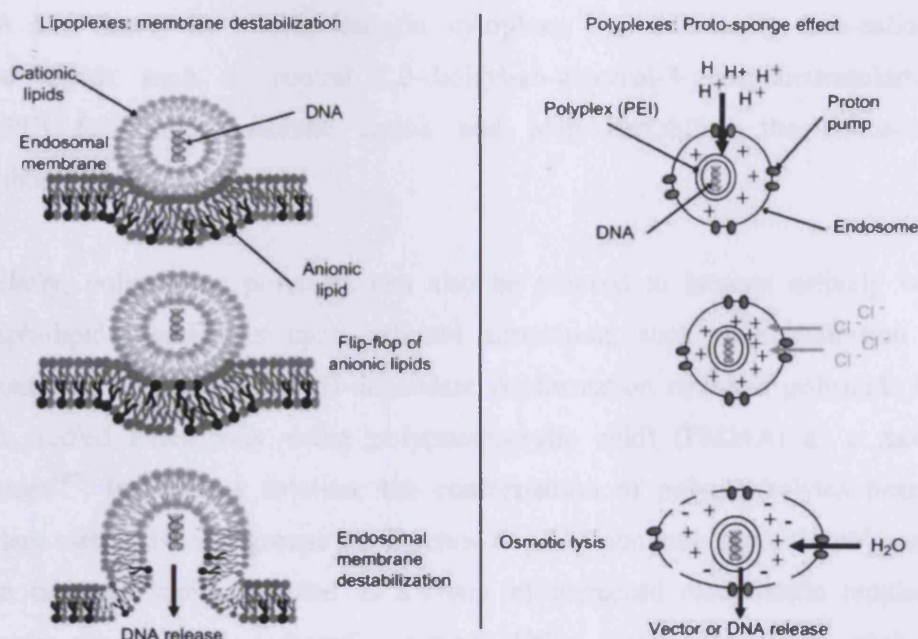


Figure 1.6 ; Hypothesis of endosomal escape of lipoplexes and polyplexes gene delivery systems⁵⁵.

The proton-sponge hypothesis assumes that polymers such as PEI and PAMAM, containing a large number of secondary and tertiary amines can buffer the pH, causing the ATPase to transport more protons to reach the desired pH. The accumulation of protons in the vesicle results in an influx of counter ions which causes osmotic swelling and rupture of the endosomal membrane, in turn releasing the polyplexes into the cytoplasm^{98,100,101}.

In the case of cationic lipid-based vectors, another model has been proposed for local endosomal membrane destabilization, in which electrostatic interactions between the cationic lipids and the endosomal membrane induce the displacement of anionic lipids from the cytoplasm-facing monolayer of the endosomal membrane, by a way called flip-flop mechanism (figure 1.6). The formation of a neutral ion pair between anionic lipids present in the endosomal membrane and the

cationic lipids of the vector will then cause subsequent decomplexation of the DNA and finally its release into the cytoplasm¹⁰². Additionally, non-cationic helper lipids such as neutral 1,2-dioleoyl-sn-glycerol-3-phosphoethanolamine (DOPE) facilitate membrane fusion and help destabilize the endosomal membrane^{103,104}.

Similarly, polyanionic polymers can also be tailored to interact actively with phospholipid membranes upon external simulation, such as acidification of surrounding medium. The pH-dependent conformation of weak polyacids has been studied extensively using poly(methacrylic acid) (PMMA) as a model polymer¹⁰⁵. In aqueous solution, the conformation of polyelectrolytes bearing pendant carboxylic acid groups is a function of pH. Upon ionization, the polymeric chain becomes more extended as a result of increased electrostatic repulsion between the charged carboxylic groups. Other interacting forces such as hydrophobic interactions and hydrogen bonding, due to the presence of alkyl groups or backbone stiffness, may also influence the conformation adopted by a polyelectrolyte in solution.

1.4.6 Cytosolic transport and nucleus entry

Polyplexes that enter the cytosol, either directly upon cellular internalization or upon escaping the endo-lysosomal pathway, are immediately faced with a physically and metabolically hostile environment. Within the cytosolic environment, nucleolytic enzymes ready to degrade unprotected nucleic acids are interspersed amongst microtubules, intermediate filaments, and microfilaments that are organised into a dense network to form the cytoskeleton¹⁰⁶. These filaments provide an internal structure to the cell and function in cell motility and intracellular transport of vesicles, chromosomes and macromolecules. It has been shown that the mesh-like structure of the cytoskeleton, and more specifically cross-linked actin filaments (figure 1.7), can severely impede the

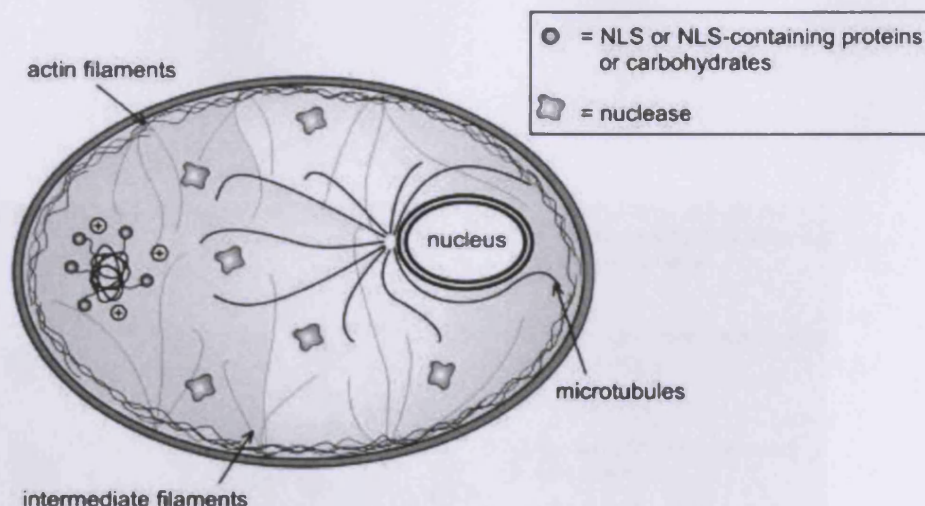


Figure 1.7 ; Cytosolic transport and nuclear import²¹.

diffusion of naked DNA greater than 250 bp in size with an extended linear length of approximately 85nm^{107,108}. An important factor in nucleic acid transport through the cytoplasm is the rate of mobility which depends on the size and shape of the molecule (circular plasmid DNA > linear DNA)¹⁰⁹. But in the case of DNA complexed with gene delivery systems, the state of DNA when present in the cytoplasm is poorly documented.

The nuclear envelope, a double membrane, is interrupted by large protein structures called nuclear pore complexes (NPCs). These proteins allow the passage of molecules up to 9nm in size (40-60 kDa), but in the case of larger molecules, the transfer needs shuttle molecules and is energy dependent¹¹⁰. The NPC is able to mediate the transport of ions, small molecules, proteins, RNA, and ribonucleoproteins in and out of the nucleus. Specific sequences on proteins expected to enter the nucleus, named nuclear localization sequence (NLS), allow intracellular protein trafficking toward the nuclear pores¹¹¹. The first NLS described was the derived sequence of the simian cancer virus large T antigen¹¹². These NLS are recognised in the cytoplasm by a soluble protein, importin- α ¹¹¹. The complex of NLS/importin- α connects to another protein, importin β , and this trimeric complex then docks at the NPC and can enter the nucleus (figure 1.8)¹¹³.

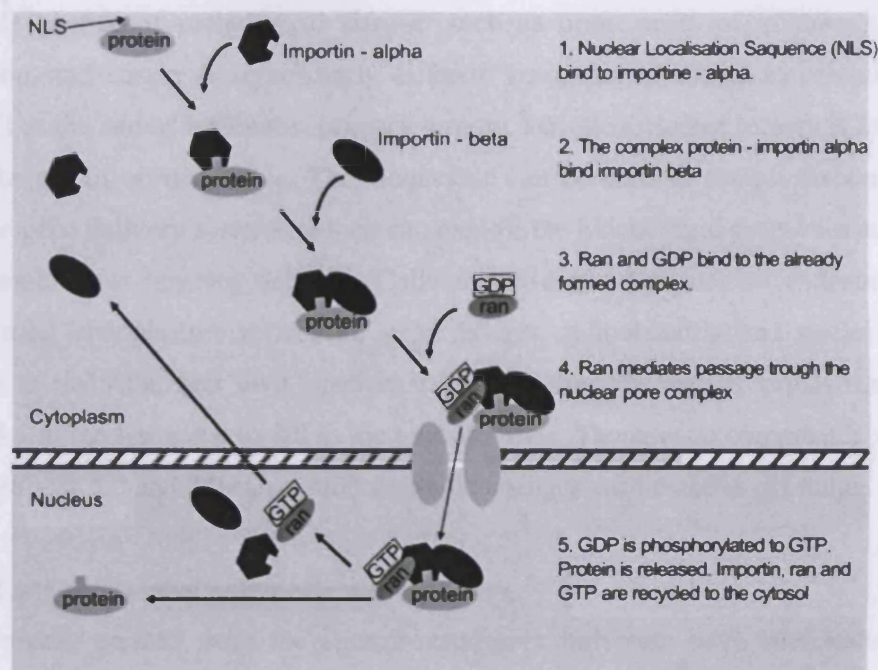


Figure 1.8 ;Schematic representation of nuclear entry mechanism through nuclear pore complexes⁵⁵.

Cytoplasm mixing and the loss of nuclear membrane during mitosis could be a way to overcome this problem. Consistent with this hypothesis, gene transfer in cultured cells has been shown to be greatly enhanced by mitotic activity for both lipoplexes^{114,115} and polyplexes¹¹⁴. This would mean that non-dividing cells are rarely transfected, and this could be a positive point for targeting tumoral cells, especially in the brain where healthy cells have no or low dividing activity.

1.5 Stimuli-responsive delivery

1.5.1 pH differences for stimuli-responsive delivery

The pH profile of pathological tissues, such as upon onset of inflammation, infection, and cancer is significantly different from that of the normal tissue¹¹⁶. The pH at the site of infections, primary tumors, and metastasized tumors is lower than the pH of normal tissue. This behaviour can be used in stimuli-responsive drug or gene delivery systems, which can exploit the biochemical properties at the diseased site for targeted delivery. Cellular sub-organelles such as endosomes, lysosomes, endoplasmic reticulum, golgi bodies, mitochondria and nuclei are known to maintain their own characteristic pH values¹¹⁶. The pH values ranged from 4.5 in the lysosome to 8.0 in the mitochondria. Therapeutic compounds with pKa between 5.0 and 8.0 can exhibit dramatic changes within above pH range.

1.5.1.1 pH-responsive polymeric nanocarriers

Nanocarriers created from the stimuli-responsive polymers have been used as anticancer drug delivery systems. The physical properties, such as swelling/deswelling, particle disruption and aggregation of stimuli-responsive nanocarriers change in response to the changes in environmental condition. The pH-sensitive poly(β -amino ester) (PbAE) constitutes a novel class of biodegradable cationic polymer for development of site-specific drug and gene-delivery systems. In the acidic environment of the tumor, PbAE undergoes rapid dissolution and releases its contents at once. Using PbAE nanoparticles, it has shown significant enhancement of paclitaxel accumulation in the tumour tissue as compared to poly-(ϵ -caprolactone) (PCL) nanoparticles containing paclitaxel¹¹⁷. In another study, pullulan acetate, a linear polysaccharide has been introduced with sulfadimethoxine (SDM) to prepare pH-sensitive and self-assembled hydrogel nanoparticles, which also demonstrated enhanced adriamycin (ADR) release in response to lower pH and increased cytotoxicity¹¹⁸.

Polyanionic polymers can also be tailored to interact actively with phospholipid membranes upon external stimulation, such as acidification of the surrounding

medium. The pH-dependent conformation of weak polyacids has been studied extensively using poly(methacrylic acid) (PMAA) as a model polymer¹⁰⁵. In aqueous solution, the conformation of polyelectrolytes bearing pendant carboxylic acid groups is a function of pH. Once ionised the polymer, polymer chain become more extended due to electrostatic repulsion between the charged carboxylic groups.

Kim and co-workers attached the amino histidine (His) as an endosomolytic agent to poly(2-hydroxyethyl aspartamide) (PHEA-His) and C₁₈-grafted PHEA (PHEA-g-C₁₈-His) via an ester linkage¹¹⁹. PHEA-g-C₁₈-His series formed stable self-assembled particles due to the hydrophobic interaction between grafted alkyl chains. The size, zeta potential and micropolarity of the PHEA-g-C₁₈-His series greatly increased at pH 5.0, because aggregates swelled by a positive surface charge and the electrostatic repulsion of ionized histidine moieties in the aggregate surface.

1.5.1.2 pH-responsive polymer-drug conjugates

Anticancer drugs can be conjugated to pH-sensitive polymers to exploit the acidic environment of tumor. Presence of acid-sensitive spacers between the drug and polymer enables release of drug either in relatively acidic extracellular fluids or, after endocytosis in endosomes or lysosomes of tumor cells. Kamada and colleagues¹²⁰ synthesized a pH-sensitive polymeric carrier, in which a poly(vinylpyrrolidone-co-dimethyl maleic anhydride) (PVD) was conjugated to doxorubicin (DOX), that could gradually release free drug in response to changes in pH [i.e., from near neutral (~7.0) to slightly acidic pH (~6.0)]. It was concluded that the superior anticancer activity of PVD-DOX conjugate is due to controlled release and enhanced tumor accumulation of the drug.

Thiolated protein bound drugs through acid sensitive hydrazone linker can be released in to the acid environment of endosomes and/or lysosomes during endocytosis¹²¹. Anticancer drugs conjugated to serum albumin have shown

considerable anticancer activity, for example, in vitro studies of acid-sensitive chlorambucil and anthracycline conjugates with serum albumin displayed higher antiproliferative activity, and acid-sensitive DOX albumin conjugates displayed greater antitumor activity in animal tumor models when compared to free drug^{122,123}.

1.5.1.3 pH responsive liposomes

Over the last 30 years, considerable attention has been given to the use of liposomes, bilayered phospholipid vesicles with the anticancer drugs and gene delivery. As a result some of the liposomal formulations are already approved for the clinical trials or in the market (i.e. DaunoXome, Mycet, AmBisome). To achieve the pH- sensitivity to release active contents, the liposomes can be tailored from the pH-sensitive components. The pH-sensitive liposomes are endocytosed in the intact form and fuse with the endovascular membrane as a consequence of the acidic pH inside the endosome, and release its active contents into the cytoplasm¹²⁴. Recent studies mainly focus on the development of new lipid compositions that attribute pH-sensitivity to liposomes or modification of liposomes with various pH-sensitive polymers¹²⁵ and imparting hydrophilicity to the liposomal surface for longevity and ligand-mediated targeting. This combination of pH-sensitivity, longevity and targeting ability of liposomes can effectively deliver their contents into the cytoplasm¹²⁶.

Phosphatidylethanolamine (PE) in liposomes undergoes a transition from lamellar to inverted micelle structures at low pH which allows for fusion of liposomal and endosomal membrane and consequently a destabilization of endosomes. Among various other drugs, pH-sensitive liposomes have successfully been applied for the delivery of antisense oligonucleotides into the cytoplasm¹²⁷. Lipids other than PE incorporated in liposomes also show pH-sensitive behaviour such as cholesteryl hemisuccinate (CHMS) and poly(organophosphazenes)^{126,128}.

pH-sensitive liposomes prepared from the hydrophobically-modified copolymers of poly(N-isopropylacrylamide) (PNIPAM) bearing pH-sensitive moiety have

been examined for the release of water-soluble fluorescent marker, pyranine, and an amphipathic cytotoxic drug DOX. The release from the copolymer modified liposomes is found to be depend on pH, the concentration of copolymer, the presence of other polymers such as polyethylene glycol and the method of preparation¹²⁹.

A pH stimuli release of drugs encapsulated in liposomes can be achieved both with drugs that increase, as well as decrease, membrane permeabilities upon acidification, as long as the intraliposomal buffer strength and pH is rationally selected. Lee et al.¹³⁰ investigated the folate receptor-targeted liposomes with three different compounds whose pKa is dependent on pH. Anionic 5(6)-carboxyfluorescein converts into non-ionic at endosomal pH and releases at endosomes. These compounds can be encapsulated into liposomes at neutral pH. As a result of decreasing pH of intraliposomal at endosomal acidic pH, the liposomal contents can be released to endosome. Some compounds such as sulforhodamine B retains both anionic and cationic charges and stay in endosomes for a long time. DOX in its cationic form in strong acidic buffer when loaded into liposomes, displays endocytosis triggered release, since sufficient uncharged DOX remains at endosomal pH.

1.5.2 Temperature differences for stimuli-responsive delivery

The use of hyperthermia as an adjunct to radiation or chemotherapy of various types of solid tumors has become an important area for the past 20 years¹³¹. Normally, tumor cells are more sensitive to heat-induced damage than normal cells. Super-paramagnetic iron oxide-containing liposomes or nanoparticles have been used in the majority of clinical studies of hyperthermia^{132,133}. The liposomes and nanoparticles provide a method for intracellular delivery and localization of the iron oxide particles. Unlike the external probes that can heat the surrounding normal tissues, applying magnetic nanoparticle hyperthermia can ensuring that only the intended target is heated. A typical in vivo dose of 100-120 kHz

alternating magnetic field is applied to experimental tumor models for about 30 min to achieve temperatures between 40 and 45°C.

1.5.2.1 Temperature-responsive polymeric nanocarriers

Temperature sensitivity is one of the most interesting characteristics in stimulus-responsive polymeric nanocarriers and has been extensively investigated to exploit the hyperthermia condition for drug and gene delivery^{134,135}. A thermoresponsive polymer exhibits a lower critical solution temperature (LCST), in which below this temperature polymer is water soluble and above water-insoluble (figure 1.9). Such LCST exists for both homopolymers and block copolymers. This property has been exploited in targeted delivery of anticancer drugs. For example, the rhodamine-poly(N-isopropylacrylamide) conjugates were selectively accumulated in a tumor tissue using targeted hyperthermia¹³⁴. Block copolymers of PEG as a hydrophilic block and PNIPAM or poly(N-isopropylacrylamide)-co-N-(2-hydroxypropyl) methacrylamide-dilactate as a thermosensitive block are able to self-assemble in water into temperature-responsive nanocarriers above the LCST of the thermosensitive block¹³⁶. An amphiphilic thermosensitive nanocarrier prepared from N-(2-hydroxypropyl)methacrylamide lactate and PEG displayed promising delivery system for the parental administration of paclitaxel¹³⁷.

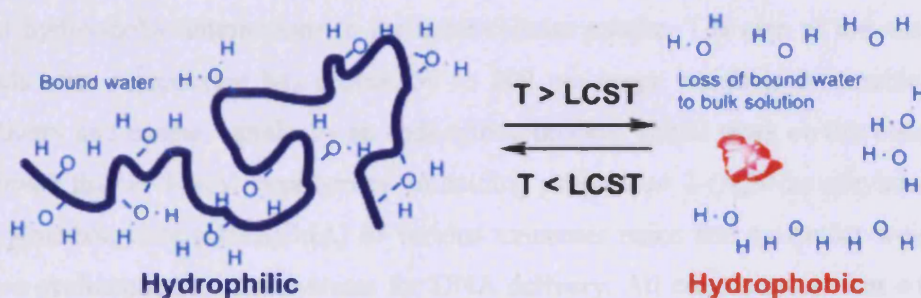


Figure 1.9; Schematic of thermoresponsive polymer response with temperature¹³⁸

Polymeric micelles have been explored for temperature induced release of actives for drug and gene delivery. Temperature-sensitive micelles are block copolymers composed of temperature-sensitive and hydrophobic blocks in which the outer shell of the polymeric micelles possess the temperature sensitive properties and the drug molecules are incorporated into the hydrophobic inner core. PNIPAM has been widely investigated for biomedical applications owing to the entropy driven change of the polymer from a water-soluble coil to a hydrophobic globule at 32⁰C. In addition, LCST of PNIPAM can be easily modified by copolymerization. AB type block copolymers consisting of a NIPAM segment and hydrophobic segment can form core-shell micellar structures below the NIPAM LCST. PEG is the most commonly used hydrophilic segment of the copolymers forming the micelles as well as for the coating of other colloidal nanocarriers, because of its biocompatibility¹³⁹. Introduction of an amino group to the NIPAM chain increases the LCST and slows down the rate of phase separation¹⁴⁰.

1.5.2.1.1 Copolymers of PNIPAM for gene delivery.

The switchable hydrophilic-to-hydrophobic properties of PNIPAM have attracted attention for nucleic acid delivery. The concept behind this is that cationic functionalized PNIPAM polymers should be able to compact large, negatively charged nucleic acids above the LCST collectively through charge neutralization and hydrophobic interactions to facilitate cellular uptake. The size of the nucleic acids after compaction lies around 50 to 200 nm range which is favourable for delivery and enables uptake by an endocytotic process. Initial work on this concept showed that PNIPAM copolymers containing protonated 2-(N,N-dimethylamino) ethylmethacrylate (DMAEMA) of various monomer ratios and molecular weights were evaluated as carrier systems for DNA delivery. All copolymers, even with a low DMAEMA content of 15mol%, were able to bind to DNA at 25⁰C. The results of this study show that the formation of stable copolymer/plasmid complexes with a size of around 200nm is a prerequisite for efficient transfection¹⁴¹. Further, Kurisawa et al¹⁴² established the precedent of varying gene transfection by

temperature-induced phase transitions in linear PNIPAM copolymers, with higher protein expression induced by incubation of cells below LCST.

Non-viral vectors based on thermosensitive polymers have been shown to be effective in vitro and in vivo gene transfection agents. Most of this research has been carried out using block copolymers of PNIPAM and polyethyleneimine (PEI) as temperature-sensitive carriers for in vitro and in vivo transfection of plasmid DNA^{143,144}. Introduction of BPEI 25K units to NIPAM chains increased the LCST values up to 39.6°C, but with linear PEI25K LCST was 36.6°C¹⁴³. Twaites et al. reported DNA binding behaviour of pH and temperature responsive PNIPAM copolymers¹⁴⁵. Plasmid DNA complexed to PNIPAM copolymers displayed variation in gel retardation behaviour above and below polymer phase-transition temperatures. High molecular weight PNIPAM copolymer forming complexes with reduced affinity above PNIPAM phase transition. PEI copolymers with side chain grafted PNIPAM were shown to be less toxic than PEI alone or PNIPAM copolymer and the effects were concentration dependent¹⁵.

In principle, thermoresponsive polymers with LCSTs below body temperature can be used to deliver tightly condensed DNA to cells. Once inside the cells, an externally applied temperature reduction to below the LCST induces the relaxed, extended-chain conformation to result in DNA release (figure 1.10)^{140,142}.

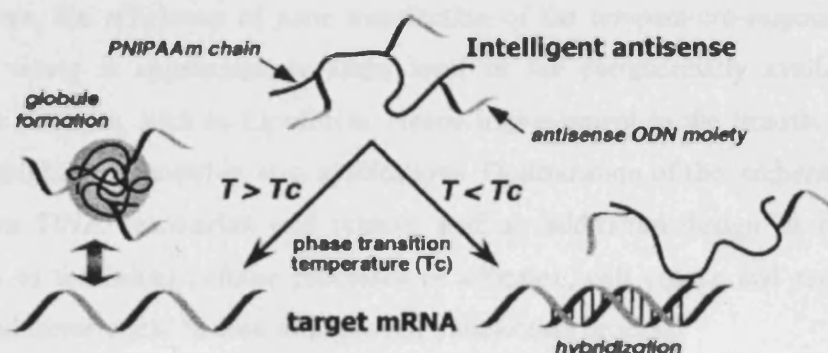


Figure 1.10; Schematic illustration of stimuli-responsive antisense reagent comprising oligonucleotide and PNIPAM¹⁴⁶.

1.6 “Challenges yet to be addressed”

1) The immense complexity of the biopolymer transport and, in the case of nucleic acids, translation and transcription processes, suggests that single component passive polymer delivery systems are not effective in many therapeutic applications. Therefore, the design of polymer systems capable of variable biopolymer binding affinities, cell membrane disruption, nuclear targeting and controlled degradation is now a particularly active area of study.

2) Another potential problem with synthetic drug delivery system is the inherent polydispersity of the polymers used in complex formation with drug/gene. There is also a need for better control of polymer architecture, in order that properties such as hydrodynamic volume and/or particle size can be tailored to avoid renal clearance. However recent advances in polymer chemistry has gone a long way to solve those problems, synthesizing polymers with narrow diversity using newly developed techniques such as living free radical and ring-opening polymerization.

3) The advances in synthetic methods, coupled with increased understanding of in vivo cell biology, are likely to lead to new functional materials with enhanced biological activity, fewer side effects and to improved therapies for the benefit of patients.

4) At present, the efficiency of gene transfection of the temperature-responsive polymeric vector is approximately same level as the commercially available transfection reagents, such as Lipofectin. Hence improvement in the transfection efficiency might be required in vivo applications. Optimization of the temperature response for DNA association and release, and an additional design to raise efficiencies of the initial cellular processes of adhesion, cell uptake and escape from the endosome could be lead to improved transfection process.

1.7 This thesis in context

The aim of the thesis was to study the solution properties of several families of polymers used in drug/gene delivery. The first study focused on physicochemical characterization of thermoresponsive PEI-PNIPAM copolymers in collaboration with Cameron Alexander. The key variable here was temperature and our goal was to quantify the structural features of these systems and relate this structural variation to their transfection efficiency. The role of vector architecture and complex structure was evaluated using Small-Angle Neutron Scattering (SANS) and Pulsed- Gradient Spin -Echo (PGSE) NMR.

Subsequently we characterized the physico-chemical behaviour of bio-responsive linear poly amidoamine as a pH-responsive polymer, following from previous work of Zeena Khayat. Initially she synthesized two different linear polyamidoamines namely ISA1 and ISA23. Small angle neutron scattering (SANS) has been used to characterize the solution properties of these polymers. Within this frame work she was able to study interaction of ISA23 with model surfaces such as surfactant. During my study I elaborated this work to study the interaction of this polymer with biologically relevant interfaces such as Lyso-PC and model membranes resembling plasma, endosomal and lysosomal mimics. Interaction between the polymer and complex interfaces were done using EPR and the results gained were supported by previously done SANS results as well.

1.8 References

1. Walther, W.; Stein, U.; Voss, C.; Schmidt, T.; Schleef, M.; Schlag, P. M., *Analytical Biochemistry* 318, 230 2003.
2. Shi, F.; Rakhmievich, A. L.; Heise, C. P.; Oshikawa, K.; Sondel, P. M.; Yang, N. S., *Molecular Cancer Therapy* 1 11, 949 2002.
3. Mansouri, S.; Lavigne, P.; Corsi, K.; Benderdour, M.; Beaumont, E.; Fernandes, J. C., *European Journal of Pharmaceutics and Biopharmaceutics* 57, 1 2004.
4. Pakunlu, R. I.; Wang, Y. C.; Saad, M.; Khandare, J. J.; Starovoytov, V.; Minko, T., *Journal of Controlled Release* 114, 153 2006.
5. Dharap, S. S.; Qiu, B.; Williams, G. C.; Sinko, P.; Stein, S.; Minko, T., *Journal of Controlled Release* 91, 61 2003.
6. Du, J. Z.; Chen, D. P.; Wang, Y. C.; Xiao, C. S.; Lu, Y. J.; Wang, J.; Zhang, G. Z., *Biomacromolecules* 7, 1898 2006.
7. Jiang, T.-Y.; Wang, Z.-Y. W.; Chen, C. C.; Mo, F.-K. M.; Xu, Y.-L. X.; Tang, L.-X. T.; Liang, J.-J. L., *Journal of Applied Polymer Science* 101, 2871 2006.
8. Zhelev, Z.; Ohba, H.; Bakalova, R., *Journal of the American Chemical Society* 128, 6324 2006.
9. Zhang, H.; Cui, W.; Bei, J.; Wang, S., *Polymer Degradation and Stability* 91, 1929 2006.
10. S. Sajeesh, C. P. S., *Journal of Biomedical Materials Research Part B: Applied Biomaterials* 76B, 298 2006.
11. Yuancai Dong; Feng, S.-S., *Journal of Biomedical Materials Research Part A* 78A, 12 2006.
12. Dixit, V.; VandenBossche, J.; Sherman, D. M.; Thompson, D. H.; Andres, R. P., *Bioconjugate Chemistry* 17, 603 2006.
13. Breunig, M.; Bauer, S.; Goepferich, A., *European Journal of Pharmaceutics and Biopharmaceutics* 68, 112 2008.
14. Duncan, R., *Nature Reviews Drug Discovery* 2, 347 2003.
15. Twaites, B.; C., d. I. H. A.; Alexander, C., *Journal of Materials Chemistry* 15, 441 2005.
16. Schmaljohann, D., *Advanced Drug Delivery Reviews* 58, 1655 2006.
17. Mulligan, R. C., *Science* 260, 926 1993.
18. Burton, E. A.; Glorioso, J. C.; Fink, D. J., *Gene Therapy* 10, 1721 2003.
19. Pawliuk, R.; Westerman, K. A.; Fabry, M. E.; Payen, E.; Tighe, R.; Bouhassira, E. E.; Acharya, S. A.; Ellis, J.; London, I. M.; Eaves, C. J.; Humphries, R. K.; Beuzard, Y.; Nagel, R. L.; Leboulch, P., *Science* 294, 2368 2001.
20. Dorothee von Laer, S. H. K. H., *The Journal of Gene Medicine* 8, 658 2006.
21. Wong, L.-F.; Goodhead, L.; Prat, C.; Mitrophanous, K. A.; Kingsman, S. M.; Mazarakis, N. D., *Human Gene Therapy* 17, 1 2006.
22. Dzau, V. J.; Beatt, K.; Pompilio, G.; Smith, K., *The American Journal of Cardiology* 92, 18 2003.
23. Alisky, J. M.; Davidson, B. L., *Human Gene Therapy* 11, 2315 2000.

24. Tuszynski, M. H., *The Lancet Neurology* 1, 51 2002.
25. Bunnell, B. A.; Morgan, R. A., *Clinical Microbiology Reviews* 11, 42 1998.
26. Kenneth, R. C., *Journal of Cellular Biochemistry* 88, 418 2003.
27. McNeish, I. A.; Bell, S. J.; Lemoine, N. R., *Gene Therapy* 11, 497 2004.
28. Kerr, D., *Nature Reviews Cancer* 3, 615 2003.
29. Vile, R. G.; Russell, S. J.; Lemoine, N. R., *Gene Therapy* 7, 2 2000.
30. Blaese, R. M.; Culver, K. W.; Miller, A. D.; Carter, C. S.; Fleisher, T.; Clerici, M.; Shearer, G.; Chang, L.; Chiang, Y.; Tolstoshev, P.; Greenblatt, J. J.; Rosenberg, S. A.; Klein, H.; Berger, M.; Mullen, C. A.; Ramsey, W. J.; Muul, L.; Morgan, R. A.; Anderson, W. F., *Science* 270, 475 1995.
31. Cavazzana-Calvo, M.; Hacein-Bey, S.; de Saint Basile, G.; Yvon, E.; Nusbaum, P.; Selz, F.; Hue, C.; Certain, S.; Casanova, J.-L.; Bousso, P.; Deist, F. L.; Fischer, A., *Science* 288, 669 2000.
32. Kay, M. A.; Manno, C. S.; Ragni, M. V.; Larson, P. J.; Couto, L. B.; McClelland, A.; Glader, B.; Chew, A. J.; Tai, S. J.; Herzog, R. W.; Arruda, V.; Johnson, F.; Scallan, C.; Skarsgard, E.; Flake, A. W.; High, K. A., *Nature Genetics* 24, 257 2000.
33. Khuri, F. R.; Nemunaitis, J.; Ganly, I.; Arseneau, J.; tannock, I. F.; Romel, L.; Gore, M.; Ironside, J.; MacDougall, R. H.; heise, C.; Randlev, B.; Gillenwater, A. M.; Bruso, P.; Kaye, S. B.; Hong, W. K.; Kirn, D. H., *Nature Medicine* 6, 879 2000.
34. El-Aneed, A., *Journal of Controlled Release* 94, 1 2004.
35. Boeckle, S.; Wagner, E., *The AAPS Journal* 8, E731 2006.
36. Hacein-Bey-Abina, S.; Le Deist, F.; Carlier, F.; Bouneaud, C.; Hue, C.; De Villartay, J.-P.; Thrasher, A. J.; Wulffraat, N.; Sorensen, R.; Dupuis-Girod, S.; Fischer, A.; Davies, E. G.; Kuis, W.; Leiva, L.; Cavazzana-Calvo, M., *New England Journal of Medicine* 346, 1185 2002.
37. Check, E., *Nature* 420, 116 2002.
38. Hacein-Bey-Abina, S.; Von Kalle, C.; Schmidt, M.; McCormack, M. P.; Wulffraat, N.; Leboulch, P.; Lim, A.; Osborne, C. S.; Pawliuk, R.; Morillon, E.; Sorensen, R.; Forster, A.; Fraser, P.; Cohen, J. I.; de Saint Basile, G.; Alexander, I.; Wintergerst, U.; Frebourg, T.; Aurias, A.; Stoppa-Lyonnet, D.; Romana, S.; Radford-Weiss, I.; Gross, F.; Valensi, F.; Delabesse, E.; Macintyre, E.; Sigaux, F.; Soulier, J.; Leiva, L. E.; Wissler, M.; Prinz, C.; Rabbitts, T. H.; Le Deist, F.; Fischer, A.; Cavazzana-Calvo, M., *Science* 302, 415 2003.
39. Marshall, E., *Science* 288, 951 2000.
40. Abdelhady, H. G.; Allen, S.; Davies, M. C.; Roberts, C. J.; Tendler, S. J. B.; Williams, P. M., *Nucleic Acids Research* 31, 4001 2003.
41. Victor, A. B., *Biopolymers* 44, 269 1997.
42. Hansma, H. G.; Golan, R.; Hsieh, W.; Lollo, C. P.; Mullen-Ley, P.; Kwoh, D., *Nucleic Acids Research* 26, 2481 1998.
43. Wagner, E.; Cotten, M.; Foisner, R.; Birnstiel, M. L., *Proceedings of the National Academy of Sciences of the United States of America* 88, 4255 1991.
44. Wong, S. Y.; Pelet, J. M.; Putnam, D., *Progress in Polymer Science* 32, 799 2007.

45. Zuber, G.; Dauty, E.; Nothisen, M.; Belguise, P.; Behr, J. P., *Advanced Drug Delivery Reviews* 52, 245 2001.
46. Rudolph, C.; Muller, R. H.; Rosenecker, J., *Journal of Gene Medicine* 4, 66 2002.
47. Luo, D.; Saltzman, W. M., *Nature Biotechnology* 18, 33 2000.
48. Wu, Y. J.; Noguchi, C. T., *Prog Clin Biol Res* 316A, 313 1989.
49. Zauner, W.; Farrow, N. A.; Haines, A. M., *Journal of Controlled Release* 71, 39 2001.
50. Wagner, S.; Knippers, R., *Oncogene* 5, 353 1990.
51. Pack, D. W.; Hoffman, A. S.; Pun, S.; Stayton, P. S., *Nature Reviews in Drug Delivery* 4, 581 2005.
52. Merdan, T.; Kunath, K.; Fischer, D.; Kopecek, J.; Kissel, T., *Pharm Res* 19, 140 2002.
53. Conner, S. D.; Schmid, S. L., *Nature* 422, 37 2003.
54. Kirkham, M.; Parton, R. G., *Biochimica et Biophysica Acta* 1746, 349 2005.
55. Morille, M.; Passirani, C.; Vonarbourg, A.; Clavreul, A.; Benoit, J.-P., *Biomaterials* 29, 3477 2008.
56. Hood, J. D.; Bednarski, M.; Frausto, R.; Guccione, S.; Reisfeld, R. A.; Xiang, R.; Cheres, D. A., *Science* 296, 2404 2002.
57. Plank, C.; Zatloukal, K.; Cotten, M.; Mechtler, K.; Wagner, E., *Bioconjugate Chemistry* 3, 533 1992.
58. Ziady, A.-G.; Ferkol, T.; Dawson, D. V.; Perlmutter, D. H.; Davis, P. B., *Journal of Biological Chemistry* 274, 4908 1999.
59. Kim, T.-G.; Kang, S.-Y.; Kang, J.-H.; Cho, M.-Y.; Kim, J.-I.; Kim, S.-H.; Kim, J.-S., *Bioconjugate Chemistry* 15, 326 2004.
60. Xu, L.; Pirollo, K. F.; Tang, W.-H.; Rait, A.; Chang, E. H., *Human Gene Therapy* 10, 2941 1999.
61. Wolschek, M. F.; Thallinger, C.; Kurs, M.; Rössler, V.; Allen, M.; Lichtenberger, C.; Kircheis, R.; Lucas, T.; Willheim, M.; Reinisch, W.; Gangl, A.; Wagner, E.; Jansen, B., *Hepatology* 36, 1106 2002.
62. Buschle, M.; Cotten, M.; Kirlappos, H.; Mechtler, K.; Schaffner, G.; Zauner, W.; Birnstiel, M. L.; Wagner, E., *Human Gene Therapy* 6, 753 1995.
63. Chiu, S.-J.; Ueno, N. T.; Lee, R. J., *Journal of Controlled Release* 97, 357 2004.
64. Zhang, Y.; Zhang, Y.-f.; Bryant, J.; Charles, A.; Boado, R. J.; Pardridge, W. M., *Clinical Cancer Research* 10, 3667 2004.
65. Hildebrandt, I. J.; Iyer, M.; Wagner, E.; Gambhir, S. S., *Gene Therapy* 10, 758 2003.
66. Kircheis, R.; Schüller, S.; Brunner, S.; Ogris, M.; Heider, K.; Zauner, W.; Wagner, E., *The Journal of Gene Medicine* 1, 111 1999.
67. Gabizon, A.; Shmeeda, H.; Horowitz, A. T.; Zalipsky, S., *Advanced Drug Delivery Reviews* 56, 1177 2004.
68. Kim, H.; Muller, W. J., *Experimental Cell Research* 253, 78 1999.
69. Blessing, T.; Kurs, M.; Holzhauser, R.; Kircheis, R.; Wagner, E., *Bioconjugate Chemistry* 12, 529 2001.

70. Kircheis, R.; Blessing, T.; Brunner, S.; Wightman, L.; Wagner, E., *Journal of Controlled Release* 72, 165 2001.
71. Sosnowski, B. A.; Gonzalez, A. M.; Chandler, L. A.; Buechler, Y. J.; Pierce, G. F.; Baird, A., *Journal Biological Chemistry* 271, 33647 1996.
72. Mislick, K. A.; Baldeschwieler, J. D., *Proceedings of the National Academy of Sciences of the United States of America* 93, 12349 1996.
73. Hardingham, T. E.; Fosang, A. J., *FASEB J.* 6, 861 1992.
74. Yanagishita, M.; Hascall, V. C., *Journal of Biological Chemistry* 267, 9451 1992.
75. Kichler, A.; Mason, A. J.; Bechinger, B., *Biochimica et Biophysica Acta (BBA) - Biomembranes* 1758, 301 2006.
76. Takigawa, D. Y.; Tirrell, D. A., *Macromolecules* 18, 338 1985.
77. Thomas, M.; Klibanov, A. M., *Proceedings of the National Academy of Sciences of the United States of America* 99, 14640 2002.
78. Ignatovich, I. A.; Dizhe, E. B.; Pavlotskaya, A. V.; Akifiev, B. N.; Burov, S. V.; Orlov, S. V.; Perevozchikov, A. P., *Journal of Biological Chemistry* 278, 42625 2003.
79. Rudolph, C.; Plank, C.; Lausier, J.; Schillinger, U.; Muller, R. H.; Rosenecker, J., *Journal of Biological Chemistry* 278, 11411 2003.
80. El-Andaloussi, S.; Holm, T.; Langel, U., *Current Pharmaceutical Design* 11, 3597 2005.
81. Rejman, J.; Bragonzi, A.; Conese, M., *Molecular Therapy* 12, 468 2005.
82. Simões, S.; Slepishkin, V.; Pires, P.; Gaspar, R.; Pedroso de Lima, M. C.; Düzgünes, N., *Biochimica et Biophysica Acta (BBA) - Biomembranes* 1463, 459 2000.
83. Mellman, I., *Annual Review of Cell and Development Biology* 12, 575 1996.
84. Matsui, H.; Johnson, L. G.; Randell, S. H.; Boucher, R. C., *Journal of Biological Chemistry* 272, 1117 1997.
85. Harbottle, R. P.; Cooper, R. G.; Hart, S. L.; Ladhoff, A.; McKay, T.; Knight, A. M.; Wagner, E.; Miller, A. D.; Coutelle, C., *Human Gene Therapy* 9, 1037 1998.
86. Khalil, I. A.; Kogure, K.; Akita, H.; Harashima, H., *Pharmacological Reviews* 58, 32 2006.
87. Rejman, J.; Oberle, V.; Zuhorn, I. S.; Hoekstra, D., *Biochemical Journal* 377, 159 2004.
88. von Gersdorff, K.; Sanders, N. N.; Vandenbroucke, R.; De Smedt, S. C.; Wagner, E.; Ogris, M., *Molecular Therapy* 14, 745 2006.
89. Erbacher, P.; Roche, A. C.; Monsigny, M.; Midoux, P., *Experimental Cell Research* 225, 186 1996.
90. Curiel, D. T.; Agarwal, S.; Wagner, E.; Cotten, M., *Proceedings of the National Academy of Sciences of the United States of America* 88, 8850 1991.
91. Cristiano, R. J.; Smith, L. C.; Woo, S. L., *Proceedings of the National Academy of Sciences of the United States of America* 90, 2122 1993.
92. Wagner, E.; Zatloukal, K.; Cotten, M.; Kirlappos, H.; Mechtler, K.; Curiel, D. T.; Birnstiel, M. L., *Proceedings of the National Academy of Sciences of the United States of America* 89, 6099 1992.

93. Cotten, M.; Wagner, E.; Zatloukal, K.; Phillips, S.; Curiel, D. T.; Birnstiel, M. L., *Proceedings of the National Academy of Sciences of the United States of America* 89, 6094 1992.
94. Zhang, Z.-Y.; Smith, B. D., *Bioconjugate Chemistry* 11, 805 2000.
95. Bieber, T.; Meissner, W.; Kostin, S.; Niemann, A.; Elsasser, H.-P., *Journal of Controlled Release* 82, 441 2002.
96. Merdan, T.; Kunath, K.; Fischer, D.; Kopecek, J.; Kissel, T., *Pharmaceutical Research* 19, 140 2002.
97. Akinc, A.; Thomas, M.; Klivanov, A. M.; Langer, R., *The Journal of Gene Medicine* 7, 657 2005.
98. Boussif, O.; Lezoualc'h, F.; Zanta, M. A.; Mergny, M. D.; Scherman, D.; Demeneix, B.; Behr, J. P., *Proceedings of the National Academy of Sciences of the United States of America* 92, 7297 1995.
99. Grabe, M.; Oster, G., *Journal of General Physiology* 117, 329 2001.
100. Yamashiro, D. J.; Fluss, S. R.; Maxfield, F. R., *Journal of Cell Biology* 97, 929 1983.
101. Maxfield, F. R.; Yamashiro, D. J., *Advances in Experimental Medicine and Biology* 225, 189 1987.
102. Xu, Y.; Szoka, F. C., *Biochemistry* 35, 5616 1996.
103. Hafez, I. M.; Maurer, N.; Cullis, P. R., *Gene Therapy* 8, 1188 2001.
104. Ellens, H.; Bentz, J.; Szoka, F. C., *Biochemistry* 25, 285 1986.
105. Yessine, M.-A.; Leroux, J.-C., *Advanced Drug Delivery Reviews* 56, 999 2004.
106. Lechardeur, D.; Lukacs, G. L., *Human Gene Therapy* 17, 882 2006.
107. Dauty, E.; Verkman, A. S., *Journal of Biological Chemistry* 280, 7823 2005.
108. Lukacs, G. L.; Haggie, P.; Seksek, O.; Lechardeur, D.; Freedman, N.; Verkman, A. S., *Journal of Biological Chemistry* 275, 1625 2000.
109. Ward, C. M.; Read, M. L.; Seymour, L. W., *Blood* 97, 2221 2001.
110. Wentz, S. R., *Science* 288, 1374 2000.
111. Gorlich, D.; Mattaj, I. W., *Science* 271, 1513 1996.
112. Kalderon, D.; Roberts, B. L.; Richardson, W. D.; Smith, A. E., *Cell* 39, 499 1984.
113. Moroianu, J.; Blobel, G.; Radu, A., *Proceedings of the National Academy of Sciences of the United States of America* 92, 2008 1995.
114. Brunner, S.; Furtbauer, E.; Sauer, T.; Kurs, M.; Wagner, E., *Molecular Therapy* 5, 80 2002.
115. Escρίου, V.; Carrière, M.; Bussone, F.; Wils, P.; Scherman, D., *The Journal of Gene Medicine* 3, 179 2001.
116. Gerweck, L. E.; Seetharaman, K., *Cancer Research* 56, 1194 1996.
117. Devalapally, H.; Shenoy, D.; Little, S.; Langer, R.; Amiji, M., *Cancer Chemotherapy and Pharmacology* 59, 477 2007.
118. Na, K.; Lee, E. S.; Bae, Y. H., *Journal of Controlled Release* 87, 3 2003.
119. Yang, S. R.; Lee, H. J.; Kim, J.-D., *Journal of Controlled Release* 114, 60 2006.

120. Kamada, H.; Tsutsumi, Y.; Yoshioka, Y.; Yamamoto, Y.; Kodaira, H.; Tsunoda, S.-i.; Okamoto, T.; Mukai, Y.; Shibata, H.; Nakagawa, S.; Mayumi, T., *Clinical Cancer Research* 10, 2545 2004.
121. Kratz, F.; Beyer, U.; Roth, T.; Tarasova, N.; Collery, P.; Lechenault, F.; Cazabat, A.; Schumacher, P.; Unger, C.; Falken, U., *Journal of Pharmaceutical Sciences* 87, 338 1998.
122. Beyer, U.; Roth, T.; Schumacher, P.; Maier, G.; Unold, A.; Frahm, A. W.; Fiebig, H. H.; Unger, C.; Kratz, F., *Journal of Medicinal Chemistry* 41, 2701 1998.
123. Drevs, J.; Hofmann, I.; Marme, D.; Unger, C.; Kratz, F., *Drug Delivery: Journal of Delivery and Targeting of Therapeutic Agents* 6, 89 1999.
124. Torchillin, V. P., *Nature Reviews Drug Discovery* 4, 145 2005.
125. Papanicolaou, I.; Briggs, S.; Alpar, H. O., *Journal of Drug Targeting* 12, 541 2004.
126. Simões, S.; Moreira, J. N.; Fonseca, C.; Düzgünes, N.; Pedroso de Lima, M. C., *Advanced Drug Delivery Reviews* 56, 947 2004.
127. Fattal, E.; Couvreur, P.; Dubernet, C., *Advanced Drug Delivery Reviews* 56, 931 2004.
128. Couffin-Hoarau, A.-C.; Leroux, J.-C., *Biomacromolecules* 5, 2082 2004.
129. Leroux, J.-C.; Roux, E.; Le Garrec, D.; Hong, K.; Drummond, D. C., *Journal of Controlled Release* 72, 71 2001.
130. Lee, R. J.; Wang, S.; Turk, M. J.; Low, P. S., *Biosci. Rep.* 18, 69 1998.
131. Dewhirst, M. W.; Vujaskovic, Z.; Jones, E.; Thrall, D., *International Journal of Hyperthermia* 21, 779 2005.
132. Jin, H.; Kang, K. A. In *Oxygen Transport to Tissue XXVIII*, 2008.
133. Gupta, A. K.; Naregalkar, R. R.; Vaidya, V. D.; Gupta, M., *Nanomedicine* 2, 23 2007.
134. Meyer, D. E.; Shin, B. C.; Kong, G. A.; Dewhirst, M. W.; Chilkoti, A., *Journal of Controlled Release* 74, 213 2001.
135. Rijcken, C. J. F.; Soga, O.; Hennink, W. E.; Nostrum, C. F. v., *Journal of Controlled Release* 120, 131 2007.
136. Kim, S. Y.; Ha, J. C.; Lee, Y. M., *Journal of Controlled Release* 65, 345 2000.
137. Bae, K. H.; Choi, S. H.; Park, S. Y.; Lee, Y.; Park, T. G., *Langmuir* 22, 6380 2006.
138. De Las Heras, A. C.; Pennadam, S. S.; Alexander, C., *Chemical Society Reviews* 34, 276 2005.
139. Molineux, G., *Cancer Treatment Reviews* 28, 13 2002.
140. Yokoyama, M., *Drug Discovery Today* 7, 426 2002.
141. Hinrichs, W. L. J.; Schuurmans-Nieuwenbroek, N. M. V.; Van De Wetering, P.; Hennink, W. E., *J. controlled Release* 60, 249 1999.
142. Kurisawa, M.; Yokoyama, M.; Okano, T., *Journal of Controlled Release* 69, 127 2000.
143. Turk, M.; Dincer, S.; Yulu, I. G.; Piskin, E., *J. of controlled release* 96, 325 2004.
144. Türk, M.; Dinçer, S.; Piskin, E., *Journal of Tissue Engineering and Regenerative Medicine* 1, 377 2007.

145. Twaites, B. R.; de las Heras Alarcon, C.; Cunliffe, D.; Lavigne, M. D.; Pennadam, S. S.; Smith, J. R.; Gorecki, D. C.; Alexander, C., *Journal of Controlled Release* 97, 551 2004.
146. Murata, M.; Kaku, W.; Anada, T.; Soh, N.; Katayama, Y.; Maeda, M., *Chemistry letters* 322003.

Techniques

2.1 Pulsed-Gradient Spin-Echo NMR (PGSE-NMR)

2.1.1 Introduction

The NMR effect was first observed in 1946, and since 1960 it has been routinely applied in chemistry and physics. Owing to its non-invasive and wide applicability, the pulsed-gradient spin-echo NMR (PGSE-NMR) has become a powerful technique to measure the self-diffusion coefficients of molecules in the solution state¹. The diffusion coefficient quantifies the random translational motion of the molecules and is sensitive to the size of the molecule and any interactions it experiences in the solution.

2.1.1.1 NMR diffusion measurements in retrospective

The traditional way to measure self-diffusion coefficients is through radioactive tracer techniques; self-diffusion coefficients are also frequently called tracer diffusion coefficients in the literature. However, tracer experiments require difficult synthetic work and measurement periods that may be of the order of days or weeks for a single component. A further disadvantage of the technique is the inherent system perturbation by isotope substitution. In contrast, NMR techniques can provide individual multicomponent self-diffusion coefficients with good precision in a few minutes, without the need for isotopic labelling, providing the species of interest contains a viable NMR signal.

Self-diffusion measurements by NMR were developed following the discovery of spin-echoes by Hahn². In that pioneering study, several effects on spin-NMR signal echoes were observed, one of which was the diffusional effect on echo amplitudes in an inhomogeneous magnetic field. In its basic form, the spin-echo (SE) technique for measuring diffusion entails monitoring of the amplitude of a spin-echo in the presence of a linear gradient in the B_0 -field. The SE experiment was significantly improved in the mid-sixties in the form of the pulsed-field gradient spin-echo (PGSE) technique. The basic idea that the gradients are pulsed

was proposed by McCall et al³, but the methodology, first experiments and the detailed analysis were developed by Stejskal and Tanner⁴.

2.1.2 Diffusion

When the liquid system is heated, the internal kinetic energy of the system will increase resulting in an increase in the overall rates of molecular and particle motion. Molecular motions of interest are, motional portioning into internal molecular motions and overall reorientation and translational diffusion of molecules and aggregates. Even though there are macroscopic convection-like phenomena, those will not be discussed here.

2.1.3 Self-diffusion

Self-diffusion is defined as random molecular motion of the molecules induced by thermal energy. The process of translational in solution is commonly referred to as self-diffusion and is defined with a self-diffusion coefficient (D). Much interest in diffusion arises because of the connection between self-diffusion coefficient and molecular size/shape and any aggregation between molecules⁵. For macromolecules, this connection is usually made through the Stokes-Einstein equation¹;

$$D = \frac{kT}{f} \quad (2.1)$$

where k is the Boltzmann constant, T is temperature, and f is the friction coefficient.

For a spherical particle with hydrodynamic radius R_h immersed in a fluid of viscosity η , the friction factor is given by,

$$f = 6\pi\eta R_h \quad (2.2)$$

Analytical expressions are also available for the friction factors for oblate and prolate ellipsoids.

The self-diffusion coefficients can be studied using two different NMR methods. One is analysis of relaxation data and the other one is pulsed-field gradient Spin-Echo (PGSE) NMR.

2.1.4 Basic principles

The basis of all NMR diffusion and flow measurements is spatially resolved NMR. In most circumstances this is achieved by artificially superimposing magnetic field gradients on the static magnetic field (B_0), in some cases by utilising magnetic field gradients intrinsically present in certain regions of the field profile of the magnets or, in rare cases, by generating gradients of the radiofrequency (RF) field. If the magnetic field varies locally, the Larmor frequencies of the nuclei also vary. Following the pioneering work by Hahn² and Carr and Purcell⁶, translational displacements of the spins are then observed by acquisition of the effects on their precession.

$$\omega_0 = \gamma B_0 \quad (2.3)$$

where ω_0 is the Larmor frequency (radians s^{-1}), γ is the gyromagnetic ratio (radT⁻¹s⁻¹), B_0 (T) is the strength of the static magnetic field.

In most experiments an inhomogeneous magnetic field is produced by a magnetic field gradient g controlled externally by suitable gradient coils. In three dimensions the gradient is described by

$$g = \frac{\partial B_z}{\partial x} i + \frac{\partial B_z}{\partial y} j + \frac{\partial B_z}{\partial z} k \quad (2.4)$$

where, i, j, k are unit vectors in the x, y and z direction of the main field of strength B_0 . The total field at position r is then given by,

$$B=B_0+g.r \quad (2.5)$$

For simplicity only a z-gradient of magnitude $g=g.k$ in the direction of main field is considered. Due to this gradient, the magnetic field varies according to;

$$B(r)=B_0(r)+\Delta B(r) \quad (2.6)$$

Hence the Larmor frequency ω of the nuclei becomes

$$\omega = \gamma\{B_0(r) + \Delta B(r)\} \quad (2.7)$$

γ is the gyromagnetic ratio. Accordingly, the Larmor frequency changes once the nucleus changes its location. This frequency change is observed in a spin-echo (SE) experiment. The spin-echo results from refocusing of the dephasing magnetisation in inhomogeneous fields. This refocusing is highly sensitive to translational displacements of the particles in the inhomogeneous field.

2.1.4.1 Relaxation process

In NMR, a strong magnetic field is used to partially polarize the nuclear spins. The excess of proton spin in the direction of the magnetic field constitutes a small net magnetization of the material. To observe a NMR signal, strong radio frequency radiation is applied to the sample at the appropriate frequency to produce spin flips. The RF radiation absorbed by some of the protons will flip from parallel to the magnetic field to anti-parallel- a higher energy state. When the exciting RF field is switched off, the protons tend to return to their lower energy state. This “relaxation” to a state where the spins are parallel to the static magnetic field produces a small amount of RF radiation which is detected as the NMR signal. Two different time constants for decay are typically observed.

The longer of the two time constants is usually labelled T_1 (spin-lattice/longitudinal relaxation) and is associated with the decay of the field

component that is parallel to the applied static magnetic field (B_0). This field direction is usually taken to define the Z-axis of the system.

The shorter time constant is usually labelled T_2 (spin-spin/transverse relaxation) and is associated with the decay of the field component that is perpendicular or transverse to the applied static magnetic field (B_0).

2.1.4.2 Measuring diffusion with magnetic field gradients

It was earlier mentioned that well-defined magnetic field gradient can be used to label the position of a spin, indirectly, through the Larmor frequency. This provides the basis for measuring diffusion. The most common approach is to use equal rectangular gradient pulses of duration δ that are inserted into each π period (figure 2.1). Applying the magnetic field gradient in pulses instead of continuously diminishes a number of experimental limitations¹.

- 1) since the gradient is off during acquisition, the line width is not broadened by the gradient, and thus method is suitable for measuring the diffusion coefficient of more than one species simultaneously.
- 2) the RF power does not have to be increased to cope with a gradient-broadened spectrum.
- 3) smaller diffusion coefficients can be measured since it is possible to use larger gradients.
- 4) as gradient is applied in pulses it is possible to separate the effects of diffusion from spin-spin relaxation.

2.1.4.3 The nuclear spin-echo (SE) method:

The basic pulse sequence for the spin-echo (SE) experiment and spin arrangement after each pulse is illustrated in figure 2.1 and figure 2.2.

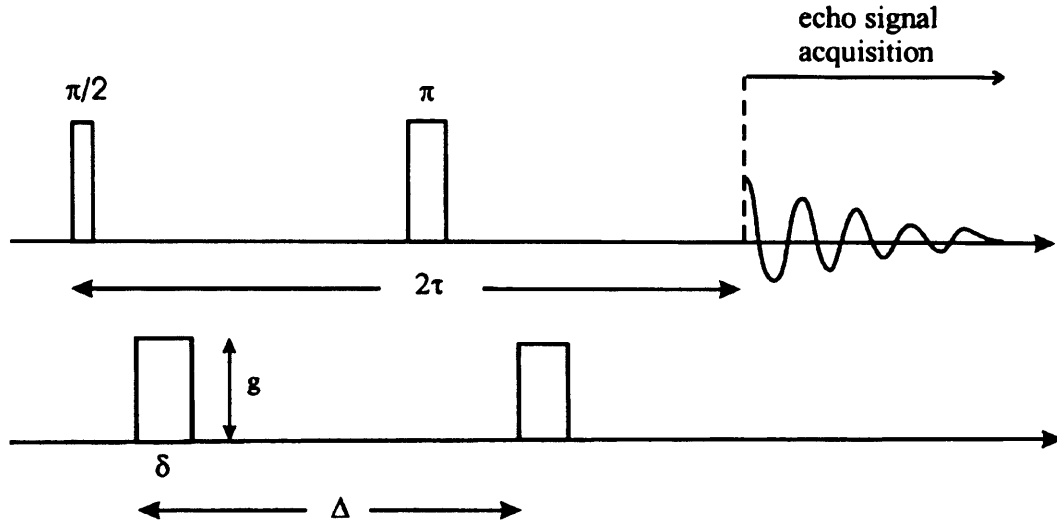


Figure 2.1; The Stejskal-Tanner experiment

A $\pi/2$ radio frequency pulse is applied which rotates the macroscopic magnetisation from the static B_0 field into the x-y plane and creates phase coherence. Subsequently, spins dephase due to inhomogeneity of the magnetic field during a time τ . Application of π radio frequency pulse reverses the dephasing effect, and the spin phases begin to cluster again. Thus, at time 2τ , if the spins have not undergone any translational motion with respect to the z-axis, the effects of the two applied gradient pulses cancel and a non-attenuated spin-echo is observed in signal acquisition.

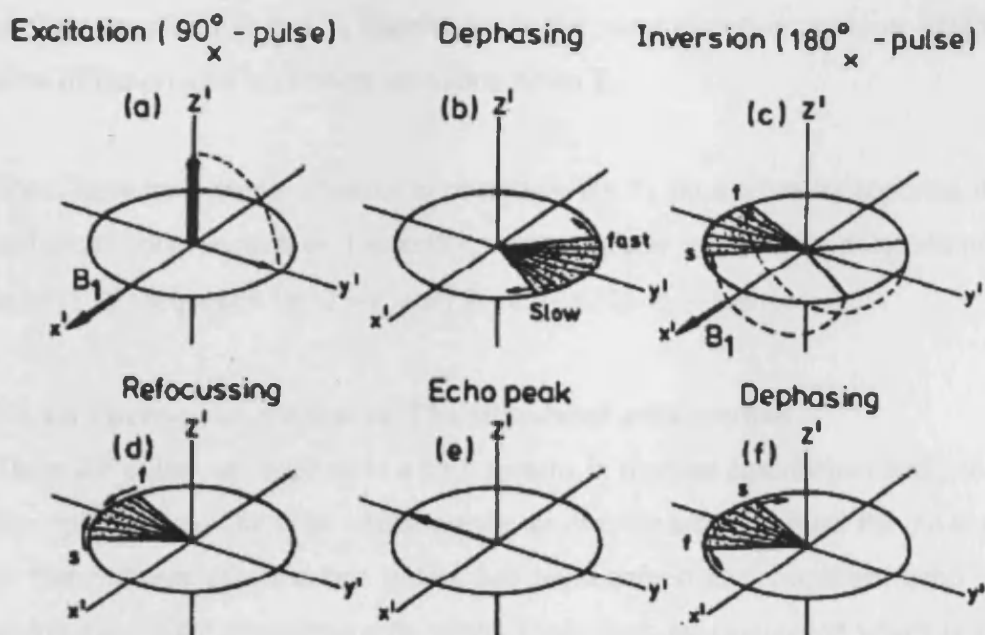


Figure 2.2; Spin arrangement after each pulsed sequence⁷

When the spins have undergone translational motion, the second field gradient pulse does not completely refocus the magnetization, and an attenuated SE is detected.

This method yields an echo attenuation given by;

$$S = S_0 \exp \left[-\frac{2\pi}{T_2} - 2\gamma^2 D g^2 \tau^3 / 3 \right] \quad (2.8)$$

where S_0 is the initial amplitude at time $\tau=0$. T_2 is the transverse relaxation time of the spin system^{2,6}.

Unfortunately, eqn. (2.8) shows spin dispersion due to transverse relaxation is also not refocused. Thus, T_2 constitutes the main limiting factor in applying PGSE-NMR to polymeric systems measurements become extremely difficult when excessively rapid transverse spin-relaxation occurs. This in practise makes diffusion measurements difficult or impossible for many nuclei. For a given

nucleus, trends in D and T_2 usually act in the same direction; systems exhibiting slow diffusion also have short relaxation times T_2 .

There have been many attempts to overcome the T_2 limitations by applying three- and multi-pulse sequences. Generally, many of these use a three- pulse stimulated echo (STE) sequence ($\pi/2 - \tau_1 - \pi/2 - \tau_2 - \pi/2 - \tau_1 - echo$).

2.1.4.4 Three-pulse sequences: The stimulated echo method

Three RF pulses are applied to a spin system in thermal equilibrium and generate five spin-echoes. The echo which occurs an interval after the third RF pulse equal to that between the first two pulses has been named as “stimulated echo”. The attenuation of the stimulated echo which arises from magnetization which is stored in the longitudinal (B_0) direction in the period between the second and third RF pulses competes with T_1 instead of T_2 -relaxation. But in 90° - 180° (normal echo) experiment the SE attenuates according to T_2 as its time of occurrence after the initial RF pulse is delayed. When chemical exchange occurs, T_2 may be much less than T_1 , hence this would be advantageous to use the PGSE-based stimulated echo technique to understand diffusion and flow properties.

Thus, in systems where $T_1 > T_2$, much information is available to study the effect of relaxation on the signal by observing the diffusional attenuation of the stimulated echo, instead of the normal echo.

In a 90° - 90° - 90° three pulse sequence, the first pulse (at time zero) rotates the magnetization into $x'y'$ -plane. This pulse leads to a loss of the phase coherence of spins at different rates and they acquire various phase angles in the rotating frame. The second pulse (at time τ_1) stores the memory of the current phase angles in the z -direction. Normally those are unaffected by field gradients and relax in the longitudinal direction. The third pulse (at time τ_2) restores the phase angles with a reversed sign and presses to form an echo time $\tau' = \tau_1 + \tau_2$ (figure 2.3).

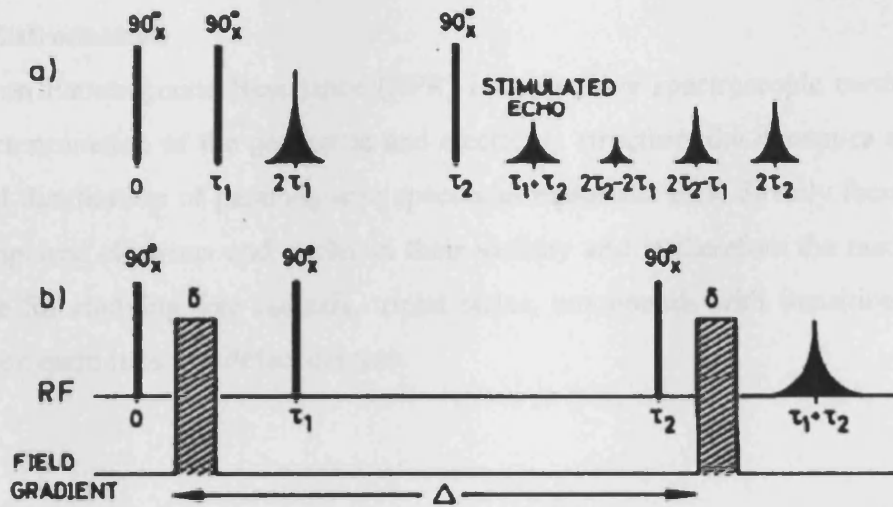


Figure 2.3; (a) Echo formation as a result of three 90° pulses; (b) Pulsed-gradient Spin Echo, as based on the stimulated echo⁷.

In terms of relaxation its amplitude is given by

$$S(\tau_1 + \tau_2) = [S_0/2] \exp[-(2\tau/T_2 + T/T_1)] \quad (2.9)$$

As shown in figure 2.3, when the static field-gradient is zero the height of the stimulated echo is at most 50% of the initial magnetisation. The dependence of $A(\tau_1 + \tau_2)$, the stimulated echo amplitude, on T_1 and T_2 as follows

$$A(\tau_1 + \tau_2) = A(0) 0.5 \exp[-(\tau_2 - \tau_1)/T_1 - 2\tau_1/T_2 - (\gamma G \delta)^2 D(\Delta - \delta/3)] \quad (2.10)$$

Hence, a plot of A vs. $-(\gamma G \delta)^2 (\Delta - \delta/3)$ allows one to measure D .

2.2 Electron Paramagnetic Resonance (EPR)

2.2.1 Introduction

Electron Paramagnetic Resonance (EPR) is a sensitive spectroscopic method for the determination of the geometric and electronic structure, the dynamics and the spatial distribution of paramagnetic species in materials. EPR directly focuses on the unpaired electrons and nuclei in their vicinity and is therefore the method of choice for studying free radicals, triplet states, compounds with transition metal and rare earth ions and defect centers.

2.2.2 Theory

The sample material is immersed in a strong static magnetic field and exposed to an orthogonal low-amplitude high-frequency field. EPR usually requires microwave-frequency radiation (GHz), while NMR is observed at lower radio frequencies (MHz). Most bulk materials formed under normal conditions have net zero electronic spin and are EPR silent. The possible elements that can give a EPR signal are as follows.

- a) Transition-metal and rare-earth species which contain unpaired nd and/or mf electrons. Ex: Mn^{2+} , Fe^{3+} , Cu^{2+} , Cr^{3+}
- b) A small number of organic molecules contain a single unpaired electron. Ex: 1,1-Diphenyl-2-picryl-hydrazyl (DPPH)
- c) Organic ion-radicals: very reactive species created by redox reactions and stable at certain conditions.
- d) Triplet-state organic molecules and biradicals.

The structure of molecules can be obtained from the analysis of the molecular absorption spectra. The spectra are acquired by measuring the attenuation versus frequency (or wave length) of a beam of electromagnetic radiation as it passes through a sample. Lines or bands in a spectrum represent transitions between energy levels of absorbing species. The absorption of energy causes a transition

from the lower energy state to the higher energy state (figure 2.4). The frequency of each line or band measures the energy separation of two levels. According to Planck's law, electromagnetic radiation will be absorbed if:

$$\Delta E = h\nu \quad (2.11)$$

where h is Planck's constant and ν is the frequency of radiation.

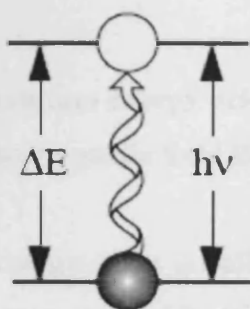


Figure 2.4; Transition associated with the absorption of electromagnetic energy⁸.

2.2.2.1 The Zeeman effect

The energy differences in EPR spectroscopy is due to the interaction of unpaired electrons in the sample with magnetic field. The electron has a magnetic moment and acts as a compass or a bar magnet in the presence of external magnetic field B_0 . In the absence of any magnetic field the magnetic moment, associated with the electron spin, is randomly oriented and the two energy levels are degenerate. The application of an external magnetic field B_0 results in a splitting of the two energy levels as the electron spin S can only be oriented parallel or anti-parallel to the magnetic field vector. As electron is a spin $\frac{1}{2}$ particle, the parallel state is numbered as $M_s = -1/2$ and the antiparallel state is $M_s = +1/2$ ⁹ (figure 2.5).

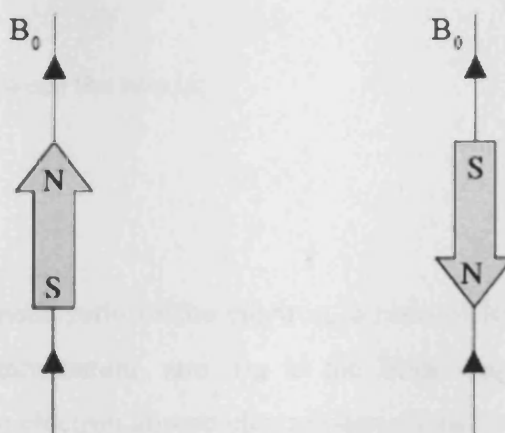


Figure 2.5; Minimum and maximum energy orientations of ν with respect to the magnetic field B_0 .

The splitting between the two energy states is called electron Zeeman interaction (EZI) and is proportional to the magnitude of B_0 (figure 2.6).

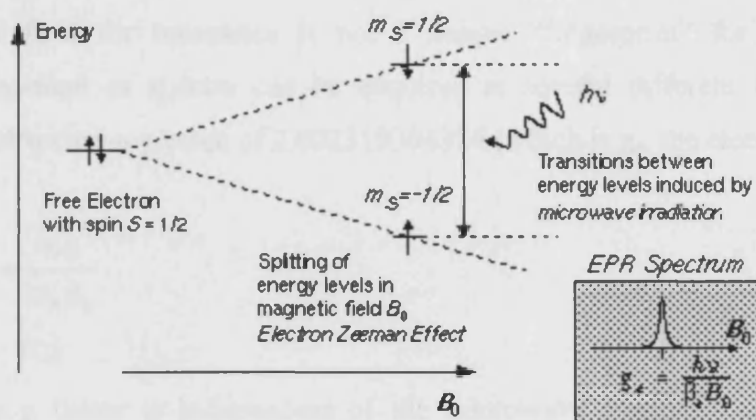


Figure 2.6; Energy level scheme for the simplest system (e.g free electron) as a function of applied magnetic field B_0 , showing EPR absorption¹⁰

Resonant absorption occurs if the frequency is adjusted so that

$$\Delta E = h\nu, \quad (2.12)$$

and energy separation between the two is;

$$\Delta E = g_e \nu_B B_0 \quad (2.13)$$

where g_e is the gyromagnetic ratio of the electron, a ratio of its magnetic dipole moment to its angular momentum, and ν_B is the Bohr magneton. Electron transition occurs when the electron absorb electromagnetic radiation of the correct energy.

$$\Delta E = h\nu = g_e \nu_B B_0 \quad (2.14)$$

This (2.14) is the fundamental equation of EPR spectroscopy⁸. The paramagnetic centre is placed in a magnetic field and the electron caused to resonate between the two states, energy absorbed and displayed this as a EPR spectrum.

The field for resonance is not a unique “fingerprint” for identification of a compound as spectra can be acquired at several different frequencies. A free electron has a g value of 2.002319304386 (which is g_e , the electronic g factor);

$$g_e = \frac{h\nu}{\nu_B B_0} \quad (2.15)$$

The g factor is independent of the microwave frequency. A list of fields for resonance for a $g=2$ signal at microwave frequencies commonly available in EPR spectrometers is presented in table 2.1. This means that for radiation at the commonly used frequency of 9.75 GHz (known as X-band microwave radiation, and thus giving rise to X-band spectra), resonance occurs at a magnetic field of about 3480 gauss¹¹.

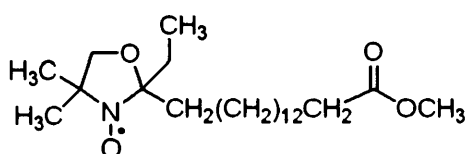
Microwave Band	Frequency (GHz)	B _{res} (G)
L	1.1	392
S	3.0	1070
X	9.75	3480
Q	34.0	12 000
W	94.0	34 000

Table 2.1; Field for resonance, B_{res}, for a g=2 signal at selected microwave frequencies

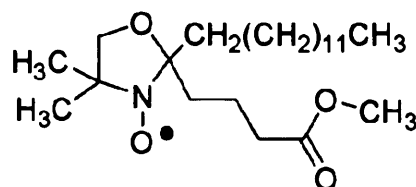
2.2.2.2 Spin probes

In biological environments it is impossible to get high concentration of radicals as they are very reactive. To obtain information on the biological system there are some specially designed non-reactive radical molecules which can be attached to specific sites in a biological cell. These are called spin-label or spin - probe molecules

The successful use of nitroxides as spin-probes (figure 2.7) has resulted in the unique possibility to vary their chemical structure without changing paramagnetic properties. Nitroxide radicals are widely used as spin-probes because their spectra are very sensitive to the environment and they are reasonably simple to prepare.



16-Doxyl-stearic acid methyl ester



5-Doxyl-stearic acid methyl ester

Figure 2.7; Structures of spin-probes used in this thesis

2.2.3 EPR spectral parameters

2.2.3.1 The g factor

The g factor gives important information about the paramagnetic center's electronic structure. When the unpaired electron is an atom, it feels not only the presence of external magnetic field B_0 , but also effects of any local magnetic fields. Therefore, the effective field B_{eff} felt by the electron is;

$$B_{\text{eff}} = B_0(1 - \sigma) \quad (2.16)$$

where σ is the effect of local fields. Therefore the resonance conditions is;

$$\Delta E = h\nu = g_e \nu_B B_{\text{eff}} = g_e \nu_B B_0(1 - \sigma) \quad (2.17)$$

The quantity $g_e(1 - \sigma)$ is called the g factor, given the symbol g, hence;

$$\Delta E = h\nu = g \nu_B B_0 \quad (2.18)$$

When g differs from g_e (2.0023), the ratio of the electron's magnetic moment to its angular momentum has changed from the free electron value. Since the electron's magnetic moment is constant (Bohr magneton), then the electron must have gained or lost angular momentum. This occurs through spin-orbit coupling and gives information about the nature of the atomic or molecular orbital containing the electron.

2.2.3.2 Hyperfine interactions

Even though g factor gives useful information about the paramagnetic center's electronic structure, it does not give any information about molecular structure of the sample. If the molecule contains nuclei with magnetic moments, such as protons this magnetic moment interact with the magnetic moment of the electron. This is defined as hyperfine interactions. This gives more information about

identity and number of atoms of the sample as well as their distances from the unpaired electron¹².

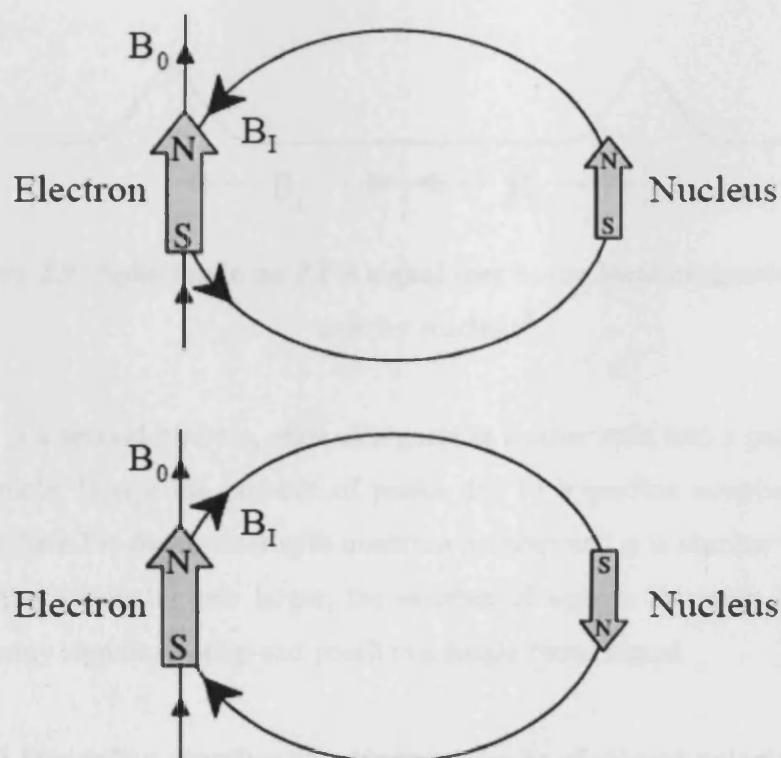


Figure 2.8; Local magnetic field at the electron, B_1 , due to a nearby nucleus⁸.

The figure 2.8 describes the origin of the hyperfine interaction. The magnetic moment of the nucleus acts like a bar magnet and produces magnetic field at the electron, B_1 . When B_1 is aligned to B_0 , the field for resonance will be lowered by B_1 whilst the opposite occurs when B_1 opposes B_0 . For a spin $\frac{1}{2}$ nucleus (hydrogen nucleus), the EPR absorption signal splits into two each, located B_1 away from the original signal (figure 2.9).

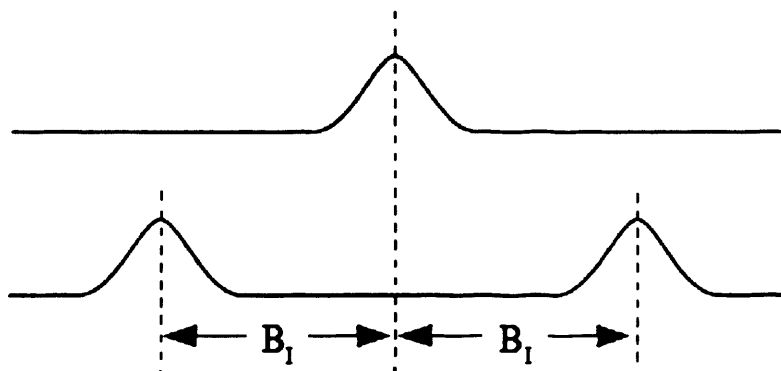


Figure 2.9; Splitting in an EPR signal due to the local magnetic field of a nearby nucleus⁸.

If there is a second nucleus, each of signals is further split into a pair, resulting in four signals. Hence the number of peaks due to hyperfine coupling is equal to $2nI+1$, where I is the nuclear spin quantum number and n is number of nuclei. As the number of nuclei gets larger, the number of signals increases exponentially, hence many signals overlap and result is a single broad signal.

2.2.3.2.1 Hyperfine coupling constant as a probe of solvent polarity

A typical EPR field-sweep spectrum of a doxyl steric methyl ester is shown in figure 2.10.



Figure 2.10; EPR spectrum of 16-DSE in 25mM SDS solution

In the case of aminoxyl radicals, hyperfine coupling to the ^{14}N yields results in three possible nuclear spin states ($m_I = -1, 0, +1$). Transitions between these spin states, as governed by the EPR selection rules ($\Delta m_S = \pm 1, \Delta m_I = 0$) thereby gives rise to three lines in the EPR spectrum

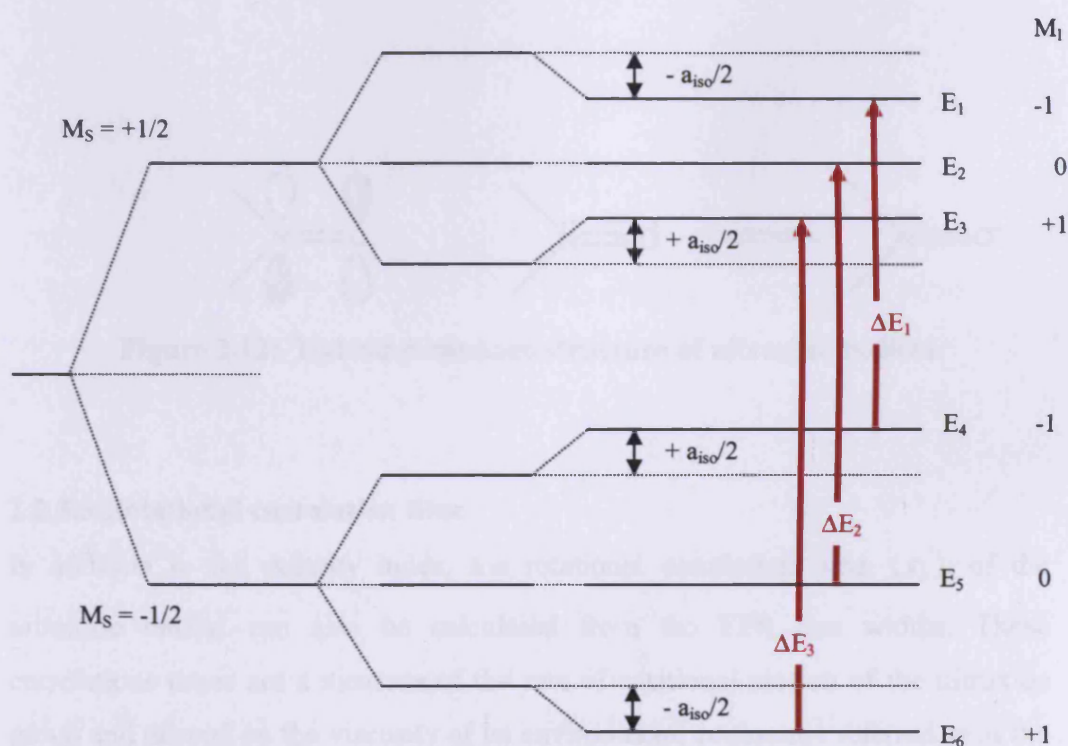


Figure 2.11; Energy level diagram for an unpaired electron interacting with a nucleus of spin $I = 1$.

The isotropic hyperfine coupling constant, A_0 , is measured as half the separation of the resonance fields of the two outermost lines (figure 2.10).

The use of nitroxides as spin-probes for analysis of the microenvironment is particularly relevant, as the value of hyperfine coupling (a_N) of the radical depends critically on the medium in which the nitroxide is dissolved. Nitroxide radicals are π radicals, in which the unpaired electron occupies a π^* orbital between the oxygen and nitrogen atoms. The nitroxide radical is frequently represented as a

resonance structure, as shown in figure 2.12. In solvents with high polarity, the resonance favours the pseudo ionic structure II where the electron spin is largely centred on the nitrogen atom, thereby resulting in a larger value of nitrogen hyperfine coupling. Particularly high values of a_N are obtained in protic solvents that are hydrogen-bond donors.

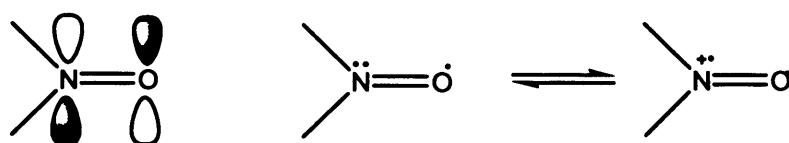


Figure 2.12; Hybrid resonance structure of nitroxide radical.

2.2.3.3 Rotational correlation time

In addition to the polarity index, the rotational correlation time, (τ_c), of the nitroxide radical can also be calculated from the EPR line widths. These correlations times are a measure of the rate of rotational motion of the nitroxide group and depend on the viscosity of its environment, commonly referred to as the “microviscosity”. The relationship between the τ_c and viscosity, η , is expressed by the Debye-Stokes-Einstein equation.

$$\tau_c = 4\pi\eta R^3 / 3kT \quad (2.19)$$

where R is the hydrodynamic radius of the spin probe, k is the boltzman constant and T is the absolute temperature. In most studies^{13,14}, falling into the motional narrowing region ($10^{-11} < \tau_c < 10^{-9}$ s), the effective rotational correlation time has been calculated using equation (2.20).

$$\tau_c = (6.51 \times 10^{-10}) \Delta H(0) \{ [h(0)/h(-1)]^{1/2} + [h(0)/h(1)]^{1/2} - 2 \} s, \quad (2.20)$$

where $\Delta H(0)$ is the line width (in gauss) of the central line of the nitroxide spectrum and $h(-1)$, $h(0)$ and $h(1)$ are the peak heights of the $M = -1, 0$ and $+1$ lines respectively.

2.3 Small Angle Neutron Scattering (SANS)¹⁵⁻¹⁷

2.3.1 Introduction

The determination of molecular arrangement within the colloidal system is an important fact when studying relationships between physical properties and molecular structures. Scattering techniques (light, X-rays, neutrons) provide useful information on molecular size, and shape of particles. The most fundamental difference between the neutron and electromagnetic scattering is the way that the radiation interacts with the matter. Light and X-rays are both scattered by the electron cloud surrounding the atomic nuclei, whereas neutrons are scattered by the nucleus. As X-rays are scattered by electrons, light atoms such as hydrogen (the most abundance atom in colloidal and polymeric materials) do not scatter strongly. SANS however can differentiate the different isotopes of a given element, the most striking difference being that between hydrogen (H) and deuterium (D) which permits experimental approach called “contrast variation” (discussed later). An electron –which is charged- is unable to travel long distances inside a material without being attracted by the nucleus or repelled by the electrons present in the material. As such X-ray beam techniques are surface specific as require thin sample. As neutrons are without charge, they are capable of penetrating deeply into matter.

2.3.2 Neutron production

The neutron beam can be produced in two different ways: by nuclear fission in reactor-based neutron sources, or by spallation in accelerator-based neutron sources. The most obvious of these two is to use a nuclear reactor, which involves fission of uranium-235. Each fission, results in 2-3 neutrons, though one of these is needed to continue the chain reaction. The most powerful reactor in the world is

the 57MW High-flux reactor at Institute Max von Laue-Paul Langevine (ILL) in Grenoble, France (figure 2.13).

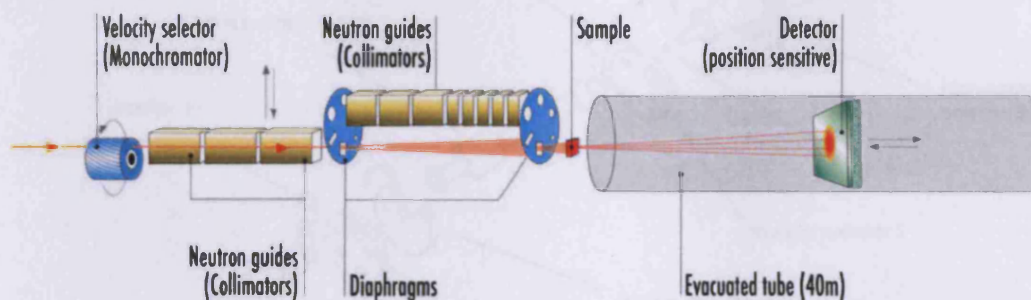


Figure 2.13; High flux reactor in France (taken from <http://www.ill.fr>)¹⁸

In accelerator-based neutron sources, neutrons are released by bombarding a heavy-metal target (e.g., U, Ta, W), with high energy particles (e.g., H^+) from a high-power accelerator- a process known as spallation. The wavelengths of the neutron produced using above methods lie between 0.1-30 Å, which covers the range of micelles, micro emulsions and colloidal dispersions. The most powerful spallation neutron source is ISIS, located near Oxford, in the UK (figure 2.14).

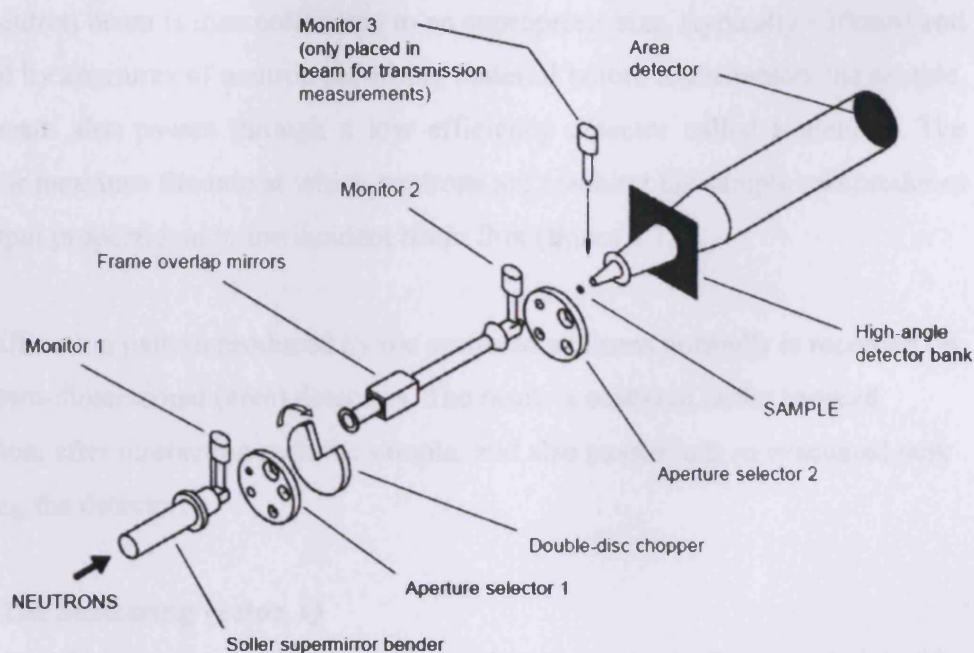


Figure 2.14; Schematic diagram of the spallation neutron source at the ISIS facility, Oxford, UK, (taken from the ISIS website)¹⁹.

2.3.3 Detailed Instrumentation at ISIS

Collisions between a proton beam and the target atom nuclei produce neutrons with very high energies. Immediately after production of neutrons, neutrons are moderated to the correct energy (wave length) by passing through a material such as liquid hydrogen, to which they lose kinetic energy.

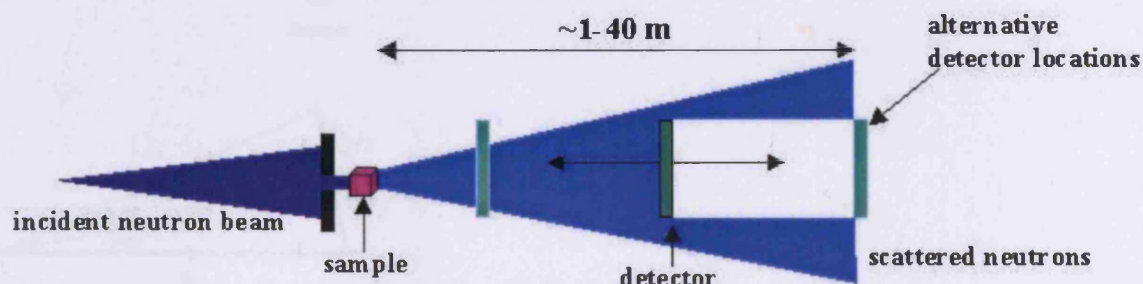


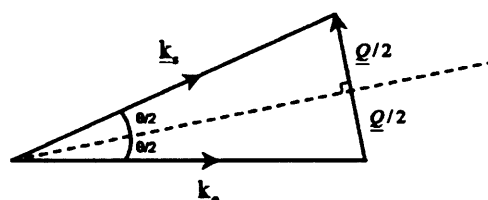
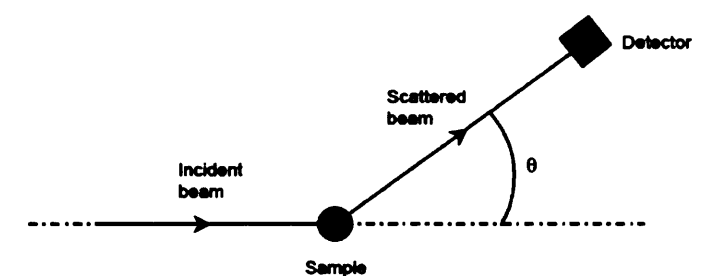
Figure 2.15 Schematic for a SANS experiment

The neutron beam is then collimated to an appropriate size, (typically ~10mm) and shaped by apertures of neutron absorbing material before it encounters the sample. The beam also passes through a low efficiency detector called a monitor. The monitor measures the rate at which neutrons are reaching the sample and produces an output proportional to the incident beam flux (figure 2.15).

The diffraction pattern produced by the scattered neutrons normally is recorded on large two-dimensional (area) detectors. The beam is scattered in the forward direction, after interaction with the sample, and also passes into an evacuated tank housing the detector.

2.3.4 The Scattering vector, Q

During a SANS experiment, the neutron beam is elastically scattered by the nucleus of any atom in its path and the relevant scattering events are coherent. Thus, scattering properties of the nuclei are related to their location in the sample. The scattering data are recorded in terms of wave vector (Q), (or scattering vector) which is the modulus of the resultant between incident (\underline{K}_0) and scattered (\underline{K}_s) wave vectors and its value is given by²⁰,



$$\sin \theta = (Q/2) / K_0$$

$$Q = 2K_0 \sin \theta$$

Figure 2.16; the theory behind, and the mathematical derivation of the scattering wave vector (Q).

$$Q = |Q| = \underline{K}_s - \underline{K}_0 = \frac{4\pi}{\lambda} \sin\left(\frac{\theta}{2}\right) \quad (2.21)$$

Q has dimensions of (length)⁻¹ and is normally quoted in nm⁻¹ or Å⁻¹. λ is the neutron wavelength. Substituting eq 2.21 into Bragg's law of diffraction (equation (2.22)) produces a useful expression (equation 2.23), where d is a distance,

$$\lambda = 2d \sin\left(\frac{\theta}{2}\right) \quad (2.22)$$

Then yields a expression

$$d = 2\pi/Q \quad (2.23)$$

where d is a molecular level length scale by virtue of the Q -range accessible in a SANS experiment.

Equation 2.22 provides important information on relationship between characteristic dimensions associated with d and Q ²⁰. Both equation 2.21 and 2.23 are used to configure an instrument, to select a Q -range, and size the scattering bodies in a sample from the position of any diffraction peak in Q -space. The distance (d) is inversely proportional to Q , thus small Q values are required to investigate the large-scale structure in a sample²¹.

2.3.5 Scattering intensities

The number of neutrons that are incident on an area of detector can be measured and this flux of neutrons $I(\lambda, \theta)$ can be described as;

$$I(\lambda, \theta) = I_0(\lambda) \Delta\Omega \eta(\lambda) TV \frac{\partial \sigma}{\partial \Omega}(Q) \quad (2.24)$$

where $I_0(\lambda, \theta)$ is the incident flux, $\Delta\Omega$ solid angle element that the neutrons are scattered onto, η the detector efficiency and T is the sample transmission and

$\frac{\partial\sigma}{\partial\Omega}(Q)$ is the differential cross-section,

$$\frac{\partial\sigma}{\partial\Omega}(Q) = N_p V_p^2 (\Delta\rho)^2 P(Q) S(Q) + B_{inc} \quad (2.25)$$

where N_p is the number concentration of scattering bodies, V_p is the volume of one scattering body, and $(\Delta\rho)^2$ is the square of the difference of the neutron scattering densities of the solvent and scattering body, $P(Q)$ is the form factor, $S(Q)$ is the structure factor and B_{inc} is the incoherent background²¹.

2.3.6 Contrast variation

The neutron scattering length density, ρ , of a molecule of i atoms can be calculated using;

$$\rho = \sum_i b_i \frac{\rho_{bulk} N_A}{M_w} \quad (2.26)$$

where ρ_{bulk} is the bulk density of the scattering body, N_A is Avogadro's number, M_w is the molecular weight. The contrast is the difference in ρ values between the molecule of interest, ρ_p , and the surrounding medium, ρ_m , all squared, i.e., $(\rho_d)^2 = (\rho_p - \rho_m)^2$. If $(\rho_d)^2$ is zero, there is no measurable intensity (when the solvent has been subtracted)²¹. When this condition is met the scattering bodies are said to be contrast matched. The contrast term is very useful for a polymer chemist as different isotopes of the same element have scattering length densities which are far apart from each other. (i.e. hydrogen and deuterium). This is exploited in the contrast-variation technique to allow different regions of molecular assemblies to be examined; i.e., one can “see” proton-containing hydrocarbon-type material dissolved in heavy water D_2O . The scattering length densities of commonly used

solvents and polymers in their hydrogenated and deuterated forms are listed in below.

Solvent	ρ (h form) ($\times 10^{10} \text{cm}^{-2}$)	ρ (d form) ($\times 10^{10} \text{cm}^{-2}$)	Polymer	ρ (h form) ($\times 10^{10} \text{cm}^{-2}$)	ρ (d form) ($\times 10^{10} \text{cm}^{-2}$)
Water	-0.56	+6.38	PB	-0.47	+6.82
Octane	-0.53	+6.43	PE	-0.33	+8.24
Cyclohexane	-0.28	+6.70	PS	+1.42	+6.42
Toluene	+0.94	+5.66	PEO	+0.64	+6.46
Chloroform	+2.39	+3.16	PDMS	+0.06	+4.66
Carbon Tetrachloride	+2.81		PMMA	+1.10	+7.22

Table 2.2; various scattering length densities of polymers and solvents^{17,21}

2.3.7 Form factor, P (Q)

The form factor is a mathematical function from which information on the size and shape of the particles can be obtained. General expressions of P(Q) are known for a wide range of different shapes such as homogeneous spheres, spherical shells, cylinders, and discs. Selected scattering form factors are given below.

2.3.7.1 Sphere model

A simple solid sphere with radius of gyration R_g ;

$$P(Q) = \left[\frac{3(\sin(QR) - QR \cos(QR))}{(QR)^3} \right]^2 \quad (2.27)$$

2.3.7.2 Rod model

A rod shaped object with N randomly oriented rods of length L and radius R,

$$P_{rod}(Q) = N \int_0^{\pi/2} F^2(Q) \sin(\gamma) d\gamma \quad (2.28)$$

$$\text{where } F(Q) = (\Delta\rho)^2 V \frac{\sin\left[\frac{1}{2QL\cos\gamma}\right]}{(1/2)QL\cos\gamma} \frac{2J_1 QR \sin\gamma}{QR \sin\gamma} \quad (2.29)$$

and J_1 is the first order Bessel function of the first kind.

2.3.7.3 Polyelectrolyte model

A polyelectrolyte model, obtained by incorporating a finite cross-section to the rod:

$$P(Q) = \frac{1}{QL} \exp\left(\frac{-Q^2 R_g^2}{2}\right) \left(\frac{Q^2 X^2}{1+Q^2 X^2}\right) \quad (2.30)$$

2.3.7.4 Solid ellipse model

This described by a radius R and ellipticity X.

$$P(Q, R, X) = \int_0^{\pi/2} \phi^2(u) \sin \alpha d\alpha \quad (2.31)$$

where,

$$\phi(u) = 3 \frac{\sin(u) - u \cos(u)}{u^3} \quad (2.32)$$

$$\text{and } u = QR \left[\sin^2(\alpha) - X^2 \cos^2(\alpha) \right]^{1/2} \quad (2.33)$$

X corresponds to the ellipticity of the scatterer; $X < 1$ corresponds to an oblate ellipsoid (disc-like) whereas if $X > 1$, the ellipse is a prolate (needle-like).

2.3.8 Structure factor, S(Q)

$S(Q)$ is a dimensionless function, which describes the type of interactions occurring in the system, mainly attractive, repulsive or excluded volume. The interparticle structure factor is given by;

$$S(Q) = 1 + \frac{4\pi N_p}{QV} \int_0^{\infty} [g(r) - 1] r \sin(Qr) dr \quad (2.34)$$

and is dependent on the degree of local order in the sample. Therefore scattering can be used to gain information about the location of the scattering centres, usually through the “radial distribution function” (r.d.f.);

$$r.d.f. = \frac{4\pi N_p r^2}{V} g(r) \quad (2.35)$$

where r is a radial distance outward from the centre of any scattering centre in the sample, and the density distribution $g(r)$ is obtained by Fourier inversion.

For systems where attractive interactions have to be considered, especially systems with phase separation regions or cloud points, a structure factor known as Ornstein-Zernike (OZ) expression may be used.

$$S(Q)_{critical-scatter} = \frac{S(Q=0)}{1 + \zeta^2 Q^2} \quad (2.36)$$

where ζ is a correlation length and $S(Q=0)$ corresponds to the contribution that this $S(Q)$ component makes to the overall $S(Q)$.

2.4 Surface tension

2.4.1 Introduction

Generally in a liquid sample there are various intermolecular forces operating between molecules. These forces are not equivalent for molecules at the surface and those in the bulk. In the bulk of a liquid all molecules are pulled by the equal magnitude from the surrounded molecules, but molecules at the surface is lacking pull in one direction. As the result of this, molecules at the

surface have a net attractive force which operates inward and this can be balanced only by the resistance of the liquid to compression²².

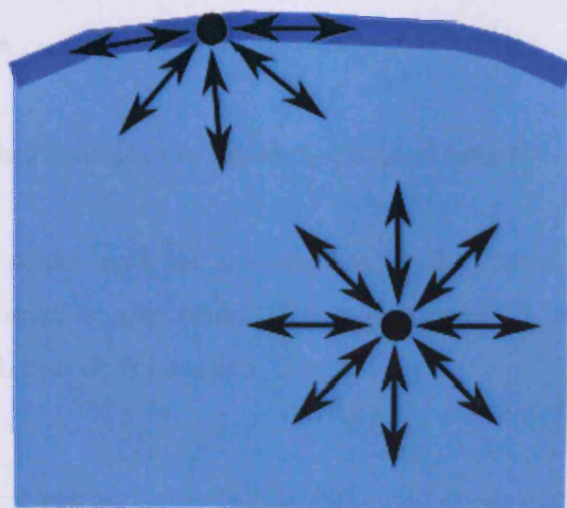


Figure 2.7; unbalanced forces between a liquid-air interface and in the interior of the liquid

This forms a surface “film” which makes it more difficult to move an object through the surface than to move it when it is completely submerged and because of these different intermolecular forces, surfaces are said to be of higher free energy. This energy is called the surface free energy and is expressed as a measure of energy/area.

Surface tension deals with air water-interface, but the same discussion can be used to describe two different liquids (interfacial tension). Since a surface always involves two phases, the surface tension depends on the nature of the two substances between which the surface is formed. Any liquid with a high intermolecular interaction will have a high surface tension. Any factor which decreases the strength of this interaction will lower the surface tension. Hence, an

increase in temperature and contamination by organic molecules will decrease surface tension.

The work dw , needed to change the surface area A of a sample by an infinitesimal amount dA is given by;

$$dw = \gamma dA \quad (2.37)$$

where the proportionality constant γ is called the surface tension.

The adsorption of a solute such as a surfactant at the liquid-air interface is characterized by the relative adsorption. This adsorption (Γ) is related to the surface tension through the Gibbs equation;

$$\Gamma = -\frac{1}{RT} \frac{d\gamma}{d \ln a_2} \quad (2.38)$$

where a_2 is the activity of the solute in bulk solution. Γ is known as surface concentration, represents excess of solute per unit area of the surface over what would be present if the bulk concentration prevailed all the way to the surface and has units of mol/m^2 . R is the gas constant and T is the temperature.

As the concentration of surfactant in the bulk solution is very low below the CMC value (the concentration that surfactants start to form micelles), the solute activity can be replaced by the solute concentration, C_2 ;

$$\Gamma = -\frac{1}{RT} \frac{d\gamma}{d \ln C_2} \quad (2.39)$$

Thus, the surfactant adsorption is obtained from the slope of the surface tension versus the logarithm of the concentration.

2.4.2 Measurement of surface tension

2.4.2.1 Maximum bubble pressure method

The maximum bubble pressure method is a convenient approach to measure the dynamic surface tension. Through the attraction between the molecules of a liquid, air bubbles within a liquid are also subject to these forces. The resulting pressure rises with the decreasing bubble radius. This increased pressure, in comparison to the outside of the bubble, is used to measure surface tension.

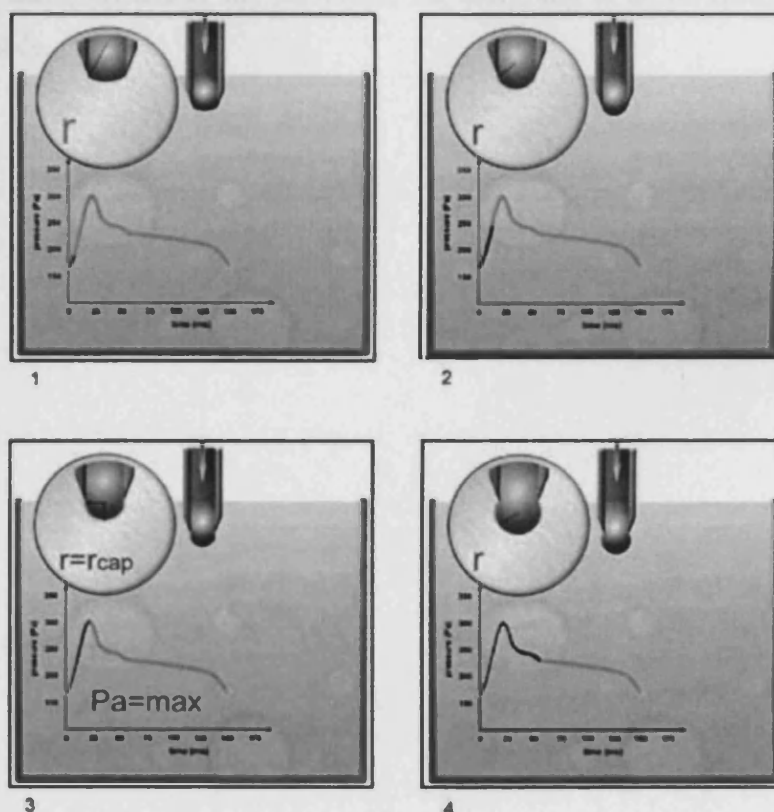


Figure 2.8; The schematic illustration of the changing pressure inside the bubble with bubble life time²³.

During this process, the pressure rises to a maximum pressure. Here the bubble has smallest radius which is equal to the radius of the capillary and forms a half sphere. Beyond this point, the size of the bubble increases exponentially with time and the pressure inside the bubble decreases. Ultimately the bubble is detached from the capillary and travels to the surface. The maximum pressure reached is

proportional to the surface tension; the pressure is converted into surface tension via the Laplace's relation²³.

$$\sigma = \frac{\rho_{\max} - \rho_0}{2} R \quad (2.40)$$

where σ the surface tension, ρ_{\max} is the maximum pressure inside the bubble and ρ_0 is the hydrostatic pressure at the tip of the capillary and R is the maximum radius of the bubble.

2.5 References

1. Price, W. S.; Webb, G. A. In Annual Reports on NMR Spectroscopy; Academic Press, 1996.
2. Hahn, E. L., Physical Review Letters 801950.
3. McCall, D. C.; Douglass, D. C.; Anderson, E. W., Ber. Bunsenges. Physics Chemistry 671963.
4. Stejskal, E. O.; Tanner, J. E., Journal of Chemical Physics 42, 288 1965.
5. Stilbs, P., Analytical Chemistry 531981.
6. Carr, H. Y.; Purcell, E. M., Physical Review Letters 941954.
7. Stilbs, P., Progress in NMR spectroscopy 19, 1 1987.
8. Weil, J. A.; Bolton, J. R., Electron paramagnetic resonance; John Willey & Sons, Inc, copyright 2007.
9. Hoff, A. J., Ed. Advanced EPR: applications in biology and biochemistry, Oxford, Elsevier, 1989.
10. www.epr.ethz.ch.
11. Weber, R. T.; Jiang, J.; Barr, D. P.; Bruker Instrument, Inc; Billerica, MA USA: 1998.
12. McConnell, H. M., Journal of Chemical Physics 24, 764 1956.
13. Kivelson, D., Journal of Chemical Physics 33, 1094 1960.
14. Coderch, L.; Fonollosa, J.; Pera, M. D.; Estelrich, J.; Maza, A. D. I.; Parra, J. L., Journal of controlled release 68, 85 2000.
15. Roe, R.-J., Methods of X-ray and neutron scattering in polymer science; Oxford University press, 2000.
16. Lindner, P.; Zemb, T., Neutrons, X-rays and light: Scattering methods applied to soft condensed matter; Elsevier, Amsterdam, 2002.
17. Higgins, J. S.; Benoit, H. C., Polymers and neutron scattering; Oxford science, 1994.
18. ILL, www.ill.fr/YellowBook/D11/.
19. ISIS, www.ISIS.rl.uk.
20. Griffiths, P. C.; King, S. M. in Encyclopedia of surface and colloidal science; Hubbard, A. T., Ed.: 2002, p 4700.
21. King, S. M.; ISIS, Oxford: 1995.
22. Evans, D. F.; Wennerstrom, H., The colloidal domain; John Willy & Sons, 1999.
23. www.KRUSS.com.

Derivatizing weak polyelectrolytes & implications for their use in drug delivery - Solution properties

3.1 Introduction

The presence of charged or ionisable groups on a polymer offers the opportunity to control many aspects of the behaviour of the polymer - solubility, tendency to adsorb at surfaces - by changes in external variables such as pH or ionic strength¹. The overall behaviour of the polymer is determined by the chemical nature of the polymer, its molecular weight and effective charge. The presence of hydrophobic moieties can perturb the structure of the polymer, either directly through the association of these hydrophobic moieties²⁻⁴, or through the impact the modification has on the ability of the polymer to charge at a given pH. Hydrophobically modified polyelectrolytes such as cellulose^{5,6}, poly(acrylamide)^{7,8}, poly(ethyleneoxide)⁹, and sulfonated poly(vinyl alcohol)¹⁰ have attracted considerable attention as the associated hydrophobic domains are capable of promoting the solubilisation of hydrophobic materials in aqueous solutions.

Gene therapy is an attractive approach for the treatment of genetic defects, as well as diseases such as cancer and chronic viral infection. Efficient and safe gene transfer systems are the fundamental requirement for such gene therapy. Viral systems are, in general, very effective for gene transfer, although there are concerns about their use on grounds of safety and immunogenicity. Therefore, a number of non - viral synthetic polymer based systems have been developed, in order to overcome the drawbacks in viral mediated drug delivery.

The polymer should be hydrophilic, stable, possess a neutral structure that will circulate inside the body for a significant period exhibiting reduced toxicity, provide stability against cytosolic degradation but be sufficiently small to preclude capture by the kidneys. Cationic polymers, with nitrogen functionalities have been developed for drug and gene delivery^{11,12}. However, in gene delivery, a neutral

polymer will result in poor DNA condensing ability whilst a cationic structure will facilitate a nonselective interaction with cell membranes, promote DNA condensation but may not subsequently release the DNA.

The structure of any optimized polymeric construct that meets these often contradictory criteria will need to incorporate the competition between hydrophobic attraction and electrostatic repulsion, and this is sensitive to the degree of charging of the polymer, the solution structure and the interaction with other serum components. However, delivery efficiency of synthetic vehicles in general is still poor and much effort is being expended to optimize the structure of the polymeric component. Targeting of PEI-based so-called polyplexes has been attempted by modifying the PEI by incorporation of galactose¹³, mannose¹⁴, transferin¹⁵, and various antibodies¹⁶. Acetylation,¹⁷ grafting of aminoacids (alanine, leucine, and histidine), thermoresponsive¹⁸ or hydrophobic moieties¹⁹ have also been explored to increase delivery efficiency.

In this chapter, characterization of different molecular weight hyperbranched poly(ethylene imines) denoted BPEI was carried out through the analysis of self-diffusion coefficients. BPEI polymers are variably polydisperse, a feature that is unfortunate but tolerated in many studies. The distribution of self-diffusion coefficients measurable in the PGSE-NMR experiment reflects indirectly, the molecular weight distribution. Two semi-empirical approaches have been used to determine the range of diffusion coefficient present, a stretched exponential and an Inverse Laplace Transformation (ILT) via Provencher's CONTIN programme.

Most of the therapeutic agents one may wish to deliver by incorporation into a polymeric vehicle are hydrophobic and therefore, insoluble in water. The aim here is to probe the fundamental effects that derivatization with hydrophobic moieties - in this study, introduced by grafting dodecyl groups - has on the solution conformation and the interaction of the polymer with a negatively charged surface, a micelle formed from the surfactant sodium dodecylsulfate (SDS). This study

employed electron paramagnetic resonance (EPR) and small-angle neutron scattering (SANS) experiments.

3.2 Materials and methods

Branched poly(ethylene imine) (BPEI) samples of nominal molecular weights 2,000, 25,000, and 750,000 g mol⁻¹ were obtained from Aldrich, whilst a 50,000 g mol⁻¹ sample was sourced from Acros Organics. 1,2-epoxydodecane (Aldrich), 16-doxyzyl stearic acid methyl ester (16-DSE) (Aldrich) were both used as received, whereas sodium dodecylsulfate (SDS) (Aldrich) was recrystallized from ethanol until no minimum around the CMC was observed in the surface tension data.

Hydrophobically modified samples prepared at 2 statistical degrees of loading were kindly donated by Sarah Waters 1 hydrophobe per 100 EI units (1 mol%), the second higher at 1 hydrophobe per 10 EI units (10 mol%). These materials are denoted HM_{1%}BPEI_{25K} and HM_{10%}BPEI_{25K} where the B underlines the fact that these polymers are hyperbranched, the subscript “25K” indicated the molecular weight of the PEI and HM_{1%} the degree of hydrophobic modification.

Pulsed - gradient spin - echo NMR (PGSE-NMR)

Measurements were conducted on a Bruker AMX 360 NMR spectrometer using a stimulated echo – sequence as described in chapter 2. This configuration uses a 5mm diffusion probe (Cryomagnet Systems, Indianapolis) and a Bruker gradient spectroscopy accessory unit.

Electron Paramagnetic Resonance (EPR)

An aliquot of an ethanol solution of spin-probe 16-DSE (2 mM) was dried in a glass vial, to which the sample is added, mixed and allowed to equilibrate. The final spin-probe concentration is around 2 μM. Where appropriate, the pH was adjusted by addition of HCl. An aliquot of the sample was drawn into a capillary tube which was sealed and placed in quartz EPR tubes before taking measurements

using a Bruker EMX at room temperature ($\sim 22^\circ\text{C}$) using a frequency of 9.29 ± 0.3 GHz. Each spectrum was recorded as the average of 10 scans.

Small-angle neutron scattering (SANS)

SANS measurements were performed on the LOQ diffractometer at ISIS, Oxford, U.K. This uses neutrons of wavelength 2.2-10 Å by time - of - flight, with a 64cm square detector at 4.1m from the sample. The sample were contained in 2mm pathlength, UV-spectrophotometer grade, quartz cuvettes (Hellma) and mounted in aluminium holders on top of an enclosed, computer – controlled, sample changer. Sample volumes are approximately 0.6cm^3 . Temperature control was achieved through the use of a thermostatted circulating bath pumping fluid through the base of the sample changer.

All scattering data were (a) normalized for the sample transmission, (b) background corrected using a quartz cell filled with D_2O and (c) corrected for the linearity and efficiency of the detector response using the instrument – specific software package. The data were put onto an absolute scale by reference to the scattering from a partially deuterated polystyrene blend.

3.3 Results

3.3.1 Self - diffusion studies of different molecular weight PEI samples

The self-diffusion coefficient D_s was extracted by fitting the integrals for a given peak occurring at 2.5 – 3 ppm using equation 3.1.

$$A(\delta, G, \Delta) = A_0 \exp[(-kD_s)]^\beta \quad (3.1)$$

A is the signal amplitude in the absence (A_0) or presence ($A(\delta, G, \Delta)$), of the field gradient pulses and β is an exponent to quantify in a semiempirical fashion the linearity of the attenuation function reflecting the width of the distribution of the self-diffusion coefficient. k is given by equation 3.2,

$$k = -\gamma^2 G^2 \left(\frac{30\Delta(\delta + \sigma)^2 - (10\delta^3 + 30\sigma\delta^2 + 35\sigma^2\delta + 14\sigma^3)}{30} \right) \quad (3.2)$$

where γ is the magnetogyric ratio, Δ the diffusion time (140 ms), σ the gradient ramp time (250 μ s), δ the gradient pulse length (500 μ s < δ < 3ms), and G the gradient field strength (0.5 < G < 3 T/m).

3.3.1.1 Analysis of self-diffusion coefficient using a stretched exponential analysis

The self diffusion-coefficient of BPEI_{2K}, BPEI_{25K}, BPEI_{50K}, and BPEI_{750K} g/mol of BPEI samples were measured using PGSE-NMR as described previously. Figure 3.1 to 3.4 illustrate concentration dependence of the self-diffusion coefficient and beta value (panel (a)) and also the variation of the normalized intensity with gradient value (k value) (panel (b)) for different molecular weight PEI samples. The raw data were fitted to a stretch exponential function to evaluate the self-diffusion coefficient and β value. For ease, the raw data has also been included in the lower panel but since the more fundamental insight comes from the D_s and β value, this analysis is placed in the upper panel.

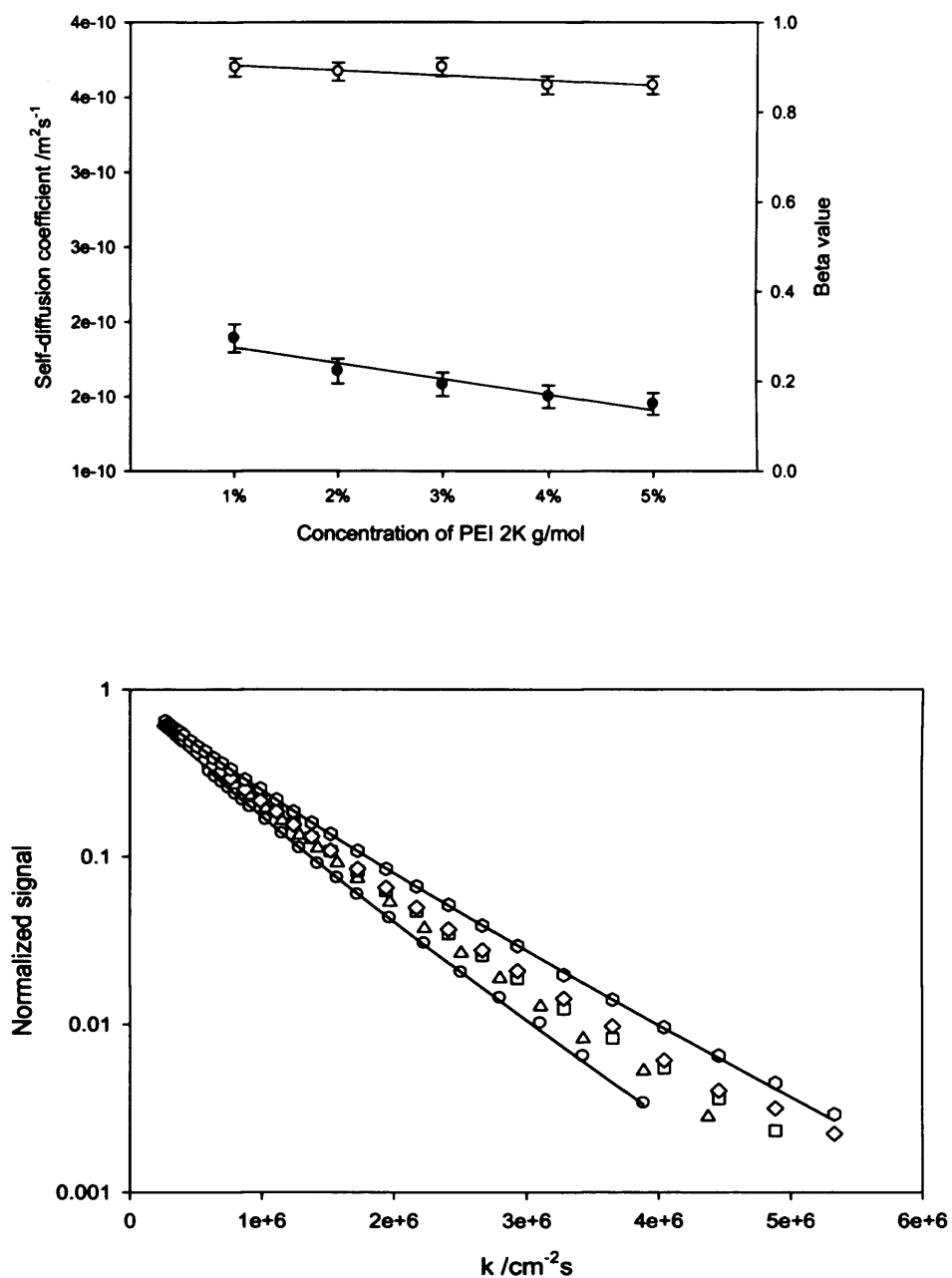


Figure 3.1; Concentration dependence of the self-diffusion coefficient (filled circles) and β value (open circles) of BPEI_{2K} panel (a). Raw attenuation function for BPEI_{2K} as a function of PEI concentration, 1wt% (circle); 2wt% (triangle); 3wt% (square); 4wt% (diamond); 5wt% (hexagon) (panel b). Representative fits only have been indicated for clarity

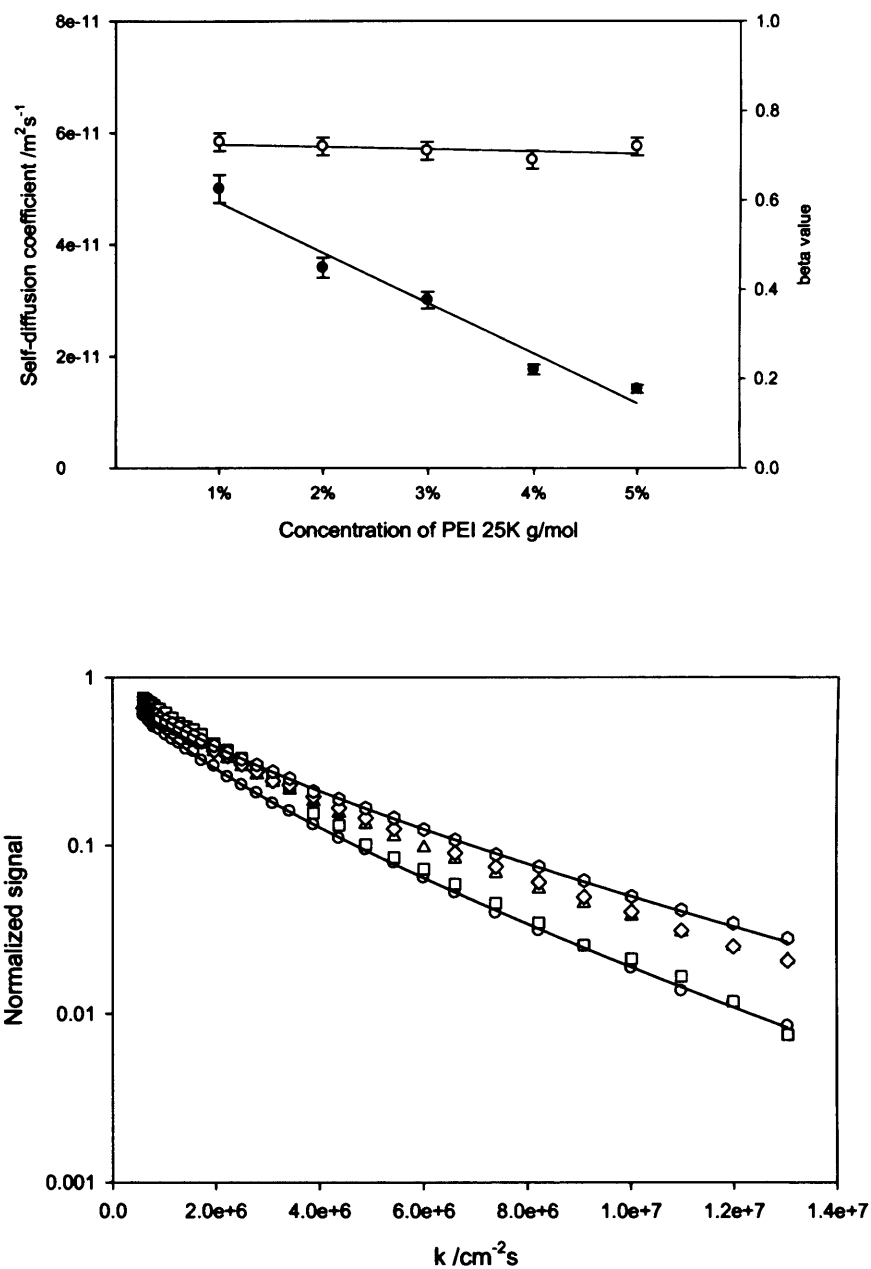


Figure 3.2; Concentration dependence of the self-diffusion coefficient (filled circles) and β value (open circles) of BPEI_{25K} panel (a). Raw attenuation function for BPEI_{25K} as a function of PEI concentration, 1wt% (circle); 2wt% (square); 3wt% (triangle); 4wt% (diamond); 5wt% (hexagon) (panel b). Representative fits only have been included for clarity

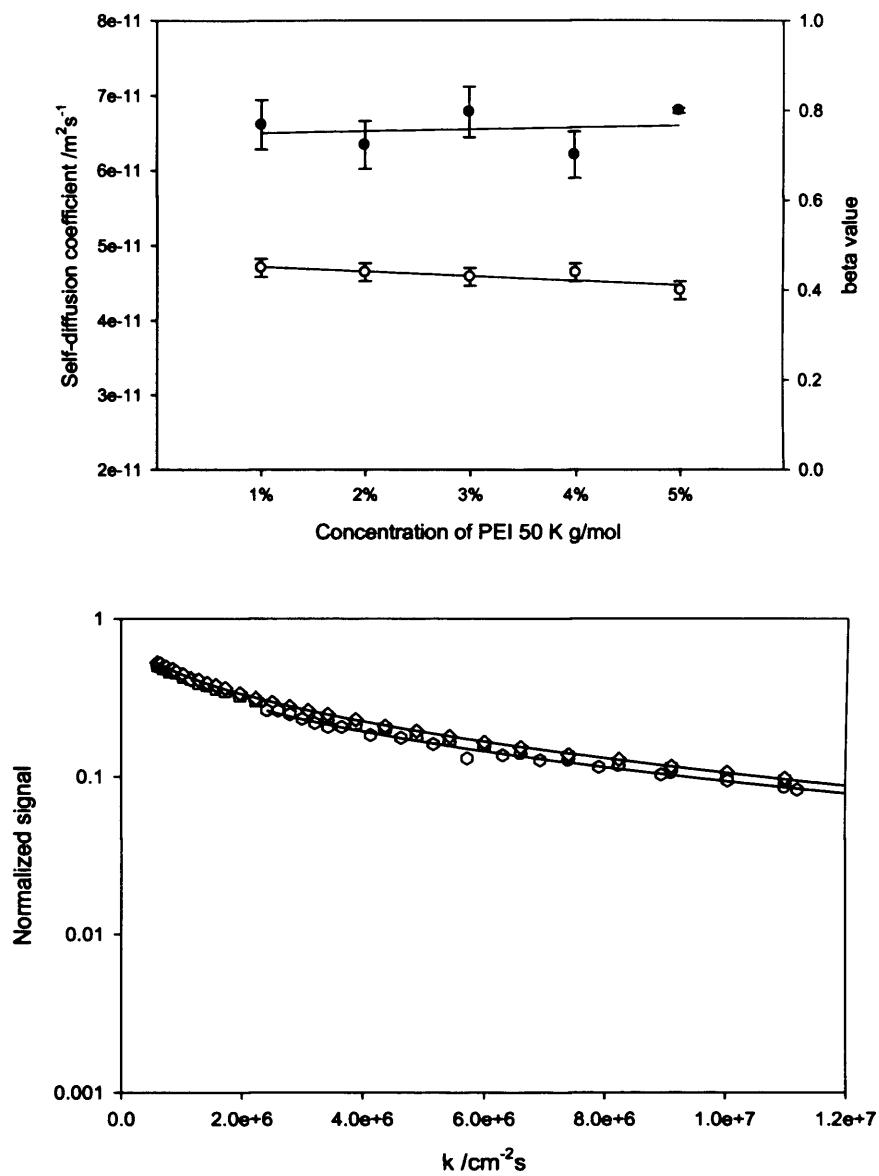


Figure 3.3; Concentration dependence of the self-diffusion coefficient (filled circles) and β value (open circles) of BPEI_{50K} panel (a). Raw attenuation function for BPEI_{50K} as a function of PEI concentration, 1wt% (circle); 2wt% (square); 3wt% (triangle); 4wt% (diamond); 5wt% (hexagon) (panel b). Representative fits only have been included for clarity.

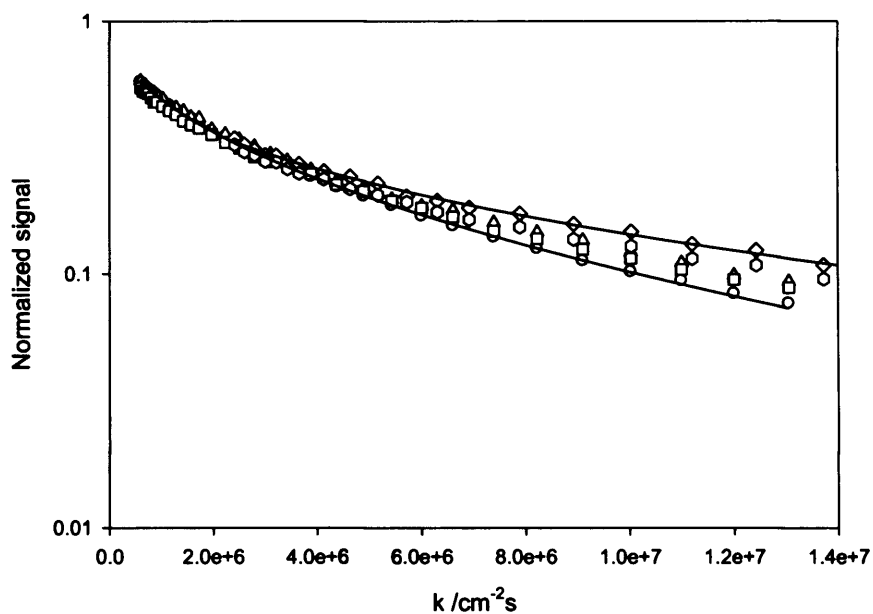
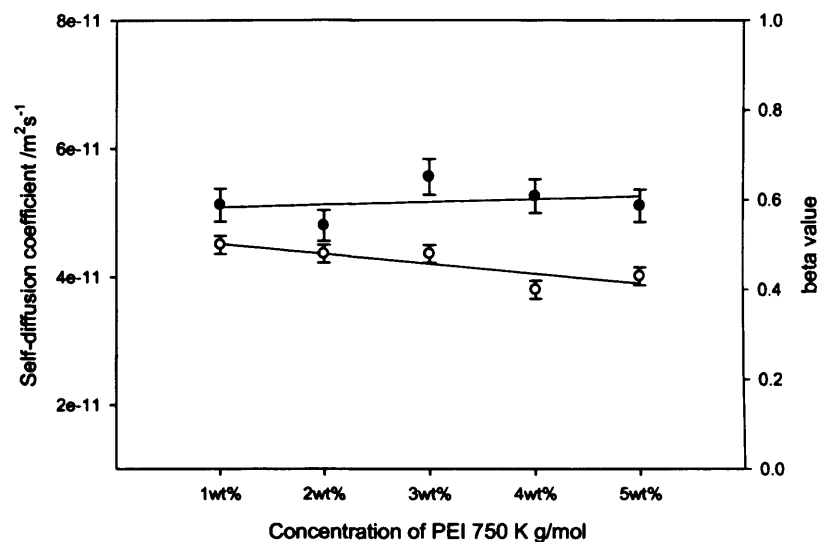


Figure 3.4; Concentration dependence of the self-diffusion coefficient (filled circles) and β value (open circles) of BPEI_{750K} panel (a). Raw attenuation function for BPEI_{750K} as a function of PEI concentration, 1wt% (circle); 2wt% (square); 3wt% (triangle); 4wt% (diamond); 5wt% (hexagon) (panel b). Representative fits have been included for clarity.

For monodisperse polymers, the attenuation plots should give a single-exponential relationship whose slope corresponds to D_s . The polydispersity results in upward curvature in the attenuation plot. The attenuation plot of BPEI_{2K} only slightly departed from linearity, indicating reasonably monodisperse behaviour. The dependence of the self-diffusion coefficient with concentration was weak as expected for a small polymer.

Upward curvature of the attenuation plot were present in the BPEI_{25K} (fig 3.2), but was particularly pronounced BPEI_{50K} (fig 3.3), and BPEI_{750K} (fig 3.4) cases indicating substantial polydispersity of these samples. The polydispersity of the 50 K and 750K samples obscures any concentration dependence of the self-diffusion coefficient due to the broad molecular weight distribution of the sample.

3.3.1.2. Analysis of self-diffusion coefficient using an Inverse Laplace transformation

An inverse Laplace Transformation (ILT) via Provencher's CONTIN program applied to an attenuation function offers a valuable opportunity to extract the self-diffusion coefficient distribution present in the sample. This information, in principle, contains the size distribution of the diffusing species. The need to process NMR data in this fashion arises when the attenuation function shows a varying degree of upward concavity and accordingly, the "measured" self-diffusion coefficient becomes a function of the experimental parameters. The ILT has been used to good effect previously by others but not without some shortcomings. Problems associated with CONTIN in particular have been discussed in considerable detail, and it is not necessary here to revisit this²⁰. Nevertheless, with a suitable standardized approach, an ILT does yield an informative picture of the self-diffusion coefficient distribution. Figure 3.5 illustrates the self-diffusion coefficient distribution for different molecular weight PEI, calculated from the ILT via Provencher's CONTIN programme.

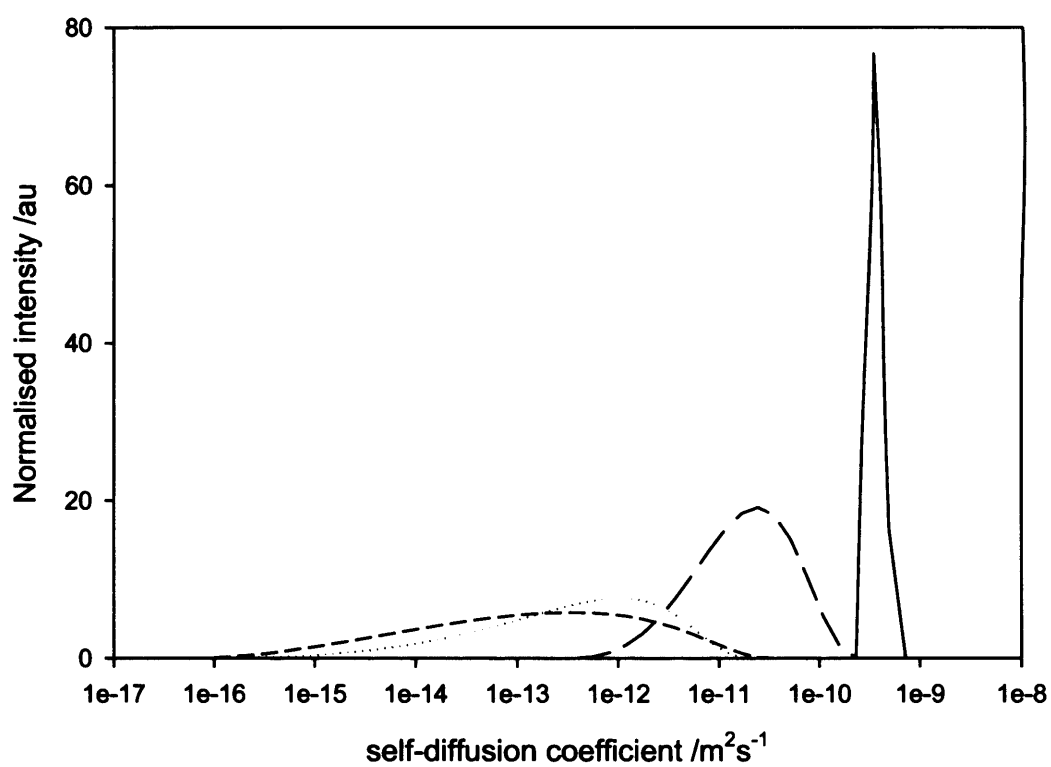


Figure 3.5; Self-diffusion coefficient distributions for the four BPEI samples: (solid line) BPEI_{2K}, (long dashed line) BPEI_{25K}, (short dashed line) BPEI_{50K}, and (dotted line) BPEI_{750K}.

Consider the CONTIN analysis of the BPEI_{2K} (fig. 3.5). This exhibits a distribution with a width comparable to the natural broadening inherent in the analysis. This distribution is reasonable for a monodisperse polymer. Further this behaviour is entirely agreement with the self-diffusion coefficient analysis using the stretched exponential approach. Except for BPEI_{2K}, all the other samples of BPEI have molecular weight distributions that are too broad to meaningfully analyse the data.

3.3.2 The effect of hydrophobe on polymer surface activity and aggregation

3.3.2.1 Solution conformation – Effect of pH

The effect of degree of hydrophobic modification on the solution conformation has been examined by SANS and presented in figure 3.6(a) and 3.6(b). The SANS data have been interpreted in terms of two models. The first approach invoked a solid ellipsoid morphology – a coarse grained version of a model previously used to describe PEI based systems⁹ – described by a radius R and ellipticity X. Here the form factor P(Q) describing the intensity of scattered radiation, I(Q), as a function

of the wave-vector, $Q = \frac{4\pi}{\lambda} \sin\left(\frac{\theta}{2}\right)$, is given by;

$$P(Q, R, X) = \int_0^{\pi/2} \phi^2(u) \sin \alpha d\alpha \quad (3.3)$$

where $\phi(u) = 3 \frac{\sin(u) - u \cos(u)}{u^3}$ and $u = QR \sqrt{\sin^2(\alpha) - X^2 \cos^2(\alpha)}$. When $X < 1$, the ellipsoid is oblate (disc-like) and $X > 1$, the ellipsoid is prolate (needle-like).

The second approach invoked a solid rod morphology. For N randomly orientated rods of length L and radius R, P(Q) is given by;

$$P(Q) = N \int_0^{\pi/2} F^2(Q) \sin(\gamma) d\gamma \quad (3.4)$$

where $F(Q) = (\Delta\rho)^2 V \frac{\text{Sin}\left(\frac{1}{2}QL\cos\gamma\right)}{\frac{1}{2}QL\cos\gamma} \frac{2J_1(QR\sin\gamma)}{QR\sin\gamma}$ and J_1 is the first order

Bessel function of the first kind.

In both approaches, a repulsive structure factor $S(Q)$ has also been included in this analysis model, calculated from RMSA approach based on a repulsive Yukawa tail (an exponentially damped electrostatic term) and the hard-core potential^{2,3}. The model is described via four parameters: a hard sphere volume fraction $\Phi_{\text{hard sphere}}$ and “particle” radius $R_{\text{hard sphere}}$, the charges on the particle and the inverse Debye screening length.

The scattering varies significantly as a function of modification, with both the form of the data and intensity varying. At pH 10 (figure 3.6a), the polymers were uncharged and with the scatters displaying a very elongated structure, and elongation increased on going from BPEI_{25K} to HM_{10%}BPEI_{25K}, i.e., with increasing degree of hydrophobic modification.

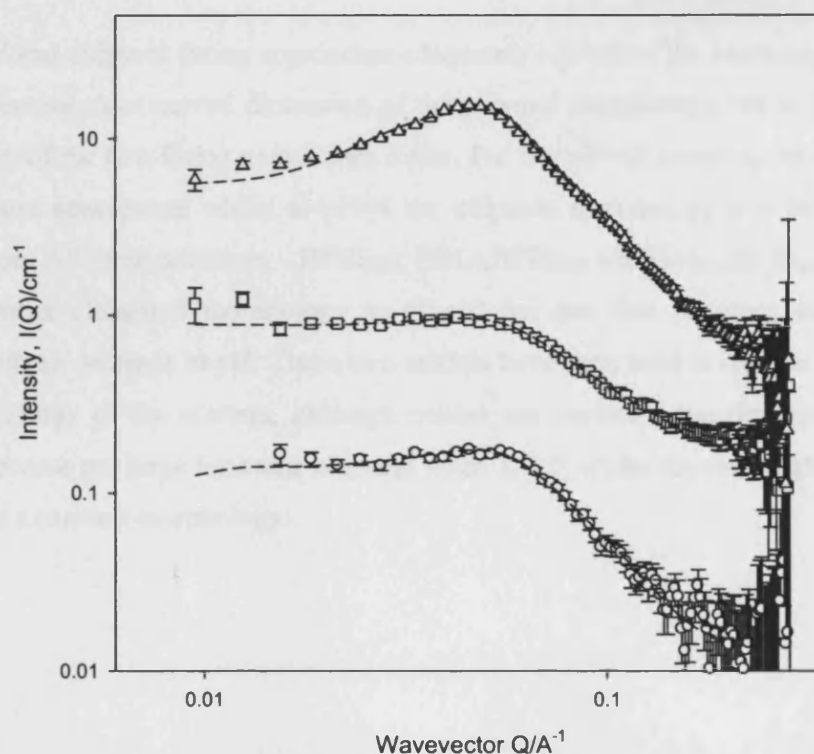
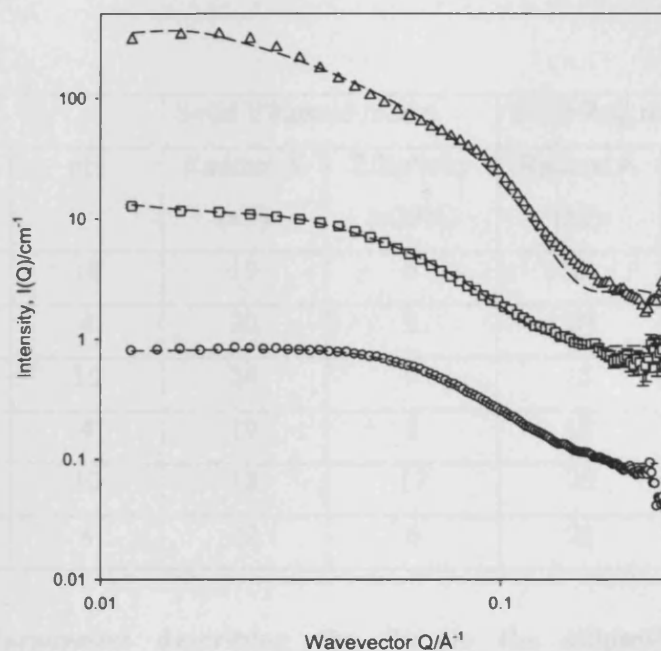


Figure 3.6; Panel (a) The effects of hydrophobic modification on the SANS from BPEI_{25K} in a 5wt% pH 10 aqueous solution; (circles) BPEI_{25K}, (squares) HM_{1%}BPEI_{25K}, and (triangles) HM_{10%}BPEI_{25K}. Broken lines correspond to fits as described in the text. Each data set has been offset by a factor of 10 for clarity. **Panel (b)** The effects of hydrophobic modification on the SANS from BPEI_{25K} in a 5wt% pH 4 aqueous solution; (circles) BPEI_{25K}, (squares) HM_{1%}BPEI_{25K}, and (triangles) HM_{10%}BPEI_{25K}. Broken lines correspond to fits to the solid ellipse model. For clarity dataset has been offset by a factor of 10 for clarity

		Solid Ellipsoid model		Solid Rod model	
Sample	pH	Radius/ Å (±3)	Ellipticity (±20%)	Radius/ Å (±3)	Length/ Å (±20)
BPEI _{25K}	10	19	5	20	160
BPEI _{25K}	4	20	3	20	180
HM _{1%} BPEI _{25K}	10	24	9	18	275
HM _{1%} BPEI _{25K}	4	19	5	18	185
HM _{10%} BPEI _{25K}	10	18	17	20	240
HM _{10%} BPEI _{25K}	4	22	6	21	450

Table 3.1; Parameters describing the fits to the ellipsoid and rod morphologies invoked to analyse the SANS data

Both the rod and ellipsoid fitting approaches adequately reproduce the scattering at high Q , reflecting more curved dimension of the polymer morphology, but at low Q the quality of the two fitting approaches differ. For the pH=10 samples, the rod model is more appropriate whilst at pH=4 the ellipsoid morphology is a better representation. All three polymers – BPEI_{25K}, HM_{1%}BPEI_{25K} and HM_{10%}BPEI_{25K} – exhibit a rather elongated morphology at pH=10 but one that becomes more spherical with an decrease in pH. These two models have been used to capture the gross morphology of the scatters, although neither are perfect – the degrees of ellipticity become too large for a true ellipsoid when $X > 5$, whilst the rod-length is too short for a true rod morphology.

3.3.2.2 16-DSE solubilised in possible hydrophobic moieties of different PEI

The effect of the hydrophobic domains present within the polymer can be assessed using EPR. The spin-probe, 16-DSE is insoluble in water, so a signal will only be observed when the spin-probe is dissolved in the hydrophobic regions. This solubility will be undoubtedly facilitated by the presence of hydrophobic domains in the PEI matrix. Freely rotating 16-DSE displays a spectrum consisting of three sharp lines, with the high field line becoming disproportionately broadened with increases in viscosity.

Figure 3.7 to 3.9 illustrate solubility of spin-probe in BPEI_{25K}, HM_{1%} BPET_{25K} and HM_{10%}BPEI_{25K} matrixes at different pHs.

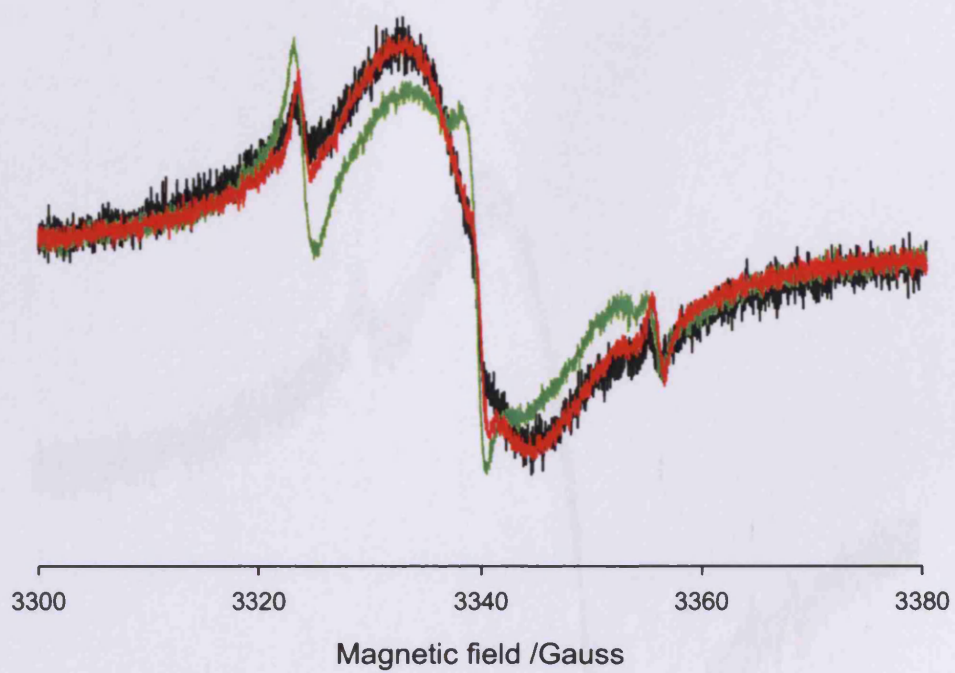


Figure 3.7; Effect of pH on the EPR spectrum of 16-DSE solubilised in BPEI_{25K} at pH 3 (black); pH 7 (red); pH 10 (green)

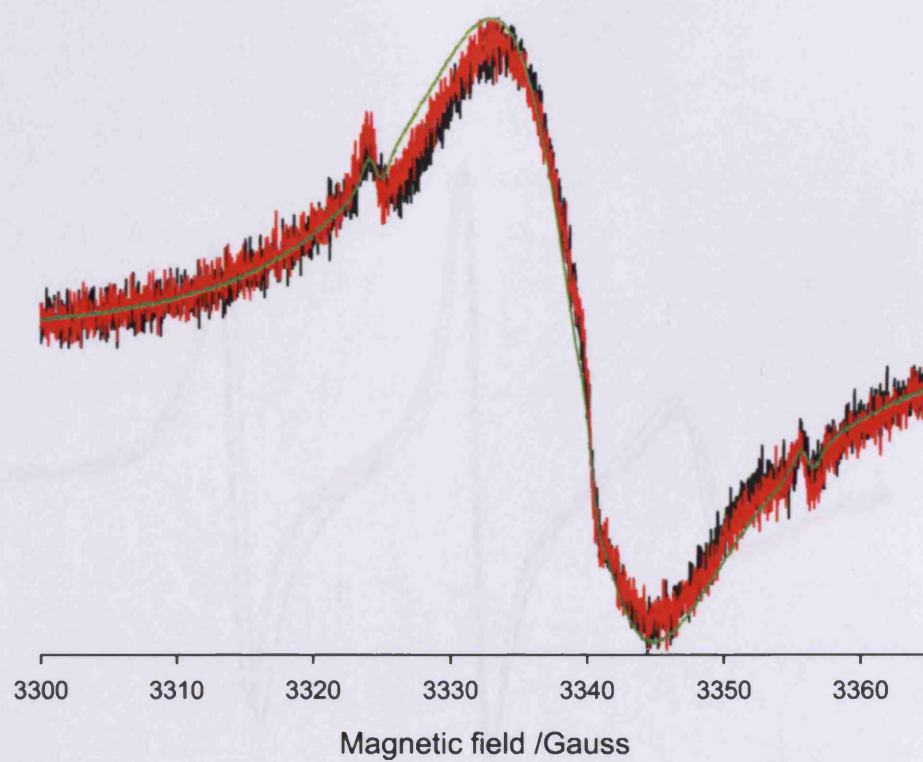


Figure 3.8; Effect of pH on the EPR spectrum of 16-DSE solubilised in HM₁%BPEI_{25K} at pH 3 (black); pH 7 (red); pH 10 (green)

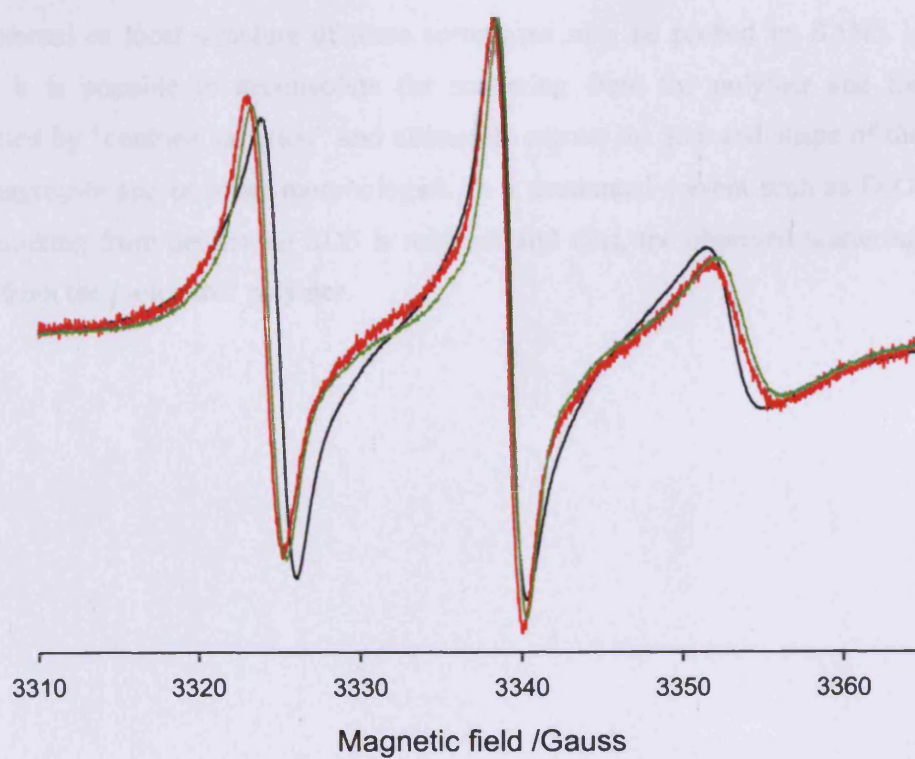


Figure 3.9; Effect of pH on the EPR spectrum of 16-DSE solubilised in HM₁₀%BPEI_{25K} at pH 3 (black); pH 7 (red); pH 10 (green)

The three line spectra characteristics of a highly mobile 16-DSE spin-probe were discernible in the BPEI_{2K} and HM_{1%}BPEI_{25K} cases at all pHs, but the spectra contain little information and suggest many unresolved interactions. The HM_{10%}BPEI_{25K} is much different resembling highly mobile spin-probe and considerable pH effect. This could be due to hydrophobic domains present or minute amount of ethanol present in the sample. According to NMR ethanol present in the sample was very little.

3.3.3 Internal structure of BPEI/SDS complexes

3.3.3.1 SANS results

The internal or local structure of these complexes may be probed by SANS in which it is possible to deconvolute the scattering from the polymer and the surfactant by “contrast variation” and ultimately extract the size and shape of the SDS aggregate and polymer morphologies. In a deuterated solvent such as D₂O, the scattering from deuterated SDS is minimal and thus, the observed scattering arises from the protonated polymer.

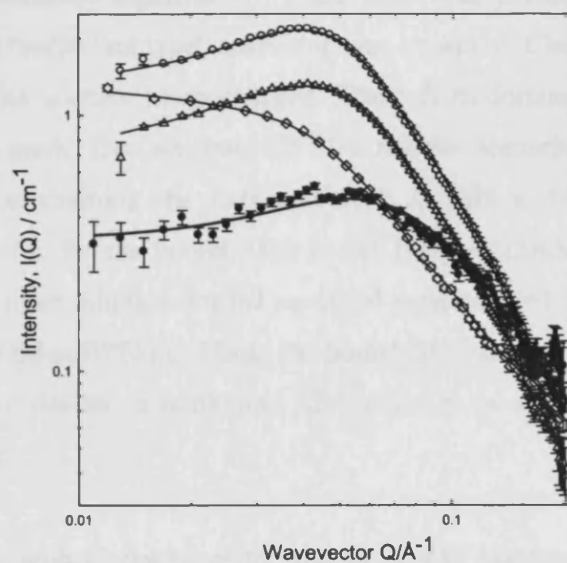
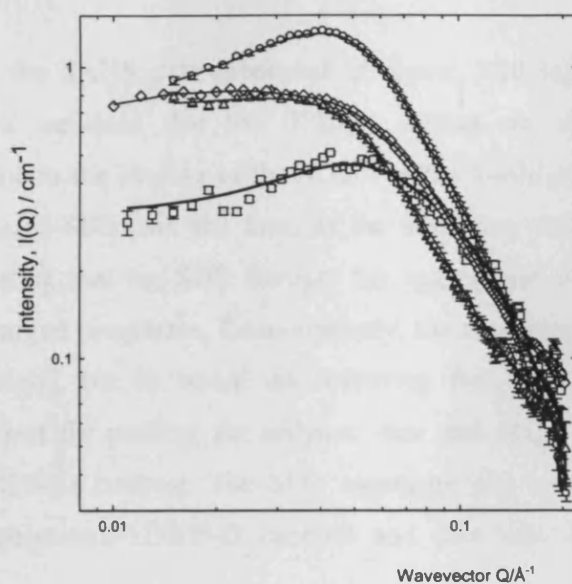


Figure 3.10; (a) Contrast variation SANS study of BPEI_{25K} ($C_{\text{polymer}}=5.0\text{wt } \%$) in the presence of 25mM SDS; (circles) BPEI_{25K}/h-SDS/D₂O, (triangles) BPEI_{25K}/d-SDS/D₂O, and (squares) BPEI_{25K}/d-SDS/H₂O. The solid line corresponds to a fit to a charged core-shell ellipse with Hayter-Penfold structure factor. For clarity, representative incoherent backgrounds have been subtracted and the data above $Q=0.2 \text{ \AA}^{-1}$ omitted. Also shown for comparison is the surfactant-free dataset BPEI_{25K}/D₂O (diamonds). (b) Contrast variation SANS study of BPEI_{25K} ($C_{\text{polymer}}=5.0\text{wt } \%$) in the presence of 25mM SDS; (circles) HM_{1\%}BPEI_{25K}/h-SDS/D₂O, (triangles) HM_{1\%}BPEI_{25K}/d-SDS/D₂O, and (squares) HM_{1\%}BPEI_{25K}/d-SDS/H₂O. The solid line corresponds to a fit to a charged core-shell ellipse with Hayter-Penfold structure factor. For clarity, representative incoherent backgrounds have been subtracted and the data above $Q=0.2 \text{ \AA}^{-1}$ omitted. Also shown for comparison is the surfactant-free dataset HM_{1\%}BPEI_{25K}/D₂O (diamonds).

According to the SANS data presented in figure 3.10 (a), scattering from h-BPEI_{25K}/d-SDS indicates that the BPEI_{25K} suffers no significant change in morphology due to the binding of the SDS. For the h-HM_{1%}BPEI_{25K}/no SDS and h-HM_{1%}BPEI_{25K}/d-SDS pair, the form of the scattering was quite different, fig. 3.10(b), indicating that the SDS disrupts the aggregation of the HM_{1%}BPEI_{25K}, resulting in charged complexes. Concomitantly, the scattering from h-SDS in H₂O would be minimal, but so would the scattering from the h-polymer; thus, the preferred contrast for probing the polymer size and shape is to employ the h-polymer/d-SDS/D₂O contrast. The SDS aggregate size and shape is accessible through a h-polymer/d-SDS/H₂O contrast and data sets are presented in fig. 3.10(a).

The intensity increased significantly when SDS was present, and pronounced peaks typical of “surfactant type” scattering was observed. Clearly, the addition of SDS rendered the scatters more charged. These SDS-dominated scattering data were fitted to a model that accounts for SDS micelle scattering, i.e., a core-shell ellipsoid, and constraining the radius at 16.7 Å with a 4Å shell yielded an ellipticity of X=12. for the bound SDS in the BPEI_{25K}/25mM SDS case, which became slightly more elliptical for the modified samples, X=1.5 for HM_{1%}BPEI_{25K} and X=2.2 for HM_{10%}BPEI_{25K}. Thus, the bound SDS state is micellar, with size and shape rather similar to nonbound SDS micelles in a low-to medium ionic strength solution.

It may simply be coincidence given the size of the PEI aggregate (R~25Å) and the size of a nonbound SDS micelle (R~16.7+4Å~21Å), but the dimensions of the bound SDS micelle significantly resemble that of the PEI/SDS complex. The obvious interpretation is that the SDS is distributed throughout the PEI aggregate.

3.3.3.2 Impact of SDS solubilized spin probe on different PEI samples

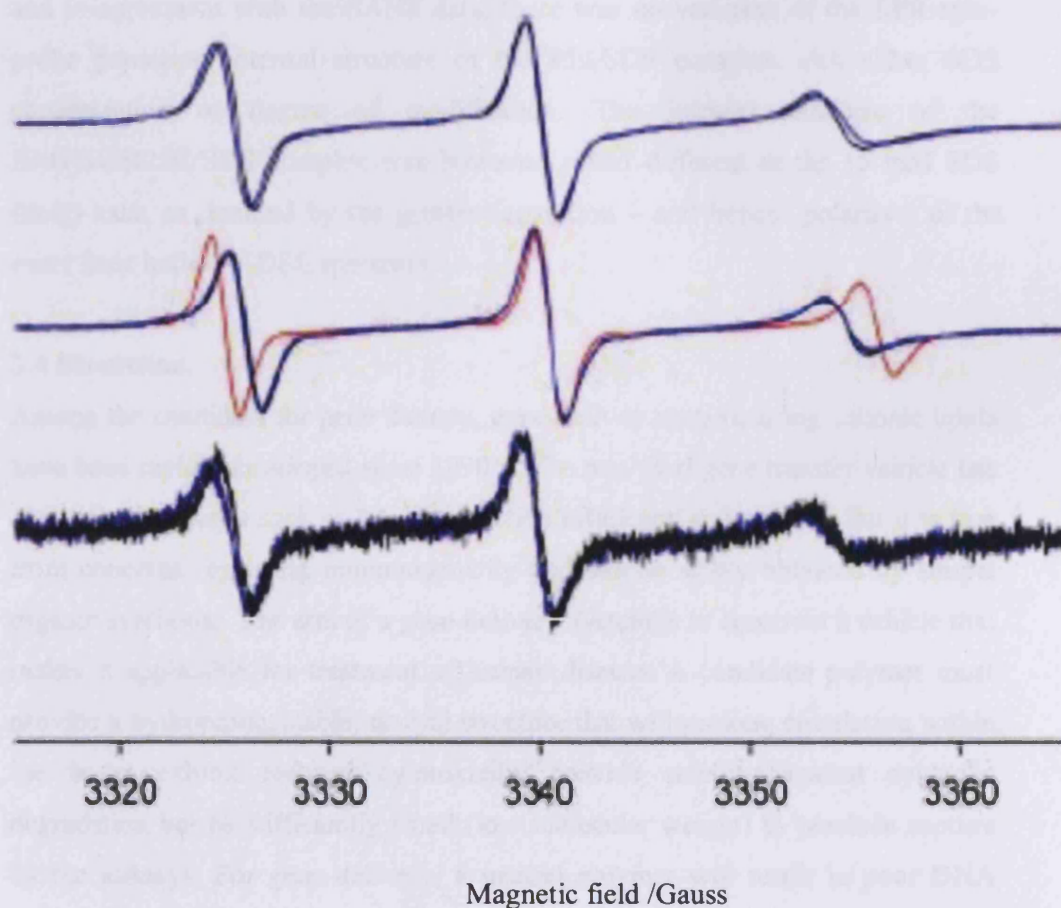


Figure 3.10; EPR spectra of 16-DSE solubilized in PEI/SDS solutions at ambient pH and with $C_{\text{polymer}}=1.0\text{wt}\%$; (black) BPEI25K; (blue) HM₁%BPEI₂₅K. Bottom spectra, [SDS] = 2 mM; middle, [SDS] = 15 mM, and top, [SDS] = 25 mM. The red spectrum corresponds to a simple 15 mM SDS solution. All vertical scales are normalized for clarity.

Further insight into the internal structure of this polymer/surfactant complex was obtained from EPR (figure 3.10), in which pair-wise comparison of BPEI_{25K} and HM_{1%}BPEI_{25K} are presented in the presence of 2, 15, and 25 mM SDS. As is obvious, the expected three line spectra of (a fluid) 16-DSE was observed, the broad feature noted earlier for the polymer-only cases being absent. Interestingly, and in agreement with the SANS data, there was no variation of the EPR spin-probe perceived internal structure of the PEI/SDS complex with either SDS concentration or degree of modification. The internal structure of the HM_{1%}PEI_{25K}/SDS complex was however, rather different to the 15 mM SDS (only) case, as denoted by the greater separation – and hence polarity - of the outer lines in the 16-DSE spectrum.

3.4 Discussion.

Among the candidate for gene therapy, gene delivery systems using cationic lipids have been rapidly developed since 1990's. The non-viral gene transfer vehicle has some disadvantages such as low transfection efficiency and stability but it is free from concerns regarding immunogenicity and can be stably obtained by simple organic synthesis. The aim of a gene delivery system is to construct a vehicle that makes it applicable for treatment of human disease. A candidate polymer must provide a hydrophilic, stable, neutral structure that will prolong circulation within the body, exhibit reduced cytotoxicity, provide stability against cytosolic degradation but be sufficiently small (low molecular weight) to preclude capture by the kidneys. For gene delivery, a neutral polymer will result in poor DNA condensing ability whilst a cationic structure will facilitate a nonselective interaction with cell membranes, promote DNA condensation but may not subsequently release DNA.

Hydrophobically modified branched poly(ethylene imine) materials based on a commercially available sample with molecular weight 25K g/mol have been studied by EPR, SANS and PGSE-NMR spectroscopy. As BPEI polymers are variably polydisperse, there is a substantial polydispersity in the polymer self-



diffusion coefficients of different molecular weight PEI in aqueous solution. Indeed, as a hyperbranched polymer with no chromophore, determination of the absolute molecular weight distribution is problematic. The distribution of self-diffusion coefficients measurable in the PGSE-NMR experiments reflects indirectly, the molecular weight distribution and is therefore a convenient method to screen out samples of BPEI that are too polydisperse to provide meaningful data. Clearly, BPEI_{2K} behaves much like a monodisperse polymer (linear attenuation function), not unexpectedly given its low molecular weight. Analyzing these data in terms of the ILT demonstrates the inherent broadening of the ILT, manifest as an approximately half order of magnitude of the self-diffusion coefficient distribution. The attenuation function for BPEI_{25K} is slightly polydisperse and the distribution of diffusion coefficients has a width that seems to span 2 orders of magnitude, but given the inherent broadening of the ILT, this equates to a “manageable” distribution of molecular weight. Clearly, BPEI_{50K} and BPEI_{750K} are too broad to work with, but interestingly rather similar.

The polyelectrolyte character of these polymers- the effective charge versus pH behaviors were largely independent of molecular weight of the polymer but there were substantial differences in the effective charge between the modified and unmodified samples; the differences, manifested as a reduced charge at a given pH, increased with degree of hydrophobic modification. All the polymers – BPEI_{25K} – aggregate at high pH into elongated structures, but became less so with increasing charge. The presence of the hydrophobic groups make polymer more surface active and led to the formation of hydrophobic domains further self-association of the hydrophobic groups led to domains able to solubilise (hydrophobic) probe molecules.

3.5 Conclusion:

The self-diffusion coefficient distribution of different molecular weight PEI samples was analyzed using stretched exponential and CONTIN analysis as a function of polymer concentration. There is a substantial polydispersity in the polymer self-diffusion coefficient of BPEI_{25K}, BPEI_{50K} and BPEI_{750K} samples compare to BPEI_{2K} sample. Both the stretched exponential analysis and CONTIN were found to fit data equally well but, in particular, the width of the distribution obtained from CONTIN is more accessible compared to beta parameters.

The presence of the hydrophobes led to a lower effective charge on the polymer at any given pH, compared to the nonmodified samples. Analysis of the SANS data showed the propensity to form highly elliptical or rod-like aggregates at higher pHs, reflecting both the changes in protonation behaviour induced by the hydrophobic modification and hydrophobic interaction, but that these structures were disrupted with decreasing pH. On addition of SDS, the onset of the formation of polymer/surfactant complexes was insensitive to the degree of modification with the resultant PEI/SDS complexes resembling the size and shape of simple SDS micelles. Indeed, the presence of the SDS effectively nullifies the effects of the hydrophobe. Hydrophobic modification is therefore a viable option to tailor pH dependent properties.

3.6 References

1. Vicent, M. J.; Greco, F.; Nicholson, R. I.; Paul, A.; Griffiths, P. C.; Duncan, R., *Angewandte Chemie International Edition* 44, 4061 2005.
2. Siegel, R. A., *Advanced Polymer Science* 109, 233 1993.
3. Matsuda, A.; Sato, J.; Yasunga, H.; Osada, Y., *Macromolecules* 27, 7695 1994.
4. Uchida, M.; Kurosawa, M.; Osada, Y., *Macromolecules* 28, 4583 1995.
5. Evertsson, H.; Nilsson, S., *Carbohydrate Polymers* 40, 293 1999.
6. Thuresson, K.; Soderman, O.; Hansson, P.; Wang, G., *Journal of Physical Chemistry* 100, 4909 1996.
7. Li, Y.; Kwak, J. C. T., *Colloids and Surfaces A: Physicochemical and Engineering Aspects* 225, 169 2003.
8. Li, Y.; Kwak, J. C. T., *Langmuir* 18, 10049 2002.
9. Karlson, L.; Malmborg, C.; Thuresson, K.; Söderman, O., *Colloids and Surfaces A: Physicochemical and Engineering Aspects* 228, 171 2003.
10. Uemura, Y.; Hirayama, H.; Hatate, Y.; Macdonald, P. M., *Journal of Chemical Engineering of Japan* 34, 1211 2001.
11. Griffiths, P. C.; Paul, A.; Khayat, Z.; Wan, K. W.; King, S. M.; Grillo, I.; Schweins, R.; Ferruti, P.; Franchini, J.; Duncan, R., *Biomacromolecules* 5, 1422 2004.
12. Khayat, Z.; Griffiths, P. C.; Grillo, I.; Heenan, R. K.; King, S. M.; Duncan, R., *International Journal of Pharmaceutics* 317, 175 2006.
13. Zanta, M. A.; Boussif, O.; Adib, A.; Behr, J. P., *Bioconjugate Chemistry* 8, 839 1997.
14. Diebold, S. S.; Kurs, M.; Wagner, E.; Cotton, M.; Zenke, K., *Journal of Biological Chemistry* 274, 19087 1999.
15. Kircheis, R.; Blessing, R.; Brunner, S.; Wightman, L.; Wagner, E., *Journal of controlled release* 72, 165 2001.
16. Wojda, U.; Miller, J. L., *Journal of Pharmaceutical Sciences* 89, 674 2000.
17. Forrest, M. L.; Meister, G. E.; Koerber, J. T.; Pack, D. W., *Pharmaceutical Research* 21, 365 2004.
18. De Las Heras, A. C.; Pennadam, S. S.; Alexander, C., *Chemical Society Reviews* 34, 276 2005.
19. Tomas, M.; Klibanov, A. M., *Proceedings of the National Academy of Sciences of the United States of America* 99, 14640 2002.
20. Morris, K. F.; Johnson, C. S., *Journal of American Chemical Society* 115 1993.

Physicochemical characterization of thermoresponsive poly(N-isopropylacrylamide)-poly(ethylene imine) copolymers

4.1 Introduction

Polymers that exhibit discontinuous sometimes large changes in their physical states as a result of small changes in environmental conditions are called “responsive polymers”¹⁻³. Stimuli such as changes in temperature⁴⁻⁶, pH⁷, ionic strength, light⁸, electrical⁹ or magnetic fields have all been explored for a range of applications. In the field of drug delivery, pH and temperature responsive polymers are the two most viable routes¹⁰. The temperature sensitivity of thermoresponsive polymers generally depends on the strength of the H-bond interaction between polymer segments with water. Increasing the temperature causes a weakening of the hydrogen bond between polymer and water molecules leading ultimately to a macroscopically observable precipitation at a well-defined lower critical solution temperature (LCST).

Poly(N-isopropyl acrylamide) (PNIPAM), is arguably the most commonly studied polymer among those exhibiting temperature induced phase separation. The ease of preparation and the fact that the LCST is around 32-33°C^{11,12} i.e. close to body temperature are key facets for use as a potential drug carrier¹³⁻¹⁵. Further, the phase transition temperature can be tuned by incorporating hydrophobic/hydrophilic groups into the PNIPAM backbone^{12,16}. The phase transition temperature of PNIPAM is directly related to the solubility of this polymer in water. Addition of hydrophilic and hydrophobic groups on to the PNIPAM chain dramatically affects the thermal behavior of PNIPAM chains such that addition of hydrophilic groups increases the solubility of the polymer and opposite for the hydrophobic groups.

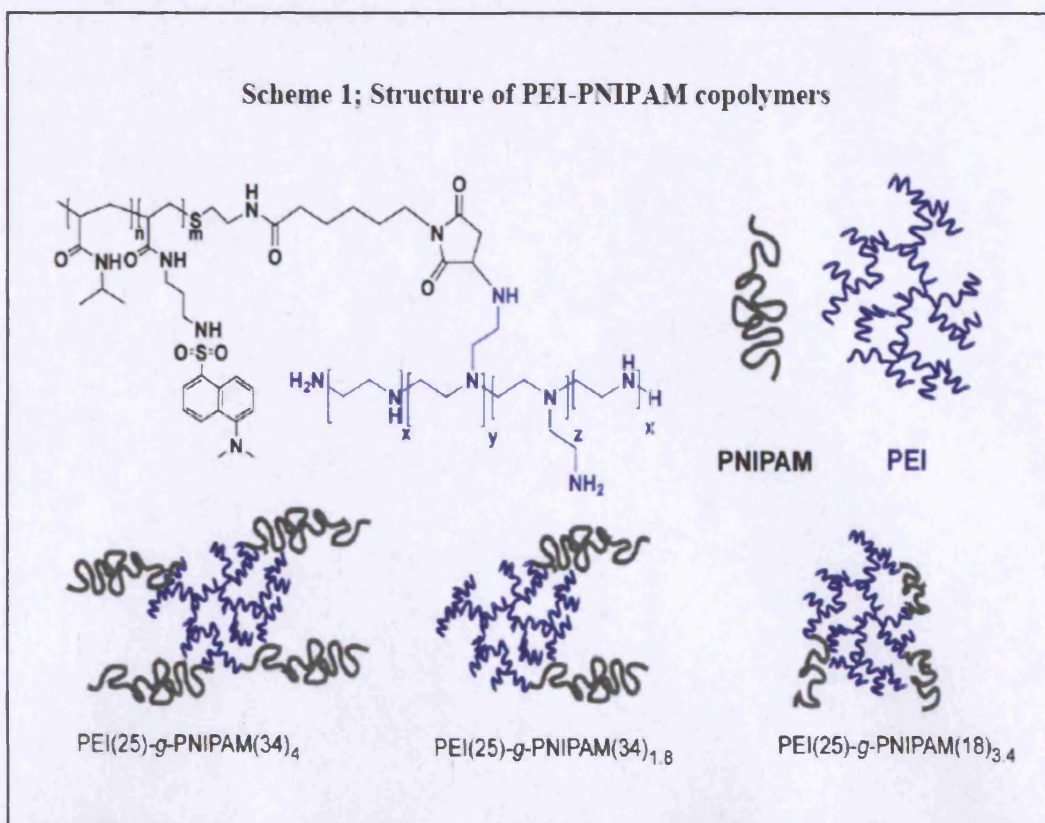
Poly(ethylene imine) (PEI) has a proven capability as a potential non viral gene delivery vector. PEI is positively charged at physiological conditions and its potency as a gene delivery vector could be due to a direct charged-based interaction with the various biological barriers¹⁷⁻²⁰. Further, PEI can influence

indirectly a particular cell or subcellular compartment, for example by acting as a proton sponge that cause ion influx and ultimately leads to a membrane rupture²¹. However, the membrane-disrupting properties are likely to be responsible for its unacceptable cytotoxicity²². To maintain the transfection efficiency of PEI but reduce the cytotoxicity, several groups have explored copolymers of PEI, either with a block of functional group that responds to temperature or pH. Generally the thermoresponsive element used has been PNIPAM, although other combinations of polycations and/or thermoresponsive segment have been used. Twaites *et al*¹⁰ have prepared a range of cationic polymers including derivatives of PEI containing short hydrophobic side chains (*i.e.*, octanamide), copolymers of PEI and PNIPAM, and polymers containing different amounts of NIPAM, DMAEMA and hexylacrylate (HA); copolymers of P(NIPAM-co-BMA-co-AAc) have been studied for the intestinal delivery of human calcitonin by Serres *et al*²³ and Ramkissoon Ganorkar *et al.*²⁴ and for the delivery of insulin by Kim *et al.*²⁵ whilst a series of water soluble poly(NIPAM-co-PEI) copolymers have been synthesised and tested for *ex-vivo* transfection of both HeLa cell lines and primary cells by Dincer *et al.*³ A range of spectroscopies and microscopies have been used to probe the interactions between these responsive copolymers and DNA over phase transitions, but characterization of polymer behaviour at molecular level detail remains incomplete.

The aim of this study was to quantify the physicochemical changes in the conformation of poly(N-isopropylacrylamide)-graft-poly(ethylene imine) (PNIPAM-g-PEI) thermoresponsive copolymers, and their interaction, by using small-angle neutron scattering (SANS) and pulsed-gradient spin-echo NMR (PGSE-NMR), to provide a fundamental understanding of their solution behavior, and a correlation with their biological activity.

4.2 Materials and methods

Three samples of PEI-g-PNIPAM copolymers (Scheme 4.1), kindly donated by Cameron Alexander (Nottingham), containing dansyl labels on the PNIPAM side chains have been examined here. The composition details are listed in Table 1. Briefly, preformed PNIPAM coils of molecular weight 17.6K g/mol or 34 K g/mol were grafted to a 25 K g/mol PEI core, with the grafting density and the molecular weight of the PNIPAM being the experimental variables. PNIPAM 20K g/mol and PEI 25 K g/mol were obtained from Sigma Aldrich. A PEI sample also obtained from Sigma Aldrich was dialysed (12KDa cut-off) against deionised water (4x1000ml) before use. Deuterated water (D_2O 99.9%) purchased from Aldrich was used to prepare all samples for SANS and NMR.



polymers	Number of pNIPAM coils per PEI coil	Molar mass of NIPAM Co-monomer/ gmol ⁻¹	Molar mass of PEI core/ gmol ⁻¹	Molar percentage pNIPAM by mass
PEI(25)-g- PNIPAM(34) ₄	4.0	34 000	25 000	85
PEI(25)-g- PNIPAM(34) _{1.8}	1.8	34 000	25 000	71
PEI(25)-g- PNIPAM(18) _{3.4}	3.4	17 600	25 000	70
PEI(25)	N/A	N/A	25 000	N/A
PNIPAM(20)	N/A	20 000	N/A	N/A

Table 4.1, Molecular Characterization of the PEI-PNIPAM Copolymers and their analogues

Polymer masses and grafts contents were calculated from NMR integral ratios and amine content via the 2,4,6-trinitrobenzenesulphonic acid (TNBS) assay and averaged as reported previously²⁶.

As an example, PEI(25)-g-PNIPAM(18)_{3.4} represents a copolymer made with PNIPAM coils with molecular weight 17.6K g/mol and PEI core of 25 K g/mol, with a effective grafting density of 3.4 PNIPAM chains attached on to the PEI core.

4.3 Results

4.3.1 PGSE-NMR

Measurements were conducted on a Bruker AMX360 NMR spectrometer using a stimulated echo sequence as described in the techniques chapter. This configuration uses a 5mm diffusion probe (Cryomagnet Systems, Indianapolis, IN) and a Bruker gradient (GRASP) spectroscopy accessory unit.

The self-diffusion coefficient D_s was extracted by fitting the integrals for a given peak to equation 4.1

$$A(\delta, G, \Delta) = A_0 \exp[(-kD_s)]^\beta \quad (4.1)$$

A is the signal amplitude in the absence (A_0) or presence of the field gradient pulses ($A(\delta, G, \Delta)$), and β is an exponent to quantify in a semiempirical fashion the linearity of the attenuation functions reflecting the width of the distribution of the self-diffusion coefficient.

$$k = -\gamma^2 G^2 \left(\frac{30\Delta(\delta + \sigma)^2 - (10\delta^3 + 30\sigma\delta^2 + 35\sigma^2\delta + 14\sigma^3)}{30} \right) \quad (4.2)$$

where γ is the magnetogyric ratio, Δ the diffusion time (240 ms), σ the gradient ramp time (250 μ s), δ the gradient pulse length (500 μ s < δ < 3ms), and G the gradient field strength (0.5 < G < 3 T/m).

4.3.1.1 Self-diffusion studies of PNIPAM

Figure 4.1 presents the typical raw PGSE-NMR attenuation plots for 1wt% PNIPAM 20 K g/mol at different temperatures. The signal decays slowly from 294K to 298K indicating difference of the self-diffusion coefficient is less within that temperature region. But from 302K to 308K regions, signal decays very fast confirming the collapse of extended conformation of PNIPAM molecules.

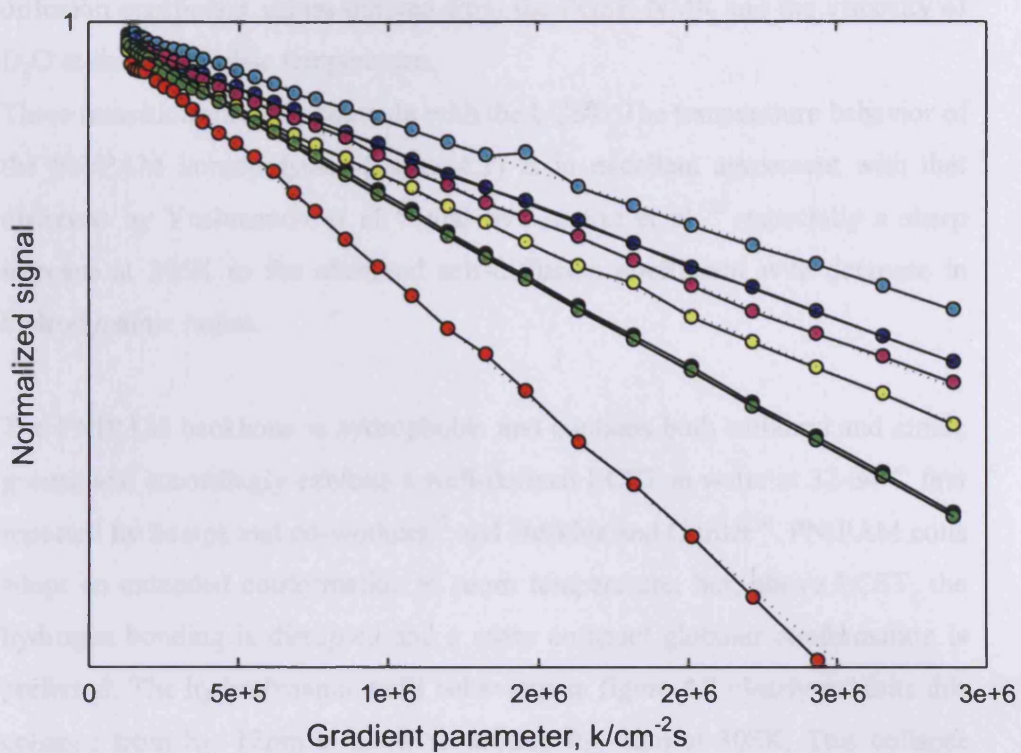


Figure 4.1; Typical attenuation functions and fits to a stretched exponential for 1wt% PNIPAM 20 K g/mol with different temperatures. 294 K, black; 298K, cyan; 302K, blue; 304K, pink; 306K, yellow; 307.5K, green; 308K, red.

Figure 4.2 illustrates self-diffusion coefficient behaviour of 20K g/mol PNIPAM as a function of temperature. Also presented the hydrodynamic radius (R_H) of PNIPAM determined from Stokes-Einstein equation using self-diffusion coefficient values derived from the PGSE-NMR and the viscosity of D_2O at the appropriate temperature.

These transitions broadly coincide with the LCST. The temperature behavior of the PNIPAM homopolymer (figure 4.1) is in excellent agreement with that observed by Yushmanov et al.²⁷ and by Larsson et al.,²⁸ especially a sharp increase at 306K in the observed self-diffusion coefficient with decrease in hydrodynamic radius.

The PNIPAM backbone is hydrophobic and contains both carbonyl and amide groups and accordingly exhibits a well-defined LCST in water at 32-34°C first reported by Scarpa and co-workers²⁹ and Heskins and Guillet³⁰. PNIPAM coils adopt an extended conformation at room temperature, but, above LCST, the hydrogen bonding is disrupted and a more compact globular conformation is preferred. The hydrodynamic radii behaviour in figure 4.2 clearly exhibits this collapse from $R_H \sim 12\text{nm}$ at 290K to around $R_H \sim 4\text{nm}$ at 308K. This collapse clearly starts to occur below the LCST, but all the samples are still homogeneous. i.e. no phase separation. Approaching the LCST, the collapse is much more pronounced and the solutions become opaque indicating phase separation. No D_s have been measured at higher temperatures due to phase separation.

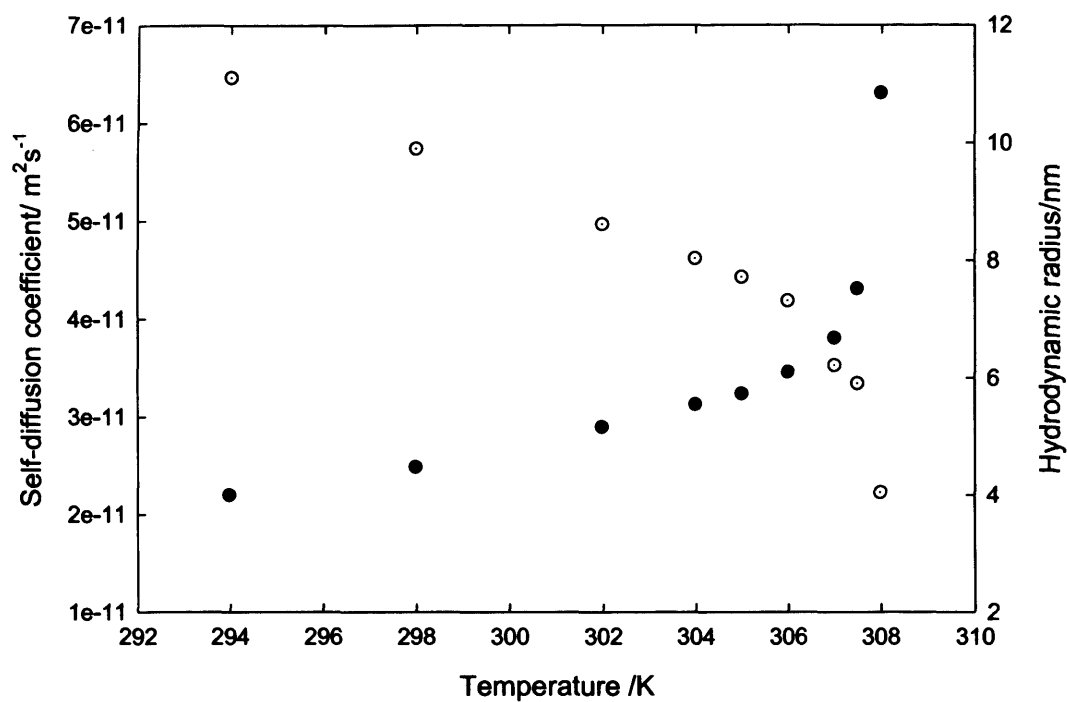


Figure 4.2; Temperature dependence of the self-diffusion coefficient of PNIPAM 20 K g/mol (filled circle) of 1wt%. Also presented is the corresponding hydrodynamic radius (open circle) of PNIPAM

4.3.1.2 Self diffusion studies of PEI-PNIPAM copolymers

4.3.1.2.1 Comparison of raw attenuation data of parent polymer (PEI 25K) and copolymers (PEI-PNIPAM)

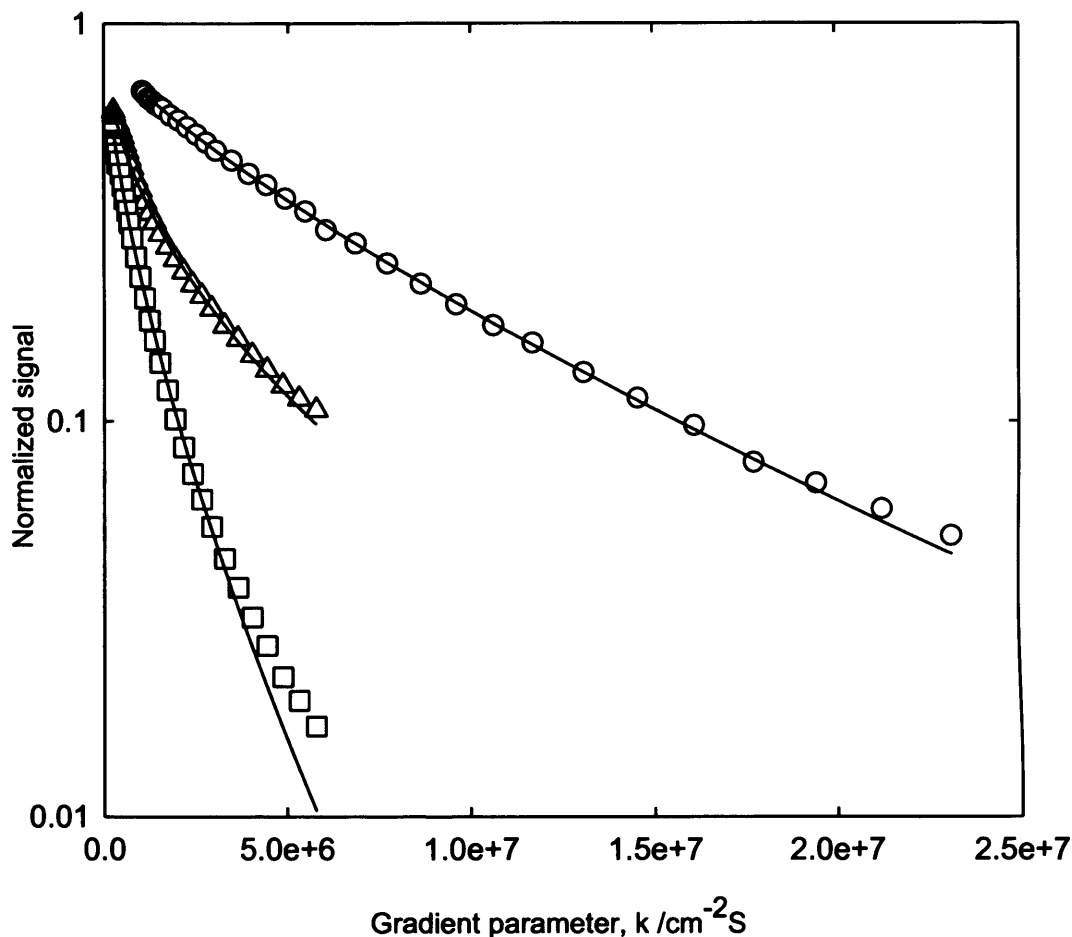


Figure 4.3, Typical attenuation functions and fits to a stretched exponential for polymer solutions with concentrations $C_{\text{polymer}}=4.5\text{wt\%}$ in D_2O and 298K; PEI 25K g/mol (\square), PEI(25)-g-PNIPAM(34)₄(\circ) and PEI(25)-g-PNIPAM(18)_{3.4} (Δ).

Figure 4.3 presents the typical raw PGSE-NMR attenuation plots plus associated fits for the branched PEI (BPEI) 25K g/mol and two copolymers, PEI(25)-g-PNIPAM(34)₄ (high PNIPAM content) and PEI(25)-g-PNIPAM(34)_{1.8} (low PNIPAM content). The signal decays fastest for the BPEI indicating that the copolymers have smaller self-diffusion coefficients thus PEI

has the smallest size. The signal for high-content PNIPAM copolymer decays slowest, reflecting it is the largest polymer.

The non-linearity of PGSE-NMR attenuation plots indicated that these polymers are polydisperse. The stretched exponential is a convenient method to quantify this polydispersity *via* the parameter β , although the methods such as CONTIN are feasible. β is largely independent of temperature and smallest (polydispersity greatest) for the parent PEI 25K ($\beta = 0.6 \pm 0.1$), but similar values are observed ($\beta = 0.8 \pm 0.1$) for the three copolymers.

4.3.1.2.2. Comparison of Self-diffusion coefficient and size of copolymers

The self-diffusion coefficients vs. temperature behavior for these copolymers are presented in figure 4.4, 4.5 and 4.6. Also shown are the associated hydrodynamic radii calculated from the Stokes-Einstein equation using the bulk viscosity of the D₂O at the appropriate temperature.

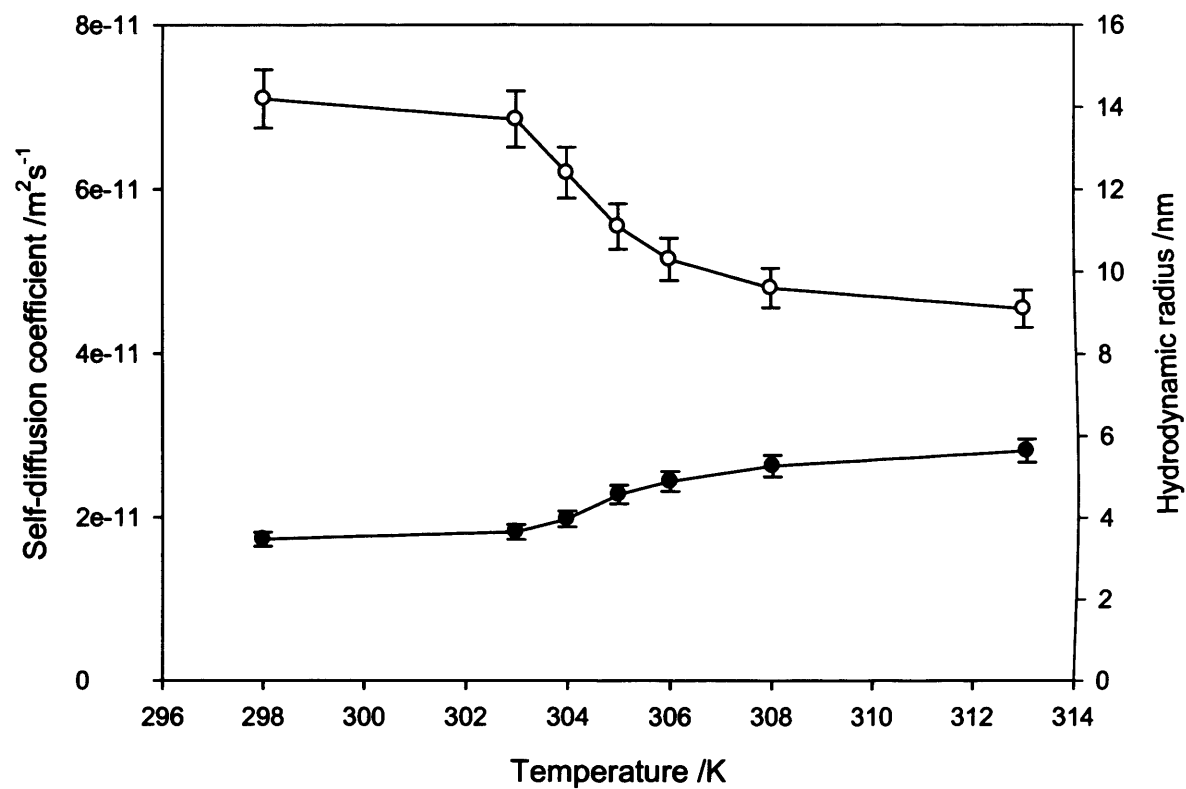


Figure 4.4; Temperature dependence of the self-diffusion coefficient (filled circles) and associated hydrodynamic radius (open circles) of copolymer PEI(25)-g-PNIPAM(34)₄ at a concentration $C_{\text{polymer}}=4.5\text{wt}\%$

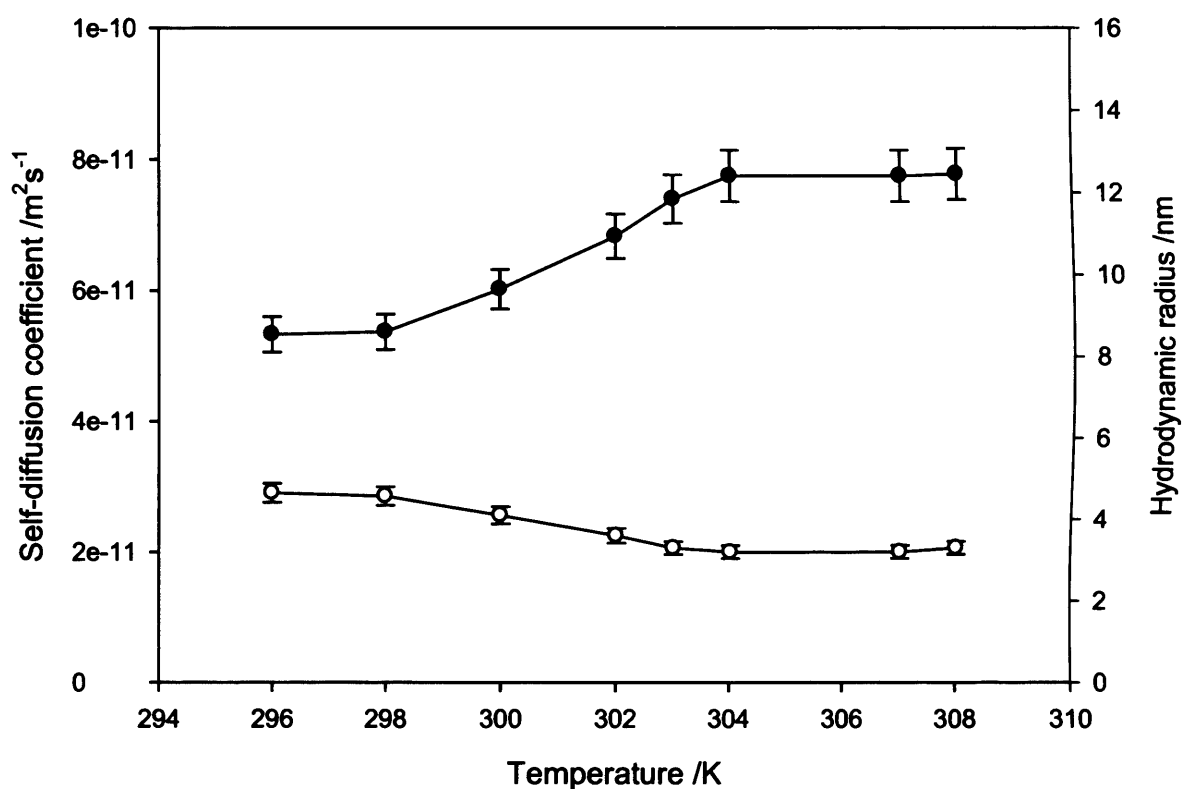


Figure 4.5; Temperature dependence of the self-diffusion coefficient (filled circles) and associated hydrodynamic radius (open circles) of copolymer PEI(25)-g-PNIPAM(34)_{1.8} at a concentration $C_{\text{polymer}}=4.5\text{wt}\%$

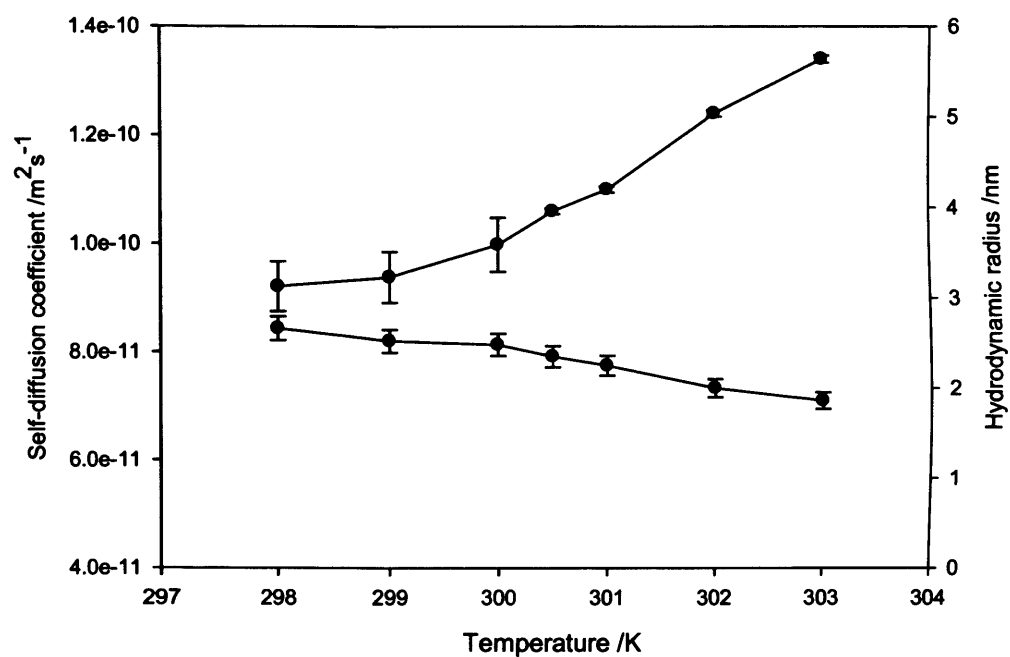


Figure 4.6; Temperature dependence of the self-diffusion coefficient (filled circles) and associated hydrodynamic radius (open circles) of copolymer PEI(25)-g-PNIPAM(18)_{3.4} at a concentration $C_{\text{polymer}}=4.5\text{wt}\%$

A similar trend was observed for all copolymers such that with increasing temperature, the self-diffusion coefficient increased, associated with a decrease in the hydrodynamic radius. But these transitions occur prior to the LCST. The behaviour of copolymer solutions was much similar to the behaviour of homopolymer. The collapse starts prior to LCST and all the solutions were still homogeneous and no phase separation observed.

The decrease in hydrodynamic radius is greater for PEI(25)-g-PNIPAM(34)₄ and PEI(25)-g-PNIPAM(34)_{1.8} than for PEI(25)-g-PNIPAM(18)_{3.4}, consistent with the higher molar mass of the PNIPAM moiety of the PEI(25)-g-PNIPAM(34)₄ and PEI(25)-g-PNIPAM(34)_{1.8} copolymers. This reflects the nature of the graft architecture and relative content of PNIPAM. Further, the hydrodynamic radii for PEI(25)-g-PNIPAM(34)₄ copolymers are greater than that for PEI(25)-g-PNIPAM(34)_{1.8}, reflecting the different number of PNIPAM chains grafted on to the PEI core. The comparative study shown in figure 4.7 indicates the change of hydrodynamic radius of the parent PEI and PNIPAM of similar molecular weights to that used in the copolymers. No significant change in the size of the PEI is observed but there is a substantial collapse of the PNIPAM on approaching its LCST.

One possible explanation is presence of PNIPAM “zone” around the PEI domain below LCST which is subsequently collapses above LCST inside the PEI regions. An alternative explanation is that these copolymers exist in solution as “interpenetrating” structures in which the PNIPAM domains lie on the inside even below LCST, as these may be more hydrophobic than PEI. In this situation collapse of PNIPAM above LCST would lead to the enhanced diffusivity observed above LCST in NMR and this is significant with higher molar mass PNIPAM grafts. PNIPAM chains collapse and coil to globule transitions are confirmed by PGSE-NMR and SANS data: the enhanced diffusivity of NMR data and the upturn at low Q in the scattering data of SANS (which discussed later in this chapter).

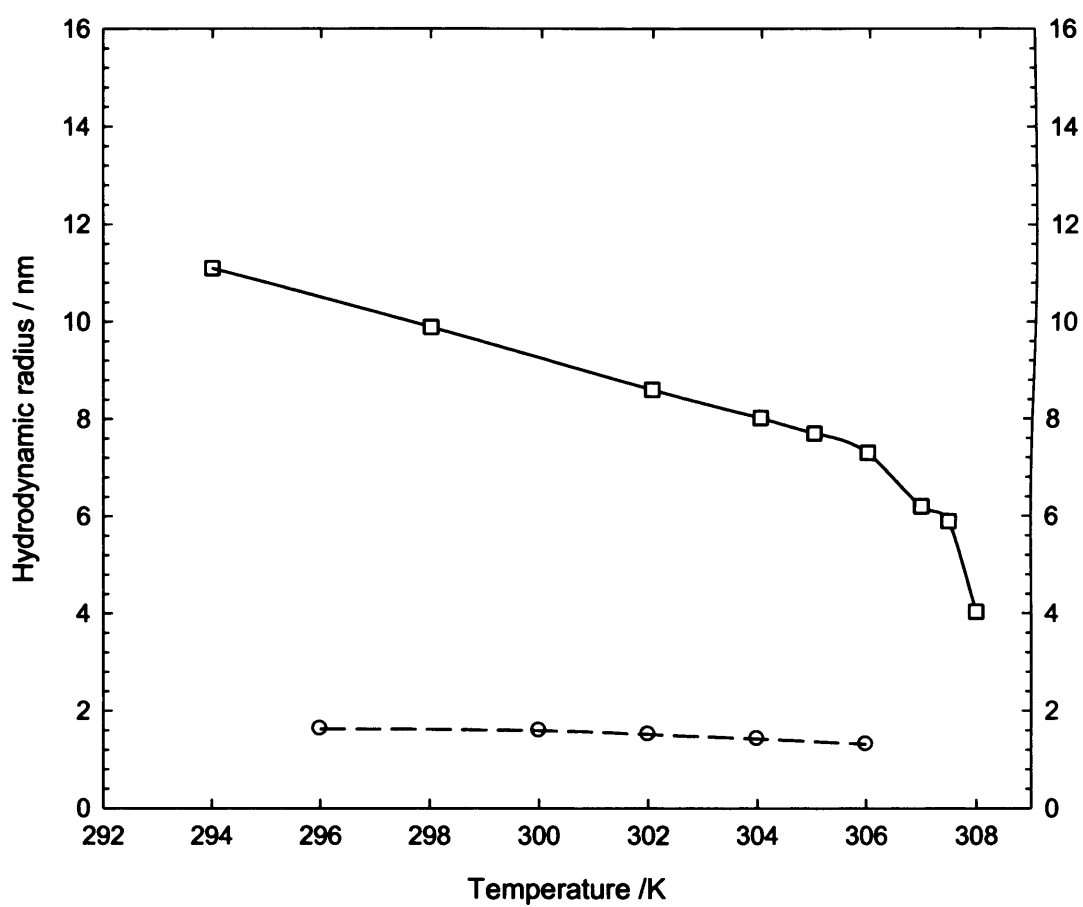


Figure 4.7; Temperature dependence of the hydrodynamic radius of homopolymers PEI 25 K g/mol (C polymer =1wt%) (O) and PNIPAM 20K g/mol (C polymer = 1wt%) (\square).

4.3.2 SANS

4.3.2.1 SANS of copolymers

Small-angle neutron scattering data and corresponding fits for the PEI 25K g/mol and for the copolymer with high PNIPAM content (PEI(25)-g-PNIPAM(34)₄) are presented in figures 4.8 and figure 4.9 respectively. At this point data is merely presented to facilitate a discussions of the differences between the various polymers, (PEI, figure 4.8; copolymers figure 4.9-4.13; and PNIPAM figure 4.14). The fits and associated underlying models are discussed in a later section.

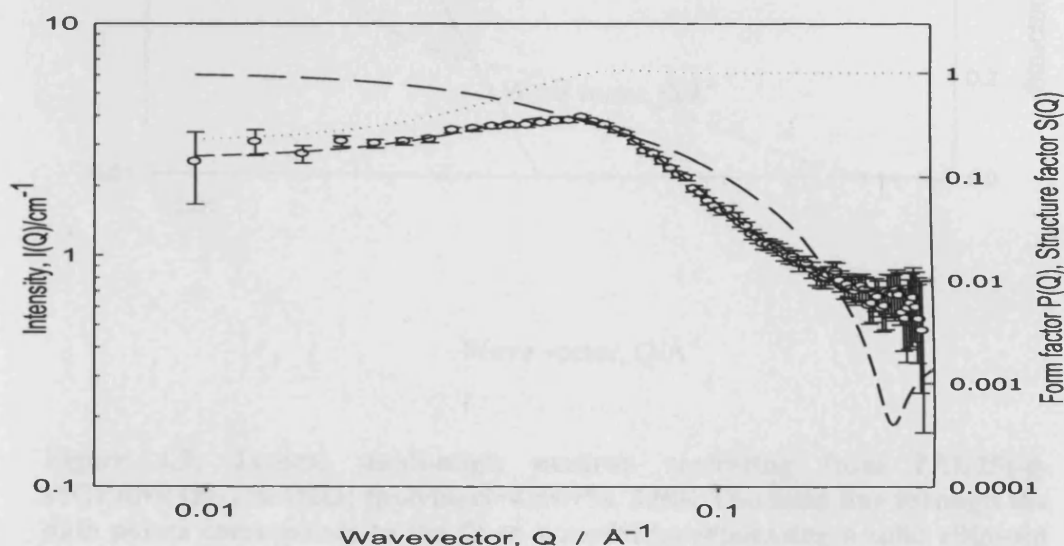


Figure 4.8; Fit (solid line) to an ellipsoidal scatterer model to the small-angle neutron scattering from PEI 25 K g/mol in a 5wt% aqueous solution at pH 7. The dashed line corresponds to the form factor $P(Q)$ and the dotted line the structure factor $S(Q)$. The ellipsoid form factor fit is parameterized with a radius of 22\AA and an ellipticity of 2.

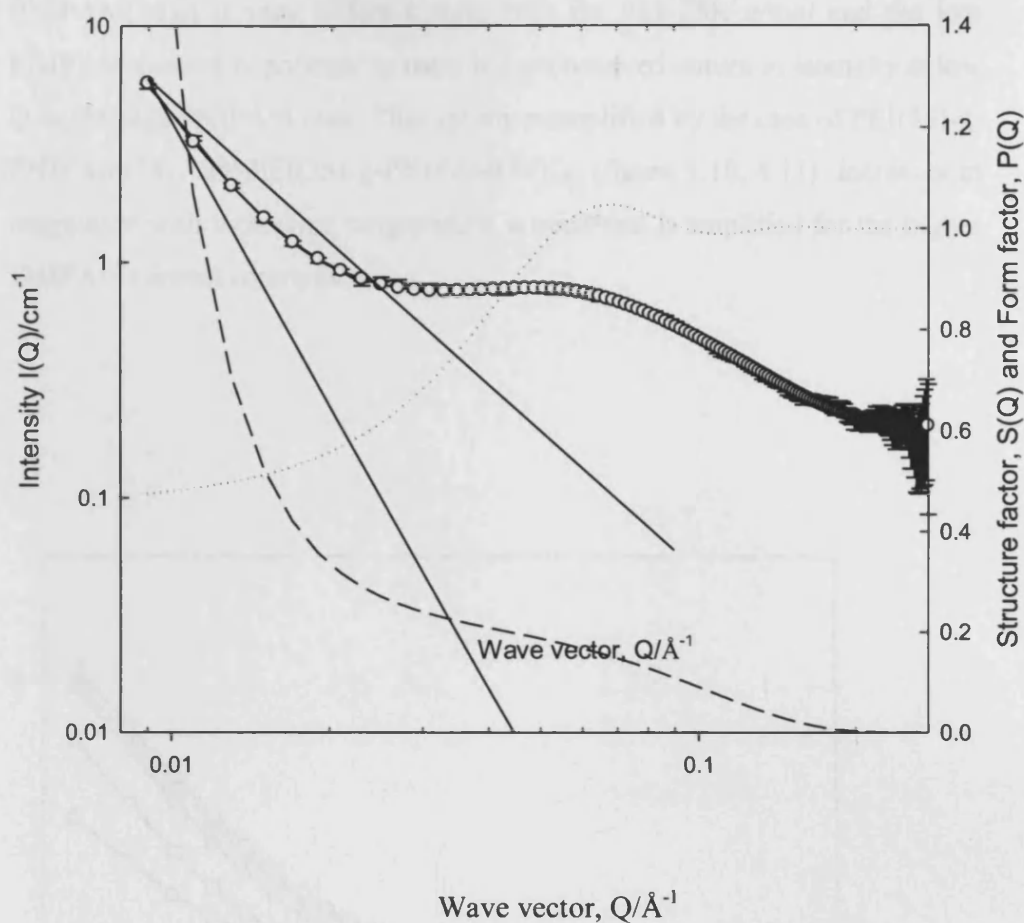


Figure 4.9; Typical small-angle neutron scattering from PEI(25)-g-PNIPAM(18)_{3,4} in D₂O; [polymer]=4.5wt%, 308K. The solid line through the data points corresponds to the fit to a model incorporating a solid ellipsoid form factor $P(Q)$, a Hayter-Penfold structure factor $S(Q)$ and a Q^{-m} power law. The dotted line corresponds to the structure factor $S(Q)$, the dashed line to a rescaled form factor Q^{-m} , while the two solid lines represent Simple Q^{-2} and Q^{-4} behaviours for comparison.

The scattering from the highest PNIPAM content copolymer (PEI(25)-g-PNIPAM(34)₄) is very different from both the PEI 25K g/mol and the low PNIPAM content copolymer as there is a pronounced upturn in intensity at low Q in the high PNIPAM case. This upturn exemplified by the case of PEI(25)-g-PNIPAM(34)₄ and PEI(25)-g-PNIPAM(34)_{1.8} (figure 4.10, 4.11) increases in magnitude with increasing temperature, a trend that is amplified for the higher PNIPAM content copolymers.

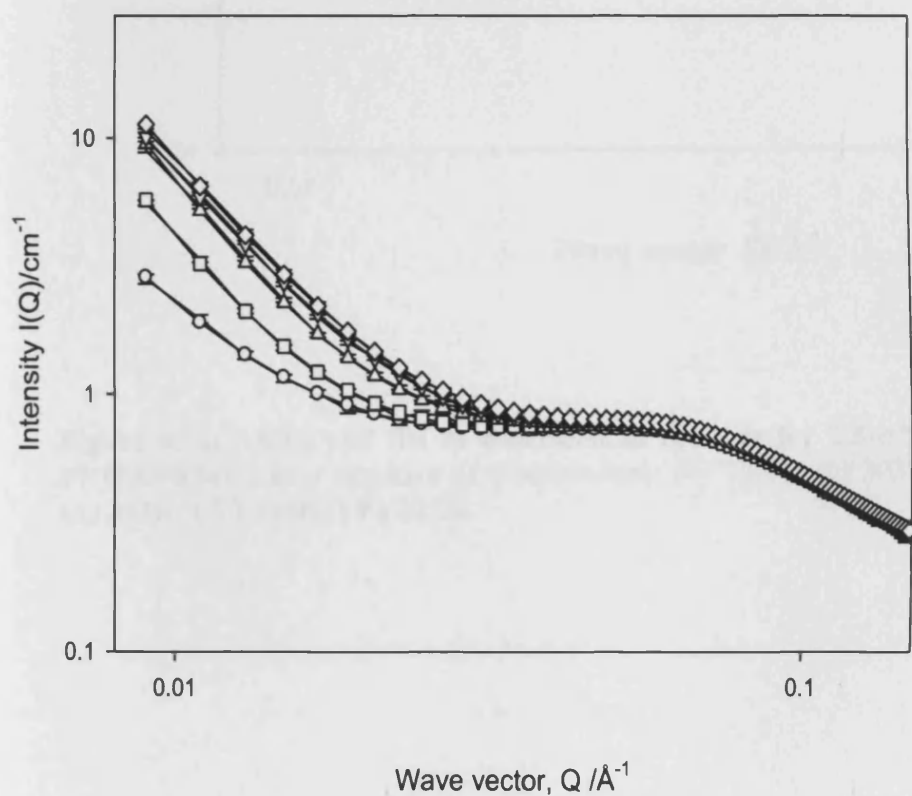


Figure 4.10; SANS and fits as described in the text for 4.5wt% PEI(25)-g-PNIPAM(34)₄ as a function of temperature: (O) 298K; (□) 308K; (Δ) 313K; (▽) 318K; (◇) 323K

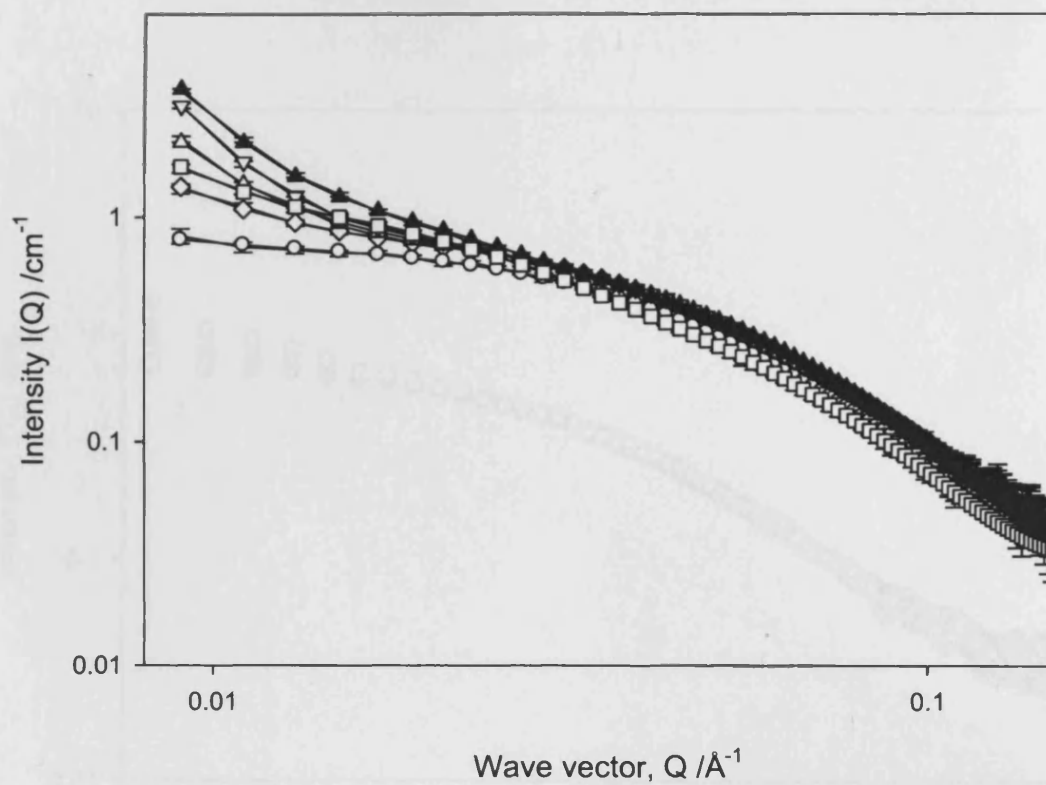


Figure 4.11; SANS and fits as described in the text for 2.5wt% PEI(25)-g-PNIPAM(34)_{1.8} as a function of temperature: (o) 298K; (◊) 303K; (◻) 308K; (Δ) 313K; (▽) 318K; (▼) 323K.

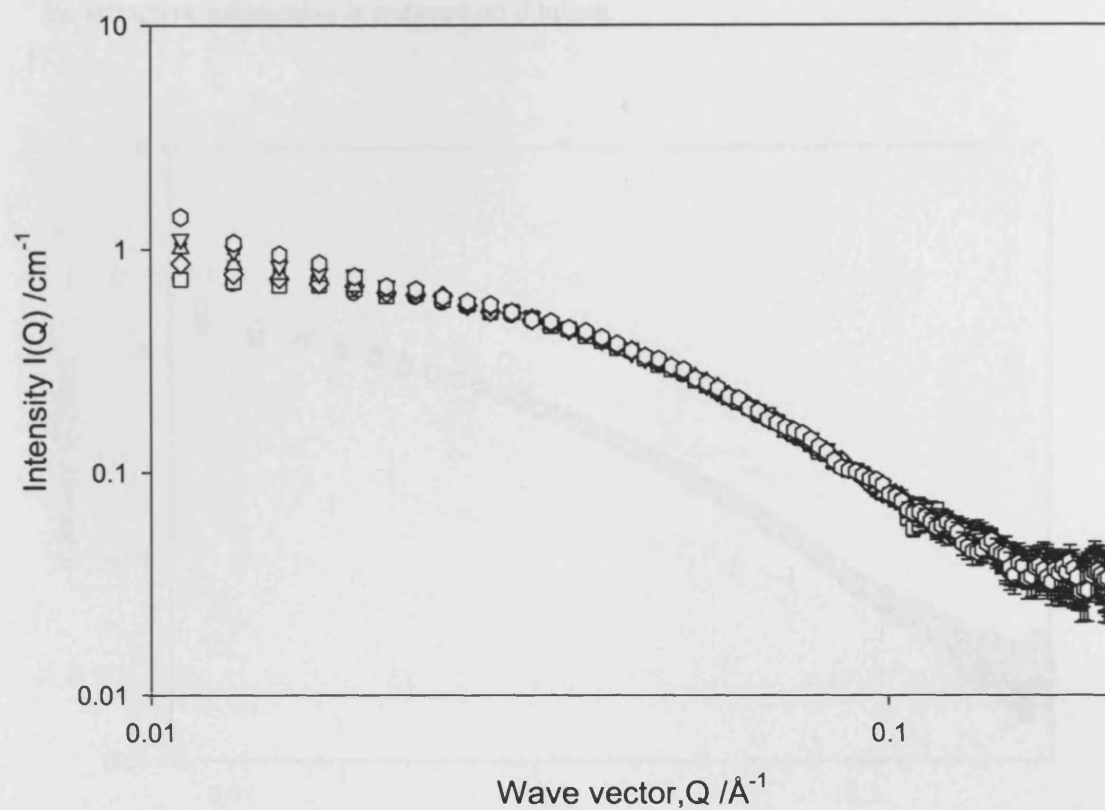


Figure 4.12; SANS from 2.5wt% PEI(25)-g-PNIPAM(34)₄ as a function of temperature: (o) 298K; (□) 303K; (◇) 308K; (Δ) 318K; (▽) 318K and (▼) 323K

Figure 4.12 illustrates scattering from 2.5wt% high PNIPAM content copolymer. The upturn with increasing temperature is less prominent compared with same copolymer with higher concentration (figure 4.10) indicating that the attractive interaction is reduced on dilution.

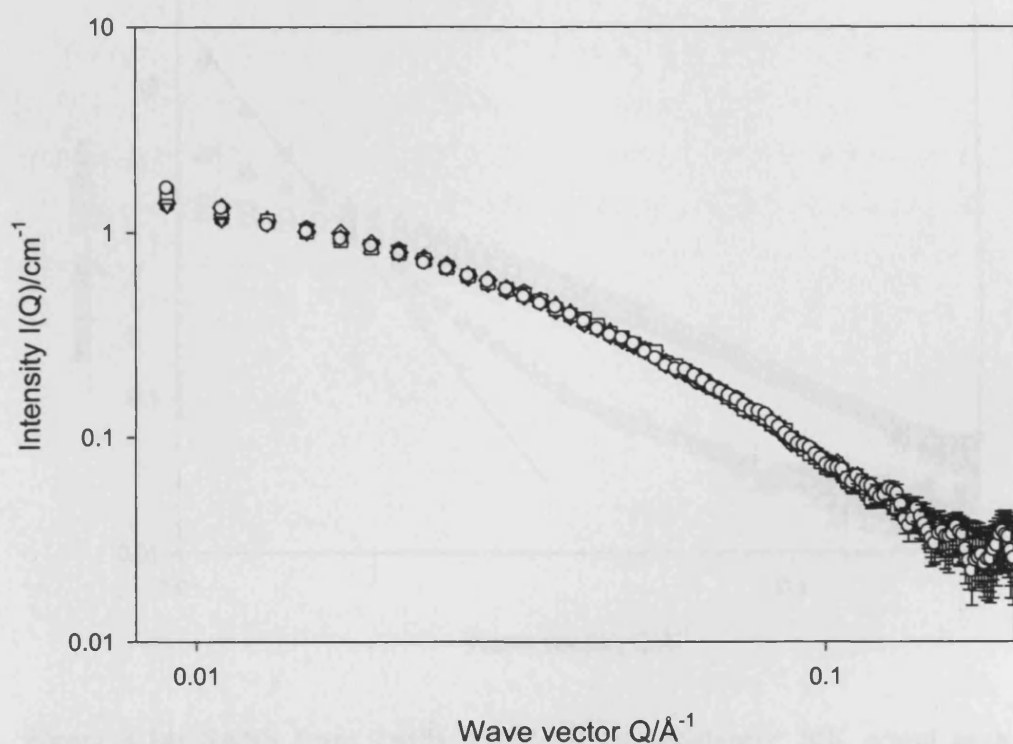


Figure 4.13; SANS and represent fit as described in the text for 2.5wt% PEI(25)-g-PNIPAM(18)_{3.4} as a function of temperature: (o) 298K; (□) 308K; (Δ) 313K; (▽) 318K; (▼) 323K.

With PEI(25)-g-PNIPAM(18)_{3.4} the upturn is less pronounced and it is clear the upturn at low Q is considerable weaker than that presented in figure 4.10 indicating that dilution weakens the cause of the upturn. Further this scattering is different from the PEI 25K g/mol.

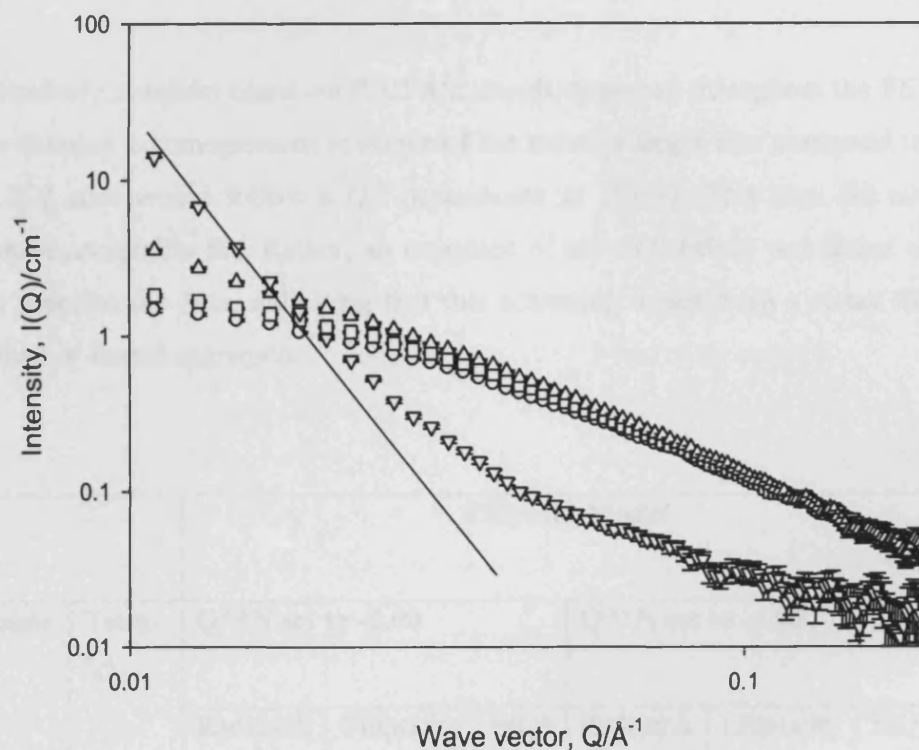


Figure 4.14; SANS from 2wt% PNIPAM homopolymer 20K g/mol as a function of temperature: open circles, 298K; squares, 303K; upward triangles, 308K; downward triangles, 313K. Also shown is a Q^{-4} term (solid line) and at the lower temperatures, fits to a Gaussian coil morphology ($R_g=6.3\text{nm}$, 298K; $R_g=6.5\text{nm}$, 303K)

An upturn in the low Q region is evident at higher temperatures for the PNIPAM homopolymer (figure 4.14) and at the highest temperature this follows a Q^{-4} dependence illustrating large solid-like particles. At lower temperatures the scattering may be adequately treated by a model invoking Gaussian coil morphology with radius of gyration $6.5 \pm 0.2\text{nm}$.

4.3.2.2 Modeling SANS data from copolymers

1) A thin shell of PNIPAM “adsorbed” onto the PEI core would be expected to demonstrate a Q^{-2} dependence, but such a simple power law term added to ellipsoidal form factor to describe the PEI core led to poor fits.

2) Similarly, a model based on PNIPAM chains dispersed throughout the PEI core forming a homogeneous scatterer of the same or larger size compared to the PEI core would follow a Q^{-4} dependence at low Q . This also did not produce acceptable fits. Rather, an exponent of $m = -3.0 (\pm 0.2)$ was found to best describe the data, indicating that this scattering arises from a rather ill-defined or fractal aggregate.

		Ellipsoid Model					
Sample	Temp. °C	Q**N set to -2.00			Q**N set to -4.00		
		Radius/Å	Ellipticity	S(Q)	Radius/Å	Ellipticity	S(Q)
PS-2-78B 2.5wt%	25	22	3.1	87	23	3.4	143
	30	23	3.1	105	23	3.3	126
	35	22	3.0	74	23	3.3	98
	40	23	2.4	70	23	3.0	90
	45	23	7.4	30	23	3.7	167
	50	23	6.2	84	24	5.0	153

Table 4.2; Parameters derived from fits of SANS

The visual appearance of the copolymers provides a clue to how to tackle this problem of rationalizing the upturn in scattering from PEI(25)-g-PNIPAM(34)₄ and PEI(25)-g-PNIPAM (34)_{1.8} copolymers. At high temperature, the copolymer solution was cloudy but not phase separated (no phase separation was observed over the temperature range studied here). With the lower PNIPAM copolymers no cloudiness was observed at higher temperatures, suggesting that the additional scattering at low Q does not arise due to PNIPAM moiety but could be due to the presence of transient aggregates via an attractive interaction.

Any model invoked to fit these data must capture a number of elements:

- 1) The morphology is that of an elongated otherwise ill-defined structure.
- 2) The interaction between the PEI segments is repulsive since the polymer bears a significant positive charge at this pH.
- 3) At higher temperature, the shape of the scattering varies due to “sticky” attractive interaction.

Considering the above facts, a model was invoked to fit SANS data that contains two structure factor terms representing interactions from the charged PEI core ($S(Q)_{\text{Hayter-penfold}}$) and a critical scatter term ($S(Q)_{\text{critical scatter}}$) to account for the upturn at low Q.

$$S(Q) = S(Q)_{\text{Hayter-penfold}} + S(Q)_{\text{critical scatter}} \quad (4.3)$$

For the $S(Q)_{\text{Hayter-penfold}}$ the effective radius, the charge on the polymer and the Debye screening length were allowed to change and constrained volume fraction. The critical scatter structure factor accounts for the attractive interaction observed as the temperature is increased;

$$S(Q)_{\text{critical}} = (S(Q=0)) / (1 + \xi^2 Q^2) \quad (4.4)$$

Where ξ is a correlation length and $S(Q=0)$ corresponds to the contribution that this $S(Q)$ component makes to the overall $S(Q)$.

The form factor for the PEI core ($P_{PEI}(Q)$) was tested against both solid ellipsoid form factors $P_{\text{ellipse}}(Q)$ or a rod form factor $P_{\text{rod}}(Q)$. $P_{\text{ellipse}}(Q)$ is parameterized by a radius R and ellipticity X :

$$P_{\text{ellipse}}(Q, R, X) = \int_0^{\pi/2} \phi^2(u) \sin \alpha d\alpha \quad (4.5)$$

$$\text{where } \phi(u) = 3 \frac{\sin(u) - u \cos(u)}{u^3} \text{ and} \quad (4.6)$$

$$u = QR[(\sin^2(\alpha) - X^2 \cos^2(\alpha))]^{1/2} \quad (4.7)$$

X corresponds to the ellipticity of the scatterer; $X < 1$ corresponds to an oblate ellipsoid (disc-like) whereas $X > 1$, the ellipse is a prolate (needle-like).

For N randomly oriented rods of length L and radius R , $P_{\text{rod}}(Q)$ is given by;

$$P_{\text{rod}}(Q) = N \int_0^{\pi/2} F^2(Q) \sin(\gamma) d\gamma \quad (4.8)$$

where

$$F(Q) = (\Delta\rho)^2 V \frac{\sin[1/2 QL \cos \gamma]}{1/2 QL \cos \gamma} \frac{2J_1(QR \sin \gamma)}{QR \sin \gamma} \text{ and } J_1 \text{ is the first order Bessel}$$

function of the first kind.

Thus, the overall intensity of scattered radiation, $I(Q)$, as a function of the wave vector, Q , is given by:

$$I(Q) = n_p V_p^2 (\rho_{\text{polymer}} - \rho_{\text{solvent}})^2 P_{PEI}(Q) [S(Q)_{\text{Hayter-Penfold}} + S(Q)_{\text{criticalscatter}}] + B_{\text{inc}} \quad (4.9)$$

The scattering from PEI 25K g/mol has been shown previously to be appropriately modeled with a charged ellipsoid morphology with radius = 22 Å with ellipticity $X=2$ and at higher pHs rod-like morphology³¹. Therefore, both

models were applied to the copolymer system; the solid rod model (Table 4.3) did not produce any satisfactory fits, but the ellipsoid gives marginally better fits (Table 4.4) and is more appropriate given the low degrees of ellipticity observed.

Solid rod model + αQ^{-m}					
Polymer	Radius /Å	Length/Å	S(Q)	α	m
PEI(25)-g- PNIPAM(18) _{3.4} $C_{\text{polymer}}=2.5\text{wt}\%$	No acceptable fits				
PEI(25)-g- PNIPAM(34) ₄ $C_{\text{polymer}}=4.5\text{wt}\%$	8	327	49	2.2e-5	-2.0
	8	300	40	0.0	-2.0
	8	153	40	1.3e-4	-2.0
	8	127	40	1.8e-4	-2.0
	8	126	40	1.8e-4	-2.0
	8	454	40	0.0	-2.0
PEI(25)-g- PNIPAM(34) ₄ $C_{\text{polymer}}=2.5\text{wt}\%$	No acceptable fits				

Table 4.3: Parameters derived from fits of SANS

polymer	temperature °C	radius Å	ellipticity	Hayter- Penfold structure factor radius/Å	charge e	inverse screening length/ Å ⁻¹	volume fraction	critical scatter Term S(Q=0) (± 0.1)	critical scatter termcorrelation length/(5%)
PEI(25)-g- PNIPAM(18) _{3,4} C _{polymer} =2.5wt%	all temperatures	26(±3)	4(±0.5)	50(±10)	5(±2)	0.04	0.025	n/a	n/a
PEI(25)-g- PNIPAM(34) ₄ C _{polymer} =4.5wt%	25	8	19	50	24.9	0.04	0.045	0.5	10
	30				24.0			0.5	10
	35				24.4			0.6	10
	40				26.5			0.7	30
	45				28.2			1.0	50
	50				30.0			2.3	100
PEI(25)-g- PNIPAM(34) ₄ C _{polymer} =2.5wt%	25	22	4.0	50	15.0	0.04	0.025	1.1	100
	30	23	4.9		16.2			1.3	100
	35	21	3.6		16.3			1.5	300
	40	22	4.1		16.2			1.8	300
	45	22	3.8		16.4			7.3	400
	50	21	4.8		16.8			8.2	500

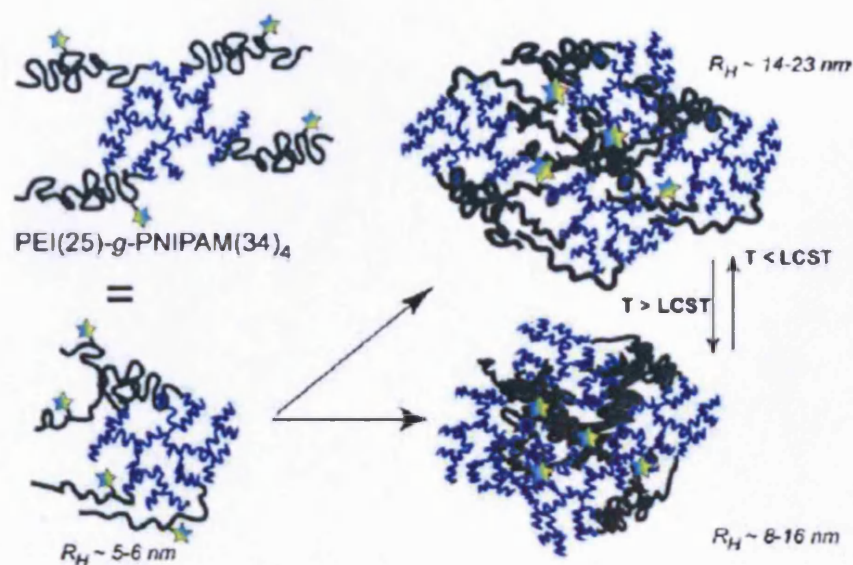
Table 4.4 Parameters derived from fits of SANS

The scattering at low Q from the higher PNIPAM content copolymers is increased with increasing temperature, but the curves superimpose at high Q implying no change in the size or shape. Further, the model fit parameters did not change with temperature, in all cases highly elliptical structures are present ($X=19$) with a minor radius of 9\AA . These fits are at extreme limits of an ellipsoid morphology, rod structure perhaps being much appropriate but the ellipsoid model has been used to facilitate a comparison with the other copolymers. The critical scatter term becomes important at higher temperatures, with the correlation length being comparable to the dimensions of scatterer. On diluting this copolymer, the upturn at low Q is much weaker and the correlation length longer as might be expected. As the critical scatter and ellipticity terms play a major role in scattering at low Q , subtle change of ellipticity can not be detected. However morphology of the scatterer is clearly less elliptical ($X=4$, $R=24\text{\AA}$) than at higher concentrations.

The morphology of the lower content PNIPAM copolymer is similar to dilute case of the higher PNIPAM content copolymer, namely $X=4$ and $R=24\text{\AA}$, and it is much closer to the morphology of PEI homopolymer, $X=2$ and $R=22\text{\AA}$.

4.4 Discussion

During this study a series of PEI-PNIPAM copolymers has been characterized by PGSE-NMR and SANS. Using PGSE-NMR, one is able to understand the nature of the graft architecture and content of PNIPAM, especially with the copolymers having higher molecular weight PNIPAM. The PNIPAM grafts are invisible in the SANS and only a gross but elongated morphology is accessible. An attractive interaction observed with high molecular weight PNIPAM copolymer at higher temperatures indicates that it is likely that the PNIPAM is forming “blobs” connected to a PEI core (Scheme2).



Scheme 2; Association and conformation changes of PEI(25)-g-PNIPAM(34)₄

Fluorescence spectroscopy of dansyl-labeled PNIPAM grafted to PEI indicates²⁶ that at concentrations above 0.05 mg mL^{-1} , the dansyl labels in the PNIPAM components of both copolymers were present in a nonpolar environment, even at temperatures below the LCST of PNIPAM. This implies some structural or associative order, most likely micelles³². The presence of the naphthyl labels attached to the fluorophore would not contribute for those structural changes as concentration of naphthyl groups are much lower compared to the PNIPAM component in the copolymer. In the solutions with lower concentration of copolymer, fluorescence data indicates the presence of nonpolar and hydrophilic domains below LCST but only hydrophobic domains above LCST. However self-diffusion coefficients from PGSE-NMR suggest that no large aggregation of polymers occurred during the experiment.

However, the collected insights from PGSE-NMR and SANS studies are very informative to construct a picture to explain the behavior of PNIPAM grafts around the phase transition temperature. One possible structure is the presence of a PNIPAM “zone” around the PEI domains below the LCST that collapses into the PEI above LCST. An alternative structure would be the presence of PNIPAM domains outside as well as inside the PEI interior below the LCST. Thus, the collapse of the PNIPAM chains above the LCST would cause the enhanced diffusivity observed in the NMR data. It should also be noted that, above LCST, the coil-to-globule transition and associated PNIPAM chain collapse are manifest in both the PGSE-NMR data and SANS data.

Biological activity correlation

Finally conformational and/or associative changes of these graft copolymers observed by the PGSE-NMR and SANS experiments offer a further insight into the gene delivery efficiencies of these materials, as shown in previous transfection studies³³. The copolymer with lower molecular weight PNIPAM grafts PEI(25)-g-PNIPAM(18)_{3,4} shown higher DNA binding in both myoblast and fibroblast cell lines below LCST, suggesting that this copolymer presents an exposed PEI region to solution, with the PNIPAM domains insufficient to mask the PEI segments, and indeed, the transfection efficiency of this copolymer in both cell lines was very similar to that of PEI both below and above LCST. However it was shown that copolymer with higher PNIPAM content has shown highest overall transfection efficiency when the temperature cycles were carried out around the LCST. Further increase in hydrophobic associations above LCST in polymer PEI(25)-g-PNIPAM(34)_{1,8} as evidenced by the PGSE-NMR and SANS data suggests that this polymer would have undergone different conformational changes than PEI(25)-g-PNIPAM(18)_{3,4} over the temperature cycles. Such conformational switching would lead to higher DNA affinity above LCST due to both electrostatic and hydrophobic interactions and less affinity towards the same because of the reduced hydrophobic interaction below LCSTs. The NMR and SANS have thus provided a unique insight into the solution behaviour which helps to understand not only the solution and associative behavior of these polymers but also the different transfection efficiencies of the copolymers in terms of graft density and length of the PNIPAM chains.

4.5 Conclusions

Gene delivery vehicles based on novel architecture synthetic polycations are being developed to improve transfection efficiency. Here we reported the effects of temperature on the size and interaction between copolymers based on a cationic core formed from poly(ethylene imine) (PEI) with differing thermoresponsive poly(N-isopropylacrylamide) (PNIPAM) grafts. An analysis of the temperature profile of the self-diffusion coefficients of the copolymer with longer chain PNIPAM grafts showed clear evidence of the collapse of the grafts with increasing temperature, same time scattering data showed some attractive interactions. For the shorter PNIPAM graft copolymer, there was a similar but much smaller collapse of the grafts with temperature, but this was not seen by SANS as a attractive interaction. The different temperature behavior of these two copolymers indicates subtle conformational rearrangements that result in various presentations of charged-core and hydrophobic moieties, central to the potential to control nucleic acid binding and cell transfection ability.

4.6 References

1. Hinrichs, W. J., *Journal of controlled Release* 60, 249 1999.
2. Yokoyama, M., *Drug Discovery Today* 7, 426 2002.
3. Dincer, S.; Turk, M.; Piskin, E., *Gene Therapy* 12, S139 2005.
4. Crassous, J. J.; Ballauff, M.; Drechsler, M.; Schmidt, J.; Talmon, Y., *Langmuir* 22, 2403 2006.
5. Tanaka, T., *Physical Review Letters* 40, 820 1978.
6. Hirokawa, Y.; Tanaka, T., *The Journal of Chemical Physics* 81, 6379 1984.
7. Osada, Y.; Okuzaki, H.; Hori, H., *Nature* 355, 242 1992.
8. Suzuki, A.; Tanaka, T., *Nature* 346, 345 1990.
9. Tanaka, T.; Fillmore, D.; Sun, S.-T.; Nishio, I.; Swislow, G.; Shah, A., *Physical Review Letters* 45, 1636 1980.
10. Twaites, B. R.; de las Heras Alarcon, C.; Cunliffe, D.; Lavigne, M.; Pennadam, S.; Smith, J. R.; Gorecki, D. C.; Alexander, C., *Journal of Controlled Release* 97, 551 2004.
11. Yu, T. L.; Lu, W.-C.; Liu, W.-H.; Lin, H.-L.; Chiu, C.-H., *Polymer* 45, 5579 2004.
12. Liu, R. C. W.; Cantin, S.; Perrot, F.; Winnik, F. M., *Polymers for Advanced Technologies* 17, 798 2006.
13. Hu, T.; You, Y.; Pan, C.; Wu, C., *Journal of Physical Chemistry B* 106, 6659 2002.
14. Kawasaki, H.; Sasaki, S.; Maeda, H.; Nishinari, K., *Langmuir* 16, 3195 2000.
15. Balamurugan, S.; Mendez, S.; Balamurugan, S. S.; O'Brien Ii, M. J.; Lopez, G. P., *Langmuir* 19, 2545 2003.
16. Sun, T.; Wang, G.; Feng, L.; Liu, B.; Ma, Y.; Jiang, L.; Zhu, D., *Angewandte Chemie - International Edition* 43, 357 2004.
17. Baker, A.; Saltik, M.; Lehrmann, H.; Killisch, I.; Mautner, V.; Lamm, G.; Christofori, G.; Gotten, M., *Gene Therapy* 4, 773 1997.
18. Abdallah, B.; Hassan, A.; Benoist, C.; Goula, D.; Behr, J. P.; Demeneix, B. A., *Human Gene Therapy* 7, 1947 1996.
19. Kunath, K.; von Harpe, A.; Fischer, D.; Petersen, H.; Bickel, U.; Voigt, K.; Kissel, T., *Journal of Controlled Release* 89, 113 2003.
20. Fischer, D.; Bieber, T.; Li, Y.; Elsasser, H. P.; Kissel, T., *Pharmaceutical Research* 16, 1273 1999.
21. Godbey, W. T.; Wu, K. K.; Mikos, A. G., *Journal of Controlled Release* 60, 149 1999.
22. Clamme, J. P.; Azoulay, J.; Mely, Y., *Biophysical Journal* 84, 1960 2003.
23. Serres, A.; Baudys, M.; Kim, S. W., *Pharmaceutical Research* 13, 196 1996.
24. Ramkissoon-Ganorkar, C.; Liu, F.; Baudys, M.; Kim, S. W., *Journal of Biomaterials Science, Polymer Edition* 10, 1149 1999.
25. Kim, Y. H.; Park, J. H.; Lee, M.; Kim, Y.-H.; Park, T. G.; Kim, S. W., *Journal of Controlled Release* 103, 209 2005.
26. Pennadam, S. S.; Ellis, J. S.; Lavigne, M. D.; Gorecki, D. C.; Davies, M. C.; Alexander, C., *Langmuir* 23, 41 2007.

27. Yushmanov, P. V.; Furo, I.; Iliopoulos, I., *Macromol. Chem. Phys.* 207, 1972 2006.
28. Larsson, A.; Kuckling, D.; Schonhoff, M., *Colloids Surf A* 190, 185 2001.
29. Scarpa, J. S.; Mueller, D. D.; Klotz, I. M., *J. Americal Chemical Society* 89 1967.
30. Heskins, M.; Guillet, J. E., *J. Macromolecular Science* 2 1968.
31. Griffiths, P. C.; Paul, A.; Fallis, I. A.; Wellappili, C.; Murphy, D. M.; Jenkins, R.; Waters, S. J.; Nilmini, R.; Heenan, R. K.; King, S. M., *Journal of colloid and interface science* 314, 460 2007.
32. Poncet-Legrand, C.; Winnik, F. M., *Polymer Journal* 33, 277 2001.
33. Lavigne, M. D.; Pennadam, S. S.; Ellis, J. S.; Yates, L. L.; Alexander, C.; Gorecki, D. G., *The Journal of Gene Medicine* 9, 44 2007.

Studies on the mechanism of interaction of a bioresponsive endosomolytic polyamidoamine with interfaces – phospholipid-rich micelle and vesicle surfaces

5.1 Introduction

Non-viral drug delivery vectors are the preferred modality for many potential treatments compared with viral vectors because of a better safety record and ease of manufacture¹, indeed a number of lipoplexes and polyplexes have been tested in clinical trials². However, further development of this technology must address one key challenge - non-toxic synthetic vehicles show poor delivery efficiencies, whereas those synthetic polymers that do demonstrate a viable delivery are often highly toxic *e.g.* poly-L-lysine (PLL)³, poly(ethylene imine) (PEI)⁴, pH-responsive polyanions such as the poly(ethylacrylic acid) (PEAAc), and related polymers⁵, and the cationic poly(amidoamine) (PAMAM) dendrimers^{6,7}.

A large family of poly(amidoamine) (PAA) polymers has now been synthesised, for a range of different biomedical applications including heparin binding in blood perfusion filters, metal ion complexation, targetable anticancer conjugates and of particular importance here, as endosomolytic polymers for cytosolic delivery⁸. The structure of the linear poly(amidoamine)s (PAAs)⁹⁻¹¹ has been systematically optimised to give relatively non-toxic polymers (IC₅₀ values > 1 mg/ml over 72 h) that are non-haemolytic at pH 7.4, but show pH-dependant breakage of model membranes¹¹. Amphoteric structures *e.g.* ISA23⁸, have been shown to not accumulate in the liver after intravenous injection, and target tumours by the enhanced permeability and retention (EPR) effect¹¹. The most viable of these polymers - ISA23 - is able to deliver genes¹² and promote cytosolic access of the non-permeant toxins ricin A chain and gelonin¹³. Quantitative subcellular fractionation studies have elaborated the trafficking of this polymer, and that after being transiently retained in the endosomal compartment, vesicles isolated from the lysosomal compartment demonstrated enhanced membrane permeability¹⁴. The permeabilising ability of these polymers was subsequently shown to be sensitive to the nature of the polymer counterion¹⁵.

Notwithstanding this progress, the non-permeant delivery efficacy is still very poor requiring many polymer molecules to deliver a single toxin molecule. To facilitate the identification of more effective PAA structures, study began to define more carefully the physicochemical properties of the hydrochloride salt form of ISA23 - ISA23.HCl specifically, the solution conformation which indicated a pH induced coil expansion; ISA23.HCl had a radius of gyration (R_g) of $\sim 2\text{nm}$ at $\text{pH} = 7$ which increased to 8nm $\text{pH} = 3$, although there was a tendency for the polymers to aggregate at higher pHs. Further, it was shown that ISA23.HCl interacted strongly with model anionic surfactant micelles (SDS) at low pH, resulting an elongation of the micelle with the polymer “wrapped around” the micelle surface. There was however no interaction at high $\text{pH}^{8,9,16}$. These observations were rationalised in terms of the relative charge of the polymer and the surface, and the presence of a significant hydrophobic effect.

Here, these studies are extended to phospholipid-rich interfaces, quantified predominantly by probe molecules or labels either solubilised into the self-assembled structures or grafted to the polymer. The use of nitroxides as spin-probes or spin-labels for the analysis of localised interactions *via* changes in the microenvironment of the probe builds on the fact that the value of hyperfine coupling (a_N) of the radical depends critically on the medium in which the nitroxide is dissolved. Nitroxide radicals are π radicals, in which the unpaired electron occupies a π^* orbital between the oxygen and nitrogen atoms. As such, the radical is frequently represented as a resonance structure, as shown in figure 2.12. In solvents with high polarity, the resonance favours the pseudo ionic structure (left) where the electron spin is largely centred on the nitrogen atom, thereby resulting in a larger value of nitrogen hyperfine coupling. Particularly high values of a_N are obtained in protic solvents that are hydrogen-bond donors. The molecular level information, combined with the sensitivity of electron paramagnetic resonance, provides an unique insight into the polymer/interface interaction.

5.2 Material and methods

5.2.1 Materials

The spin-probes 16-doxyl stearic acid methyl ester (16-DSE) and 5-doxyl stearic acid methyl ester (5-DSE) were of analytical grade and obtained from Fluka . Two samples of polymer were employed; ISA23.HCl ($M_w = 24,000 \text{ g mol}^{-1}$ polydispersity 1.5) and a lower molecular weight ($M_w = 10,600 \text{ g mol}^{-1}$, polydispersity 1.55) spin-labelled analogue (ISA23HCl-TEMPO) (Scheme 5.1) kindly donated by Paolo Ferruti (University of Milan, Italy). This polymer is analogous to ISA23 but has been modified by the inclusion of 10mol% of TEMPO monomer. Obviously this will perturb the behaviour of the polymer, such that the labeled-ISA23 is rather different to non-labelled ISA23. The literature¹⁷ also calls this “ISA23” which is less than ideal, and we also use this nomenclature with the stated caveat. Sodium dodecylsulfate (SDS) (Aldrich) was purified by repeated recrystallization from ethanol until no impurities could be detected as a local minimum around the critical micelle concentration (CMC) in the surface tension data. The phospholipids 1-palmitoyl-2-hydroxy-*sn*-glycero-3-phosphocholine (*lyso*-PC), 1,2-dipalmitoyl-*sn*-glycero-3-phosphocholine (DPPC), 1,2-dipalmitoyl-*sn*-glycero-3-[phosphor-L-serine] (sodium salt) (DPPS) & 1,2-dipalmitoyl-*sn*-glycero-3-phosphoethanolamine (DPPE) were obtained from Avanti Polar Lipids Inc., (USA) as a powder and used without further purification. 1,2-diheptanoyl-*sn*-phosphatidylcholine (DHPC) was obtained from Sigma Chemical as a solution in chloroform.

5.2.2 Sample Preparation

5.2.2.1 Micellar Solutions

Micellar solutions of spin-probe were prepared by addition of 5ml of SDS (25mM in pure water) to a glass vial containing an aliquot of pre-dried spin-probe (16-DSE or 5-DSE 0.04mg/ml) ethanol solution, mixed and allowed to equilibrate. The pH was adjusted by addition of 0.1M HCl solution.

The polymer *plus* surfactant series were prepared in a similar fashion by mixing stock solutions of SDS (50mM, 2.5ml) and ISA23.HCl (0.4 wt/v% 2.5ml) to a glass vial containing pre-dried spin-probe ethanol solution such that the final concentrations were 25mM SDS and 0.2 w/v% ISA23.HCl. The pH was adjusted by addition of 0.1M HCl solution

SDS/DHPC micellar solutions were prepared by weighing the required mass of solid or chloroform solution into glass vials containing pre-dried spin-probe ethanol solution, evaporating the chloroform and the subsequent addition of 100mM SDS solution. Finally, the polymer solution (0.4wt/v%) was added.

5.2.2.2 Vesicle preparation

The widely used freeze/thaw extrusion method^{18,19} was used to prepare liposomes whose composition mimicked - at least to a first approximation - the plasma, endosomal and lysosomal membranes (Table 5.1). Stock phospholipid solutions were prepared from DPPC in chloroform (10mg/ml), DPPE in chloroform (4mg/ml) and DPPS in 3:1 ratio of chloroform: methanol (2mg/ml).

To prepare the liposomes the required amounts of each phospholipid were placed in a round bottom flask, to which 1ml of chloroform was added and thoroughly mixed. The chloroform was evaporated using a rotary evaporator, to give a phospholipid film around the bottom of the flask. The film was left to evaporate for a further 60 min, at 25°C. Then 2 ml of PBS, at pH 7.4, was added, and the film left to hydrate in a water bath (70°C) for around 50 min. The hydrated film was then subjected to 5 freeze/thaw cycles (5 min freezing in liquid nitrogen, 2 min thawing in water at room temperature and 5 min vortex mixing). Finally, the liposome mixture was extruded first through a 200nm polycarbonate membrane (ten times) and secondly through a 100nm polycarbonate membrane (twenty times). The spin-probe was incorporated into these vesicles *via* simple mixing as in the micelle case. Finally the pH was adjusted to the desired value the

microstructure, size and stability of the vesicles using small-angle neutron scattering and photon correlation spectroscopy (PCS)²⁰.

5.2.2.3 Hydrophobically modified PEI

Samples of hydrophobically modified PEI were kindly donated by Sarah Waters and they were prepared at 2 statistical degrees of loading; 1 hydrophobe per 100 EI units, the second higher at 1 hydrophobe per 10 EI units. These materials are denoted HM_{1%}BPEI_{25 K} and HM_{10%}BPEI_{25 K} where the B underlines the fact that these polymers are hyperbranched, the subscript “25 K” indicated the molecular weight of the PEI and HM_{1%} the degree of hydrophobic modification.

5.2.2.4 Hydrophobically modified ISA23-TEMPO

The hydrophobically modified ISA23-TEMPO was prepared using epoxydodecane and loading capacity was 1 hydrophobe for every 10 ISA23 units. ISA23-TEMPO and modifying agent were separately dissolved in ethanol and mixed. The resultant mixture was stirred at room temperature for one day. Finally, the mixture was extracted with chloroform in order to remove unreacted epoxydodecane. The residual was freeze dried.

5.2.3 Electron Paramagnetic Resonance

The EPR spectra reported were recorded on a Bruker EMX spectrometer fitted with a high-sensitivity cavity (ER 4119HS) operating at X-band frequencies (~ 9.5 GHz). All spectra were recorded at room temperature using 100 kHz field modulation and 10 mW microwave power. The experimental EPR lines were analysed in terms of a Lorentzian-Gaussian sum function using the program LOWFIT²¹, to yield the position of the resonance field of each of the three EPR lines to a precision of few milligauss, and also separates the Lorentzian and Gaussian contributions to the line shapes. Small changes in peak intensity arising due to slight changes in instrument gain were removed by normalizing each spectrum to the maximum peak intensity in each spectrum.

5.2.3.1 Polarity determination

The polarity sensed by a spin-probe can be detected by measuring its EPR spectrum. Hyperfine coupling results from the magnetic interactions between the electron and nuclear spins of atomic neighbours²². In the case of aminoxyl radicals, hyperfine coupling to the ^{14}N yields results in three possible nuclear spin states ($m_I = -1, 0, +1$). Transitions between these spin states, as governed by the EPR selection rules ($\Delta m_I = \pm 1, \Delta m_I = 0$) thereby gives rise to three lines in the EPR spectrum (see for example figure 2.11). The hyperfine coupling constant (A_o) is the distance between the nuclear transitions, measured in mT or MHz. For simplicity, in the case of hyperfine coupling arising from interaction of an unpaired electron with a nitrogen nucleus A_o is often determined as half the separation of the two outermost lines. The hyperfine coupling constant, a_N , varies with the local polarity in the vicinity of the aminoxyl group. The polarity is defined by a hydration index, H , which is the volume fraction of OH dipoles in the spin-probe neighbourhood. Due to their polarity nitroxide radical, spin-probes are believed to be localized in the micelle/water interface, and hence the water associated with micelle surface.

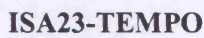
It has been shown²³ that the spacing, A^+ , between the $m_I = -1$ and $m_I = 0$ transitions in the EPR spectrum is a more reliable probe of polarity, and is a linear function of the hydration index H as follows,

$$A_+(H) = c + mH \quad (5.1)$$

where for 16 DSE, $c = 14.21$ Gauss, $m = 1.52$ units and $c = 15.08$, $m = 1.81$ for the TEMPO labelled polymer.



ISA23



Scheme 5.1; Chemical structures of polymers used in this chapter

5.3 Results and discussion

5.3.1 Sodium dodecyl sulphate (SDS) as model surface

Preliminary studies were carried out using simple SDS micelles to investigate the impact of pH on interaction of spin-probe and spin-labelled polymer at different pH.

5.3.1.1 Raw EPR spectra of ISA23.HCl with 16-DSE and 5-DSE as spin probes.

Pairwise spectral comparisons of the effect of pH on the EPR spectrum of the spin-probe (16-DSE or 5-DSE) in the presence and absence of the polymer are therefore particularly informative. Figure 5.1 reproduces early data for 16-DSE solubilised into SDS micelles at different pH and same time figure 5.2 illustrates the same with different spin probe- 5-DSE. With both spin probes interaction is prominent at low pH.

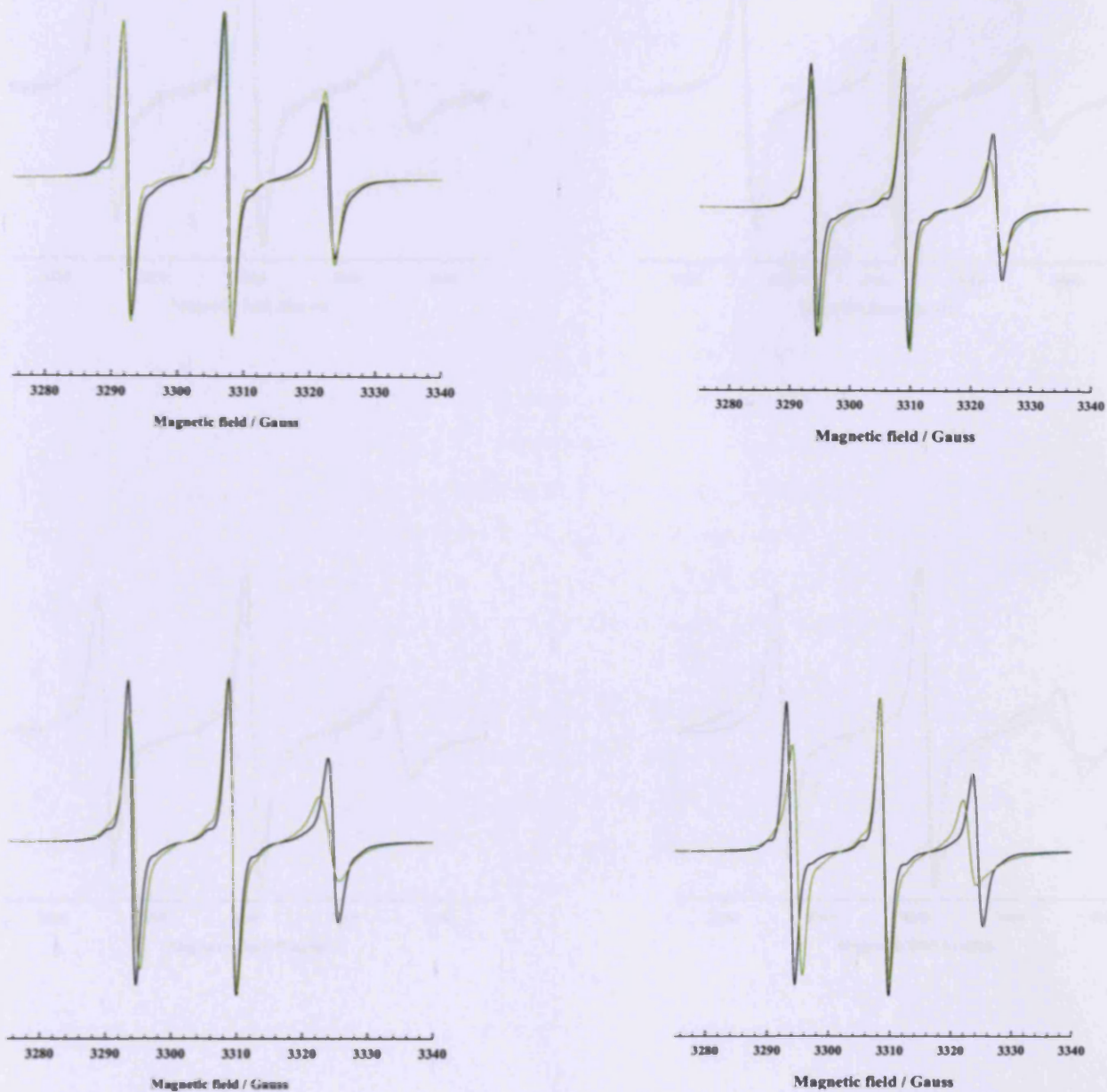


Figure 5.1; The effect of pH on the EPR spectrum of 16-DSE solubilised in 25mM SDS (black) and presence (green) of 0.2wt% ISA23.HCl solution at pH 7.4 (upper panel left), pH 6.5 (upper panel right), pH 5.5 (lower panel left) and pH 4.0 (lower panel right).

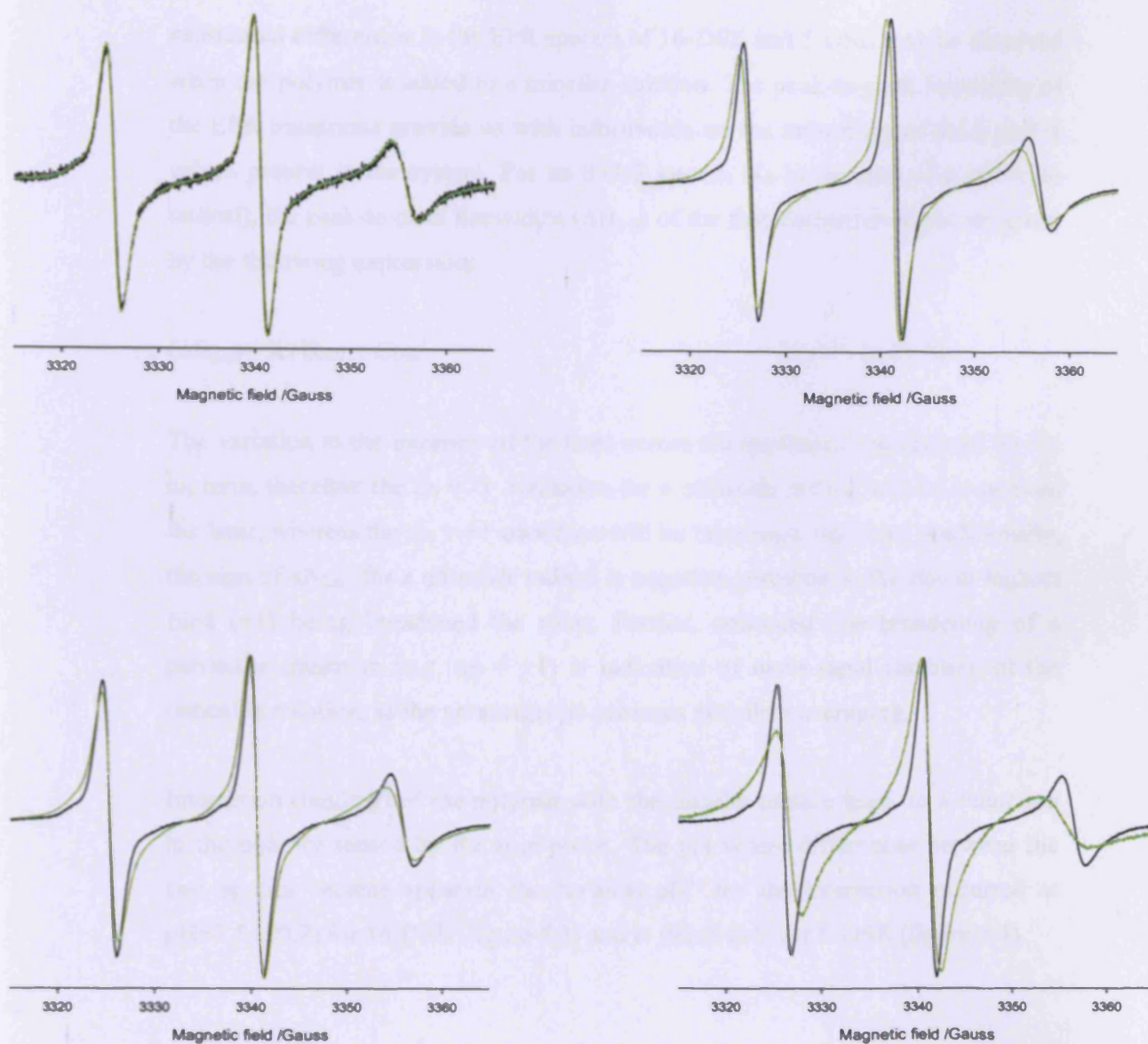


Figure 5.2; The effect of pH on the EPR spectrum of 5-DSE solubilised in 25mM SDS (black) and presence (green) of 0.2wt% ISA23.HCl solution at pH 9 (upper panel left), pH 7.2 (upper panel right) , pH 5.5 (lower panel left) and pH 3.0 (lower panel right).

substantial differences in the EPR spectra of 16-DSE and 5-DSE may be observed when the polymer is added to a micellar solution. The peak-to-peak linewidths of the EPR transitions provide us with information on the anisotropy of the g and A values present in the system. For an $S=1/2$ system (as in the case of a nitroxide radical), the peak-to-peak linewidths (ΔB_{p-p}) of the first derivative signal are given by the following expression;

$$(\Delta B_{p-p}) = A + Bm_l + Cm_l^2 \quad (5.2)$$

The variation in the intensity of the lines across the spectrum is dominated by the m_l term, therefore the $m_l = -1$ transition for a nitroxide radical will be broadened the least, whereas the $m_l = +1$ transition will be broadened the most. Additionally, the sign of $aN_{(iso)}$ for a nitroxide radical is negative, resulting in the line at highest field (+1) being broadened the most. Further, enhanced line-broadening of a particular transition (e.g. $m_l = +1$) is indicative of more rapid tumbling of the radical in solution, as the paramagnetic achieves complete averaging.

Interaction (binding) of the polymer with the micelle surface leads to a reduction in the polarity sensed by the spin-probe. The pH where differences between the two spectra became apparent the “critical pH” for the interaction occurred at $pH=7.5 (\pm 0.2)$ for 16-DSE (figure 5.3) and at $pH=5 (\pm 1)$ for 5-DSE (figure 5.4).

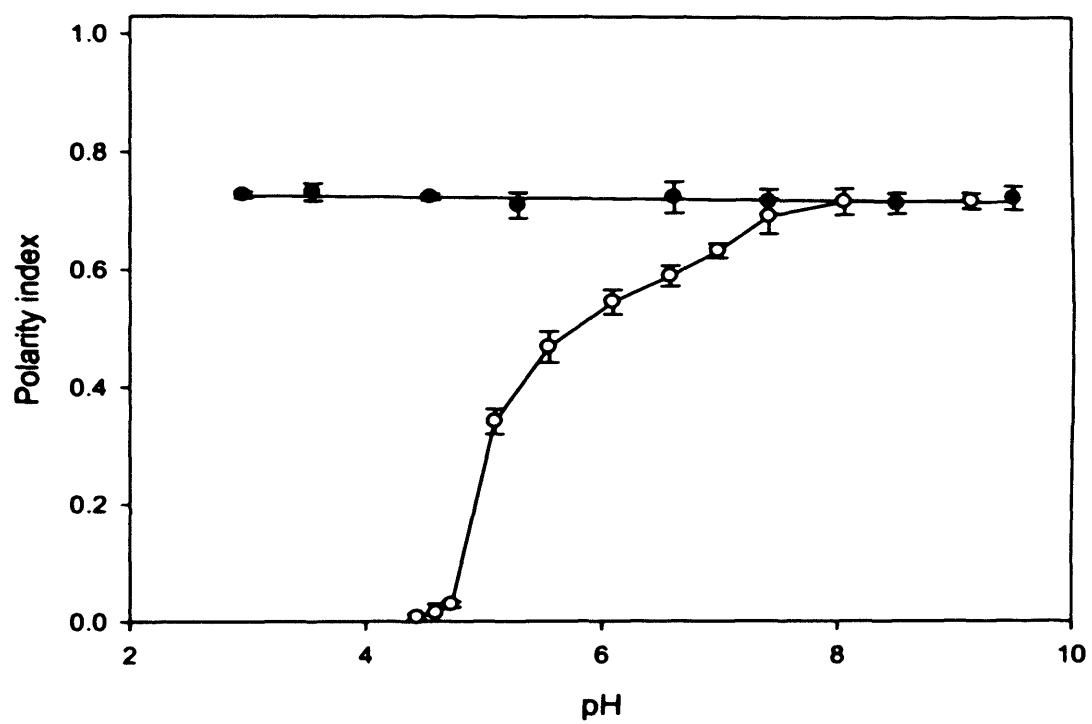


Figure 5.3; pH dependence of the polarity index of 16-DSE solubilised into SDS solutions (25mM) in the absence (filled circles) and presence (open circles) of 0.2wt% ISA23.HCl

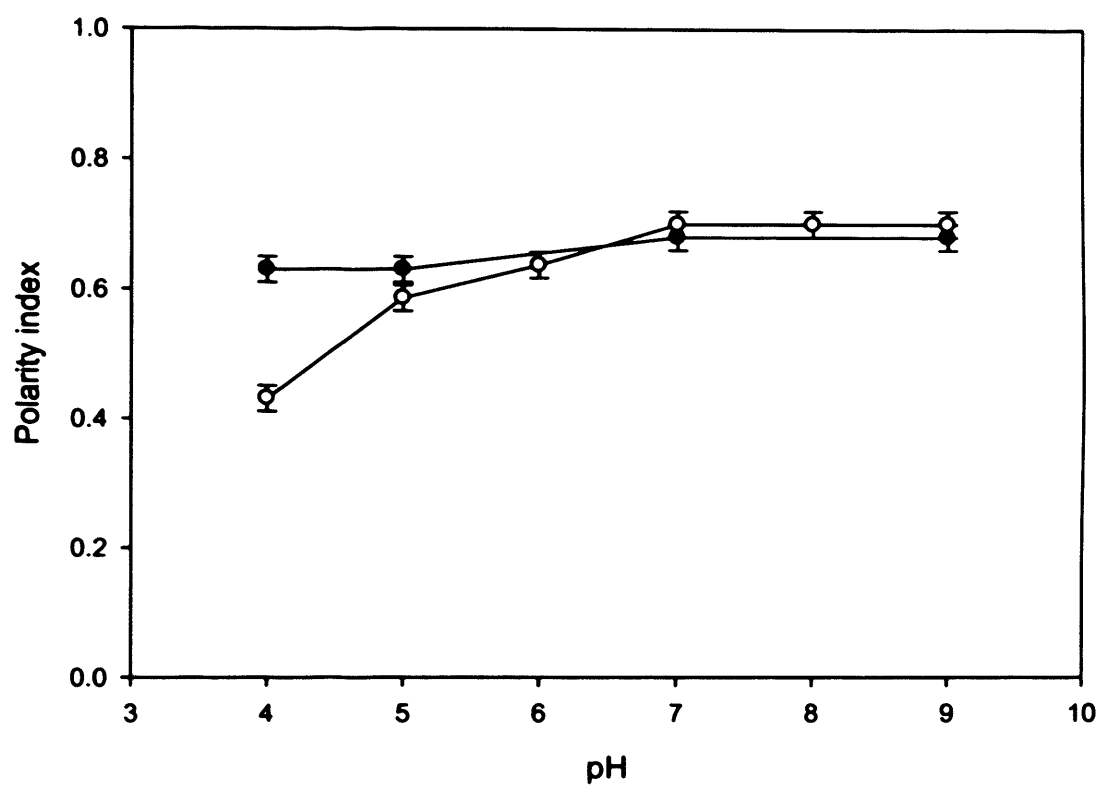


Figure 5.4; pH dependence of the polarity index of 5-DSE solubilised into SDS solutions (25mM) in the absence (filled circles) and presence (open circles) of 0.2wt% ISA23.HCl

The critical pH reflects the balance of the electrostatic and hydrophobic contributions to the interaction at a depth commensurate with the location of the spin-probe. The surface of an SDS micelle (16-DSE) is negatively charged across the whole pH range, whereas the polymer becomes net positive only below pH~4 as the carboxylic group protonates, although at the critical pH one of the two nitrogens has undergone some protonation. The observation of any interaction between two (net) negatively charged moieties indicates the presence of a significant hydrophobic contribution, the driving force for which is binding of the polymer into the micelle palisade layer thus reducing the fraction of the hydrocarbon core exposed to the aqueous phase. 5-DSE reports much smaller effect of the polymer, and one that occurs at significantly lower pH, reflecting the fact that the polymer is largely interacting with the micelle surface.

A complementary insight may be gained by examining the behaviour of the polymer via its spin-label. Any interaction between the polymer and the micelle surface will lead likewise to changes in polarity and dynamics. Figure 5.5 demonstrates a critical pH=7.2 (± 0.1), in good agreement with the 16-DSE behaviour, especially given the difference in the two spin-labelled and non-labelled polymer.

There are significant differences in the EPR spectra obtained in the absence and presence of the SDS micelle revealing how the interaction between the polymer and micelle affects the mobility of the spin-label. Under pH conditions where there is no interaction e.g. pH=9, the spin-label does not sense the presence of the micelles and therefore, the observed spectrum is that of a freely-mobile spin. However, at low pH e.g. pH=5.5, very significant changes in both linewidth and intensity are evident (figures 5.2). The broad nature of the peaks, in particular that of the third peak, indicates that the motion of the spin-label has become either anisotropic and or very slow, consistent with the polymer collapsing onto the micelle surface.

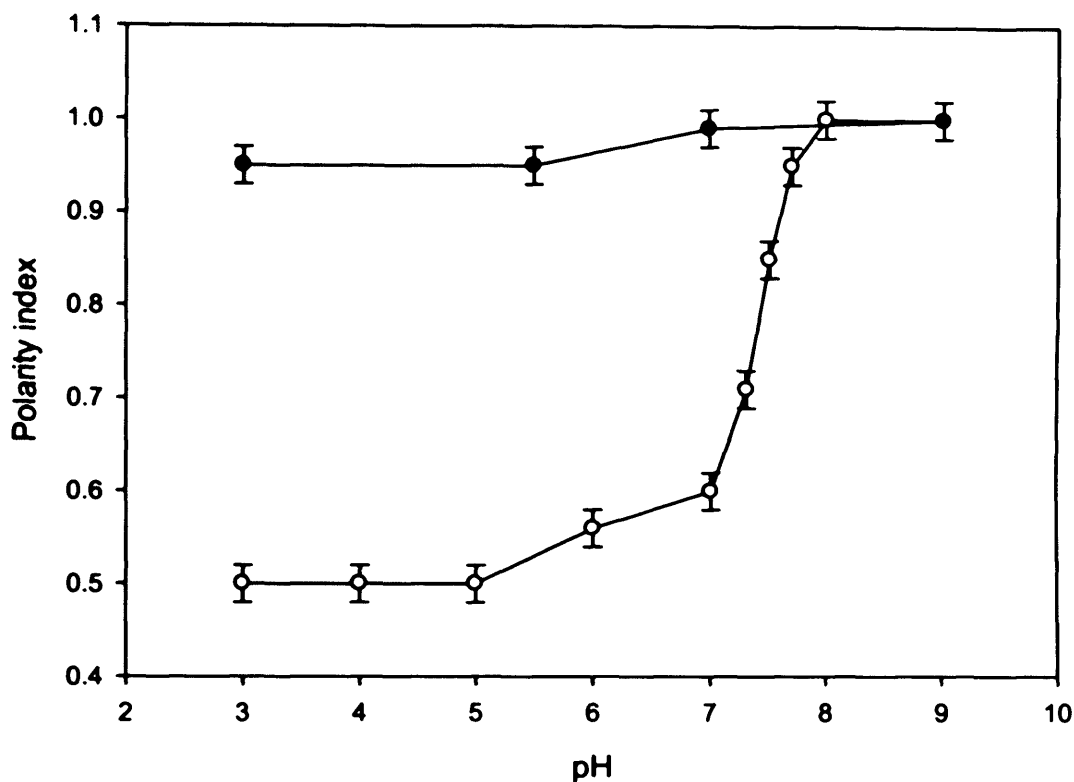


Figure 5.5; pH dependence of the polarity index of a tempo spin-label grafted to ISA23-TEMPO in the absence (filled circles) and presence (open circles) of 25mM SDS.

5.3.2 Lyso PC as model system

The small anionic headgroup of the SDS surfactant, and hence the interface it forms on self-assembly is not a good model for phospholipid rich interfaces such as membranes. lyso-PC is a phospholipid-based surfactant but unlike usual phospholipids, the lyso-PC contains only one hydrophobic chain. This forms spherical micelles and not the lamellar sheet or liposomes that are observed with phospholipids with two fatty acid chains. Due to this property, and the fact that phosphatidylcholine is the most abundant phospholipid found in the biological membrane; lyso-PC was chosen as a more realistic surfactant model to investigate polymer/membrane interaction.

5.3.2.1 Interaction of lyso-PC with BPEI_{25K} and hydrophobically modified PEI

As a comparison, the interaction of PEI with lyso-PC was first investigated. BPEI_{25K} was chosen as it is widely accepted as the most efficient candidate for transfection of genes among all PEI derivatives. BPEI_{25K} and HM_{1%}BPEI_{25K} and HM_{10%}BPEI_{25K} were used as polymers and the experiment performed at different pH. Figure 5.6 illustrates the raw EPR spectrum of 16-DSE solubilised in lyso-PC at different pH. The third peak of the spectrum is broad implying low motion of the spin-probe within the lyso-PC micelles. But pH has no effect on solubility of the spin-probe.

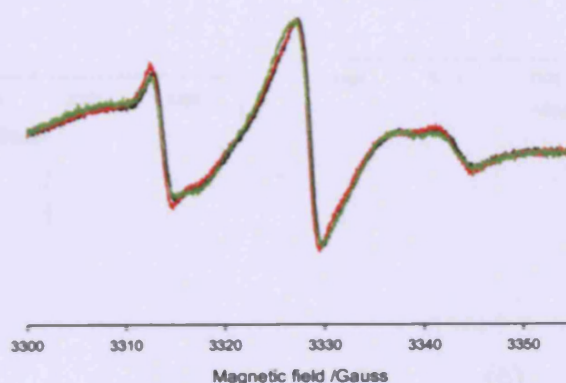


Figure 5.6; The effect of pH on the EPR spectrum of 16-DSE solubilised 25mM lyso-PC at pH 7.2 (black), pH 5.5 (red) and pH 4 (green)

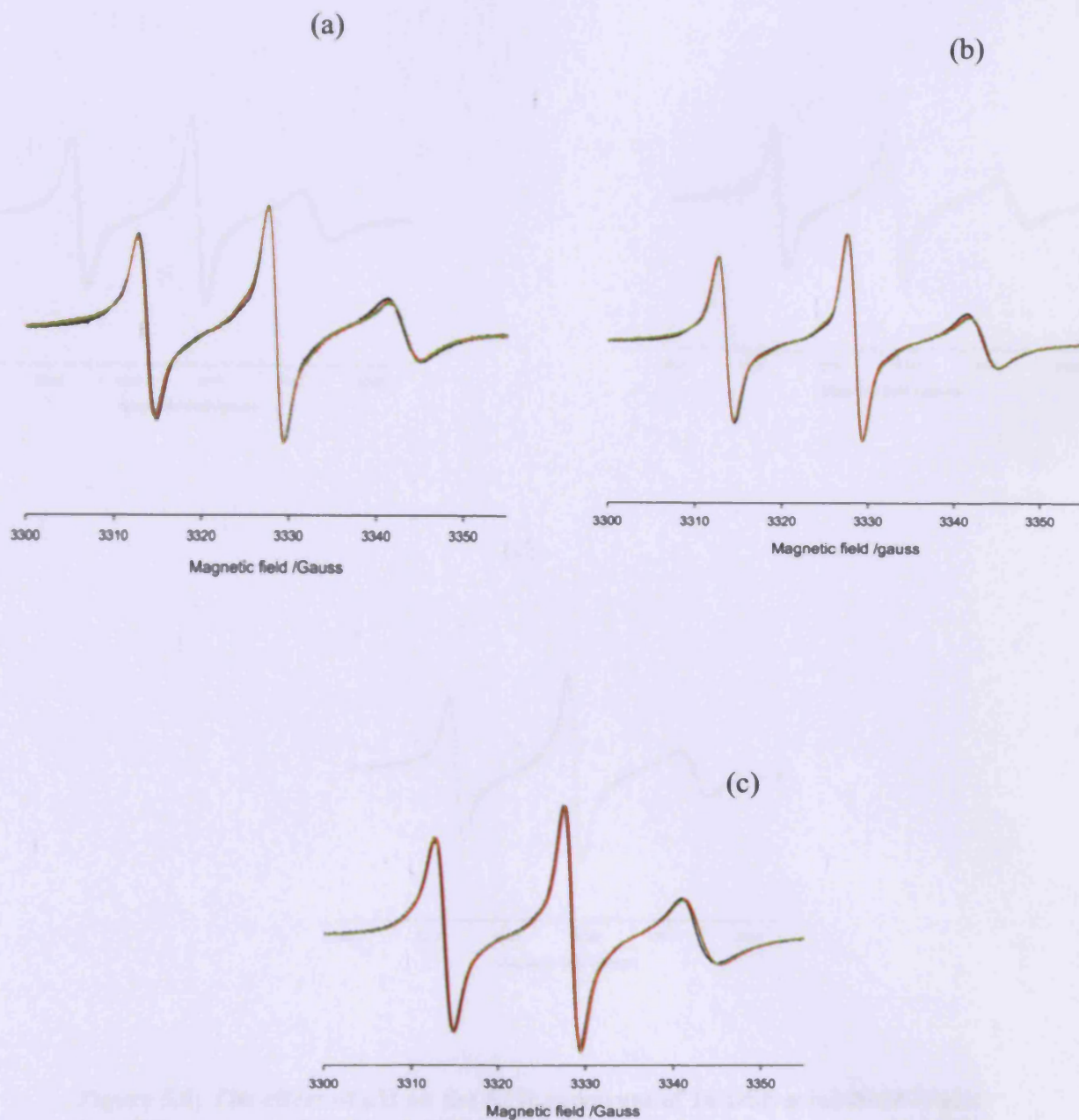


Figure 5.7; The effect of pH on the EPR spectrum of 16-DSE solubilised 25mM lyso-PC presence of 25K g/mol PEI (a), presence of 1wt% hydrophobically modified PEI (b), presence of 10wt% hydrophobically modified PEI (c) at pH 7.2 (black); pH 5.5 (red); and pH 4 (green).

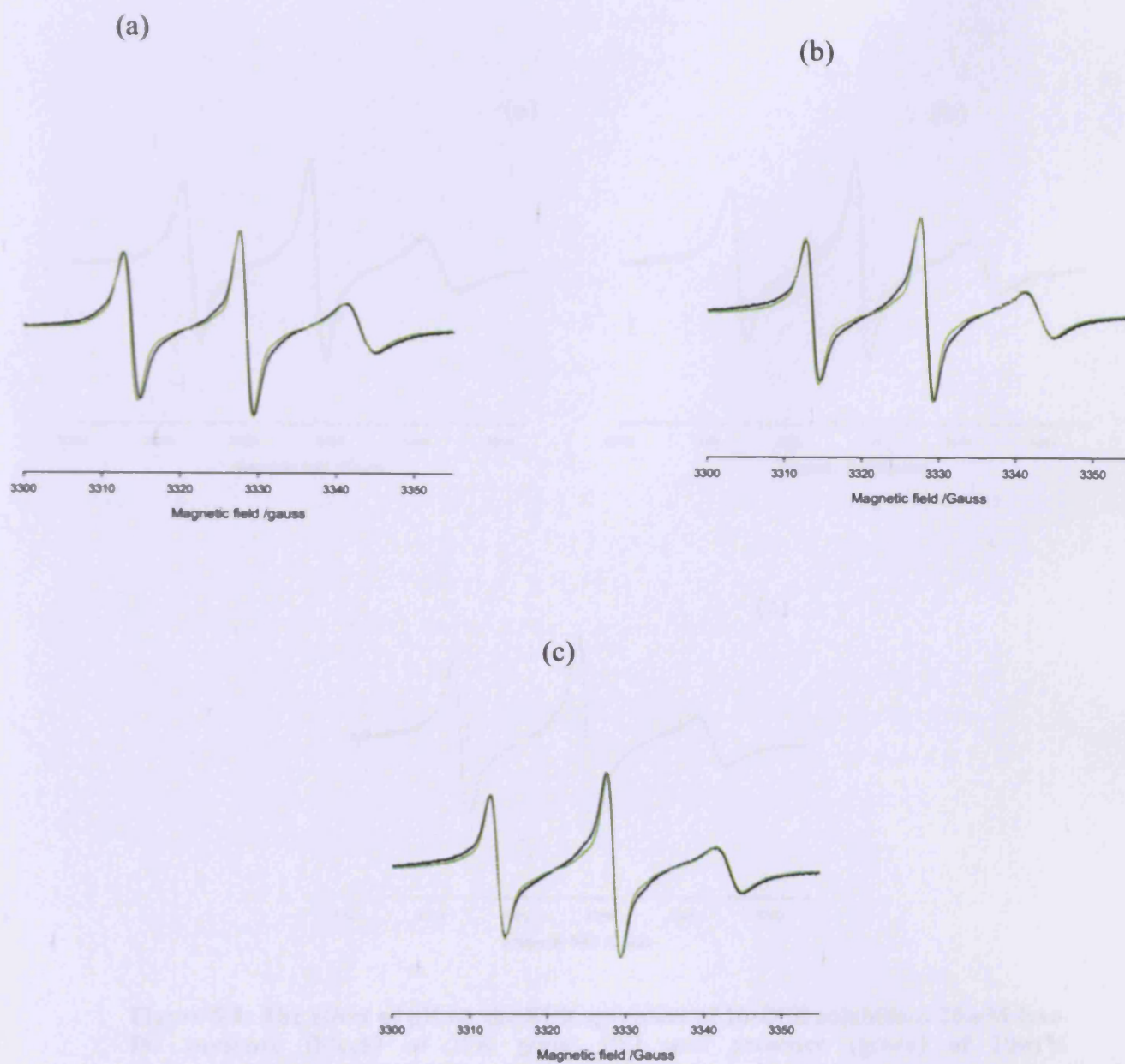


Figure 5.8; The effect of pH on the EPR spectrum of 16-DSE solubilised 25mM lyso-PC presence (black) of 25K g/mol PEI and presence (green) of 1wt% hydrophobically modified PEI at pH 7 (a), pH 5.5 (b) and pH 4 (c).

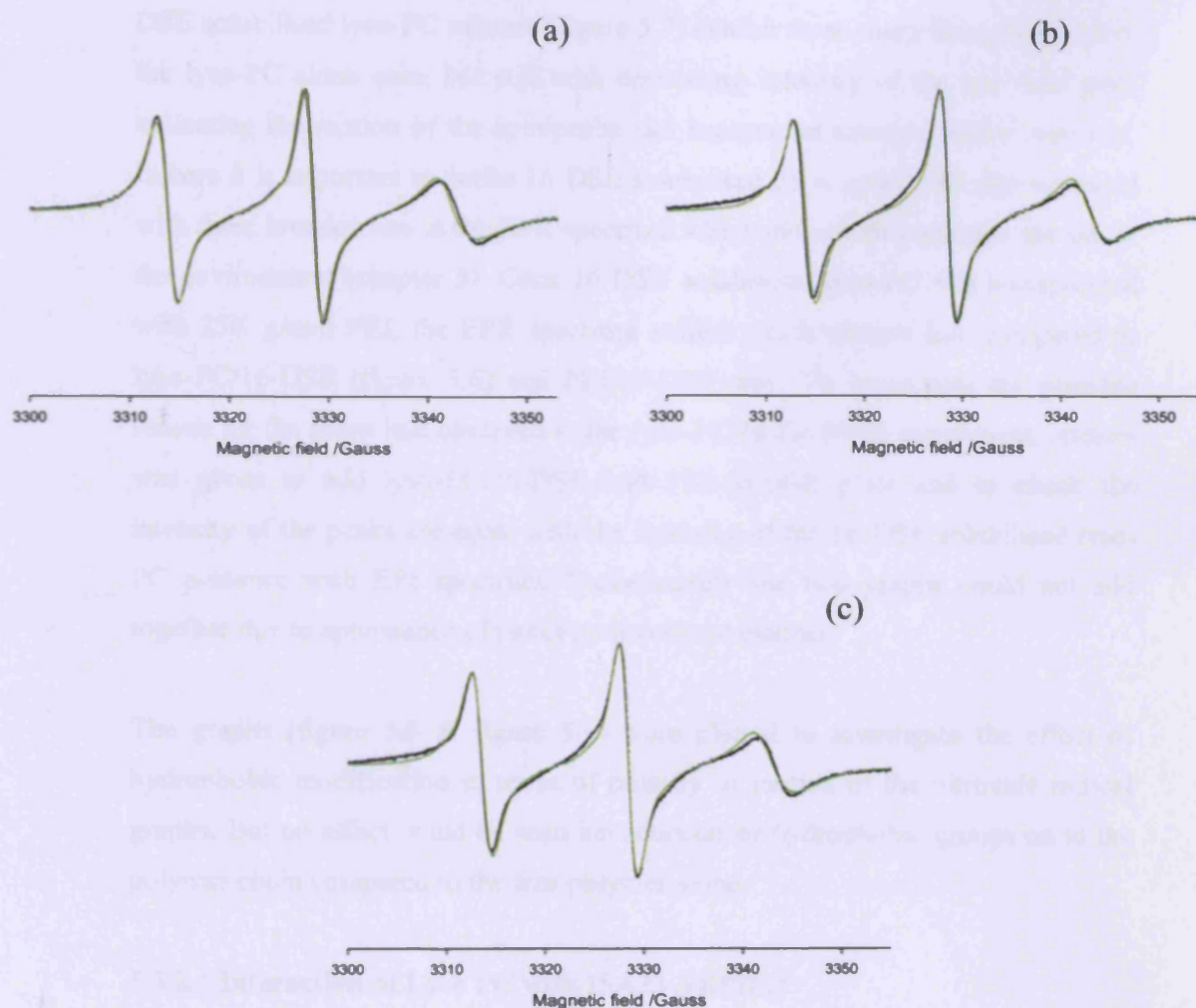


Figure 5.9; The effect of pH on the EPR spectrum of 16-DSE solubilised 25mM lyso-PC presence (black) of 25K g/mol PEI and presence (green) of 10wt% hydrophobically modified PEI at pH 7 (a), pH 5.5 (b) and pH 4 (c).

The EPR spectrum of 16-DSE solubilised lyso-PC (figure 5.6) is broader compared with SDS implying anisotropic or slow motion of the nitroxide radical. Introduction of PEI 25K g/mol or 1wt% HMPEI or 10wt% HM PEI into the 16-DSE solubilised lyso-PC mixture (figure 5.7) exhibit three sharp lines compared to the lyso-PC alone case, but still with decreasing intensity of the low field peak indicating the motion of the spin-probe had become anisotropic and/or very low. In here it is important to notice 16-DSE solubilised 25 K g/mol PEI also appeared with three broader line in the EPR spectrum which did not change upon the pH of the environment (chapter 3). Once 16-DSE solubilised lyso-PC was incorporated with 25K g/mol PEI, the EPR spectrum exhibit much sharper line compared to lyso-PC/16-DSE (figure 5.6) and PEI/16-DSE case. To investigate the possible reason for the sharp line observed in the lyso-PC/16-DSE/PEI experiment, attempt was given to add lyso-PC/16-DSE and PEI-16-DSE plots and to check the intensity of the peaks are equal with the intensity of the 16-DSE solubilised lyso-PC presence with EPI spectrum. Unfortunately the two graphs could not add together due to appearance of peaks in disordered manner.

The graphs (figure 5.8 & figure 5.9) were plotted to investigate the effect of hydrophobic modification in terms of polarity or motion of the nitroxide radical graphs. But no effect could be seen introduction of hydrophobic groups on to the polymer chain compared to the free polymer alone.

5.3.2.1 Interaction of Lyso PC with ISA23-TEMPO

In this study, spin-labelled polymer used to analyse the possible interaction with the biologically relevant phospholipid lyso-PC. Unlike the EPR discussed with HMPEI in above, here the water soluble spin-probe was chemically attached to the polymer and hence some difference in reactivity was expected but EPR studies showed no spectral changes (no change of effective OH dipoles sensed by the spin-probe) (figure 5.10) over the pH change studied, confirming no interaction. But unlike with spin-probe/ polymer interaction, we observed sharp three line with spin-labelled polymer indicating rapid or isotropic motion of the spin-probe.

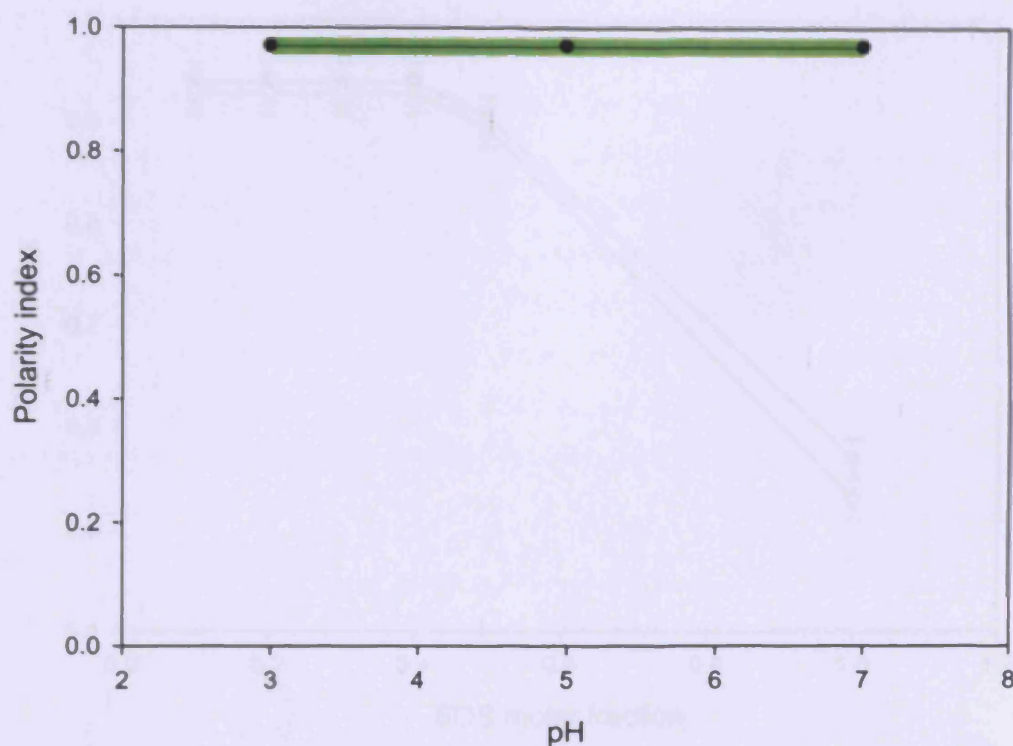


Figure 5.10; The pH dependence of the polarity index of 0.2wt% ISA23-TEMPO (black circles) and presence (green line) of 25mM lyso-PC

5.3.2.1 Interaction of SDS/Lyso PC mixed system with 10wt% hydrophobically modified ISA23-TEMPO

The above experiment suggested that no interaction occurred between lyso-PC with spin-labelled polymer at different pH's. As SDS/ISA23.HCl showed a hydrophobic contribution at pH 7, in this experiment attempt was given to hydrophobically modify spin-labelled polymer with some epoxydodecane. Hence try to explore the possible hydrophobic interaction that would occur with hydrophobic modified part of the polymer and SDS/lyso-PC mixed system.

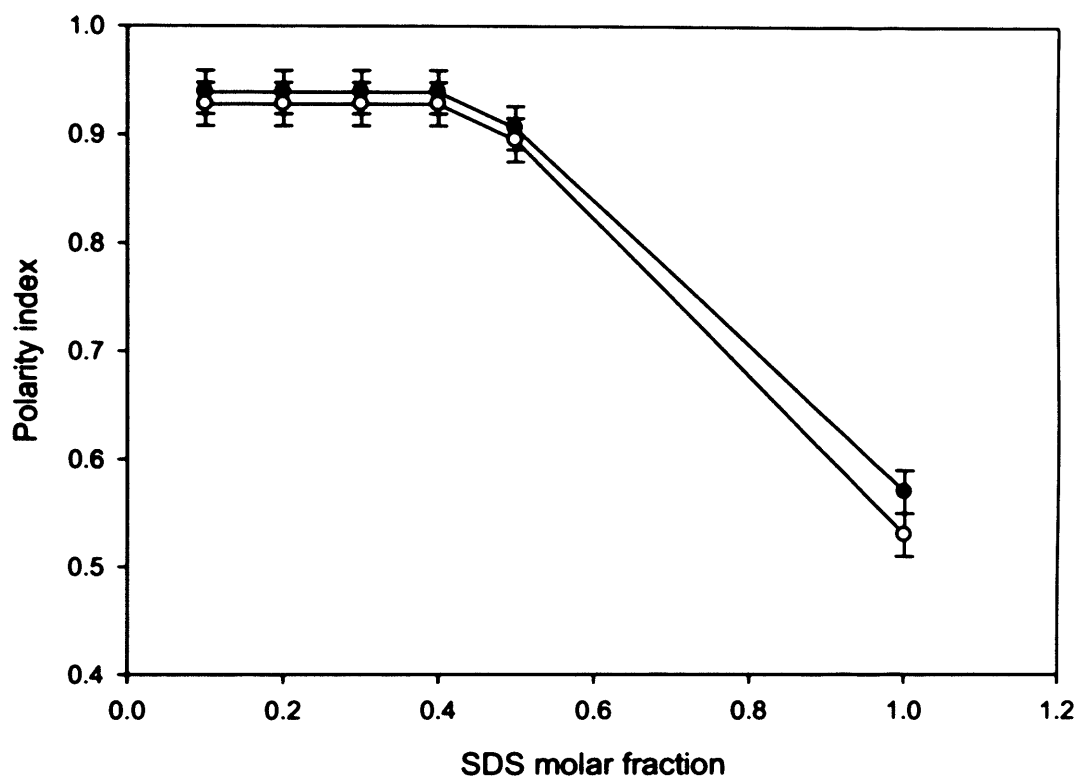


Figure 5.11; pH dependence of the polarity index of a 10wt% HM ISA23-TEMPO (filled circles) and ISA23-TEMPO (open circles) in the presence of mixed micelles of SDS/lyso-PC (25mM) at pH 5.

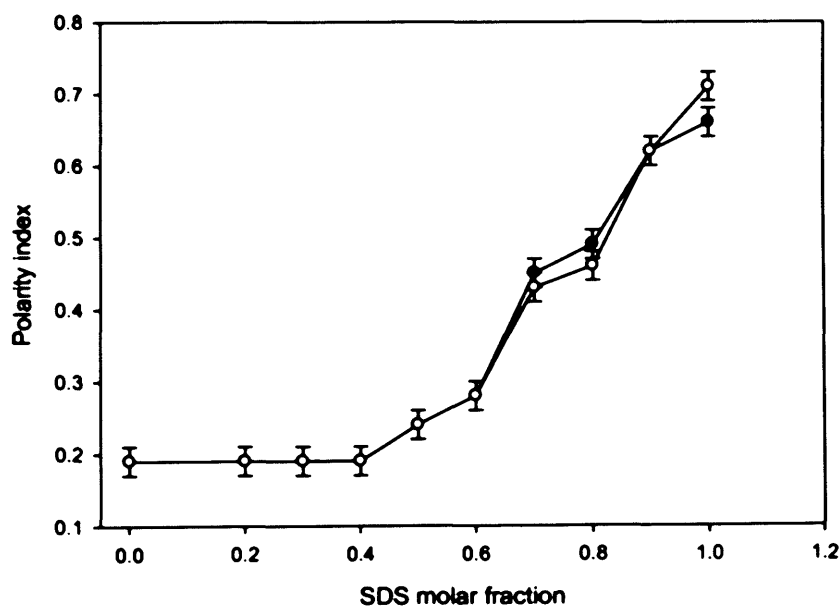
The hydrophobically modified polymer also behave as same as non modified polymer. Further interaction observed with SDS rich region only ($\alpha_{\text{SDS}} > 0.5$)

5.3.3 SDS/DHPC mixed micelles as model system

5.3.3.1 SDS/DHPC mixed micelles with spin probe polymer

The EPR of lyso-PC with PEI, HMPEI and spin labelled ISA23 showed no interaction. Accordingly, the interaction of the polymer with previously studies mixed micelles of SDS and 1,2-diheptanoyl-sn-phosphatidylcholine (DHPC) was examined with both the 16-DSE spin-probe and the spin-labelled polymer. The polarity indices for 16-DSE solubilised into mixed SDS/DHPC micelles in the absence and presence of the polymer as a function of SDS solution mole fraction are presented in figure 5.12; (a) pH = 9, (b) pH = 7 and (c) pH = 5.

(a)



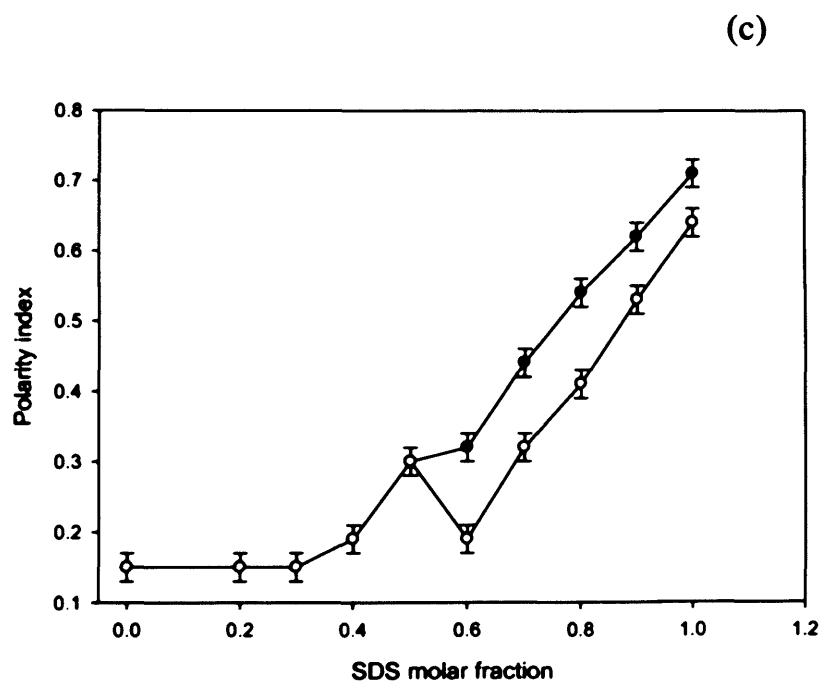
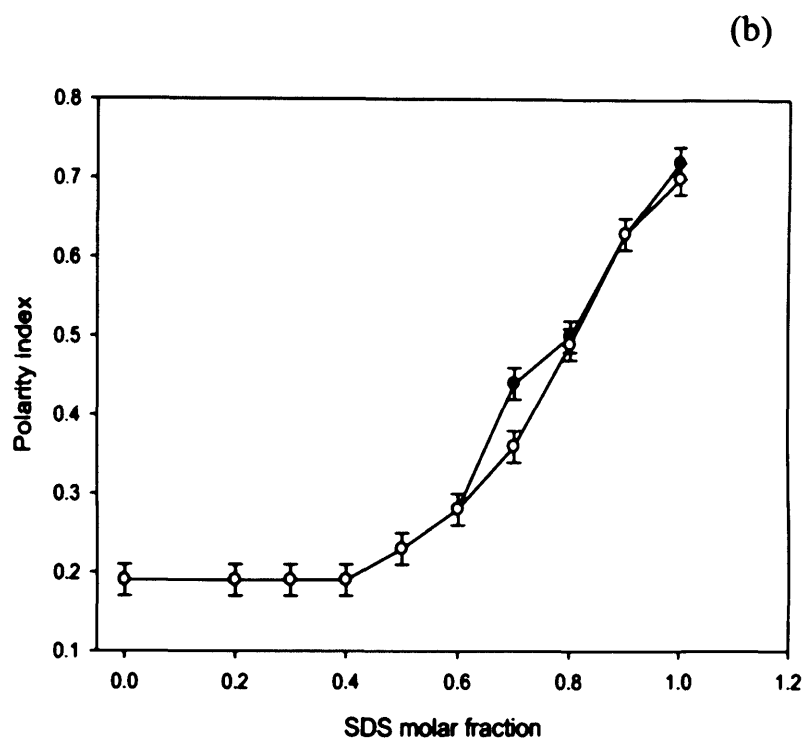


Figure 5.12; Solution composition dependence of the polarity index of 16-DSE solubilised into mixed micelles of SDS/DHPC (25mM) in the absence (filled circles) and presence of 0.2wt% ISA23.HCl (open circles) at pH 9 (a); pH 7 (b); and pH 5 (c).

The behaviour of the polarity in the absence of the polymer at each pH is rather similar – for $0 < \alpha_{\text{SDS}} < 0.4$, there is no significant change in the polarity index with solution composition suggesting that as the aggregation number of the micelle increases, the morphology of the micelle adjusts to maintain the cylindrical structure and thus, a constant headgroup hydration. Above $\alpha_{\text{SDS}} > 0.5$, the micelle adopts a more spherical morphology and changes in micelle size and shape are far less pronounced, the substitution of each SDS molecule for the DHPC introduces more water into the headgroup region, as shown by increase in polarity.

Addition of the polymer to these series of surfactant mixtures at pH = 9 and pH = 7 causes no change in the polarity and one concludes there to be no interaction between the polymer and the headgroup region comprising mixed anionic and amphoteric groups. Presumably, the fraction of exposed hydrocarbon core that may be masked by the adsorption of the polymer is insufficient to overcome the electrostatic and entropic penalties of binding. At pH = 5, a difference between the two series and hence an interaction is observed but only above $\alpha_{\text{SDS}} = 0.5$.

5.3.3.2 SDS/DHPC mixed micelles with spin-labelled polymer

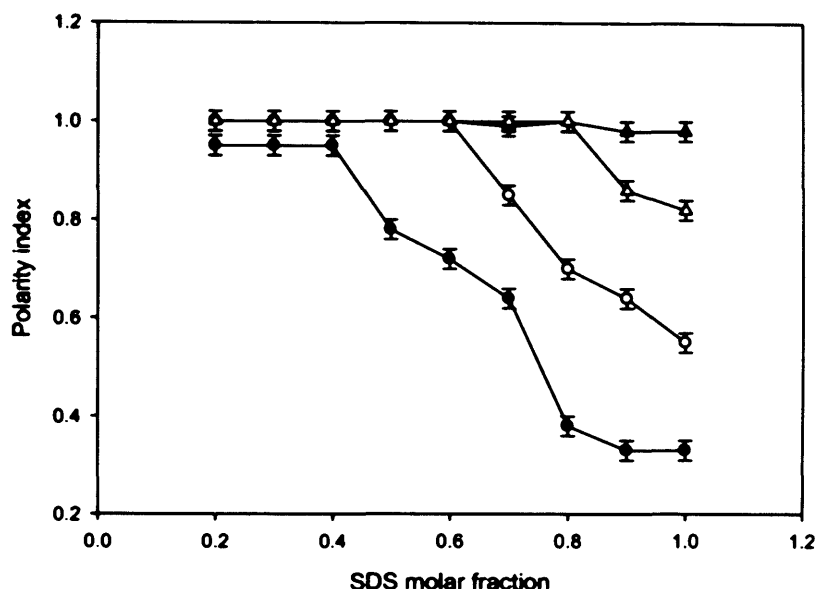


Figure 5.13; pH dependence of the polarity index of a ISA23-TEMPO in the presence of mixed micelles of SDS/DHPC (25mM) at pH 5 (filled circles), pH 7 (open circles), pH 7.5 (open triangles) and pH 9 (filled triangles).

The spin-labelled polymer in the presence of these mixed micelles, (figure 5.13), behaves in a rather similar fashion although the pH behaviour is rather more sensitive to composition. For example, no change in polarity is observed over the entire composition range at pH = 9, no change in polarity over $0 < \alpha_{\text{SDS}} < 0.85$ (± 0.05) for pH 7.5 and $0 < \alpha_{\text{SDS}} < 0.65$ (± 0.05) for pH 7 whilst no change is observed for $0 < \alpha_{\text{SDS}} < 0.4$ (± 0.05) for pH = 5.

Clearly, these respective insights gained from the 16-DSE and spin-labelled polymer reflect the hydrophobic and electrostatic balance. At the higher pHs, the

like charges on the polymer and surface are of sufficient magnitude to oppose any interaction. For the phospholipid rich surface, there will be only a small amount of exposed hydrocarbon core on account of the bulky nature of the phospholipid headgroup. Therefore, in the absence of any specific interaction and irrespective of the charged nature of the polymer, there is no driving force for adsorption. At the lower pHs, the electrostatic repulsion will be weaker (i.e reduced nett negative charge overall) and an interaction more likely, provided there is an appropriate hydrophobic component. For phospholipid rich surfaces, at least with the aggregation numbers associated with DHPC rich micelles (Nagg ~ 150), the hydrophobic term is clearly very weak.

5.3.4 Membrane mimics as model surface

To explore the role of curvature and the possibility of specific interactions with particular membrane relevant phospholipids, this approach has been extended to the study of the interaction of the polymer with vesicles of a composition intended to reflect particular membranes, table 1.

Composition (percentage) of the different biological membranes			
	Plasma	Endosomal	
Lysosomal			
Phosphatidylcholine	39.89	55.41	31.34
Phosphatidylethanolamine	19.37	22.35	16.96
Phosphatidylinositol	4.36	1.35	4.68
Phosphatidylserine	8.73	4.7	11.54
Sphingomyelin	15.21	16.02	26.82
Cholesterol	12.43	0	8.68

Adapted from Quinn, 1976; Robinson, 1975; Gallegos et al, 2002; Bergstrand et al, 2003; Evans and Hardison, 1984; Urade et al, 1988

Table 5.1; Phospholipid composition of model membranes (percentage in molar terms)

5.3.4.1 EPR studies of ISA23.HCl with model membranes (plasma, endosomal and Lysosomal) using 5-DSE as spin probes.

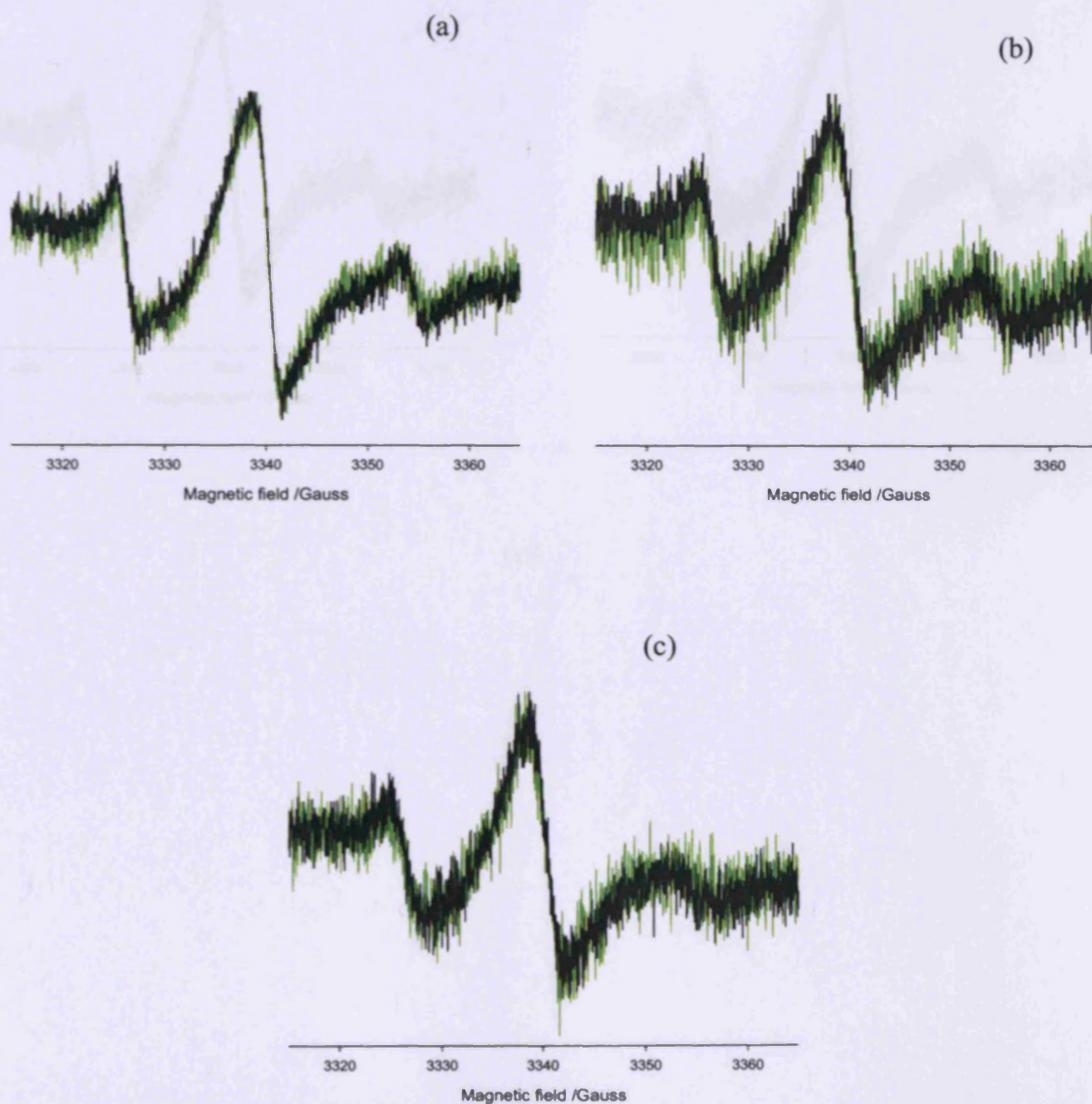


Figure 5.14; The effect of pH on the EPR spectrum of 5-DSE solubilised in model plasma membrane (green) and presence (black) of 0.2wt% ISA23.HCl at pH 7.2 (a); pH 5.5 (b) and pH 4.0 (c)

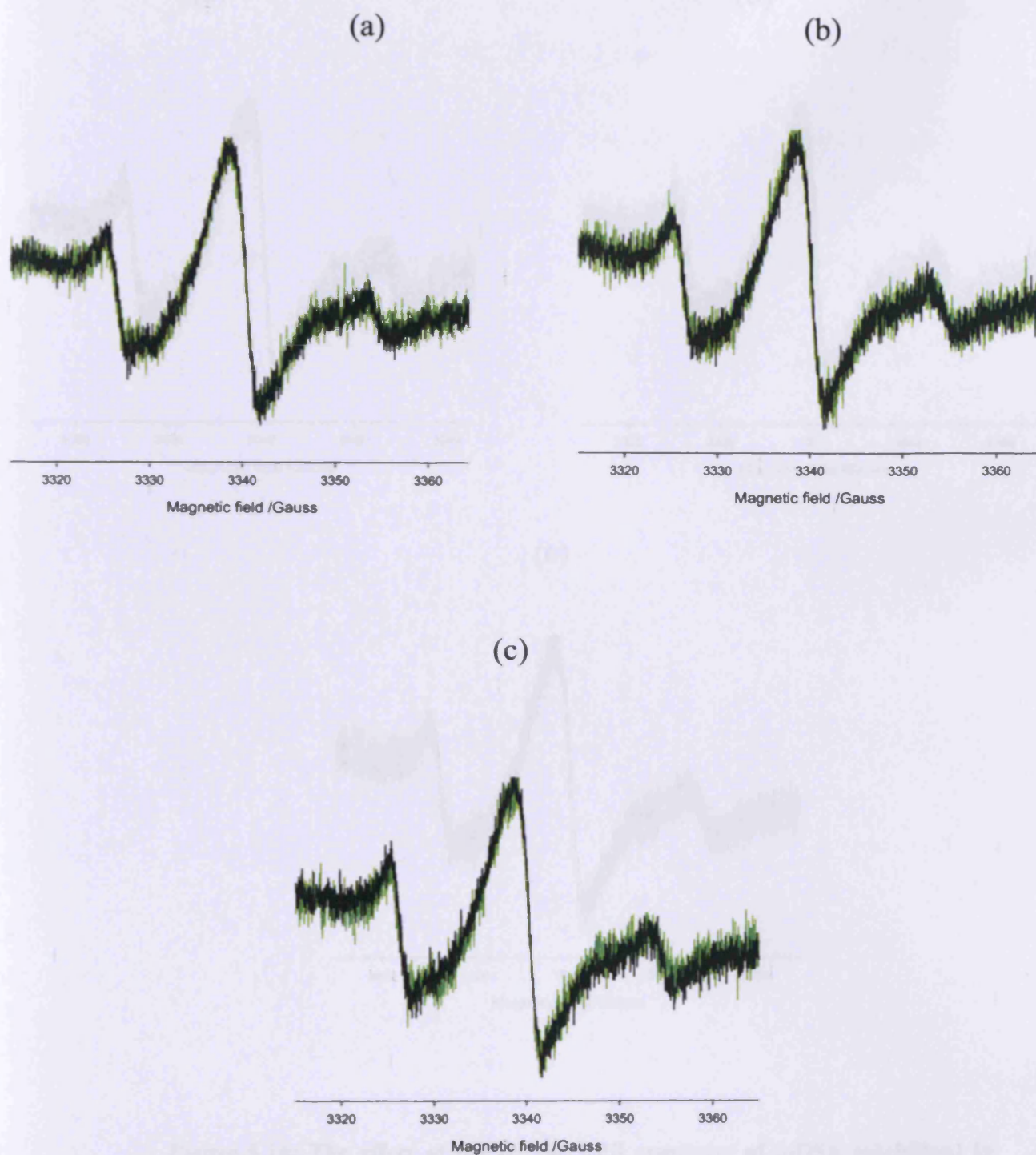


Figure 5.15; The effect of pH on the EPR spectrum of 5-DSE solubilised in model endosomal membrane (green) and presence (black) of 0.2wt% ISA23.HCl at pH 7.2 (a); pH 5.5 (b) and pH 4.0 (c)

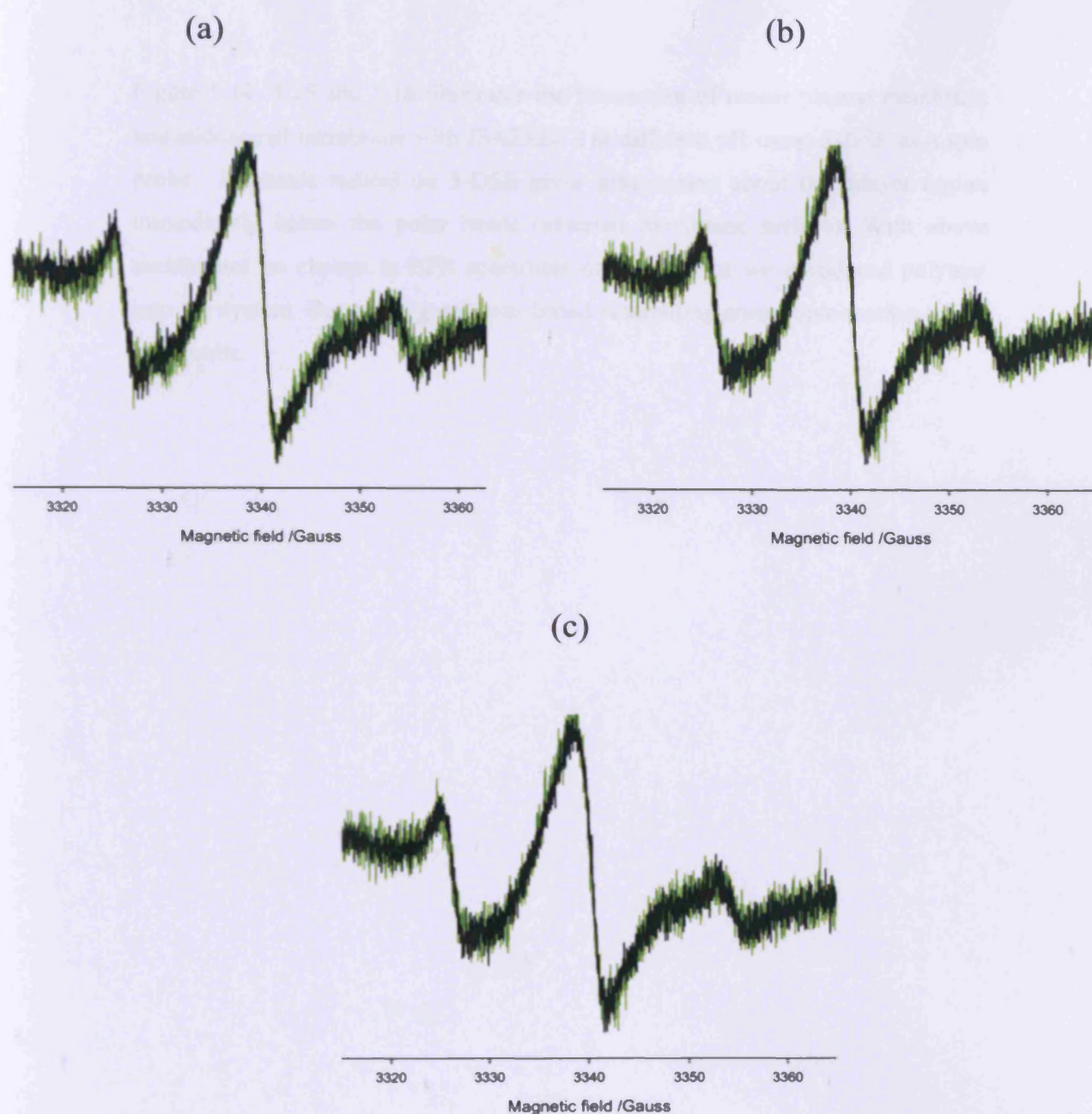


Figure 5.16; The effect of pH on the EPR spectrum of 5-DSE solubilised in model lysosomal membrane (green) and presence (black) of 0.2wt% ISA23.HCl at pH 7.2 (a); pH 5.5 (b) and pH 4.0 (c)

Figure 5.14, 5.15 and 5.16 illustrates the interaction of model plasma membrane and endosomal membrane with ISA23.HCl at different pH using 5-DSE as a spin probe. Nitroxide radical on 5-DSE gives information about the bilayer region immediately below the polar heads (external membrane surface). With above membranes no change in EPR spectrums observed once we introduced polymer into the system. But every graph was broad resembling anisotropic motion of the spin probe.

5.3.4.2 EPR studies of ISA23.HCl with model membranes (plasma, endosomal and Lysosomal) using 16-DSE as spin probes.

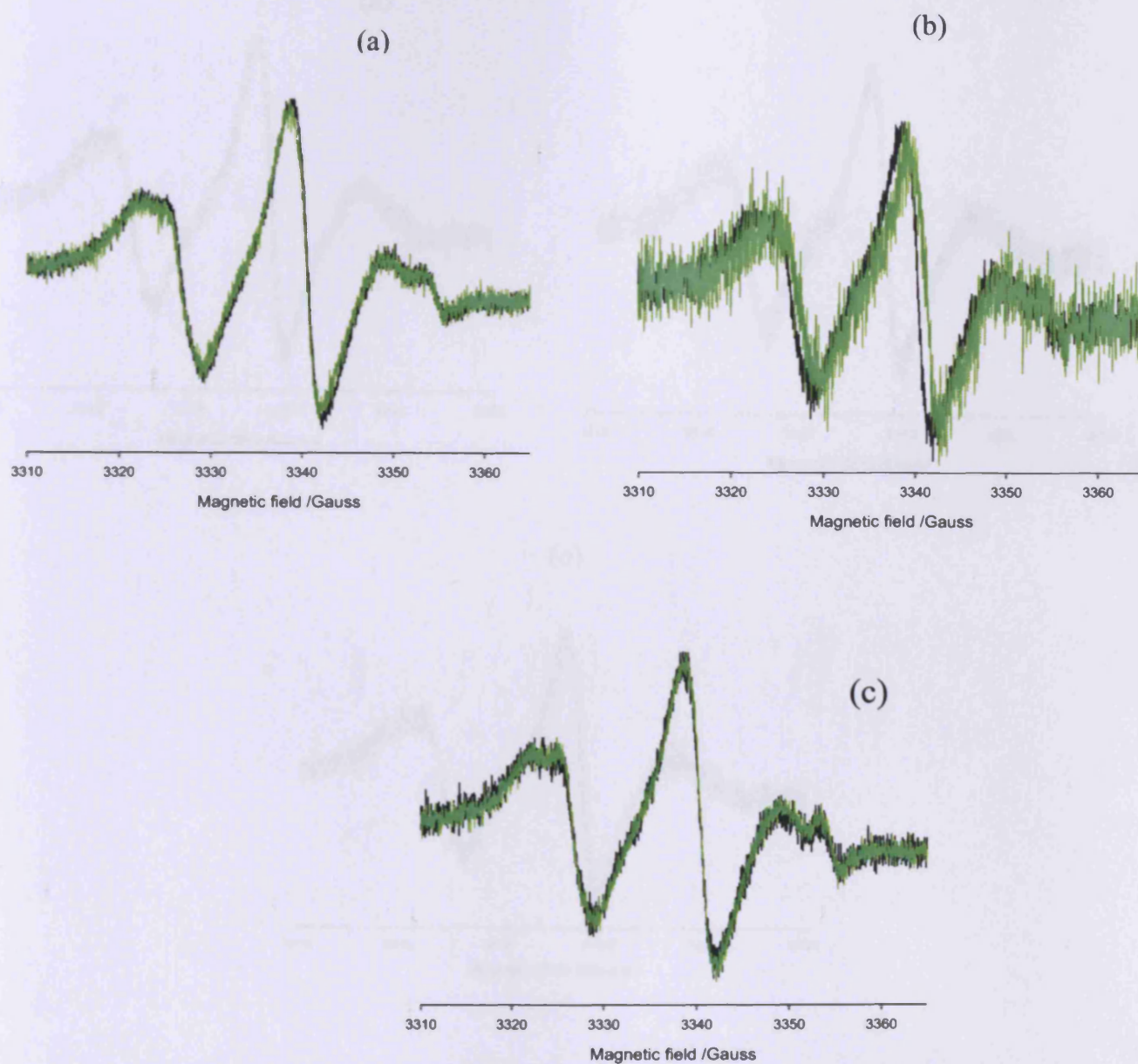


Figure 5.16; The effect of pH on the EPR spectrum of 16-DSE solubilised in model plasma membrane (green) and presence (black) of 0.2wt% ISA23.HCl at pH 7.2 (a); pH 5.5 (b) and pH 4.0 (c)

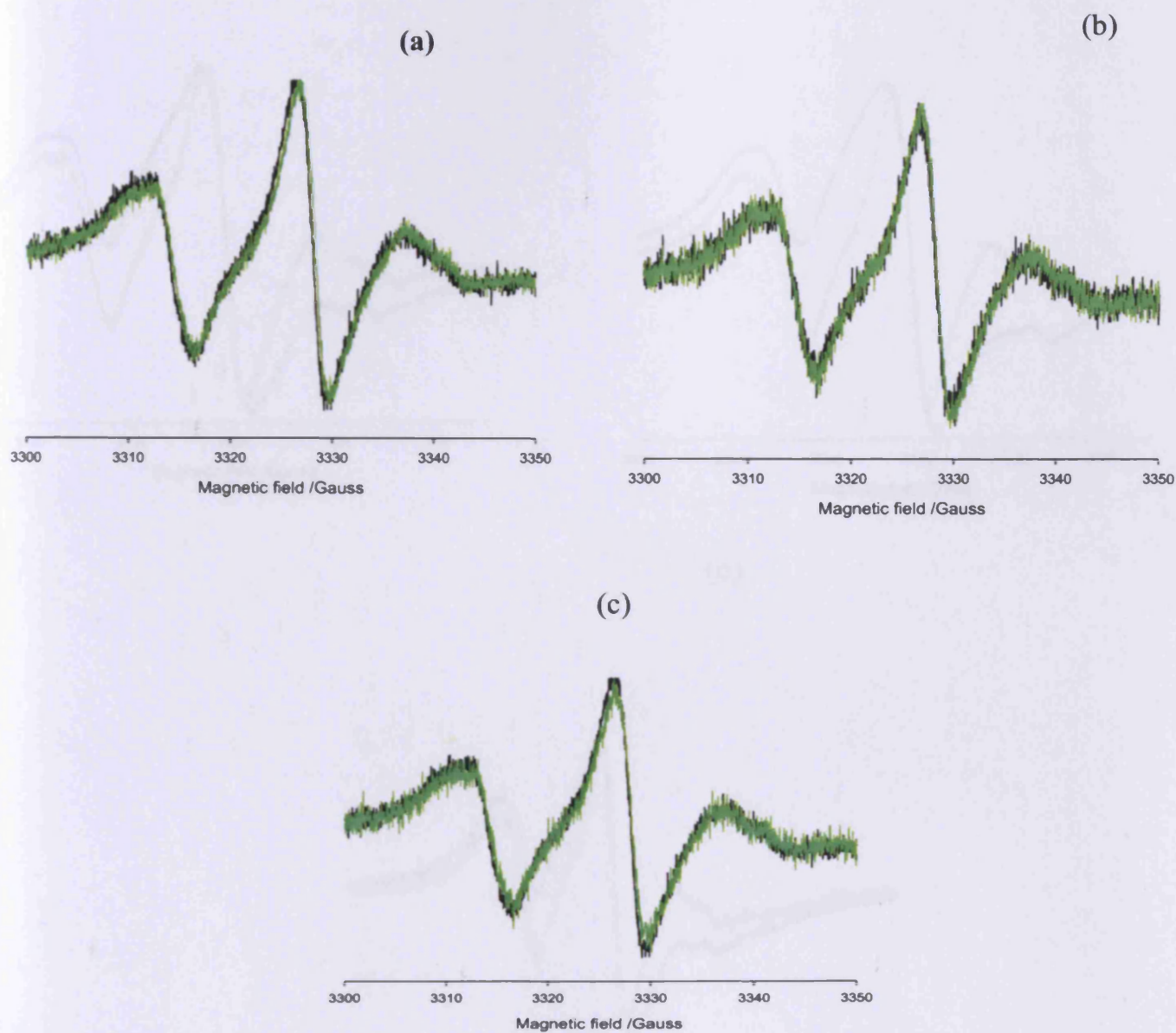


Figure 5.17; The effect of pH on the EPR spectrum of 16-DSE solubilised in model endosomal membrane (green) and presence (black) of 0.2wt% ISA23.HCl at pH 7.2 (a); pH 5.5 (b) and pH 4.0 (c)

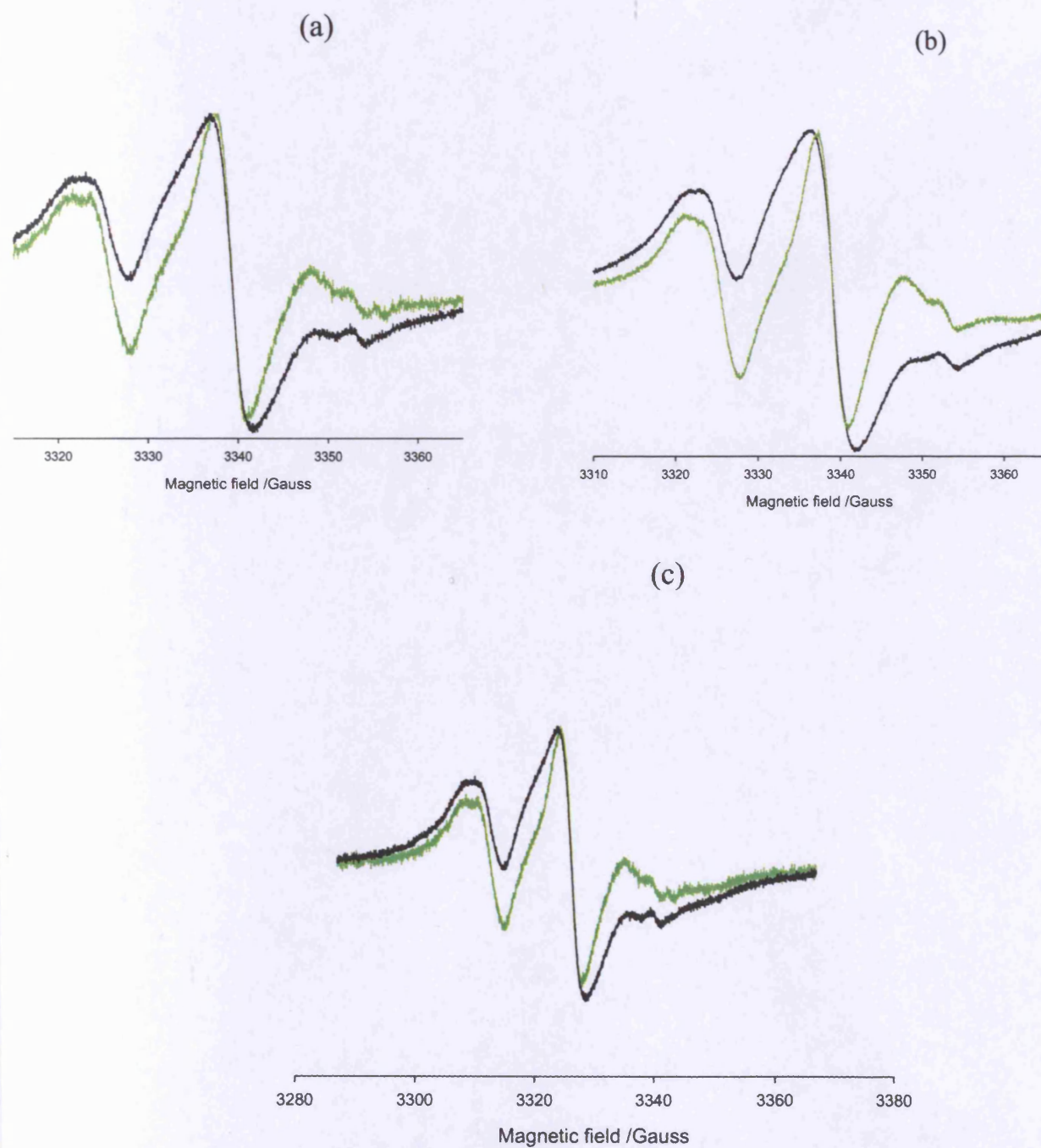


Figure 5.18; The effect of pH on the EPR spectrum of 16-DSE solubilised in model lysosomal membrane (green) and presence (black) of 0.2wt% ISA23.HCl at pH 7.2 (a); pH 5.5 (b) and pH 4.0 (c)

Figure 5.16, 5.17, 5.18 illustrates 16-DSE solubilised model membranes with ISA23.HCl at different pHs. Unlike 5-DSE, 16-DSE senses internal regions of the micelles. But system behaves same way as with 5-DSE - there is no change of EPR spectrum once introduced polymer into the system. But spectrums are broad implying motionally constrained or anisotropic systems and/or presence of many superimposed microenvironments. The intrinsic value of the data is therefore limited.

5.3.4.2 EPR studies of ISA23.TEMPO with model membranes (plasma, endosomal and Lysosomal)

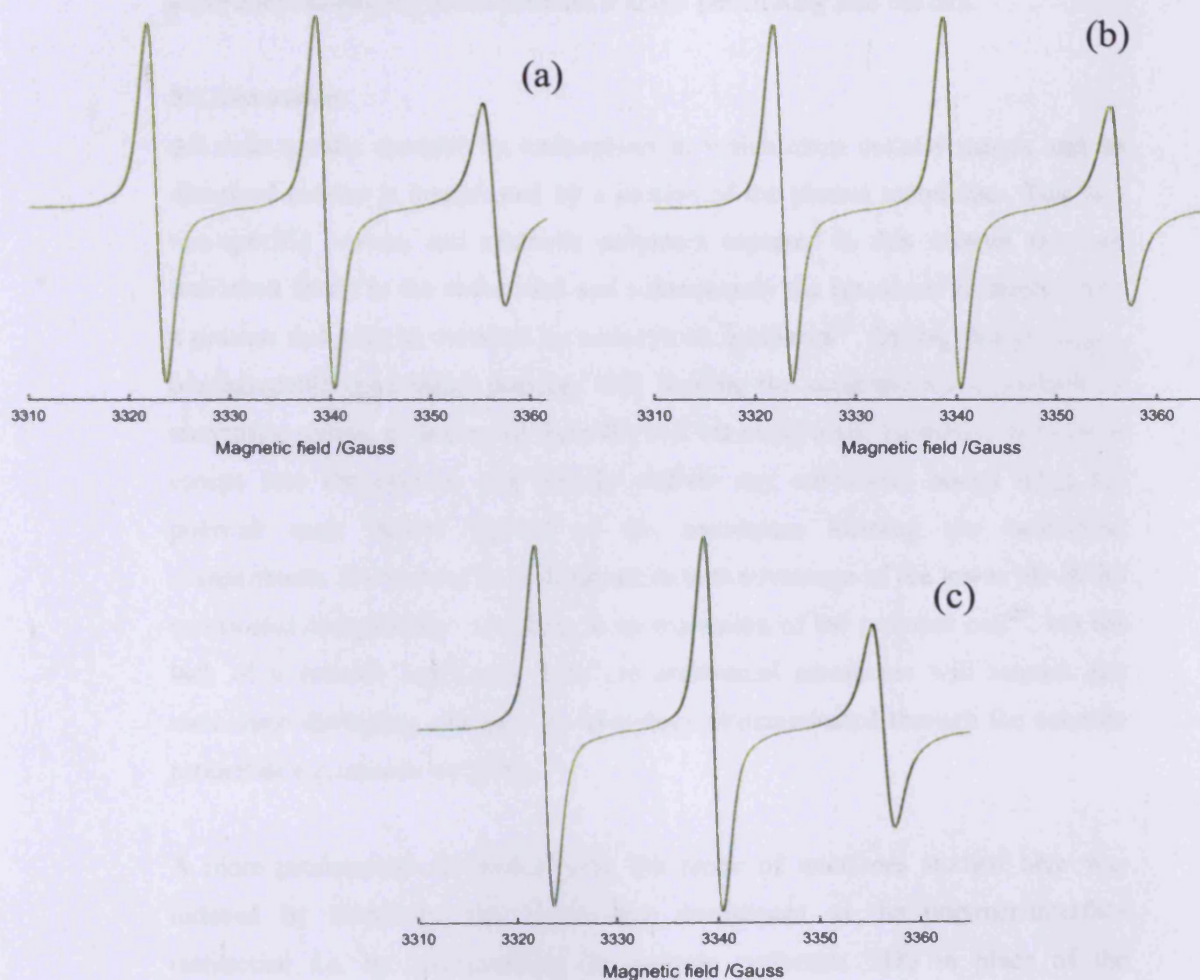


Figure 5.19; The effect of pH on the EPR spectrum of 0.2wt% ISA23-TEMPO (black) and presence (green) of model plasma membrane at pH 7.2 (a); pH 5.5 (b) and pH 4.0 (c)

The EPR spectrums of spin-labelled polymer with all three model membranes (endosomal and lysosomal membrane figures are not included) are same irrespective of the pH studied. The spin-labelled polymer however, shows the sharp lines spectra indicative for rapid motion in solution.

5.3.5 Living cell as model surface

EPR experiment with spin-labelled polymer was carried out with living cell extracted from rat as a model surface. The cell and the dipped medium was test for the EPR signal and no signal was observed from living cell, but sharp signal observed from dipped medium (supernatant) indicating all the polymer used in the experiment remaining in the medium without penetrating into the cell.

5.4 Discussion.

All cells uptake material by endocytosis in which extra cellular matrix and its dissolved solutes is invaginated by a portion of the plasma membrane. This is a non-specific process and synthetic polymers captured in this manner are then trafficked firstly to the endosomal and subsequently the lysosomal compartments, a process that may be curtailed by endocytosis inhibitors²⁴. During this journey, a biodegradable (non-toxic) polymer will become the substrate for a plethora of enzymatic routes, or is cleared from the cell via exocytosis. However, in order to escape into the cytosol, and thereby deliver any covalently bound drug, the polymer must induce rupture of the membrane forming the endosomal compartment. PAAs have been designed to take advantage of the lower pH of the endosomal compartment, resulting in an expansion of the polymer coil²⁵, but the lack of a specific interaction with the endosomal membrane will require any membrane disrupting character to have been communicated through the solution properties e.g.osmotic swelling.

A more pronounced interaction with the range of interfaces studied here was induced by increasing the electrostatic component to the polymer/interface interaction *i.e.* by incorporating the anionic surfactant SDS in place of the

polyamphoteric phospholipids, or by reducing the pH to decrease the anionic charge on the polyamphoteric polymer. Neither of these avenues – whilst highly informative – is viable from a biological standpoint in the development of a polymer delivery vehicle. However, this insight gained points to the factors that need to be addressed. To promote the interaction of a synthetic polymer with a particular interface requires a favourable electrostatic or hydrophobic interaction in order to overcome the inherent loss of entropic and steric constraints the polymer will suffer on binding. Increasing the hydrophobic nature of the polymer is likely to promote reduced polymer solubility and the concomitant tendency to self-associate. Modifying the electrostatic interaction offers some limited potential *via* precise tailoring of polymer architecture or monomer structure, but the inherent toxicity of the many polymer would appear to have its origins here (poly-L-lysine (PLL), poly(ethylene imine) (PEI), poly(ethylacrylic acid) (PEAAc), and related polymers, poly(amidoamine) (PAMAM) dendrimers).

5.5 Conclusions

Nitroxide containing spin-probes and a spin-labelled polymer have been examined by EPR to evaluate the polarity sensed by the nitroxide moiety as an indication for an interaction of the polymer with several model interfaces, selected to resemble simple globular micelles and more complex mixed micelles systems and membrane mimics. For phospholipid rich interfaces, no interaction is observed, although introduction of the anionic surfactant SDS did induce some binding of the polymer. The driving force for the interaction is a complex balance of the electrostatic and hydrophobic characters of both the interface and polymer, the lack of any interaction between the phospholipid rich surface reflecting the greatly reduced hydrophobic component on account of the bulky phospholipids headgroup.

A lack of interaction would account for the weak endosomolytic character of this polymer during trafficking and offers one possible explanation for the poor delivery efficacy of ISA23.HCl in that the polymer does not escape into the

endosomal compartments, but rather accumulates in lysosomal compartments rendering them more permeable.

5.6 References

1. Pack, D. W.; Hoffman, A. S.; Pun, S.; Stayton, P. S., *Nature Reviews in Drug Delivery* 4, 581 2005.
2. Ohana, P.; Gofrit, O.; Ayesh, S.; Al-Sharef, W.; Mizrahi, A.; Birman, T.; Schneider, T.; Matouk, I.; de Groot, N.; Tavdy, E.; Sidi, A. A.; Hochberg, A., *Gene Therapy and Molecular Biology* 8, 181 2004.
3. Wu, J.; Zhou, B.; Hu, Z., *Physical Review Letters* 90, 048304 2003.
4. Boussif, O.; Lezoualc'h, F.; Zanta, M. A.; Mergny, M. D.; Scherman, D.; Demeneix, B.; Behr, J. P., *Proceedings of the National Academy of Sciences of the United States of America* 92, 7297 1995.
5. Murthy, N.; Robichaud, J.; Tirrel, D.; Stayton, P.; Hoffman, A., *Journal of Controlled Release* 61, 137 1999.
6. Qin, L. H.; Pahud, D. R.; Ding, Y. Z.; Beilinska, A. U.; Kukowska-Latallo, J. F.; Baker, J. R.; Bromberg, J. S., *Human Gene Therapy* 9, 553 1998.
7. Fischer, D.; Li, Y. X.; Ahlemeyer, B.; Kriegelstein, J.; Kissel, T., *Biomaterials* 24, 1121 2003.
8. Ferruti, P.; Manzoni, S.; Richardson, S. C. W.; Duncan, R.; G., P. N.; Mendichi, R.; Casolaro, M., *Macromolecules* 33, 7793 2000.
9. Duncan, R.; Ferruti, P.; Sgouras, D.; Tuboku-Metzger, A.; Ranucci, E.; Bignotti, F. A., *Journal of Drug Targeting* 2, 341 1994.
10. Ferruti, P.; Marchisio, M. A.; Duncan, R., *Macromolecular Rapid Communications* 23, 332 2002.
11. Richardson, S.; Ferruti, P.; Duncan, R., *Journal of Drug Targeting* 6, 391 1999.
12. Richardson, S. C. W.; Patrick, N. G.; Man, Y. K. S.; Ferruti, P.; Duncan, R., *Biomacromolecules* 2, 1023 2001.
13. Patrick, N. G.; Richardson, S. C. W.; Casolaro, M.; Ferruti, P.; Duncan, R., *Journal of Controlled Release* 77, 225 2001a.
14. Patrick, N. G.; Ferruti, P.; Duncan, R., *Proc. Int. Symp. contr. Release Bioact. Mater.* 28, 864 2001b.
15. Wan, K.-W.; Malgesini, B.; Verpilio, L.; Ferruti, P.; Griffiths, P. C.; Paul, A.; Hann, A. C.; Duncan, R., *Biomacromolecules* 5, 1102 2004.
16. Putnam, D., *Nature Materials* 5, 439 2006.
17. Gussoni, M.; Greco, F.; Ferruti, P.; Ranucci, E.; Ponti, A.; Zetta, L., *New Journal of Chemistry* 32, 323 2008.
18. Mayer, L. D.; Hope, M. J.; Cullis, P. R., *Biochimica et Biophysica Acta (BBA)* 858, 161 1986.
19. Hope, M. J.; Bally, M. B.; Webb, G.; Cullis, P. R., *Biochimica et Biophysica Acta (BBA)* 812, 55 1985.
20. Khayat, Z. in *Chemistry*; University of Cardiff: 2006.
21. Halpern, H. J.; Peric, M.; Yu, C.; Bales, B. L., *Journal of Magnetic Resonance Series A* 103, 13 1993.
22. Griffith, O. H.; Dehlinger, P. J.; Van, S. P., *Journal of Membrane Biology* 151974.
23. Bales, B. L.; Messina, L.; Vidal, A.; Peric, M., *Journal of Physical Chemistry* 102, 10347 1998.

24. Kitchens, K. M.; Kolhatkar, R. B.; Swaan, P. W.; Ghandehari, H., *Molecular Pharmaceutics* 5, 364 2008.
25. Griffiths, P. C.; Khayat, Z.; Tse, S.; Heenan, R. K.; King, S. M.; Duncan, R., *Biomacromolecules* 8, 1004 2006.

“Future work”

6.1 Introduction

This chapter contains various avenues of study that were initiated as part of this thesis, are highly collaborative in nature, and for various reasons are still on-going at the completion of the PhD candidature. These are included as different projects but not comprehensively presented.

6.2 Definition of the effect of polymer stereochemistry on the physicochemical behavior of polymer therapeutics

6.2.1 Introduction

The behaviour of polyelectrolytes in solution remains an active area of research as their controllable behaviour to different stimuli and also importance of water soluble polymers. The application of these polymers in different areas depend on magnitude and extent of conformational changes. These extend from semiconductor devices, molecular sensors, nanoscale pumping devices, controlled wetting, new optics, microelectronics, drug delivery, flocculants, and super-absorbents. Such knowledge may also assist in elucidating the roles that complex biological polyelectrolytes such as DNA play in biochemical process when interact with membrane-forming lipids (surfactants). Same manner, the association of ionic surfactants (ex; cationic ones, S^+) with oppositely charged polyelectrolytes (anionic ones, P^-) is interested due to its importance in biological systems. The technological relevance of such studies is a consequence of an extremely wide range of applications of mixed surfactant-polymer systems. The numerous studies based on synthetic polyelectrolytes have shown that the interaction between S^+ / P^- is very strong. This is a consequence of strong electrostatic interaction between charged surfactant aggregates and the polyion and is demonstrated by the very low critical aggregation concentration (CAC). Those CAC values are orders of magnitude lower than the critical micelles concentration. In order to evaluate these results one should know detailed properties of the surfactant ion and polyion. The relevant characteristics of the polyelectrolyte chain are; charge density, chain

flexibility and hydrophobicity¹. These properties are determined by the structure of the polymer backbone and by the nature of the attached groups and are reflected in the equilibrium conformation of the polymer chain in solution.

It has been demonstrated that stereoregular polymer often have characteristic local conformation in solution, although their overall conformation can well be approximated by random coils^{2,3}. For example, syndiotactic poly(methyl methacrylate), s-PMMA, in benzene has a locally preferred curvature and appears to be more strongly coiled than isotactic PMMA, i-PMMA. However, i-PMMA has a rather random conformation with local helical sequences³. Further, it has been shown that local conformations are not much affected by the presence of charges; i.e., they are similar for the corresponding stereoregular poly(sodium methacrylates) in aqueous solution.

In this study, explore the solution properties of syndiotactic and atactic polymethacrylic acid (PMA) using different techniques use in colloidal chemistry, such as PGSE-NMR, EPR, SANS and surface tension in order to find a better explanation for different behavioural pattern exhibit by two stereoregular conformations.

6.2.2 Materials and methods

Isotactic (a-PMA) and syndiotactic (s-PMA) PMA were kindly donated by Lorella Izzo and table 6.4 illustrates the characterization of both polymers.

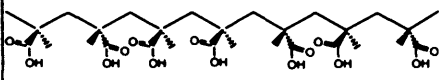
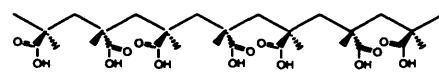
Starting Polymers	M _w (kDa)	M _w /M _n	Strucuture
Atactic-PMA	48	1.54	
Syndiotactic-PMA	43	1.02	

Table 6.1; Characterization of syndio and atactic PMA

Surface tension

The surface tension measurements were made by using a maximum bubble pressure tensiometer (SITA Online t60) with bubble lifetime of 15s. The instrument was calibrated using distilled water. In all cases, measurements were made at 25°C ± 0.5. All glassware was thoroughly cleaned with Decon 90 and rinsed with copious quantities of distilled water. First, stock surfactant solutions were prepared by dissolving the appropriate mass of surfactant in distilled water to produce a total surfactant concentration of 100 mM. The stock solutions of a-PMA and s-PMA (0.4 w/v% in double distilled water) were also prepared, and these solutions mixed in appropriate ratios to obtain solutions of constant polymer ratios to obtain solutions of constant polymer concentration with varying surfactant concentration. The surface tension of these polymer/surfactant solutions was then measured after following for temperature equilibration (10 min).

6.2.3 Results

6.2.3.1 Surface tension

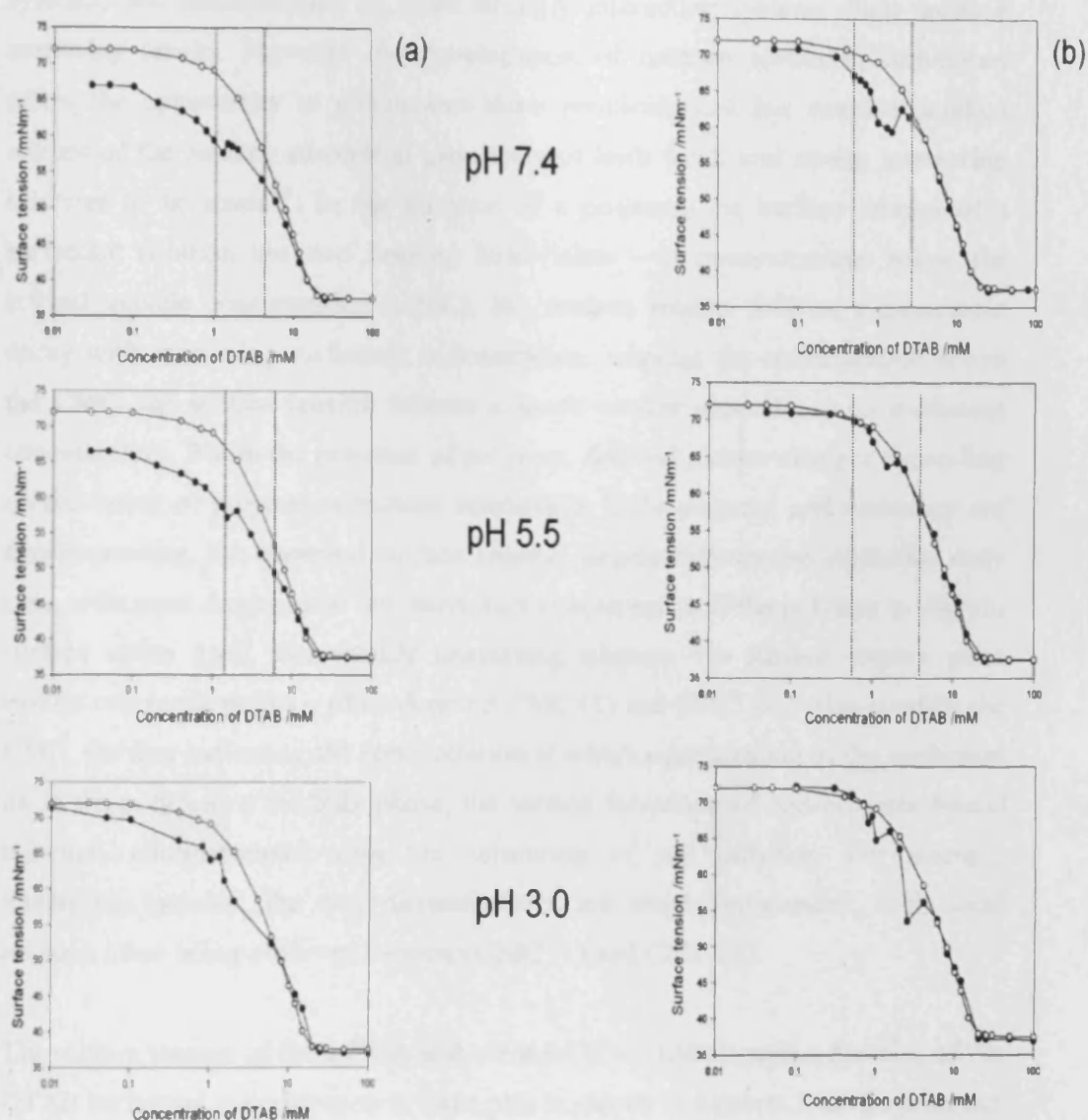


Figure 6.1; Concentration dependence of surface tension of 0.2wt% atactic polymer (panel a) and 0.2wt% syndiotactic polymer (panel b), surface tension of DTAB (open circles) and surface tension of polymers (closed circles), further dotted line indicates the precipitated region.

Surface tension has been the main tool for the study of the air/solution interface and the patterns of behaviour have been well established for weakly interacting systems, but measurements on more strongly interacting systems often produce confusing results. However the development of neutron scattering techniques offers the opportunity to circumvent these problems and has enabled detailed studies of the surface adsorption properties of both weak and strong interacting mixtures to be made^{4,5}. In the absence of a polymer, the surface tension of a surfactant solution has two limiting behaviours – at concentrations below the critical micelle concentration (CMC), the surface tension follows a monotonic decay with increasing surfactant concentration, whereas for concentration above the CMC, the surface tension follows a much weaker dependence on surfactant concentration. But in the presence of polymer, detailed picture changes depending on the extent of polymer-surfactant interaction. If the polymer and surfactant are non-interacting, the observed surface tension largely follows the surfactant only case, with some deviation at low surfactant concentration if the polymer is slightly surface active itself. For weakly interacting systems, the surface tension plots exhibit two break points – often denoted CMC (1) and CMC (2) – that straddle the CMC, the first indicating the concentration at which micellization of the surfactant on to the polymer in the bulk phase, the second formation of non-polymer bound micelles, commensurate with the saturation of the polymer. For strongly interacting systems, the two discontinuities are much pronounced, with local maxima often being observed between CMC (1) and CMC (2).

The surface tension of the a-PMA and s-PMA/DTAB solutions as a function of the DTAB surfactant concentration at three pHs is shown in figure 6.1. In the presence of DTAB, the surface tension of the a-PMA/DTAB solution is lower than that of the DTAB alone over the entire surfactant concentration range studied at pH 7.4 and 5.5, and lower over the intermediate surfactant concentration range at pH=3.0. For the s-PMA, at all pHs, the distinction between the DTAB-only and the s-PMA/DTAB cases is less distinct, in particular the surface tension at very low surfactant concentration.

6.2.3.2 SANS and EPR

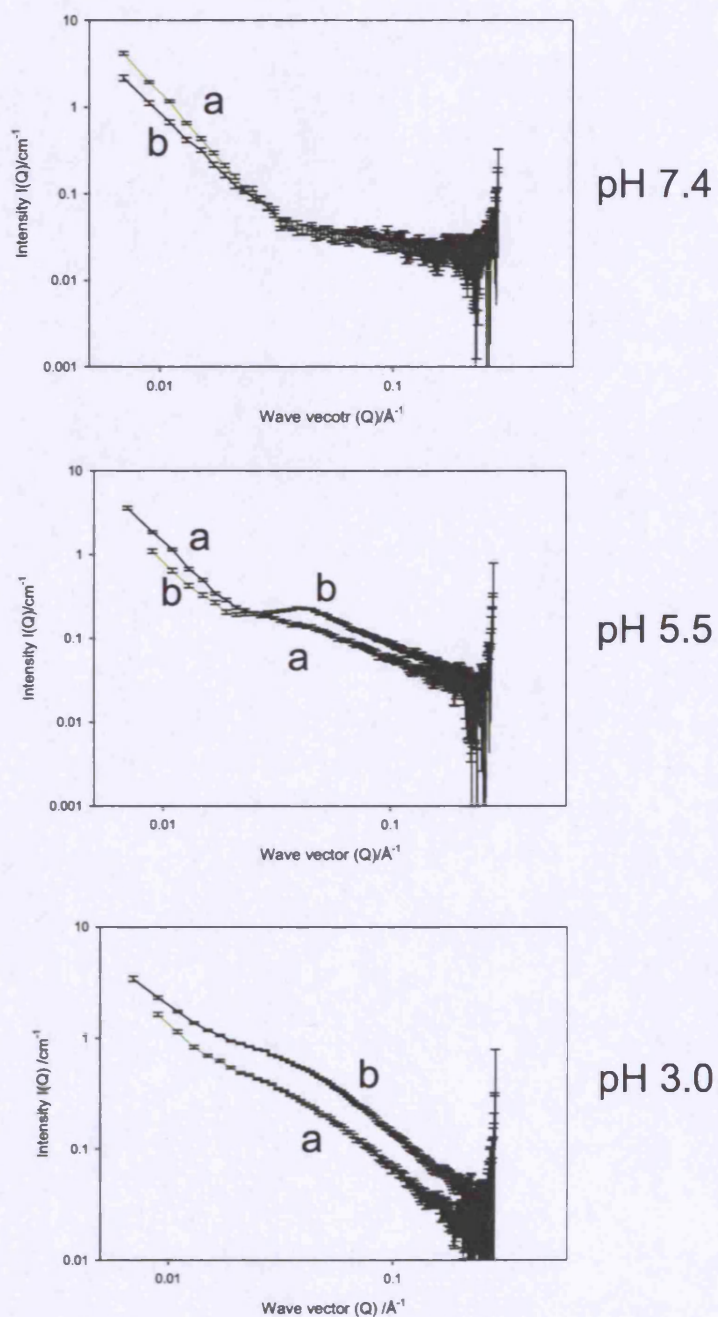
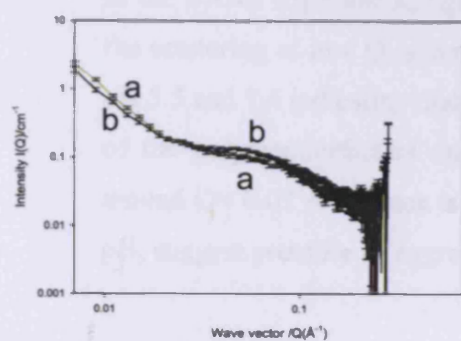
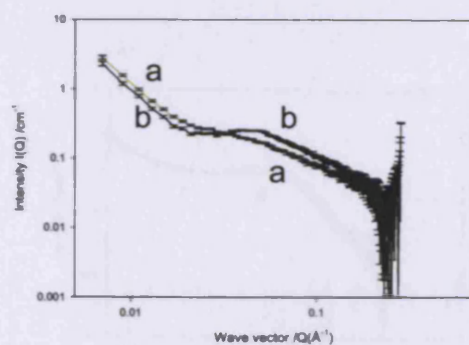
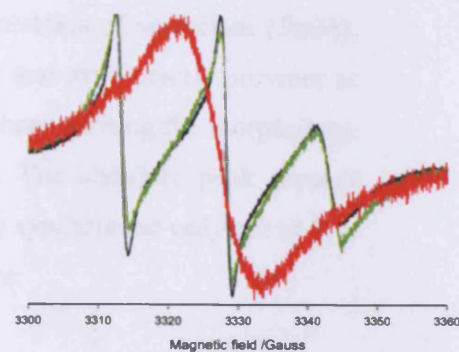


Figure 6.2; The effect of pH on the small-angle neutron scattering from aqueous solution of atactic (a) and Syndiotactic (b) 2 wt% PMA.



pH 7.4



pH 5.5

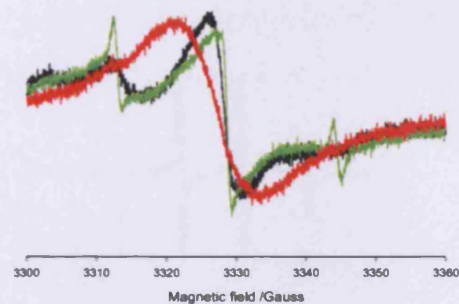


Figure 6.3; Comparison of effect of pH on small-angle neutron scattering and electron paramagnetic resonance spectra.

SANS from 5 mM d-DTAB aqueous solution of atactic(a) and syndiotactic (b) PMA 2 wt% concentration.

EPR of 16-DSE solubilised in 5 mM DTAB (red) in presence of atactic (green line) and syndiotactic (black line) 2 wt% PMA.

The structure of the polymer/surfactant complex – and the role of the polymer tacticity in controlling or influencing the association behaviour of the various PMAs with the DTAB micelle can be examined by small angle neutron scattering (SANS) and electron paramagnetic resonance (EPR).

In the SANS experiment, figure 6.3, at a low concentration of surfactant (5mM), the scattering at low Q is similar for both the atactic and syndiotactic polymer at pH 5.5 and 7.4 indicating that the larger dimensions characterising the morphology of the polymer/surfactant complex are comparable. The shoulder peak present around $Q = 0.07 \text{ \AA}^{-1}$, which is more significant for the syndiotactic polymer at low pH, suggest presence of aggregate or micellar structure.

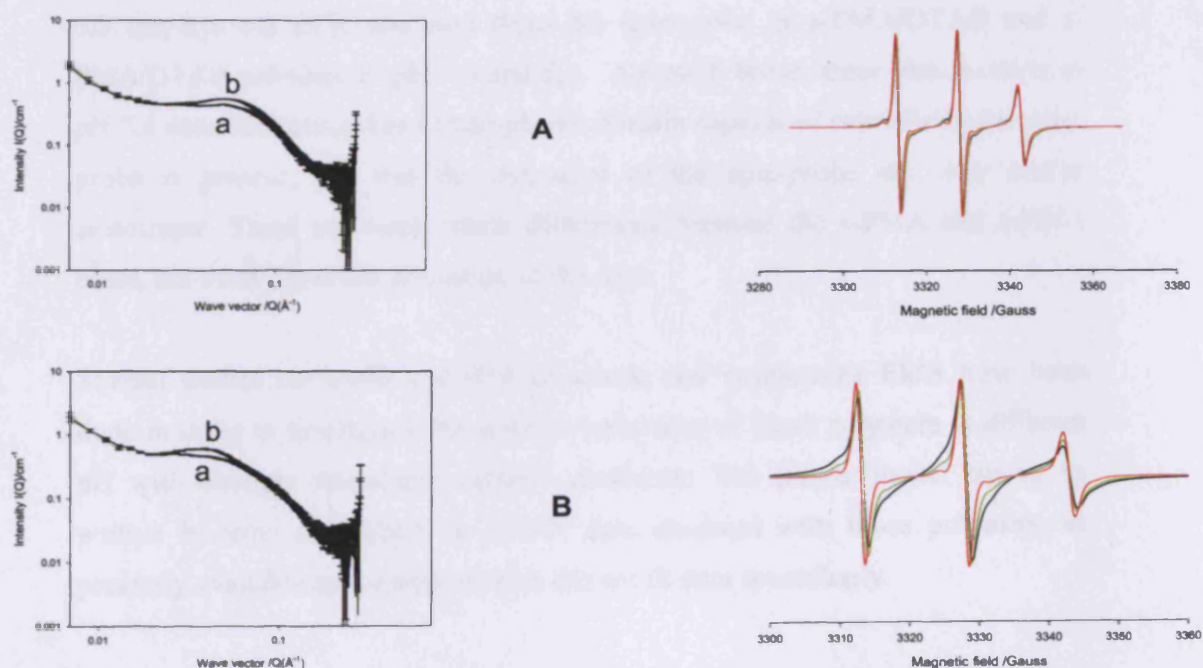


Figure 6.4; Comparison of small-angle neutron scattering and electron paramagnetic resonance spectra at different d-DTAB concentration and PMA low degree of neutralisation (pH 3.0).

SANS from 200 mM (A) and 100 mM (B) d-DTAB aqueous solution of atactic(a) and syndiotactic (b) PMA 2 wt% concentration.

EPR of 16-DSE solubilised in 200 mM (A) and 100 mM (B) DTAB (red) in presence of atactic (green line) and syndiotactic (black line) 2 wt% PMA.

At higher concentrations of surfactant (100mM and 200 mM), the scattering from the respective polymer/surfactant complex adopt a form that is only weakly dependent on the stereo-conformation, the only difference being the slightly more pronounced maximum in the range $0.05 < Q < 0.1 \text{ \AA}^{-1}$ (figure 6.4) shown by the syndiotactic form compared to the atactic form. In the corresponding EPr spectra, the syndiotactic PMA shows a more pronounced decrease in intensity of the low field peak indicates that the motion of the spin-probe had become slower than in the atactic case.

Nitroxide radicals show three sharp lines when dispersed in a fluid environment, with the separation of the low- and mid- field peaks reflecting the polarity sensed by the probe, and the line shape defined by the mobility of the spin-probe. Figure 6.3 displays the EPR spectrum from the spin-probe in a-PMA/DTAB and s-PMA/DTAB solutions at pH 7.4 and 5.5. Although broad, three lines evident in pH 7.4 data, indicating that a hydrophobic domain capable of solubilising the spin-probe is present, but that the dynamics of the spin-probe are slow and/or anisotropic. There are some subtle differences between the s-PMA and a-PMA cases, but these are at the resolution of the data.

Several studies on SANS and EPR of atactic and syndiotactic PMA have been done in order to investigate the solution behaviour of those polymers at different pH with strongly interacting cationic surfactant. The proper model has to be written in order to analyse the SANS data observed with those polymers, as presently available appropriate models did not fit data accordingly.

6.3 Physicochemical characterization of dendronised PEG based polymers

6. 3. 1 Introduction

Since the introduction of dendrimers in the mid-1980s, this novel class of polymeric material has attracted considerable attention, because of their unique structure⁶. In comparison with the traditional linear polymers, dendrimers have much more accurately controlled structures, a single molecular weight rather than a distribution of molecular weights, and a large number of controllable 'peripheral' functionalities and a tendency to adopt a globular shape once a certain size reached. During their discovery, earlier studies in dendrimer chemistry focused mainly on the development of methods of synthesis, as well as the investigation of their physical and chemical properties. As a result, a large number of dendrimers with a broad variety of architectures have been prepared, and the basis for understanding their physical properties was well established. The maturity of methods of synthesis and the relative availability of dendritic materials have led to a significant switch of research emphasis from the fundamental aspects to the exploration of practical applications.

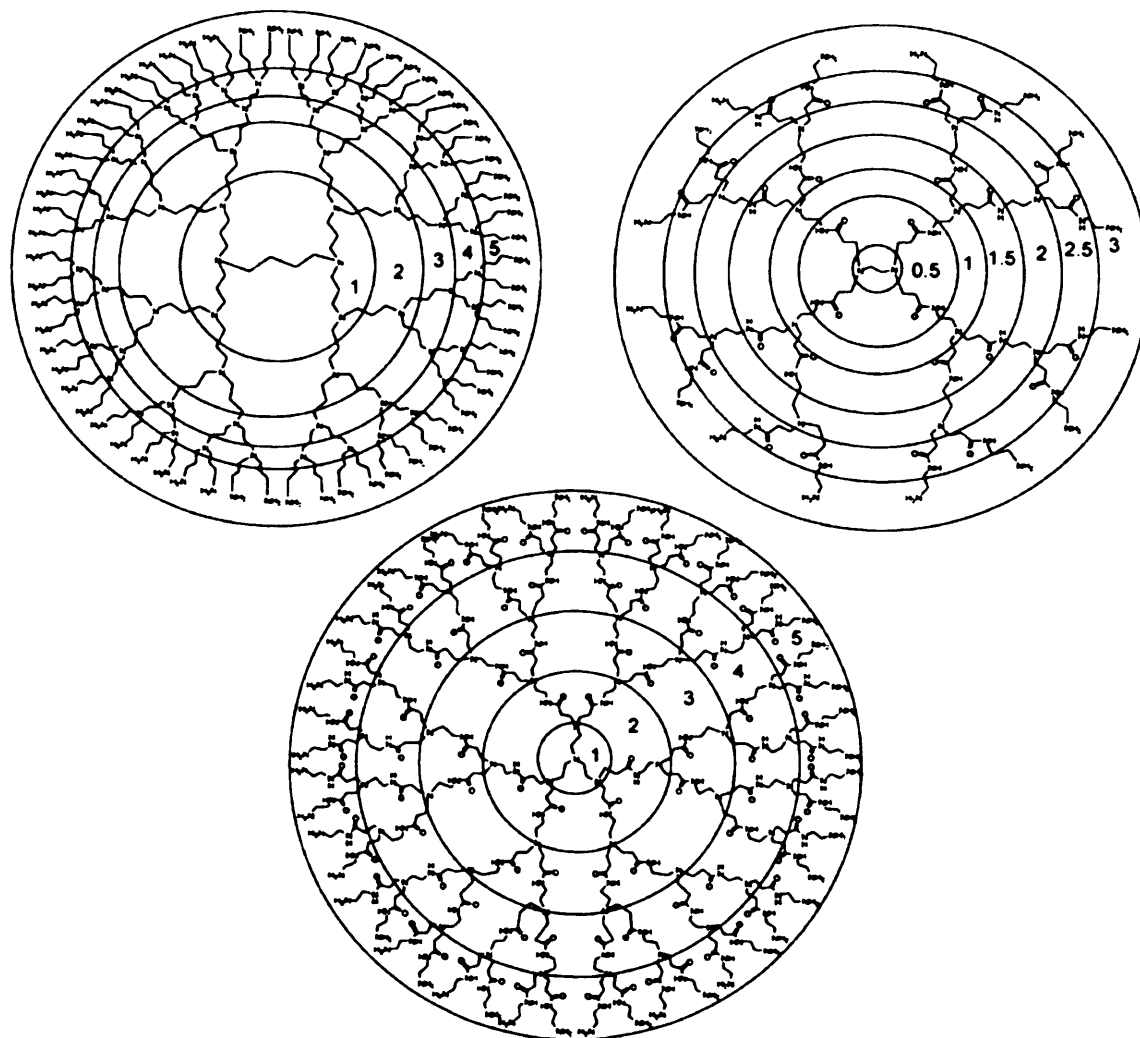


Figure 6.2; Common commercially available dendrimers; top left: Polypropylene imine dendrimer (G5). Top right: Polyamido amine dendrimer (G3). Bottom: Polyamido amine (Starbust) dendrimer (G5). Each generation is marked with a circle⁷

The well-defined structure, compact globular shape, size monodispersity and controllable 'surface' functionalities of dendrimers make them excellent candidates for evaluation as drug carriers⁸. Although the use of dendrimers as drug-delivery agents has been attracted as a major area of their potential application, this area has actually been little studied. Dendrimers can be used as potential drug-delivery agents in at least two ways: firstly, the drug molecules can be physically entrapped inside the dendritic structure; secondly, the drug molecules can be covalently attached on to the surface or other functionalities to afford dendrimer-drug conjugates.

During this study, different generations of polyethylene glycol dendrimers were characterised using small-angle neutron scattering and pulsed-gradient spin-echo NMR to evaluate their conformation.

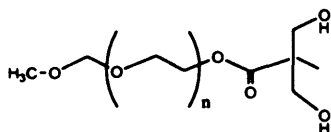
6. 3. 2 Materials and method

The polymers were kindly donated by Lorella Izzo and table 6.1 represents the polydispersity of each polymer used in this experiment

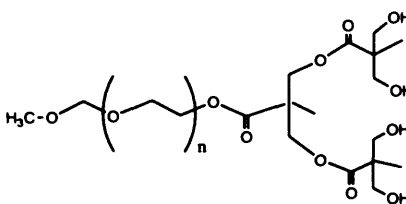
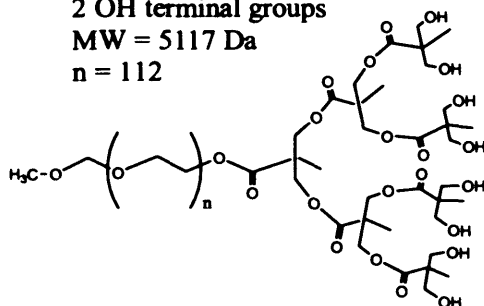
Polymer	Molecular weight/gmol ⁻¹	Polydispersity index (PDI)
PEG G1	5100	1.3
PEG G2	5300	1.3
PEG G3	5800	1.3
PEG G4	6700	1.3
20K 4 arm	2934	1.6
PEG 20K linear	2000	2.6
PEG 5K	5000	1.3

Table 6.2; Molecular weight and polydispersity of polymers

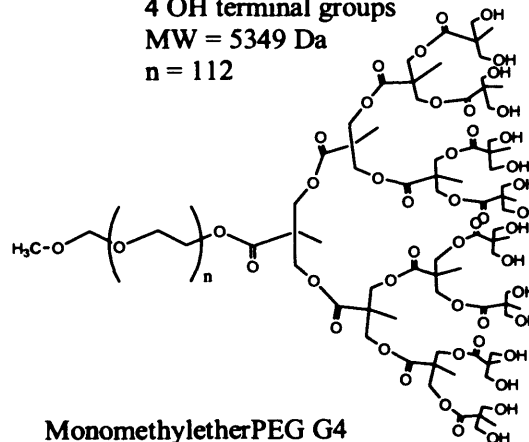
Structures of different generations of PEG



MonomethyletherPEG G1
2 OH terminal groups
MW = 5117 Da
n = 112

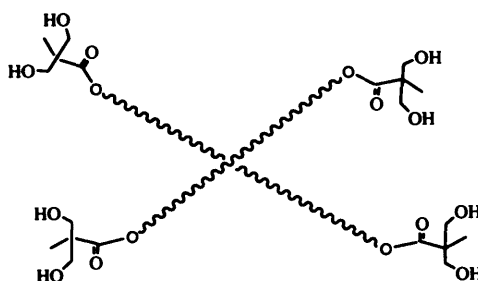


MonomethyletherPEG G2
4 OH terminal groups
MW = 5349 Da
n = 112

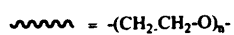


MonomethyletherPEG G3
8 OH terminal groups
MW = 5814 Da
n = 112

MonomethyletherPEG G4
16 OH terminal groups
MW = 6743 Da
n = 112



PEG 4arms
MW = 2934



SANS were carried out with dendrimers and data were fitted to polydisperse Gaussian coil while constraining the polydispersity to the experimentally determined value to calculate radius of gyration.

The diffusion data were measured on AMX 360 with diffusion time 480ms at 25°C. Radii of hydration have been calculated from Stokes-Einstein equation using viscosity of D₂O at 25°C.

6. 3. 3 Results

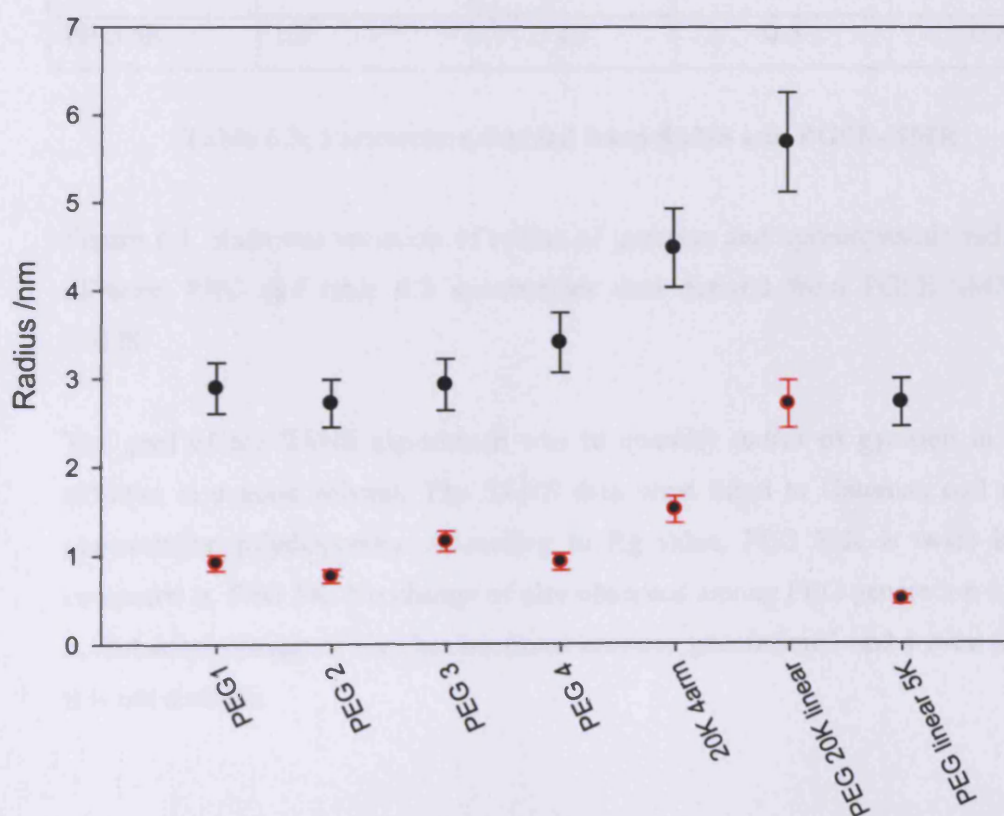


Figure 6.5; Variation of radius of gyration (black) and hydrodynamic radius (red) with different PEG molecular architectures

Polymer	Polydispersity	Radius of gyration $R_g(\text{nm})$ ($\pm 0.1\text{nm}$)	Hydrodynamic radius R_h (nm) (± 0.2)	R_h/R_g
PEG G1	1.3	2.9	1.0	0.3
PEG G2	1.3	2.7	0.7	0.25
PEG G3	1.3	2.9	1.15	0.4
PEG G4	1.3	3.4	0.9	0.3
20K 4 arm	1.6	4.5	1.5	0.3
PEG20K linear	2.6	5.7	2.7	0.5
PEG 5K	1.3	2.7	0.5	0.2

Table 6.3; Parameters derived from SANS and PGSE-NMR

Figure 6.1 illustrates variation of radius of gyration and hydrodynamic radius of different PEG and table 6.2 summarizes data derived from PGSE-NMR and SANS.

The goal of the SANS experiment was to quantify radius of gyration in dilute solution in a good solvent. The SANS data were fitted to Gaussian coil model constraining polydispersity. According to R_g value, PEG 20K is twice in size compared to PEG 5K. No change of size observed among PEG generation 1,2 and 3. But some change of size has occurred between generation 3 and 4 even though it is not sizeable.

6.4 Physicochemical characterization of dendronised pluronics polymer

6.4.1 Introduction

Amphiphilic copolymers of the poly(ethylene oxide)-b-poly(propylene oxide)-b-poly(ethylene oxide) (PEO-PPO-PEO) type, available commercially as Poloxamers or Pluronics, find widespread use as surface active agents⁹. The hydrophilic-lipophilic character of these polymers can be tailored by varying their molecular weight and relative block size. A number of PEO-PPO-PEO copolymers have been shown to associate in aqueous solutions to form micelles consisting of a PPO core and a corona dominated by hydrated PEO segments¹⁰.

The size and morphology of Pluronic copolymer aggregates depend on polymer concentration, environmental effects, and hydrophilic/lipophilic balance. For most pluronic copolymers, the critical micelle temperature (CMT) values range from 25 to 40°C, above which they self-assemble to form a spherical micellar structure by dehydration of the PPO middle block within the structure. At concentration above about 25% (w/v), the Pluronic copolymers exhibit a sol-gel transition behaviour around CMT.

6.4.2 Materials and methods

Three Pluronics described below were kindly donated by collaborator Lorella Izzo (Salerno, Italy) and their chemical details are listed in table 6.4.

Polymer	Molecular weight	No of PEO units	No of PPO units	% PEO	% PPO
PEO-PPO- PEO Dendron G1	14 834	280	40	83.0	15.6
PEO-PPO- PEO Dendron G2	15 298	280	40	80.5	15.1
PEO-PPO- PEO Dendron G3	16 228	280	40	75.9	14.3

Table 6.4; Molecular characterization of different generation of Pluronics

Surface tension

The surface tension measurements were made by using a maximum bubble pressure tensiometer (SITA Online t60) with bubble lifetime of 30s. The instrument was calibrated using distilled water. All glassware was thoroughly cleaned with Decon 90 and rinsed with copious quantities of distilled water. The surface tension measured in range of temperatures for each polymer concentration. Concentration of polymer varied from 0.1wt% (w/v) to 5.0wt% (w/v) and temperature changed from 24⁰C to 34⁰C and measurements were continued in each two degree intervals.

SANS

SANS studies were performed in same configuration described in chapter 3.

6.4.3 Results

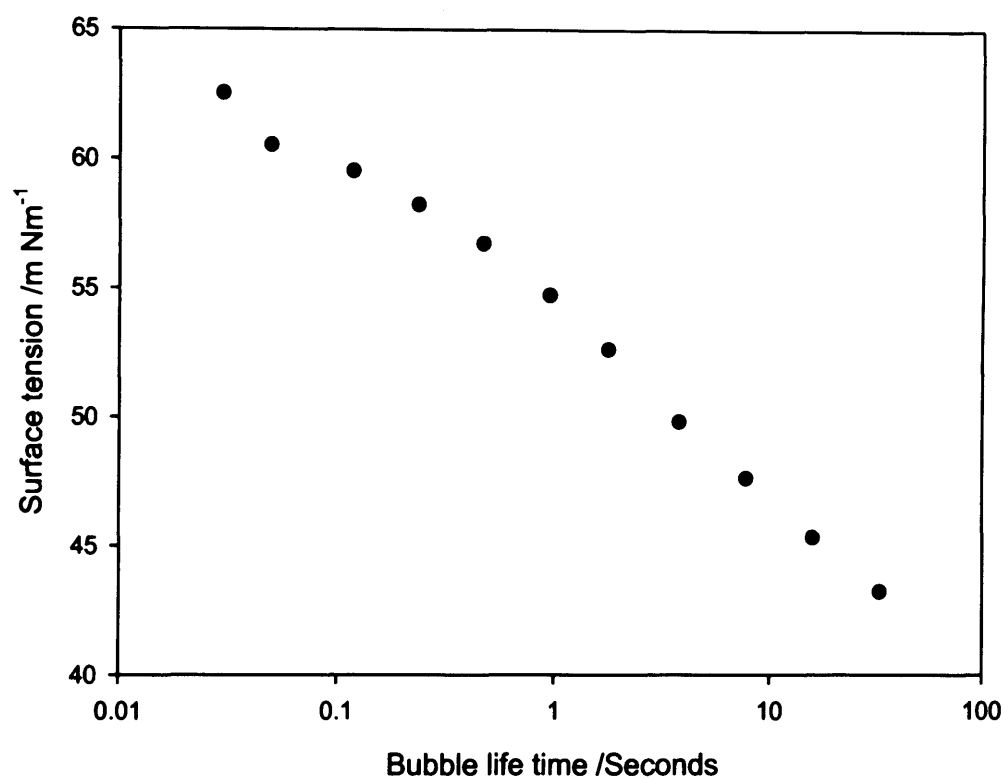


Figure 6.6; The bubble life time dependence of the surface tension of 2.5wt% (w/v) PEO-PPO-PEO G1 at 23°C.

Surface tension variation with different bubble life time of 2.5wt% Pluronic generation 1 illustrates system tends to equilibrate approaching bubble life time of 30 seconds which was used for rest of the experiment.

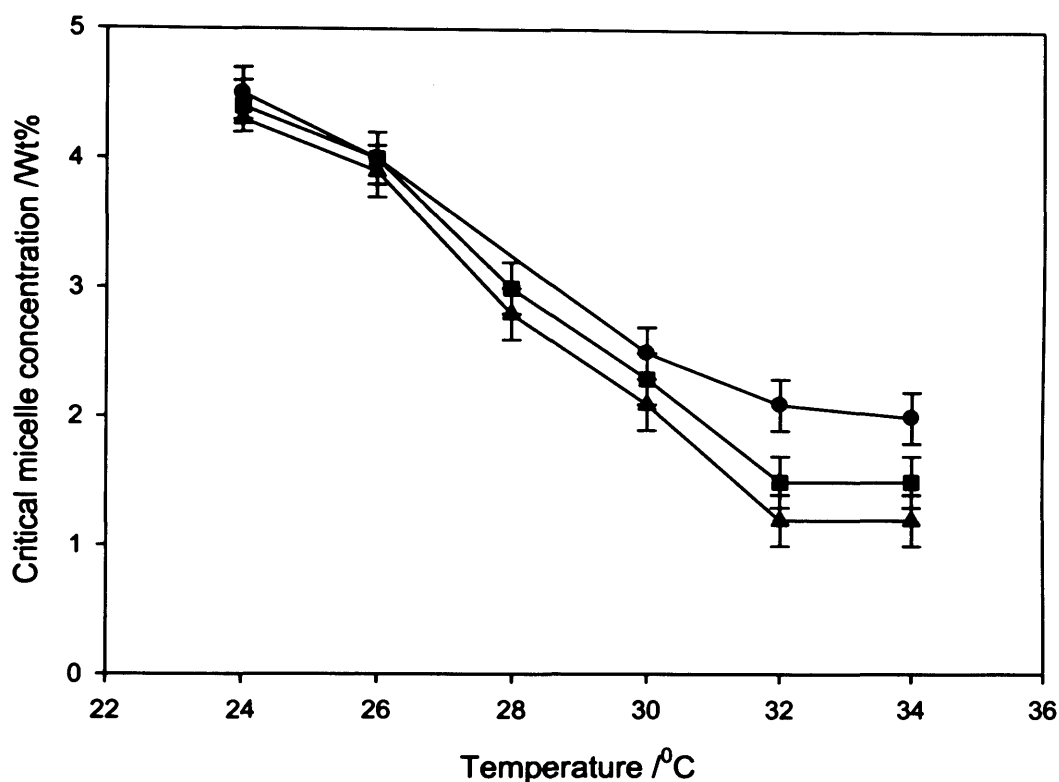
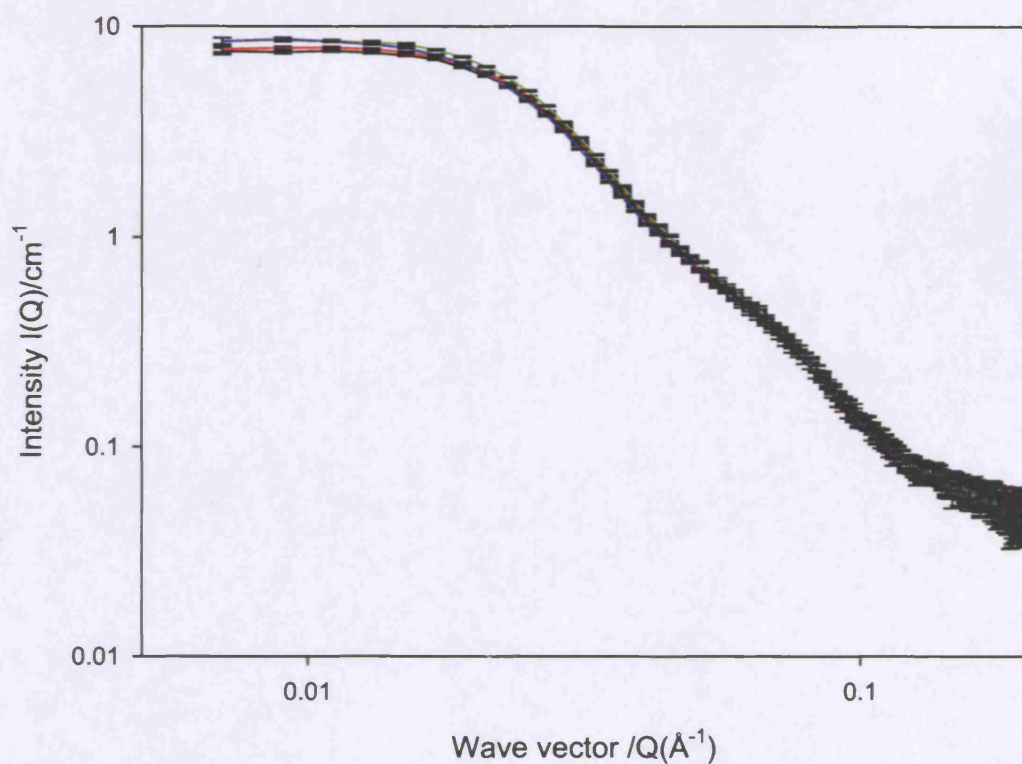


Figure 6.7; Temperature dependence of critical micelle concentration of PEO-PPO-PEO G1: (closed circle); G2: (closed square) and G3: (closed

According to figure 6.3, no significant variation of critical micelle temperature (CMT) for three generation of the polymers studied here. Since the all three samples have the same molecular weight, it may not be possible to observe the considerable variation of CMTs, but it is surprising why the difference of PEO content of each polymer does not contribute in this regard.

Further SANS (figure 6.4) of three different generations and linear polymer observed no variation in scattering which support the discussion made with surface tension data.



SANS of pluronics linear (black), G1 (red), G2 (green) and G4 (blue).

Figure 6.8; Small-angle neutron scattering of PEO-PPO-PEO G1: (red); G2: (green) and G3: (blue) and linear PEO-PPO-PEO (black).

6.5 Physico-chemical characterization of Ion-sensitive ‘isothermal’ responsive polymers

6.5.1 Introduction

Responsive or ‘smart’ materials that can undergo conformational or phase changes in response to variations in temperature and or pH are being developed for uses in field diverse as bulk engineering and microscale medicine. Potential applications of these materials include drug, gene and cell delivery, surface engineering, sensing and actuation. Generally, most responsive polymers change their properties according to in situ temperature stimulus. But the polymers describe here use the side-chain functionality normally exploited for aqueous solubility is used as an ion-responsive component. Of key importance is that the ionic response allows a phase transition to be triggered in thermo-sensitive polymers without a temperature change. By designing polymer architectures such that the coil-to-globule transition affects micellisation, the effect of a polymer response to the presence of ions should lead to formation or destruction of supramolecular architectures. This in turn enables the generation of ‘isothermal’ ionic-responsive release systems.

6.5.2 Materials and methods

Hybrid block co-polymers namely P6 and P7 were kindly donated by Cameron Alexander, Nottingham University. P6 and P7 composed of statistical sequences of polyethylene glycol ethyl ether methacrylate (PEGMA-EE, M_n 246) and polyethylene glycol methyl ether methacrylate (PEGMA-ME, M_n 475, from which were grown an outer block of PEGMA-ME 475.

Polymer-n:m ^a	M _{nth} ^b	M _n ^c	M _w /M _n ^c	% m ^d	LCST °C ^e
P6- Hybrid block-g-PEGMA ME 475 ([n:m]:m = 85:15:6)	26.4	22.2	1.46	44	45
P7- Hybrid block-g- PEGMA ME 475 ([n:m]:m =89:11:17)	15.5	14.7	1.33	30	37

Table 6.5 a) n:m molar ratio of PEGMA-EE 246: PEGMA-ME 475; b) theoretical, from monomer: initiator ratio; c) from GPC (THF, poly(styrene) standard)s, d) NMR integrals; e) from sharp increase I UV adsorption of solutions in water at 550nm¹¹

6.5.3 Results

SANS of these polymers were conducted at ISIS according to the configuration mentioned in chapter 3. Two samples from each polymer were prepared presence and absence of the salt and scattering pattern observed at different temperatures. PGSE-NMR of these polymers was done at different temperature by Abdul Jangher to analyse diffusion coefficient and hydrodynamic radius.

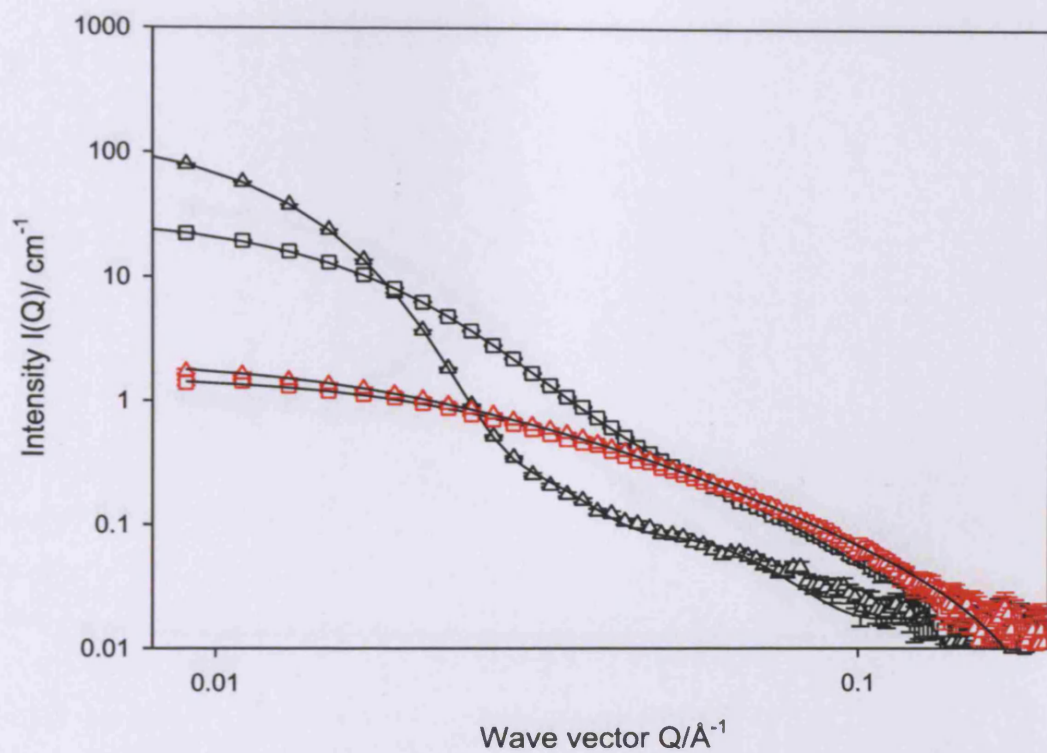


Figure 6.9; Small angle neutron scattering from P6: with salt 50°C, (triangle up); without salt 50°C, (square); salt 20°C, (red triangle); without salt 20°C, (red square); black line represent fitted data to polydispersed two shell hard sphere model

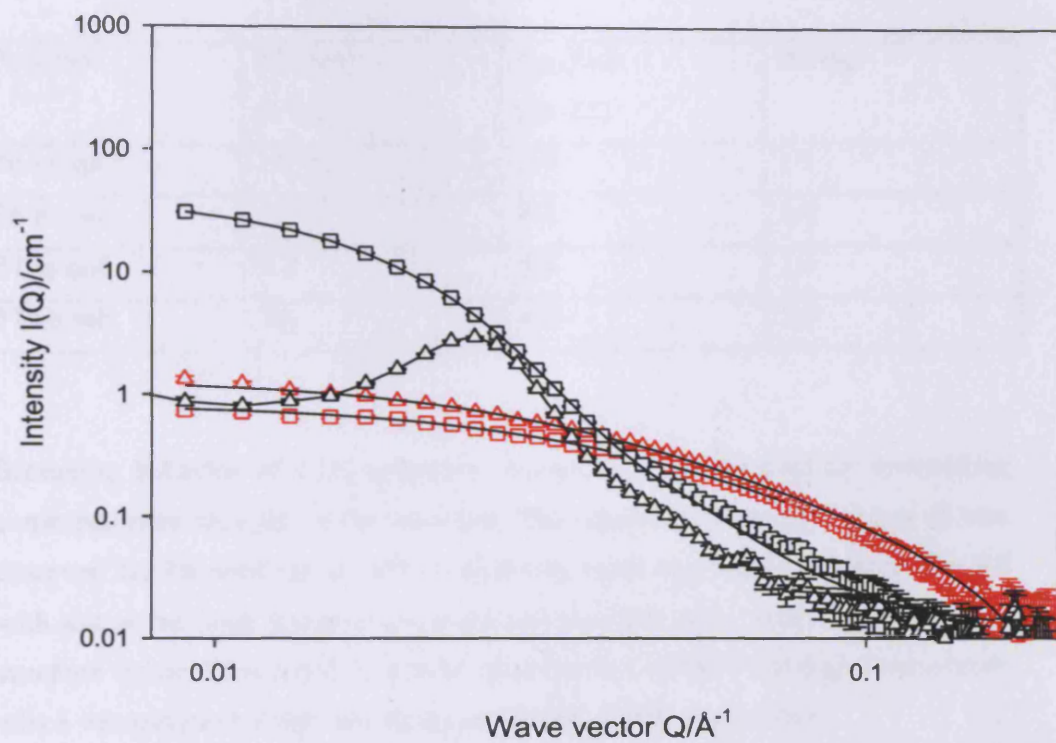


Figure 6.10; Small angle neutron scattering from P7: with salt 50°C, (triangle up); without salt 50°C, (square); salt 20°C, (red triangle); without salt 20°C, (red square); black line represent fitted data to polydispersed two shell hard sphere model

According to the SANS data, both polymer scattered in same way at low temperature and data were fitted to polydispersed Gaussian coil. Both from SANS and PGSE-NMR data, it was shown that P6 is small compare to P7.

Polymer	Rh (nm) (± 0.2)	Rg (nm) (± 0.1)	Rh/Rg
P6 in salt	12.80	8.4	1.5
P6 no salt	12.28	7.8	1.6
P7 in salt	9.2	5.8	1.6
P7 no salt	7.6	4.8	1.6

Scattering behavior of both polymers changed at high temperature resembling conformational changes of the structure. The significant scattering at low Q was observed for P6 with salt at 50°C resembling some aggregated structure. But P7 with salt at the same temperature, produced shoulder peak, implying pronounced structure factor. This could be due to micellisation of the P7 at high temperature which was evident by light scattering and PGSE-NMR data as well.

6.5.4 References

- 1. Walin, T.; Linse, P., Langmuir 14, 2940 1998.**
- 2. Muroga, Y.; Noda, I.; Nagasawa, M., Macromolecules 18, 1580 1985.**
- 3. Apel, U. M.; Hentschke, R.; Helfrich, J., Macromolecules 28, 1778 1995.**
- 4. Taylor, D. J. F.; Thomas, R. K.; Penfold, J., Langmuir 18, 4748 2002.**
- 5. Taylor, D. J. F.; Thomas, R. K.; Hines, J. D.; Humphreys, K.; Penfold, J., Langmuir 18, 9783 2002.**
- 6. Lee, C. C.; Yoshida, M.; Frechet, J. M. J.; Dy, E. E.; Szoka, F. C., Bioconjugate Chemistry 16, 535 2005.**
- 7. Boas, U.; Heegaard, P. M. H., Chemical Society Reviews 33, 43 2004.**
- 8. Gossel, I.; Shu, L.; Schluter, A. D.; Rabe, J. P., Journal of the American Chemical Society 124, 6860 2002.**
- 9. Yang, L.; Alexandridis, P.; Steytler, D. C.; Kositza, M. J.; Holzwarth, J. F., Langmuir 16, 8555 2000.**
- 10. Zhou, D.; Alexandridis, P.; Khan, A., Journal of Colloid and Interface Science 183, 339 1996.**
- 11. Magnusson, J. P.; Khan, A.; Pasparakis, G.; Saeed, A. O.; Wang, W.; Alexander, C., Journal of the American Chemical Society 130, 10852 2008.**

Appendix 1

1) Poster presented as a oral presentation

Renuka Nilmini, Peter Griffiths, Zeena Khayat, Ruth Duncan, Emma Carter, Paolo Ferruti, Probing the interaction of a bioresponsive endosomolytic polyamidoamine with model surfaces using neutron scattering and electron spin-resonance. **International Symposium on Polymer Therapeutics, Valencia, Spain, May 2008.**

2) Posters

R. Nilmini, P.C. Griffiths, C. Alexander, S.S. Pennadam, S.M. King, R.K.Heenan, Physicochemical characterization of thermoresponsive poly(N-isopropylacrylamide) - poly(ethylene imine) graft copolymers, **International Symposium on Polymer Therapeutics, Valencia, Spain, May 2008.**

Renuka Nilmini, Peter Griffiths, Ruth Duncan, Probing membrane – polymer interaction: taking a lead from colloid chemistry, **Summer school in nano medicine, Cardiff, June 2007.**

3) Papers

Derivatizing weak polyelectrolytes-solution properties, self-aggregation, and association with anionic surfaces of hydrophobically modified poly(ethylene imine); Peter C. Griffiths, Alison Paul, Ian A. Fallis, Champa Wellappilli, Damien M. Murphy, Robert Jenkins, Sarah J. Waters, Renuka Nilmini, Richard K. Heenan, Stephen M. King; *Journal of Colloid and Interface Science*, 314 (2007) 460-469

Physicochemical characterization of thermoresponsive Poly(N-isopropylacrylamide) –poly(ethyleneimine) graft copolymers; Peter C. Griffiths, Cameron Alexander, Renuka Nilmini, Sivanand S. Pennadam, Stephen M. King, Richard K. Heenan; *Biomacromolecules* 2008, 91 1170-1178.

The interaction of bioresponsive endosomolytic polymers with biologically relevant interfaces 2 – Phospholipid rich surfaces; Peter Griffiths, Renuka Nilmini, Zeena Khayat, Ruth Duncan, Emma Carter and Paolo Ferruti (ready to submit)

Definition of the effect of polymer stereochemistry on the physicochemical behaviour of polymer therapeutics; Lorella Izzo, Peter C. Griffiths, Renuka Nilmini, Kerri-Lee Wallom, Elaine Ferguson, Ruth Duncan (ready to submit)

Physicochemical characterization of stimuli responsive “smart polymers”;
Johannes Pall Magnusson, Cameron Alexander, Peter Griffiths, Abdulhakim
Jangher and Renuka Nilmini (ready to submit)

Derivatizing weak polyelectrolytes—Solution properties, self-aggregation, and association with anionic surfaces of hydrophobically modified poly(ethylene imine)

Peter C. Griffiths^{a,*}, Alison Paul^a, Ian A. Fallis^a, Champa Wellappili^a, Damien M. Murphy^a, Robert Jenkins^a, Sarah J. Waters^a, Renuka Nilmini^a, Richard K. Heenan^b, Stephen M. King^b

^a School of Chemistry, Cardiff University, Main Building, Park Place, Cardiff CF10 3AT, UK

^b ISIS Facility, Rutherford Appleton Laboratory, Chilton, Didcot, OX11 0QX, UK

Received 3 March 2007; accepted 23 May 2007

Available online 7 June 2007

Abstract

The physical properties of weak polyelectrolytes may be tailored via hydrophobic modification to exhibit useful properties under appropriate pH and ionic strength conditions as a consequence of the often inherently competing effects of electrostatics and hydrophobicity. Pulsed-gradient spin-echo NMR (PGSE-NMR), electron paramagnetic resonance (EPR), small-angle neutron scattering (SANS) surface tension, fluorescence, and pH titration have been used to examine the solution conformation and aggregation behavior of a series of hydrophobically modified hyperbranched poly(ethylene imine) (PEI) polymers in aqueous solution, and their interaction with sodium dodecylsulfate (SDS). PGSE-NMR gave a particularly insightful picture of the apparent molecular weight distribution. The presence of the hydrophobes led to a lower effective charge on the polymer at any given pH, compared to the (parent) nonmodified samples. Analysis of the SANS data showed that the propensity to form highly elliptical or rod-like aggregates at higher pHs, reflecting both the changes in protonation behavior induced by the hydrophobic modification and an hydrophobic interaction, but that these structures were disrupted with decreasing pH (increasing charge). The parent samples were not surface active yet the hydrophobically modified samples show pronounced surface activity and the presence of small hydrophobic domains. The surface activity increased with an increase in the degree of modification. On addition of SDS, the onset of the formation of polymer/surfactant complexes was insensitive to the degree of modification with the resultant PEI/SDS complexes resembling the size and shape of simple SDS micelles. Indeed, the presence of the SDS effectively nullifies the effects of the hydrophobe. Hydrophobic modification is therefore a viable option to tailor pH dependent properties, whose effects may be removed by the presence of surfactant.

© 2007 Elsevier Inc. All rights reserved.

Keywords: Weak polyelectrolyte; Poly(ethylene imine); Hydrophobically modified polymer; Solution conformation; pH behavior; Radius of gyration; Neutron scattering; Diffusion coefficient distribution; Inverse Laplace transform

1. Introduction

The presence of charged or ionisable groups on a polymer offers the opportunity to control many aspects of the behavior of the polymer—solubility, tendency to adsorb at surfaces—by changes in external variables such as pH or ionic strength [1]. The overall behavior of the polymer is determined by the chemical nature of the polymer, its molecular weight and effective

charge. The presence of hydrophobic moieties can perturb the structure of the polymer, either directly through the association of these hydrophobic moieties [2–4], or through the impact the modification has on the ability of the polymer to charge at a given pH. Hydrophobically modified polyelectrolytes such as cellulose [5–7], poly(acrylamide) [8–10], poly(ethylene oxide) PEO [11], and sulfonated poly(vinyl alcohol) [12] are attracting considerable attention as the associated hydrophobic domains are capable of promoting the solubilization of hydrophobic materials in aqueous solutions.

Charged polymers, especially those bearing nitrogen functionalities, are being developed for drug delivery [13–15]

* Corresponding author. Fax: +44 29 20874030.
E-mail address: griffithspc@cardiff.ac.uk (P.C. Griffiths).

and gene (plasmid [16–18], oligonucleotide [19–21]) therapy. A candidate polymer must provide a hydrophilic, stable, neutral structure that will prolong circulation within the body, exhibit reduced cytotoxicity, provide stability against cytosolic degradation but be sufficiently small (low molecular weight) to preclude capture by the kidneys. For gene delivery, a neutral polymer will result in poor DNA condensing ability whilst a cationic structure will facilitate a nonselective interaction with cell membranes, promote DNA condensation but may not subsequently release the DNA.

The structure of any optimized polymeric construct that meets these criteria will need to incorporate the competition between hydrophobic attraction and electrostatic repulsion, and this is sensitive to the degree of charging of the polymer, the solution structure and the interaction with other serum components. However, to date, such synthetic vehicles are poorly efficient at delivering their payload, and much effort is being expended to optimize the structure of the polymeric component. Targeting of PEI-based so-called polyplexes has been attempted by modifying the PEI by incorporation of galactose [22], mannose [23], transferrin [24], and various antibodies [25]. Acetylation [26], grafting of amino acids (alanine, leucine, and histidine), thermoresponsive [27], or hydrophobic moieties [28] has been attempted to increase the delivery efficacy.

Most of the therapeutic agents one may wish to deliver by incorporation into a polymeric vehicle are hydrophobic and therefore, insoluble in water. Our aim here is to probe the fundamental effects that derivatization with hydrophobic moieties—in this case, introduced by grafting dodecyl groups—may have on the solution conformation of the polymer, the effect this has on the pH dependent degree of protonation and the interaction of the polymer with a negatively charged surface, a micelle formed from the surfactant sodium dodecylsulfate (SDS).

Previous studies of PEI/SDS systems have indicated some unusual pH and conductivity changes. The increase in pH of the PEI solution with increasing SDS concentration was qualitatively interpreted via the concept of ion exchange reactions [29] and in terms of specific amine group–SDS interaction [30–32]. On the basis of their NMR study, Winnik et al. [31] interpreted the unusual conductivity increase of SDS in the presence of PEI as a consequence of special ion transport processes within the polyamine/surfactant complex. They showed that at low concentrations of SDS, PEI showed an exothermic interaction with SDS, attributed to the binding of individual SDS molecules to the polymer. At high concentration of SDS, the interaction was endothermic, due to repulsion between dodecyl ions ($C_{12}H_{25}OSO_3^-$) bound to the polymer. In the first binding process, the $C_{12}H_{25}OSO_3^-$ ions bind in monomer form to the protonated amine groups, driving an increase in pH. Above a critical amount of the bound surfactant, the PEI/SDS complex molecules collapsed and precipitated. The precipitated complex dissolved in the excess surfactant due to a collective (micelle-like) polymer–surfactant interaction. No major conformational changes were observed by small-angle neutron scattering in branched PEI at pH 10.1, as a result of association of SDS, with the polymer remaining in an elongated ellipsoidal form. At pH 4.9, the PEI/SDS association forms three-dimensional

aggregates, involving surfactant bilayers separated by PEI and water in a lamellar arrangement [33].

Recently, Penfold et al. [34] reported a neutron reflectivity study of (both linear and branched) PEI/SDS mixtures at the air–water interface. Not surprisingly, both the surface tension and adsorption results showed a pronounced pH dependence. The SDS adsorption was greatest for the branched polymer and at higher pHs, i.e., under conditions when the polymer is least charged. The branched polymer showed a pH and surfactant concentration dependent transition from monolayer (thickness ~ 20 Å) to multilayer coverage. Ordered structures—leading to Bragg peaks in the reflectivity—were also observed.

Such phase separation of oppositely charged polymers and surfactants can be avoided by grafting water soluble oligomeric groups such as poly(ethylene oxide) to the polymer [35,36]. In such poly(ethoxylated) derivatives, the hydrogen atoms attached to the primary and secondary nitrogen are replaced by an ethoxylated chain. The degree of ethoxylation ensures that when positively charged (protonation of amine groups), the strong interaction with the SDS does not cause phase separation. Indeed, the observed surface tension behavior of ethoxylated PEI {PEI(EO)₇}/SDS was intermediate between that expected of a weak polymer/surfactant interaction (PEO/SDS) and a strong polymer/surfactant interaction (PEI/SDS). The surface tension of PEI(EO)₇/SDS mixtures at all SDS concentrations decreased with an decrease in pH. Only at the lower pHs, i.e., pH 3, was there any indication in the surface tension data of an association [37]. The micelle aggregation number of the bound SDS aggregates are greater with (EO)₂₀PEI (95–142 depending on surfactant concentration) when compared to pure SDS micelles. The increased stability of the bound micelles resulting from electrostatic interactions with the polymer, promotes the micellar growth. For PEI(EO)₂₀/SDS systems, on increasing the pH from 2.5 to 5.5, the aggregation number increases from 44 to 95.

Bergstrom and Claesson et al. in a series of papers [33,38,39] have considered the scattering from a range of cationic polyelectrolytes, usually in the presence of anionic surfactants. At low pH, i.e., high charge density, and low SDS concentrations, disk-like structures were observed, leading to a more ordered phase with increasing surfactant concentration, interpreted in terms of stacked elliptical bilayers. At high pH and low SDS concentrations, there is little change in the polymer scattering, and hence polymer conformation.

Clearly, the PEI/SDS system is an interesting one, with significant variations in structure being observed dependent on molecular weight, pH, and nature of modification. Here, we explore the effects of hydrophobic modification on a number of these interesting structure characteristics.

2. Materials and methods

Branched poly(ethylene imine) (PEI) samples of nominal molecular weights 2000, 25,000, and 750,000 g mol⁻¹ were obtained from Aldrich, whilst a 50,000 g mol⁻¹ samples was sourced from Acros Organics. These polymers were somewhat polydisperse, a point discussed in more detail in Supplemen-

Table 1
Spectroscopic characterization of the hydrophobically modified poly(ethylene imine) derivatives employed in this study

Sample	Area of characteristic peak		Ratio (number of PEI units)/ (number of $-\text{CH}_3$ groups) ($\pm 5\%$)
	PEI $-\text{CH}_2\text{CH}_2\text{N}-$ (2.3–3.0 ppm)	Hydrophobic group $-\text{CH}_3$ group (0.96 ppm)	
HM _{1%} BPEI _{25 K}	63	0.5	93
HM _{10%} BPEI _{25 K}	40	2	15

tary material. In essence, only the data from the $25,000 \text{ g mol}^{-1}$ sample will be presented, as the other polymers were either too polydisperse or too small ($\text{PEI } 2000 \text{ g mol}^{-1}$). Nonetheless, the other polymers were interesting for comparison purposes. 1,2-epoxydodecane (Aldrich), 16-doxyl stearic acid methyl ester (16-DSE) and pyrene (Aldrich) were all used as received, whereas sodium dodecylsulfate (SDS) (Aldrich) was recrystallized from ethanol until no minimum around the CMC was observed in the surface tension data.

Hydrophobically modified samples were prepared at 2 statistical degrees of loading; 1 hydrophobe per 100 EI units, the second higher at 1 hydrophobe per 10 EI units. These materials are denoted HM_{1%}BPEI_{25 K} and HM_{10%}BPEI_{25 K} where the B underlines the fact that these polymers are hyperbranched, the subscript “25 K” indicated the molecular weight of the PEI and HM_{1%} the degree of hydrophobic modification. The degree of modification was determined by ^1H NMR, Table 1.

2.1. Surface tension measurements

Surface tension measurements were performed at 25°C ($\pm 1^\circ\text{C}$) using a Du Nöuy ring surface tension balance, incorporating a CI Electronics (Wiltshire, UK) zero displacement microbalance with a 4 cm circumference platinum ring. The platinum ring was carefully cleaned in concentrated nitric acid and rinsed several times with distilled water. The absolute value and linearity of the surface tension balance was calibrated using water/ethanol mixtures. Measurements were performed in triplicate to constant value, to ensure reproducibility and equilibrium conditions (up to times of several tens of minutes).

2.2. Fluorescence measurements

All fluorescence measurements were performed on a Perkin-Elmer luminescence spectrophotometer, LS50B. Pyrene (concentration $2 \mu\text{M}$) was used as a probe in all cases. The spectrum was recorded over the range 350–450 nm (excitation wavelength 310 nm, slit width 2.5 nm). The polarity was expressed as the common 3/1 ratio—the ratio of the first (372–373 nm) and third (382–384 nm) vibronic peaks in the pyrene spectrum.

2.3. Small-angle neutron scattering

SANS measurements were performed on the LOQ diffractometer at ISIS (Rutherford Appleton Laboratories, Oxfordshire, UK). This uses neutrons of wavelength 2.2–10 Å by time of flight, with a 64 cm square detector at 4.1 m from the sample. The samples were contained in 2 mm pathlength,

UV-spectrophotometer grade, quartz cuvettes (Hellma) and mounted in aluminium holders on top of an enclosed, computer-controlled, sample changer. Sample volumes were approximately 0.4 cm^3 . Temperature control was achieved through the use of a thermostatted circulating bath pumping fluid through the base of the sample changer. Under these conditions a temperature stability of $\pm 0.5^\circ\text{C}$ can be achieved. All measurements were carried out at 25°C . Experimental measuring times were approximately 40 min.

All scattering data were (a) normalized for the sample transmission, (b) background corrected using a quartz cell filled with D_2O (this also removes the inherent instrumental background arising from vacuum windows, etc.), and (c) corrected for the linearity and efficiency of the detector response using the instrument-specific software package. The data were put onto an absolute scale by reference to the scattering from a partially deuterated polystyrene blend.

2.4. Pulsed-gradient spin-echo NMR spectroscopy

Measurements were conducted on a Bruker AMX360 NMR spectrometer using a stimulated echo-sequence as described elsewhere [40]. This configuration uses a 5 mm diffusion probe (Cryomagnet Systems, Indianapolis) and a Bruker gradient spectroscopy accessory unit.

2.5. Electron paramagnetic resonance (EPR) spectroscopy

An aliquot of an ethanol solution of spin-probe 16-DSE (2 mM) was dried in a sample vial, to which the sample is added, mixed and allowed to equilibrate. The final spin-probe concentration is around $2 \mu\text{M}$. Where appropriate, the pH was adjusted by addition of HCl. An aliquot of the sample was drawn into a capillary tube which was sealed and placed in quartz EPR tubes before taking measurements using a Bruker EMX at room temperature ($\sim 22^\circ\text{C}$) using a frequency of $9.29 \pm 0.3 \text{ GHz}$. Each spectrum was recorded as the average of 10 scans.

3. Results and discussion

Poly(ethylene imine) (PEI) is a hyperbranched polymer containing three different types of amine groups: secondary and tertiary amino groups in the main chain and secondary and primary amino groups in the side chain. The ratio of primary to secondary to tertiary amino groups is 1:2:1. PEI becomes a strong polyelectrolyte at low pH but to all intents and purposes is uncharged at high pH [41,42].

3.1. Polydispersity assessment

BPEI polymers are variably polydisperse, a feature that is unfortunate but tolerated in many other studies. Indeed, as a hyperbranched polymer with no chromophore, determination of the absolute molecular weight distribution is problematic. The distribution of self-diffusion coefficients measurable in the PGSE-NMR experiments reflects indirectly, the molecular weight distribution and is therefore a convenient method to screen out samples of BPEI that are too polydisperse to provide meaningful data.

Figs. 1a and 1b present the raw PGSE-NMR attenuation data plus associated fits and the self-diffusion coefficient distributions respectively for the four polymers used here. Clearly, BPEI_{2K} behaves much like a monodisperse polymer (linear attenuation function), not unexpectedly given its low molecular weight. An inverse Laplace transform (ILT) of these attenuation functions will result in the distribution of apparent self-diffusion coefficients, an alternative but semi-empirical method to quantify the polydispersity. Analyzing the near monodisperse BPEI_{2K} data in this manner demonstrates the inherent broadening of the ILT, manifest as an approximately half order of magnitude of the self-diffusion coefficient distribution. The attenuation function for BPEI_{25K} is slightly polydisperse although it is not obvious on this scale so a linear “fit” has been added to emphasize this point. The ILT-derived distribution of diffusion coefficients has a width that seems to span 2 orders of magnitude, but given the inherent broadening of the ILT (cf. the BPEI_{2K} data), this equates to a “manageable” distribution of molecular weight. Clearly, BPEI_{50K} and BPEI_{750K} are too broad to work with, but interestingly rather similar. Accordingly, only data from BPEI_{25K} and its derivatives will be discussed here, but similar results were observed for the BPEI_{50K}.

3.2. Degree of ionization

The standard method for determining the charge on a polymer as a function of pH is to titrate the polymer using acid or base, and record the pH [43]. Unlike small molecules, the ability to (further) protonate a particular group on a polyelectrolyte depends on its current degree of protonation. pH titration data may be recast in a modified form of the Henderson–Hasselbach equation suitable for polyelectrolytes;

$$\log K_i = \log K_i^0 + (n - 1) \log \left(\frac{1 - \alpha}{\alpha} \right), \quad (1)$$

where $\log K_i$ is the effective protonation constant of the polymer, $\log K_i^0$ is the protonation of the completely unionized polymer, and α is the degree of protonation. n is a parameter that accounts for neighboring group effects in the protonation process. The degree of protonation is plotted in Fig. 2a as a function of pH for the four BPEI used in this study. The behavior of these samples is in excellent agreement with that presented by, for example Mészáros et al. [44]—PEI is effectively uncharged at pH > 10.5, 30% charged at pH 7 and ~65% charged at pH 4. There are subtle differences between

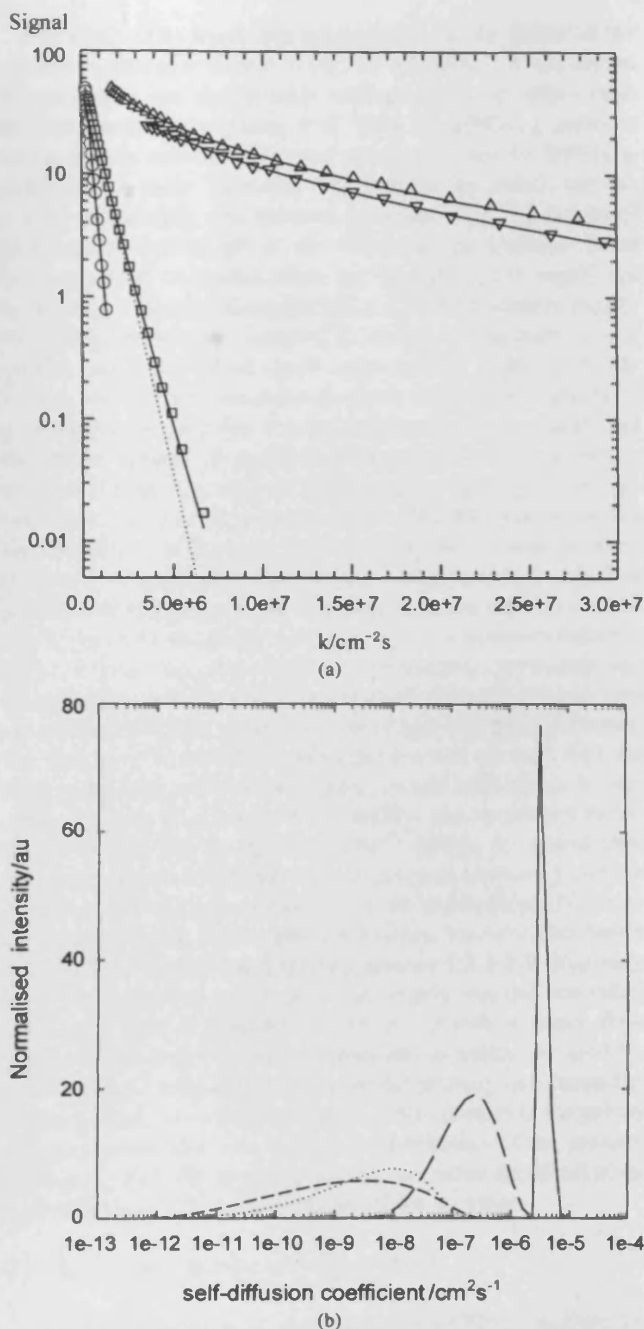


Fig. 1. (a) Raw attenuation functions for the four BPEI samples studied here; (open circles) BPEI_{2K}, (open squares) BPEI_{25K}, (triangles down) BPEI_{50K}, and (triangles up) BPEI_{750K}. Solid lines correspond to fits to a “stretched exponential” analysis as described in Supplementary material. The dotted line through the BPEI_{25K} data corresponds to “monodisperse” behavior. (b) Self-diffusion coefficient distributions for the four BPEI samples studied here; (solid line) BPEI_{2K}, (long dashed line) BPEI_{25K}, (short dashed line) BPEI_{50K}, and (dotted line) BPEI_{750K}.

the various samples, reflecting the distribution of primary, secondary, or tertiary nitrogens within the polymer, coupled with the molecular weight and architecture dependent effective pK_a s within this population of the primary, secondary or tertiary nitrogens. Attempts to quantify this distribution using NMR

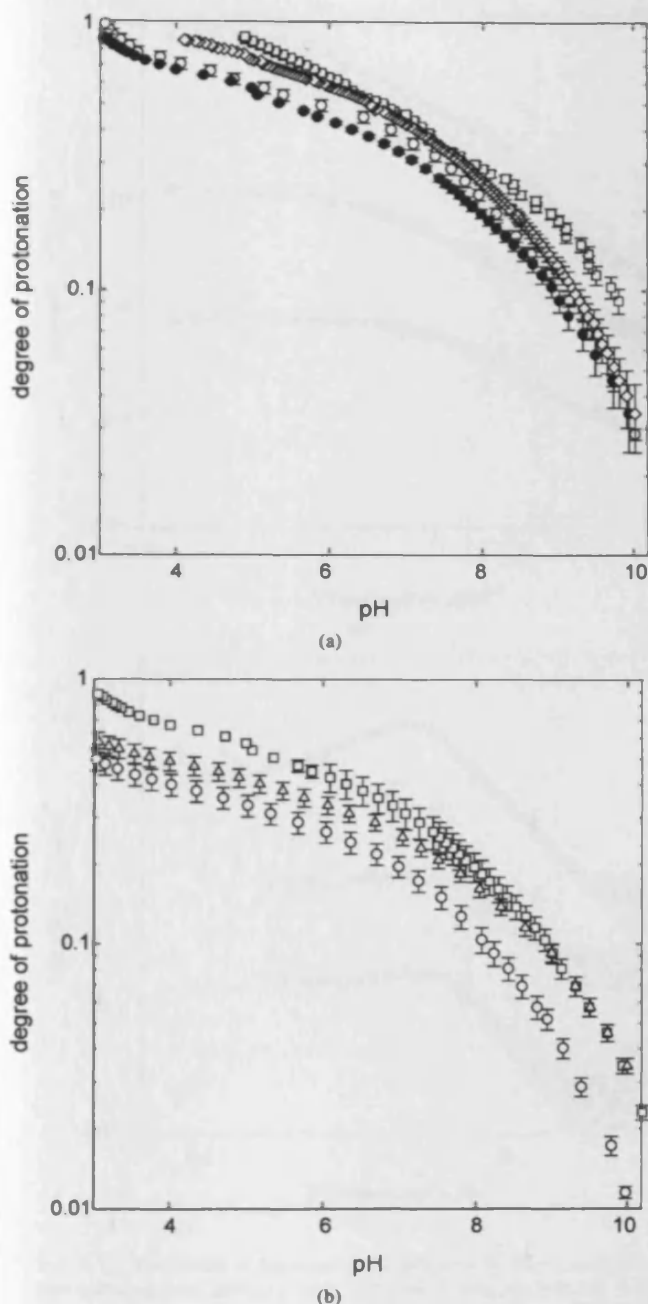


Fig. 2. (a) The degree of protonation calculated from the pH titration data for branched poly(ethylene imine) samples; (open squares) BPEI_{2K}, (open circles) BPEI_{25K}, (filled circles) BPEI_{50K}, and (open diamonds) BPEI_{750K}. (b) The degree of protonation calculated from the pH titration data for branched poly(ethylene imine) samples; (squares) BPEI_{25K}, (triangles) HM1% BPEI_{25K}, and (circles) HM10% BPEI_{25K}.

prove futile given the broad nature of the lines in the spectra. Electrophoretic NMR reports a similar conclusion, but with a significantly different degree of protonation [45] implying that charge/dynamics measurements may probe a different facet of the charging behavior compared with the macroscopic pH titration.

The effect of hydrophobic modification on the ability of the polymer to charge is shown in Fig. 2b. For pHs < 8, the degree of protonation was significantly reduced for the modified samples compared to the parent PEI. Only the BPEI_{25K} series is shown for the reasons discussed previously, but the BPEI_{50K} exhibited the same behavior. The amount by which the degree of protonation was lowered increases with the degree of modification. Above pH 8, the effects of the hydrophobe at the lower level of modification are negligible, but significant for the higher degree of modification. Clearly, hydrophobically modifying the polymer reduced its ability to protonate, i.e., it became less basic, albeit above some critical degree of modification and pH. On successively decreasing the pH, and from an inductive perspective, it is not unreasonable to assume that the tertiary amines are protonated first, followed by secondary amines with the terminal primary amines, although most accessible to the solvent, protonated last [46]. Recently, there has been significant interest in understanding the titration behavior of number of controlled architecture nitrogen bearing polymers [47,48] and extending those conclusions to the data here, these pH curves represent global averages of the protonation behavior of the polymer, i.e., the distribution of primary, secondary, and tertiary nitrogens. Hydrophobically modifying the polymer will alter this distribution of primary, secondary and tertiary amines. The hydrophobic modifier employed here will not react with the tertiary amines, and of those amine groups with which it does react, will convert primary to secondary, and secondary to tertiary moieties. For the 25,000 g mol⁻¹ sample discussed here, and assuming a 1:2:1 distribution of primary secondary and tertiary amines in the parent polymer, and if the hydrophobic modification is largely via the primary amines, the new distribution of primary secondary and tertiary amines 1:2.3:1.1. Similarly, if the hydrophobic modification is largely via the secondary amines, the new distribution is 1:1.8:1.2. Needless to say, these represents the limits of two extremes and in reality, the modifier will be more evenly distributed over the primary and secondary amine groups. To conclude therefore, the changes in the pH behavior were not due to a change in distribution of the primary, secondary, and tertiary amine groups, but rather the effect of the hydrophobes on the local structure of the polymer.

3.3. Solution conformation—Effect of pH

A detailed analysis of the SANS from PEI_{25K} and the hydrophobically modified samples as a function of pH are presented in Supplementary material. A clear insight into the solution conformation may be gained by comparing the three polymers at a given pH. The effect of degree of hydrophobic modification has also been examined, Figs. 3a and 3b. Clearly, the scattering varies significantly as a function of degree of modification, with both the form of the data and the intensity varying (note the relative offsets in intensity). At pH 10 (Fig. 3a), the polymers were uncharged with the scatterers displaying a very elongated structure, whose elongation increased on going from BPEI_{25K} to HM10% BPEI_{25K}, i.e., with increasing degree of hydrophobic modification. This “lengthening” of the aggregate is possibly the precursor to the stacked arrangement seen by Bas-

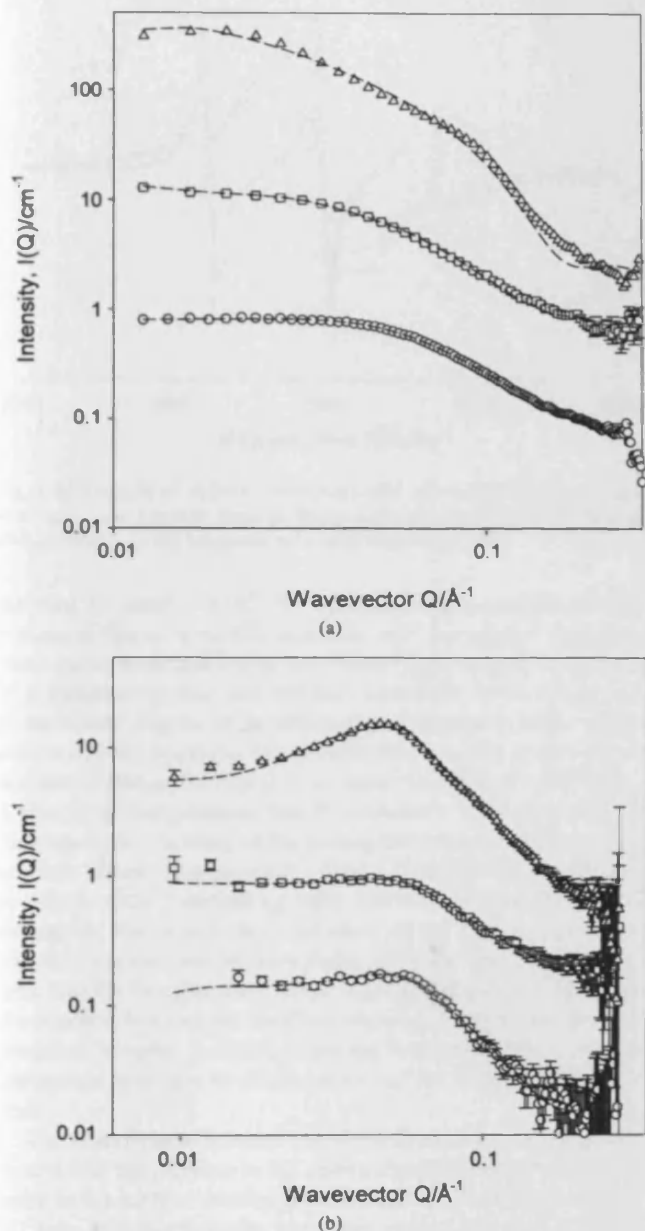


Fig. 3. (a) The effects of hydrophobic modification on the small-angle neutron scattering from BPEI₂₅K in a 5 wt% pH 10 aqueous solution; (circles) BPEI₂₅K, (squares) HM₁% BPEI₂₅K, and (triangles) HM₁₀% BPEI₂₅K. Broken lines correspond to fits as described in the text. Each dataset has been offset by a factor of 10 for clarity. (b) The effects of hydrophobic modification on the small-angle neutron scattering from BPEI₂₅K in a 5 wt% pH 4 aqueous solution; (circles) BPEI₂₅K, (squares) HM₁% BPEI₂₅K, and (triangles) HM₁₀% BPEI₂₅K. Broken lines correspond to fits to the solid ellipse model. For clarity the datasets have been offset by a factor of 3 for clarity.

tardo et al. and would suggest a hydrophobically driven “face on face” association of disc-like structures [49,50]. At pH 4 (Fig. 3b, these three polymers have a much more similar and less elongated morphology. Further, this hydrophobe-promoted aggregation was consistent with the viscosity of such solutions (Supplementary material), with the three polymers exhibiting a similar viscosity up to a polymer concentration of 4 wt%,

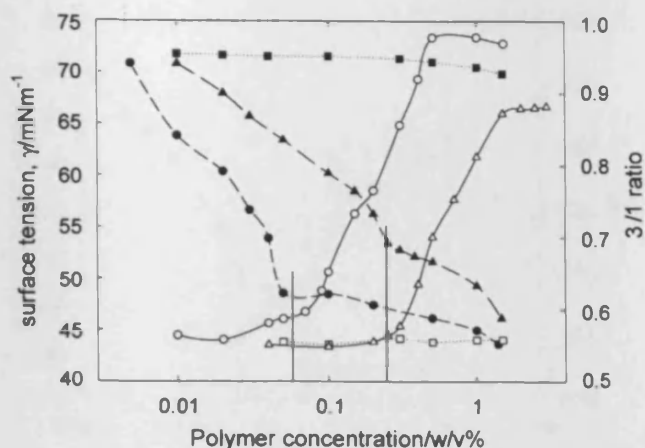


Fig. 4. Surface tension and pyrene fluorescence behavior of BPEI₂₅K and two hydrophobically modified branched poly(ethylene imine) derivatives BHM₁% PEI and BHM₁₀% PEI₂₅K as a function of polymer concentration. Fluorescence (open symbols, right-hand axis) and surface tension (filled symbols, left-hand axis) behaviors; (squares) PEI₂₅K, (triangles) BHM₁% PEI₂₅K, and (circles) BHM₁₀%.

but above which the viscosity of HM₁₀% BPEI₂₅K increases more dramatically than BPEI₂₅K. At a polymer concentration of 10 wt%, HM₁₀% BPEI₂₅K was some 5 times more viscous than the BPEI₂₅K sample.

3.4. The effect of hydrophobe on polymer surface activity and aggregation

Fig. 4 illustrates the surface tension and pyrene fluorescence behavior of BPEI₂₅K, HM₁% BPEI₂₅K, and HM₁₀% BPEI₂₅K as a function of polymer concentration. BPEI₂₅K was largely nonsurface active, with only a negligible decrease in surface tension. The situation was very different for the two modified samples, with the surface tension of both polymers decreasing significantly with an increase in polymer concentration. It is tempting to draw an analogy with classical surfactants in that a pronounced discontinuity at some characteristic concentration is evident. Of key importance, however, was that for all polymer concentrations, the surface tension of HM₁₀% BPEI₂₅K was lower than that of the less highly modified sample HM₁% BPEI₂₅K, and this was lower than the nonmodified sample.

Fig. 4 also presents the 3/1 ratio [51] of the fluorescence spectrum over the same polymer concentration range. There was no change in the 3/1 ratio for BPEI₂₅K with value of the 3/1 ratio remaining constant at 0.55, typical of an aqueous environment. Therefore, there was no association of pyrene to BPEI₂₅K. For both HM₁% BPEI₂₅K and HM₁₀% BPEI₂₅K, the 3/1 ratio dramatically increased above a well-defined critical polymer concentration with the fluorescence intensity for HM₁₀% BPEI₂₅K being greater than HM₁% BPEI₂₅K at all polymer concentrations above the critical value. Again, the sharp rise in the 3/1 ratio occurred at a lower polymer concentration for HM₁₀% BPEI₂₅K compared to the polymer with low degree of modification. The smaller maximum value of the

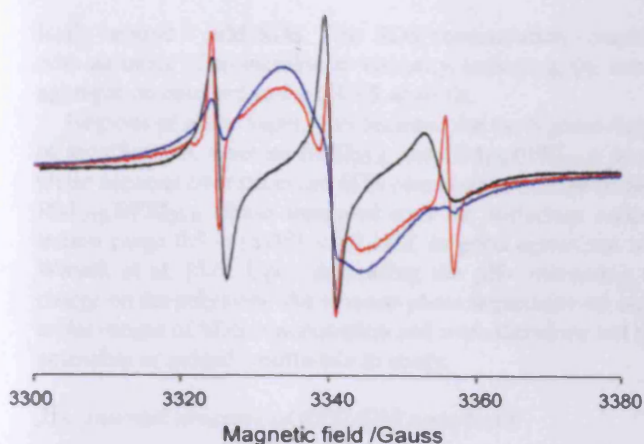


Fig. 5. EPR spectra of 16-DSE solubilized in PEI solutions at ambient pH and with $C_{\text{polymer}} = 1.0$ wt%; (blue) BPEI_{25K}, (red) HM_{1%}BPEI_{25K}, and (black) HM_{10%}BPEI_{25K}. The intensities have been scaled for clarity.

limiting 3/1 ratio (~ 0.85) for HM_{1%}BPEI_{25K} compared with HM_{10%}BPEI_{25K} (~ 0.97) indicates that the pyrene senses a more polar environment in the former case, either as a result of a partitioning that was shifted toward the water phase due to the lower degree of modification or a greater water penetration into the hydrophobic environment, i.e., the hydrophobic domain in HM_{10%}BPEI_{25K} were larger than in HM_{1%}BPEI_{25K}. It should be remembered that the fluorescence merely reflects the overall partitioning of the pyrene between the polymer and aqueous phase. The presence of the nonmodified polymer had no effect on the partitioning, but in the case of the hydrophobic analogues, the degree of partitioning of the pyrene increased, with the concomitant increase in the 3/1 ratio. What is key, however, was the fact that there are pronounced differences between the nonmodified and the modified samples, and between the two modified samples indicating that the increased partitioning of the pyrene was due to the presence of the hydrophobic moieties.

The comparison between the two techniques clearly demonstrated that the increase in 3/1 ratio coincided with the discontinuity in the surface tension data. It followed therefore, that the 3/1 ratio and discontinuity in surface tension correspond to the same physical process.

The presence and nature of the hydrophobic domains may also be assessed using EPR. The spin-probe 16-DSE is insoluble in water, so should a signal be observed from 16-DSE dispersed into a PEI solution, the spectra will reflect the hydrophobicity of the spin-probe environment. Freely rotating 16-DSE displays a spectrum consisting of three sharp lines, with the high field line becoming disproportionately broadened with increases in viscosity. The EPR spectra for 16-DSE in PEI_{25K}, HM_{1%}PEI_{25K} and HM_{10%}PEI_{25K} are presented in Fig. 5. The three line spectra was present in all cases, but superimposed on a much broader feature in the PEI_{25K} and HM_{1%}PEI_{25K} cases. The broad feature arises due to unresolved hyperfine coupling between the spin-probe and PEI, and its broad character signifies a wide distribution of dynamics were present. The expected, three line spectrum was rather more noticeable in the

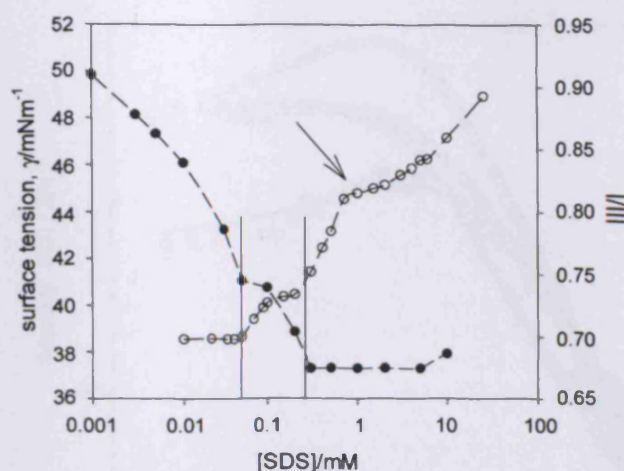


Fig. 6. Surface tension and pyrene fluorescence behavior of HM_{1%}BPEI_{25K} ($C_{\text{polymer}} = 0.5$ wt%) as a function of sodium dodecylsulfate SDS concentration. Fluorescence behavior (right-hand axis) open circles, surface tension behavior (left-hand axis) filled circles. The arrow corresponds to the breakpoint discussed in the text.

HM_{10%}PEI_{25K} case indicating that the spin-probe was located in a relatively mobile environment, presumably the hydrophobic aggregates. pH has no significant effect on these spectra (data not shown)—there may be slight differences between the uncharged (pH 10) and charged (pH < 10) cases, but these are at the limit of the resolution of the experiment, until the highest degree of modification—suggesting that the EPR experiment is probing the internal structure of the PEI complex, and not the aggregate size, such as that detected in the SANS.

At this juncture, it is not possible to state categorically whether the enhanced partitioning of both pyrene and 16-DSE was into aggregates of the hydrophobic moieties or binding of the pyrene to molecularly dispersed dodecyl moieties, or indeed, whether there would be a difference given that the size of any aggregates would necessarily be small. However, the substantial change in the EPR spectra in particular suggests small aggregates are involved.

3.5. Effect of added anionic surfactant SDS on intra- and interpolymer aggregation

Fig. 6 reports the comparison of the surface tension and pyrene fluorescence behavior of mixtures of the BPEI_{25K} derivatives studied here, in the presence of the anionic surfactant SDS. No attempt has been made in this part of the study to fix or control the pH, and the addition of SDS causes a slight increase (0.5 pH unit) in the pH, as discussed by Winnik [31].

Notwithstanding the difficulties in measuring the surface tension of oppositely charged polymers and surfactants, it is clear that the features in the fluorescence data are also present in the surface tension data; a slight increase in fluorescence intensity associated with the surface tension discontinuity at the lower surfactant concentration and a much more pronounced increase in intensity at the higher surfactant concentration.

There was an additional breakpoint in the fluorescence 3/1 ratio, one that is not observed in the surface tension data, specif-

ically around 1 mM SDS. This SDS concentration coincided with an onset of an increase in viscosity, indicating the sort of aggregation detected in the SANS analysis.

Regions of phase separation occurred for the highest degree of modification; whereas BPEI₂₅K and HM₁%BPEI₂₅K do not phase separate over the entire SDS concentration range studied, HM₁₀%BPEI₂₅K phase separated over the surfactant concentration range $0.9 < [\text{SDS}] < 10$ mM, in good agreement with Winnik et al. [52]. Upon decreasing the pH—increasing the charge on the polymer—the systems phase separated over much wider ranges of SDS concentration and were therefore, not that amenable or indeed worthwhile to study.

3.6. Internal structure of BPEI/SDS complexes

The internal or local structure of these complexes may be probed by SANS in which it is possible to deconvolute the scattering from the polymer and the surfactant by an approach known as “contrast variation,” and ultimately extract the size and shape of the SDS aggregate and polymer morphologies. In a deuterated solvent such as D₂O, the scattering from deuterated SDS (d-SDS) is minimal and thus, the observed scattering arises from the (protonated) polymer. Such an approach allows a simple picture of the morphology of the PEI/SDS complex to be obtained. In Fig. 7a, the form of the scattering from the h-BPEI₂₅K/no SDS case was very similar to that from h-BPEI₂₅K/d-SDS indicating that the BPEI₂₅K suffers no significant change in morphology due to the binding of the SDS. For the h-HM₁%BPEI₂₅K/no SDS and h-HM₁%BPEI₂₅K/d-SDS pair, the form of the scattering was quite different, Fig. 7b, indicating that the SDS disrupts the aggregation of the HM₁%BPEI₂₅K, resulting in charged complexes. Concomitantly, the scattering from h-SDS in H₂O would be minimal, but so would the scattering from the h-polymer; thus, the preferred contrast for probing the polymer size and shape is to employ the h-polymer/d-SDS/D₂O contrast. The SDS aggregate size and shape is accessible through a h-polymer/d-SDS/H₂O contrast, and typical datasets are presented in Fig. 7b.

The intensity increased significantly when SDS was present, and pronounced peaks typical of “surfactant-type” scattering were observed. Clearly, the addition of SDS rendered the scatterers more charged. These SDS-dominated scattering data were fitted to a model that accounts for SDS micelle scattering, i.e., a core-shell ellipsoid, and constraining the radius at 16.7 Å with a 4 Å shell yielded an ellipticity of $X = 1.2$ for the bound SDS in the BPEI₂₅K/25 mM SDS case, which became slightly more elliptical for the modified samples, $X = 1.5$ for HM₁%BPEI₂₅K and $X = 2.2$ for HM₁₀%BPEI₂₅K. Thus, the bound SDS state is micellar, with a size and shape rather similar to nonbound SDS micelles in a low—to medium ionic strength solution.

It may simply be coincidence given the size of the PEI aggregate ($R \sim 25$ Å) and the size of a nonbound SDS micelle ($R \sim 16.7 + 4 \text{ Å} \approx 21 \text{ Å}$), but the dimensions of the bound SDS micelle significantly resemble that of the PEI/SDS complex. The obvious interpretation is that the SDS is distributed throughout the PEI aggregate, in agreement with the conclu-

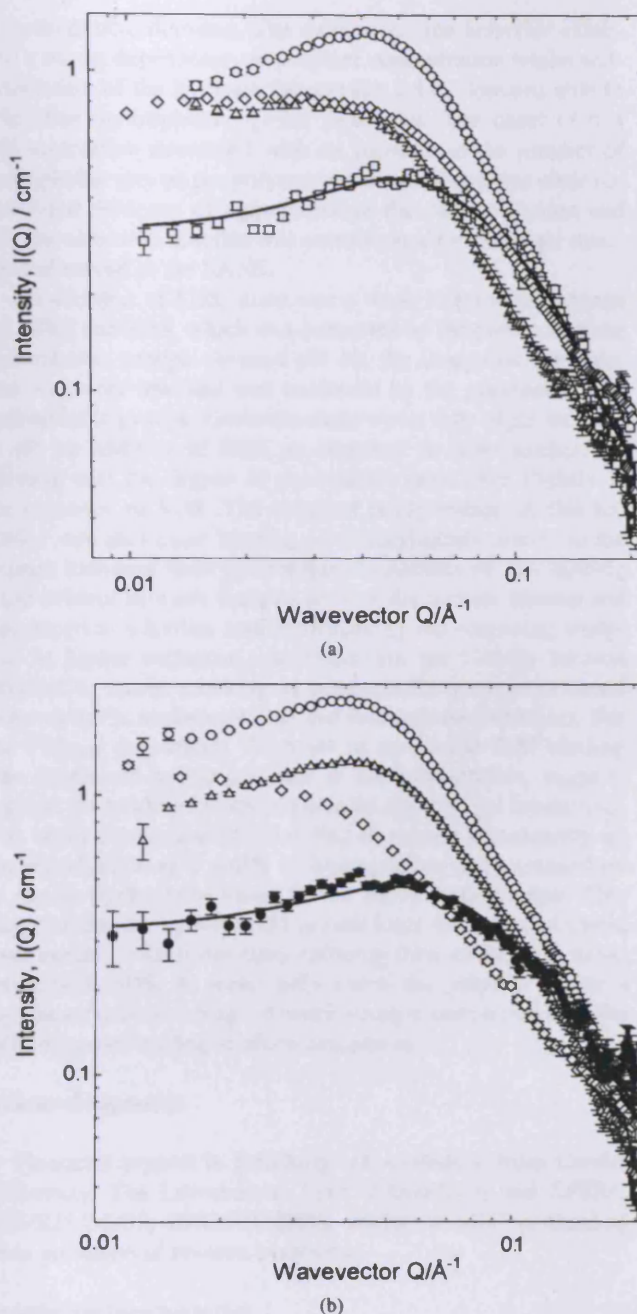


Fig. 7. (a) Contrast variation SANS study of BPEI₂₅K ($C_{\text{polymer}} = 5.0$ wt%) in the presence of 25 mM sodium dodecylsulfate SDS; (circles) BPEI₂₅K/h-SDS/D₂O, (triangles) BPEI₂₅K/d-SDS/D₂O, and (squares) BPEI₂₅K/d-SDS/H₂O. The solid line corresponds to a fit to a charged core-shell ellipse with Hayter–Penfold structure factor. For clarity, representative incoherent backgrounds have been subtracted and the data above $Q = 0.2 \text{ Å}^{-1}$ omitted. Also shown for comparison is the surfactant-free dataset BPEI₂₅K/D₂O for comparison (diamonds). (b) Contrast variation SANS study of BPEI₂₅K ($C_{\text{polymer}} = 5.0$ wt%) in the presence of 25 mM sodium dodecylsulfate SDS; (circles) HM₁%BPEI₂₅K/h-SDS/D₂O, (triangles) HM₁%BPEI₂₅K/d-SDS/D₂O, and (squares) HM₁%BPEI₂₅K/d-SDS/H₂O. The solid line corresponds to a fit to a charged core-shell ellipse with Hayter–Penfold structure factor. For clarity, representative incoherent backgrounds have been subtracted and the data above $Q = 0.2 \text{ Å}^{-1}$ omitted. Also shown for comparison is the surfactant-free dataset HM₁%BPEI₂₅K/D₂O for comparison (diamonds).

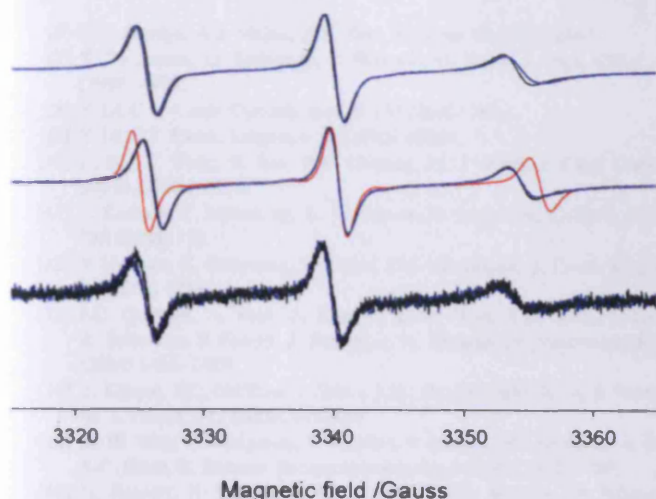


Fig. 8. EPR spectra of 16-DSE solubilized in PEI/SDS solutions at ambient pH and with $C_{\text{polymer}} = 1.0 \text{ wt\%}$; (black) BPEI_{25K}, (blue) HM_{1%}BPEI_{25K}. Bottom spectra, [SDS] = 2 mM, middle, [SDS] = 15 mM, and top, [SDS] = 25 mM. The red spectrum corresponds to a simple 15 mM SDS solution. All vertical scales are normalized for clarity.

sions reached previously that the PEI acts as a template for the SDS.

Further insight into the internal structure of this polymer/surfactant complex was obtained from EPR, Fig. 8, in which pair-wise comparisons of BPEI_{25K} and HM_{1%}BPEI_{25K} are presented in the presence of 2, 15, and 25 mM SDS. As is obvious, the expected 3 line spectra of (a fluid) 16-DSE was observed, the broad feature noted earlier for the polymer-only cases being absent. Interestingly, and in agreement with the SANS data, there was no variation of the internal structure of the PEI/SDS complex with either SDS concentration or degree of modification. The internal structure of the (HM_{1%})PEI_{25K}/SDS complex was however, rather different to the 15 mM SDS (only) case, as denoted by the greater separation—and hence polarity—of the outer lines in the 16-DSE spectrum.

4. Summary

Hydrophobically modified branched poly(ethylene imine) materials based on a commercially available sample with molecular weight $25,000 \text{ g mol}^{-1}$ have been studied by pH titration, fluorescence, surface tension, EPR and NMR spectroscopy and small-angle neutron scattering. The polyelectrolyte character of these polymers—the effective charge versus pH behaviors—were largely independent of molecular weight but there were substantial differences in the effective charge between the modified and nonmodified samples; the differences, manifested as a reduced charge at a given pH, increased with degree of hydrophobic modification. All the polymers—BPEI_{25K}—aggregate at high pH into elongated structures, but became less so with increasing charge.

The presence of the hydrophobic groups on the polymer rendered the BPEI surface active, and led to the formation

of hydrophobic domains. The surface tension behavior exhibited a strong dependence on polymer concentration whilst self-association of the hydrophobic groups led to domains able to solubilize (hydrophobic) probe molecules. The onset of this self-association decreased with an increase in the number of hydrophobic groups per polymer molecule. There was clear co-incident evidence of aggregation in the surface tension and fluorescence data, and this was corroborated by the larger structures observed in the SANS.

On addition of SDS, there was a weak interaction between the BPEI and SDS, which was promoted by the presence of the hydrophobic groups. Around pH 10, the charge on the polymer was very low and was unaltered by the presence of the hydrophobic groups. However, there was a very slight increase in pH on addition of SDS, as observed in other studies, indicating that the degree of protonation must alter slightly in the presence of SDS. The simplest interpretation of this behavior was molecular binding of dodecylsulfate anions to the amines inducing their protonation. Signatures of this binding were evident as weak features in both the surface tension and fluorescence behavior, and reinforced by the scattering analysis. At higher surfactant concentrations, the binding became micellar in nature resulting in substantially more pronounced features in the surface tension and fluorescence behaviors. For the PEI_{25K} derivatives, the onset of *molecular* SDS binding was unaffected by the presence of the hydrophobes, suggesting that the binding has its origin in an electrostatic interaction. The onset of *micellar* SDS binding decreased significantly on the introduction of 1 mol% of hydrophobes, but increased up to the no-hydrophobe value for 10 mol% hydrophobes. This suggests that the hydrophobic groups form domains that shield their contact with water, thus reducing their availability to interact with SDS. At lower pHs where the polymer attains a significant cationic charge, a much stronger interaction with the SDS occurred leading to phase separation.

Acknowledgments

Financial support is gratefully acknowledged from Cardiff University, The Leverhulme Trust (F/00407/Q) and EPSRC (GR/S25456/01; EP/C013220/1), whilst CCLRC is thanked from provision of neutron beamtime.

Supplementary material

The online version of this article contains additional supplementary material.

Please visit DOI: 10.1016/j.jcis.2007.05.082.

References

- [1] M.J. Vicent, F. Greco, R.I. Nicholson, A. Paul, P.C. Griffiths, R. Duncan, *Angew. Chem. Int. Ed.* 44 (2005) 2–6.
- [2] R.A. Siegel, *Adv. Polym. Sci.* 109 (1993) 233.
- [3] A. Matsuda, J. Sato, H. Yasunga, Y. Osada, *Macromolecules* 27 (1994) 7695.
- [4] M. Uchida, M. Kurosawa, Y. Osada, *Macromolecules* 28 (1995) 4583.
- [5] H. Evertsson, S. Nilsson, *Carbohydr. Polym.* 40 (1999) 293.

- [6] L.G. Patruyo, A.J. Muller, A.E. Saez, *Polymer* 43 (2002) 6481.
- [7] K. Thuresson, O. Soderman, P. Hansson, G. Wang, *J. Phys. Chem.* 100 (1996) 4909.
- [8] Y. Li, C.T. Kwak, *Colloids Surf. A* 225 (2003) 169.
- [9] Y. Li, C.T. Kwak, *Langmuir* 18 (2002) 10049.
- [10] G. Bai, Y. Wang, H. Yan, R.K. Thomas, J.C.T. Kwak, *J. Phys. Chem. B* 106 (9) (2002) 2153.
- [11] L. Karlson, C. Malmberg, K. Thuresson, O. Soderman, *Colloids Surf. A* 228 (2003) 171.
- [12] Y. Uemura, H. Hirayama, Y. Hatate, P.M. Macdonald, *J. Chem. Eng. Jpn.* 34 (2001) 1211.
- [13] P.C. Griffiths, A. Paul, Z. Khayat, K.-W. Wan, S.M. King, I. Grillo, R. Schweins, P. Ferruti, J. Franchini, R. Duncan, *Biomacromolecules* 5 (2004) 1422–1427.
- [14] Z. Khayat, P.C. Griffiths, I. Grillo, R.K. Heenan, S.M. King, R. Duncan, *Int. J. Pharm.* 317 (2006) 175–186.
- [15] K.-W. Wan, B. Malgesini, I. Verpilio, P. Ferruti, P.C. Griffiths, A. Paul, A.C. Hann, R. Duncan, *Biomacromolecules* 5 (2004) 1102–1109.
- [16] O. Boussif, F. Lezoualch, M.A. Zanta, M.D. Mergny, D. Scherman, B. Demeneix, J.-P. Behr, *Proc. Natl. Acad. Sci. USA* 92 (1995) 7297–7301.
- [17] B. Abdallah, A. Hassan, C. Benoist, D. Goula, J.-P. Behr, B.A. Demeneix, *Hum. Gene Ther.* 7 (1996) 1947–1954.
- [18] A. Boletta, A. Benigni, J. Lutz, G. Remuzzi, M.R. Soria, L. Monaco, *Hum. Gene Ther.* 8 (1987) 1243–1251.
- [19] B.T. Kren, P. Bandyopadhyay, C.J. Steer, *Nat. Med.* 4 (1998) 285–290.
- [20] P. Bandyopadhyay, X. Ma, C. Linehan-Stieers, B.T. Kren, C.J. Steer, *J. Biol. Chem.* 274 (1999) 10163–10172.
- [21] D.W. Pack, A.S. Hoffman, S. Pun, P.S. Stayton, *Nature Rev. (Drug Deliv.)* 4 (2005) 581–593.
- [22] M.-A. Zanta, O. Boussif, A. Adib, J.P. Behr, *Bioconjugate Chem.* 8 (1997) 839.
- [23] S.S. Diebold, M. Kurs, E. Wagner, M. Cotton, K. Zenke, *J. Biol. Chem.* 274 (1999) 19087.
- [24] R. Kircheis, R. Blessing, S. Brunner, L. Wightman, E. Wagner, *J. Controlled Release* 72 (2001) 165.
- [25] U. Wojda, J.L. Miller, *J. Pharm. Sci.* 89 (2000) 674.
- [26] M.L. Forrest, G.E. Meister, J.T. Koerber, D.W. Pack, *Pharm. Res.* 21 (2004) 365.
- [27] A.C. De Las Heras, S. Pennadam, C. Alexander, *Chem. Soc. Rev.* 34 (2005) 276.
- [28] M. Tomas, A.M. Klibanov, *Proc. Natl. Acad. Sci. USA* 99 (2002) 14640.
- [29] T.K. Bronich, T. Cherry, S.V. Vinogradov, A. Eisenberg, V.A. Kabanov, A.V. Kabanov, *Langmuir* 14 (1998) 6101.
- [30] S.M. Bystryak, M.A. Winnik, J. Siddiqui, *Langmuir* 15 (1999) 3748.
- [31] M.A. Winnik, S.M. Bystryak, C. Chassenieux, V. Strashko, P.M. Macdonald, J. Siddiqui, *Langmuir* 16 (2000) 4495.
- [32] R. Meszaros, L. Thompson, M. Bos, I. Varga, T. Gilany, *Langmuir* 19 (2003) 609.
- [33] L.A. Bastardo, V.M. Garamus, M. Bergstrom, P.M. Claesson, *J. Phys. Chem. B* 109 (2005) 167.
- [34] J. Penfold, I. Tucker, R.K. Thomas, J. Zhang, *Langmuir* 21 (22) (2005) 10061–10073.
- [35] Y. Li, R. Xu, S. Couderc, D.M. Bloor, J. Warr, J. Penfold, J.F. Holzwarth, E. Wyn-Jones, *Langmuir* 17 (2001) 5657.
- [36] Y. Li, S.M. Ghoreishi, J. Warr, D.M. Bloor, J.F. Holzwarth, E. Wyn-Jones, *Langmuir* 16 (2000) 3093.
- [37] J. Penfold, D.J.F. Taylor, R.K. Thomas, I. Tucker, L.J. Thompson, *Langmuir* 19 (2003) 7740.
- [38] L.M. Bergstrom, U.R.M. Kjellin, P.M. Claesson, I. Grillo, *J. Phys. Chem.* 108 (2004) 1874–1881.
- [39] L.M. Bergstrom, U.R.M. Kjellin, P.M. Claesson, J.S. Pederson, M.M. Nielsen, *J. Phys. Chem. B* 106 (2002) 11412–11419.
- [40] J.A. Davies, P.C. Griffiths, *Macromolecules* 36 (2003) 950.
- [41] E.J. Goethals (Ed.), *Polymer Amines and Ammonium Salts*, Pergamon, Oxford/New York, 1980.
- [42] B.L. Rivas, K.E. Geckerler, *Adv. Polym. Sci.* 102 (1992) 171.
- [43] G.H. Lindquist, R.A. Stratton, *J. Colloid Interface Sci.* 55 (1976) 45.
- [44] R. Mészáros, L. Thompson, M. Bos, P. de Groot, *Langmuir* 18 (2002) 6164.
- [45] P.C. Griffiths, A. Paul, P. Stilbs, E. Pettersson, *Macromolecules* 38 (2005) 3539–3542.
- [46] J. Suh, H. Paik, B. Keun-Hwang, *Bioorg. Chem.* 22 (1994) 318–327.
- [47] D. Cakara, J. Kleimann, M. Borkovec, *Macromolecules* 36 (2003) 4201–4207.
- [48] G.J.M. Koper, R.C. van Duijvenbode, D.D.P.W. Stam, U. Steuerle, M. Borkovec, *Macromolecules* 36 (2003) 2500–2507.
- [49] L.M. Bergstrom, U.R.M. Kjellin, P.M. Claesson, I. Grillo, *J. Phys. Chem.* 108 (2004) 1874–1881.
- [50] L.M. Bergstrom, U.R.M. Kjellin, P.M. Claesson, J.S. Pederson, M.M. Nielsen, *J. Phys. Chem. B* 106 (2002) 11412–11419.
- [51] R. Zana, *Surf. Sci. Ser.* 22 (1987) 359.
- [52] M.A. Winnik, S.M. Bystryak, C. Chassenieux, V. Strashhko, P.M. Macdonald, J. Siddiqui, *Langmuir* 16 (2000) 6101.

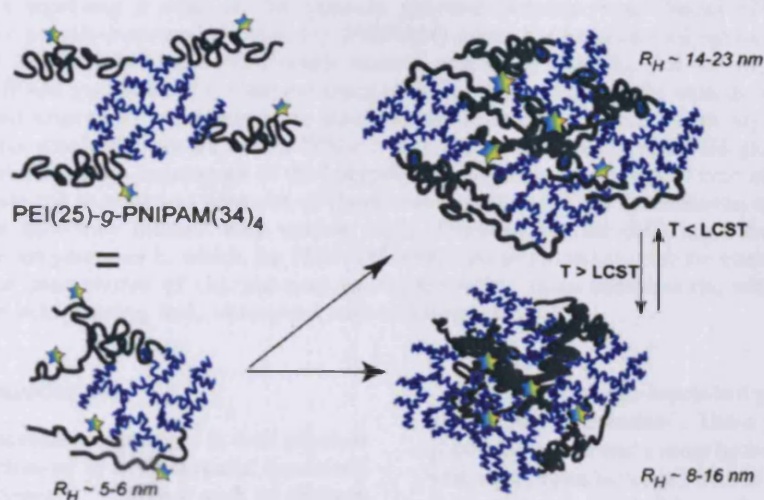
Article

Physicochemical Characterization of Thermoresponsive Poly(*N*-isopropylacrylamide)#poly(ethylene imine) Graft Copolymers

Peter C. Griffiths, Cameron Alexander, Renuka Nilmini, Sivanand S. Pennadam, Stephen M. King, and Richard K. Heenan

Biomacromolecules, 2008, 9 (4), 1170-1178 • DOI: 10.1021/bm701096p • Publication Date (Web): 19 March 2008

Downloaded from <http://pubs.acs.org> on January 15, 2009



More About This Article

Additional resources and features associated with this article are available within the HTML version:

- Supporting Information
- Links to the 2 articles that cite this article, as of the time of this article download
- Access to high resolution figures
- Links to articles and content related to this article
- Copyright permission to reproduce figures and/or text from this article

[View the Full Text HTML](#)



ACS Publications
High quality. High impact.

Biomacromolecules is published by the American Chemical Society, 1155 Sixteenth Street N.W., Washington, DC 20036

Physicochemical Characterization of Thermoresponsive Poly(*N*-isopropylacrylamide)–poly(ethylene imine) Graft Copolymers

Peter C. Griffiths,^{*,†} Cameron Alexander,[‡] Renuka Nilmini,[†] Sivanand S. Pennadam,[‡] Stephen M. King,[§] and Richard K. Heenan[§]

School of Chemistry, Cardiff University, Main Building, Park Place, Cardiff CF10 3AT, Wales, United Kingdom, The School of Pharmacy, University of Nottingham, Boots Science Building, University Park, Nottingham NG7 2RD, United Kingdom, and ISIS Facility, Rutherford Appleton Laboratory, Chilton, Didcot OX11 0QX, United Kingdom

Received October 3, 2007; Revised Manuscript Received January 13, 2008

Synthetic polycations have shown promise as gene delivery vehicles but suffer from an unacceptable toxicity and low transfection efficiency. Novel architectures are being explored to increase transfection efficiency, including copolymers with a thermoresponsive character. The physicochemical characterization of a family of copolymers comprising a core of the cationic polymer poly(ethylene imine) (PEI) with differing thermoresponsive poly(*N*-isopropylacrylamide) (PNIPAM) grafts has been carried out using pulsed-gradient spin-echo NMR (PGSE-NMR) and small-angle neutron scattering (SANS). For the copolymers that have longer chain PNIPAM grafts, there is clear evidence of the collapse of the grafts with increasing temperature and the associated emergence of an attractive interpolymer interaction. These facets depend on the number of PNIPAM grafts attached to the PEI core. While a collapse in the smaller PNIPAM grafts is observed for the third polymer, there is no appearance of the interpolymer attractive interaction. These observations provide further insight into the association behavior of these copolymers, which is fundamental to developing a full understanding of how they interact with nucleic acids. Furthermore, the differing behaviors of the three copolymers over temperatures in which the PNIPAM blocks undergo coil-to-globule transitions is indicative of changes in the presentation of charged-core and hydrophobic chain components, which are key factors affecting nucleic acid binding and, ultimately, cell transfection ability.

Introduction

Polymers that exhibit discontinuous changes in their physical states as a result of small changes in environmental conditions are called “responsive polymers”.^{1–3} Stimuli such as changes in temperature,^{4–6} pH,⁷ ionic strength, light,⁸ and electrical,⁹ or magnetic fields¹⁰ have all been explored for a range of applications. In the field of drug delivery, pH and temperature responsive polymers are two classes of materials that offer potential biomedical advantages.¹¹

The temperature sensitivity of thermoresponsive polymers depends on the extent of interaction of polymer segments with water via H-bonding.¹² Increasing the temperature causes a weakening of the hydrogen bond between polymer and water molecules, leading ultimately to a macroscopically observable precipitation at a well-defined lower critical solution temperature (LCST).^{13,14} Poly(*N*-isopropyl acrylamide) (PNIPAM) is arguably the most commonly studied polymer among those exhibiting temperature-induced phase separation. Its ease of preparation and the fact that the LCST is around 32–33 °C, i.e., close to body temperature, are key facets for use as a potential drug carrier.^{15–17} Further, the phase transition temperature can be tuned by incorporating hydrophobic or hydrophilic groups into the PNIPAM backbone.^{14,18}

Polymers with pH-dependent properties are also of interest as “intelligent materials”. These polymers comprise a hydrophobic monomer and a more hydrophilic ionizable comonomer, with a pK_a value between 3 and 10. Changes in pH and therefore the net charge can induce a phase change depending on the hydrophobic/hydrophilic balance of the copolymer. Classical examples are copolymers of methylmethacrylate with methacrylic acid or dimethylaminoethyl methacrylate (DMAEMA). The pH-responsive swelling and collapsing behavior has been used to induce controlled release of model compounds, drugs, and proteins such as caffeine, indomethacin, and lysozyme.¹⁹

Our focus is on the cationic polymer poly(ethylene imine) (PEI) as it has a proven capability as a potent nonviral gene delivery vector.^{20–24} Under normal physiological conditions, PEI is charged but has the capacity to protonate still further in certain acidic subcellular environments. Its potency as a gene delivery vector could be due to a direct charge-based interaction with the various biological barriers, such as negatively charged membranes that any polymeric drug delivery vehicle must traverse, which can result ultimately in destabilization of the membranes. It is also possible that PEI can influence indirectly a particular cell or subcellular compartment, for example, by acting as a proton sponge that causes ion influx and ultimately leads to membrane rupture.²⁵ It is this ability to traverse these biological barriers and thereby facilitate the delivery of its DNA payload to the cytoplasm that gives PEI its potent gene delivery characteristic. However, the membrane-disrupting properties are likely to be responsible for its unacceptable cytotoxicity.²⁶

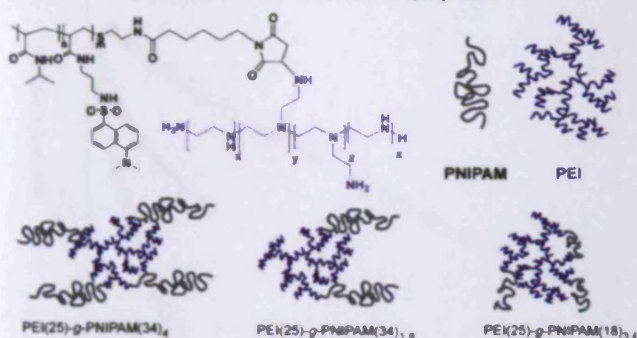
* Corresponding author. E-mail: griffithspc@cardiff.ac.uk. Telephone: +44-29 20875858. Fax: +44-29 20874030.

[†] School of Chemistry, Cardiff University.

[‡] The School of Pharmacy, University of Nottingham.

[§] ISIS Facility, Rutherford Appleton Laboratory.

Scheme 1. Structure of PEI-PNIPAM Copolymers



To maintain the transfection efficiency of PEI but reduce the cytotoxicity, several groups have explored copolymers of PEI, either with a block or functional group that responds to temperature or pH.^{27,28} Generally, the thermoresponsive element used has been poly(*N*-isopropylacrylamide) (PNIPAM), although other combinations of polycations and/or thermoresponsive segment have been used. Hinrichs et al. have synthesized pH and thermoresponsive copolymers of PNIPAM and dimethyl-aminoethyl methacrylate (DMAEMA) and investigated its transfection efficiency in ovarian cancer cells;¹ Kurisawa et al.²⁹ developed a terpolymeric gene carrier system composed of a thermoresponsive unit (PNIPAM), a cationic unit (DMAEMA), and a hydrophobic unit butyl methacrylate (BMA) and evaluated its transfection efficiency at different incubation temperatures; Twaites et al.¹¹ have prepared a range of cationic polymers including derivatives of PEI containing short hydrophobic side chains (i.e., octanamide), copolymers of PEI and PNIPAM, and polymers containing different amounts of NIPAM, DMAEMA, and hexylacrylate (HA); copolymers of *p*(NIPAM-*co*-butyl-methacrylate-*co*-acrylic acid) have been studied for the intestinal delivery of human calcitonin by Serres et al.³⁰ and Ramkissoon Ganorkar et al.³¹ and for the delivery of insulin by Kim et al.,¹⁹ while a series of water-soluble poly(NIPAM-*co*-PEI) copolymers have been synthesized and tested for *ex vivo* transfection of both HeLa cell lines and primary cells by Piskin et al.^{3,32,33} A range of spectroscopies and microscopies have been used to probe the interactions between these responsive copolymers and DNA over phase transitions, but characterization of the polymer behavior on a molecular level remains incomplete.

The aim of this study was to quantify the physicochemical changes in the conformation of poly(*N*-isopropylacrylamide)-*graft*-polyethylenimine (PNIPAM-*g*-PEI) thermoresponsive copolymers, and their interaction, by using small-angle neutron scattering (SANS) and pulsed-gradient spin-echo NMR (PGSE-NMR), to provide a fundamental understanding of their solution behavior.

Experimental Section

Materials. Three samples of PEI-*g*-PNIPAM copolymers (Scheme 1) containing dansyl labels on the PNIPAM side chains have been

examined here; these were prepared as described previously and their details listed in Table 1. Briefly, preformed PNIPAM coils ($M_w = 17600$ g mol⁻¹, $M_w/M_n = 1.9$, or 34000 g mol⁻¹, $M_w/M_n = 2.3$), containing 1 mol % of the fluorescent dansyl monomer³⁴ DANSAPP,³⁵ were grafted to a 25000 g mol⁻¹ PEI core, with the grafting density and molecular weight of the PNIPAM being varied. The polymers labeled PEI(25)-*g*-PNIPAM(34)₄ and PEI(25)-*g*-PNIPAM(34)_{1.8} differ only in a slight variation in PNIPAM graft density but serve to illustrate the sensitivity of the conformation to the number of grafts per PEI core. Branched PEI (PEI) 25 K g mol⁻¹ was purchased from Aldrich and dialyzed (12 kDa cutoff) against deionized water (4×1000 mL). All solutions for NMR and SANS analysis were prepared in deuterated water (D₂O, 99.9%), also purchased from Aldrich.

Methods. *Pulsed-Gradient Spin-Echo NMR (PGSE-NMR).* Measurements were conducted on a Bruker AMX360 NMR spectrometer using a stimulated echo sequence as described elsewhere.³⁶ This configuration uses a 5 mm diffusion probe (Cryomagnet Systems, Indianapolis, IN) and a Bruker gradient (GRASP) spectroscopy accessory unit.

The self-diffusion coefficient D_s was extracted by fitting the integrals for a given peak to eq 1;

$$A(\delta, G, \Delta) = A_0 \exp[(-kD_s)]^\beta \quad (1)$$

A is the signal amplitude in the absence (A_0) or presence of the field gradient pulses ($A(\delta, G, \Delta)$), and β is an exponent to quantify in a semiempirical fashion the linearity of the attenuation functions reflecting the width of the distribution of the self-diffusion coefficient,

$$k = -\gamma^2 G^2 \left(\frac{30\Delta(\delta + \sigma)^2 - (10\delta^3 + 30\sigma\delta^2 + 35\sigma^2\delta + 14\sigma^3)}{30} \right) \quad (2)$$

where γ is the magnetogyric ratio, Δ the diffusion time (140 ms), σ the gradient ramp time (250 μ s), δ the gradient pulse length (500 μ s < δ < 3 ms), and G the gradient field strength (0.5 < G < 3 T/m).

Small-Angle Neutron Scattering (SANS). Small-angle neutron scattering (SANS) measurements were performed on the fixed-geometry, time-of-flight LOQ diffractometer (ISIS Spallation Neutron Source, Oxfordshire, UK). By using neutron wavelengths spanning 2.2–10 Å, a $Q = 4\pi \sin(\theta/2)/\lambda$ range of approximately 0.008–0.25 Å⁻¹ (25 Hz) is accessible, with a fixed sample-detector distance of 4.1 m. The samples were contained in 2 mm path length, UV-spectrophotometer grade, quartz cuvettes (Hellma) and mounted in aluminum holders on top of an enclosed, computer-controlled, sample chamber. Sample volumes were approximately 0.4 cm³. Temperature control was achieved through the use of a thermostatted circulating bath pumping fluid through the base of the sample chamber. Under these conditions, a temperature stability of better than ± 0.5 °C can be achieved. Experimental measuring times were approximately 40 min.

All scattering data were (a) normalized for the sample transmission, (b) background corrected using a quartz cell filled with D₂O (this also removes the inherent instrumental background arising from vacuum windows, etc.), and (c) corrected for the linearity and efficiency of the detector response using the instrument-specific software package. The data were put onto an absolute scale by reference to the scattering from a partially deuterated polystyrene blend.

Dynamic Light Scattering (DLS). Hydrodynamic radii of the polymers were measured in double-distilled water via scattered light

Table 1. Molecular Characterization of the PEI-PNIPAM Copolymers^a

copolymer	average number of pNIPAM coils per PEI coil	molar mass of NIPAM comonomer/g mol ⁻¹	molar mass of PEI core/g mol ⁻¹	mass percentage PNIPAM/%
PEI(25)- <i>g</i> -PNIPAM(34) ₄	4.0	34000	25000	85
PEI(25)- <i>g</i> -PNIPAM(34) _{1.8}	1.8	34000	25000	71
PEI(25)- <i>g</i> -PNIPAM(18) _{3.4}	3.4	17600	25000	70

^a Polymer molar masses and graft contents were calculated from NMR integral ratios and amine content via the TNBS assay and averaged as reported previously.⁴⁴

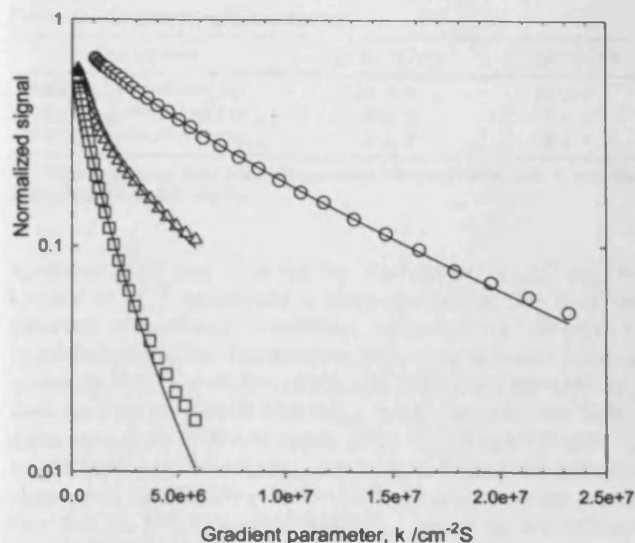


Figure 1. Typical attenuation functions and fits to a stretched exponential for polymer solutions with concentrations $C_{\text{polymer}} = 4.5$ wt % in D_2O and 298 K; PEI 25 K g mol^{-1} (\square), PEI(25)-*g*-PNIPAM(34)₄ (\circ), and PEI(25)-*g*-PNIPAM(18)_{3.4} (\triangle).

recorded at 90° angle to incident radiation in a Viscotek 802 dynamic light scattering (DLS) instrument equipped with a 50 mW internal laser operating at a wavelength of 830 nm. From standard autocorrelation functions, measured diffusion coefficients were related to hydrodynamic radius via the Stokes–Einstein equation. Software models used to derive hydrodynamic radii were based on the assumptions that polymers were random coils and noninteracting. Measurements quoted are the averages of triplicate samples of polymers recorded at each temperature with at least 10 correlation functions analyzed to obtain data. Radii quoted are averages based on the scattered light in terms of polymer molecular masses.

Results

PGSE-NMR. Figure 1 presents typical raw PGSE-NMR attenuation data plus associated fits for the parent, branched PEI (PEI) 25 K g mol^{-1} and two copolymers, PEI(25)-*g*-PNIPAM(34)₄ (high PNIPAM content) and PEI(25)-*g*-PNIPAM(34)_{1.8} (low PNIPAM content). The signal decays fastest for the parent PEI, indicating that the copolymers have larger self-diffusion coefficients, with PEI thus associated with a smaller size. Similarly, the signal from the high-content PNIPAM copolymer (PEI(25)-*g*-PNIPAM(34)₄) decays slowest, indicating it is the largest polymer. PGSE-NMR is clearly a very powerful if perhaps not fully exploited technique^{37–40} for probing perturbations to the solution conformation of responsive polymers induced by changes in appropriate external parameters, although relaxation times tend to be reported rather than the diffusion coefficient.^{41,42}

The nonlinearity of PGSE-NMR attenuation data indicated that these polymers are polydisperse. The stretched exponential is a convenient method to quantify this polydispersity via the parameter β , although other methods such as CONTIN are feasible.⁴³ β was largely independent of temperature ($\beta = 0.8 \pm 0.1$) and similar for the three copolymers studies here.

The self-diffusion coefficient vs temperature behavior for these copolymers are presented in Figure 2a,b. Also shown are the associated hydrodynamic radii calculated from the Stokes–Einstein equation using the bulk viscosities for water at the appropriate temperature. All samples exhibited a similar pattern in that, with increasing temperature, the self-diffusion coefficient increased, associated with a decrease in the hydrodynamic radius. These transitions broadly coincide with the LCST, which displays both

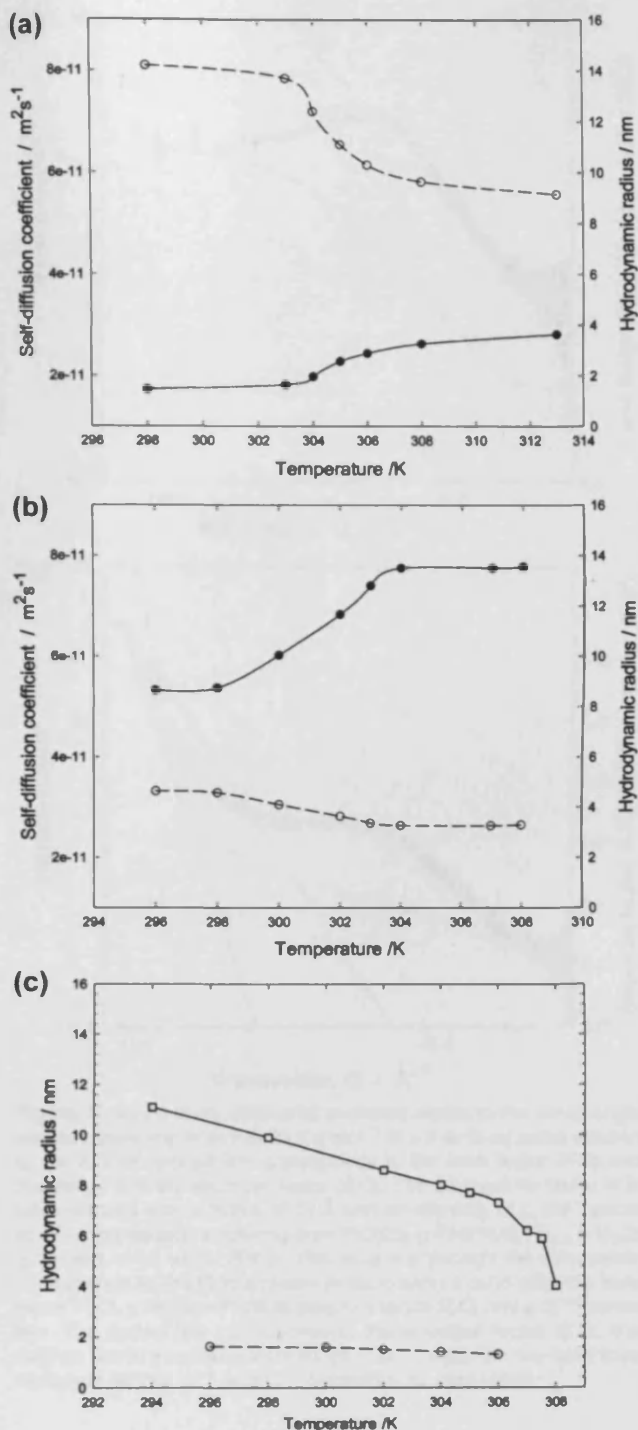


Figure 2. (a) Temperature dependence of the self-diffusion coefficient (\bullet) and associated hydrodynamic radius (\circ) of copolymer PEI(25)-*g*-PNIPAM(34)₄ at a concentration $C_{\text{polymer}} = 4.5$ wt %. The lines are simple guides to the eye. (b) Temperature dependence of the self-diffusion coefficient (\bullet) and associated hydrodynamic radius (\circ) of copolymer PEI(25)-*g*-PNIPAM(34)_{1.8} at a concentration $C_{\text{polymer}} = 4.5$ wt %. The lines are simple guides to the eye. (c) Temperature dependence of the hydrodynamic radius of homopolymers PEI 25 K g mol^{-1} ($C_{\text{polymer}} = 1$ wt %) (\circ) and PNIPAM 20 K g mol^{-1} ($C_{\text{polymer}} = 1$ wt %) (\square). The lines are simple guides to the eye.

a pronounced concentration dependence (10 K over $0 < C_{\text{polymer}} < 5$ wt %) and a weaker dependence on solvent composition, i.e., the LCST is 1–2 K lower in D_2O compared to H_2O . The temperature behavior of the PNIPAM homopolymer is in excellent

Table 2. Dynamic Light Scattering*

copolymer	R_h 20 °C/nm	R_h 50 °C/nm
PEI(25)- <i>g</i> -PNIPAM(34) ₄	24 ± 4	16 ± 5
PEI(25)- <i>g</i> -PNIPAM(34) _{1.8}	8 ± 3	5 ± 1
PEI(25)- <i>g</i> -PNIPAM(18) _{3.4}	6 ± 2	3 ± 1

* Hydrodynamic radii were determined from solutions with a polymer concentration of 0.5 mg/mL.

agreement with that observed by Yushmanov et al.³⁸ and by Larsson et al.,³⁹ specifically a sharp increase at 306 K in the observed self-diffusion coefficient, reflecting the decrease in hydrodynamic radius. The decrease in the hydrodynamic radius is greater for PEI(25)-*g*-PNIPAM(34)₄ and PEI(25)-*g*-PNIPAM(34)_{1.8} than for PEI(25)-*g*-PNIPAM(18)_{3.4}, consistent with the higher molar mass of the PNIPAM moiety of the PEI(25)-*g*-PNIPAM(34)₄ and PEI(25)-*g*-PNIPAM(34)_{1.8} copolymers. Indeed, the hydrodynamic radii for PEI(25)-*g*-PNIPAM(34)₄ copolymers are greater than that for PEI(25)-*g*-PNIPAM(34)_{1.8}, reflecting the different number of PNIPAM chains grafted to the PEI core. For comparison, the analogous behavior for the parent PEI and a PNIPAM homopolymer of comparable molecular weight are presented in Figure 2c; clearly, there is no significant change in the size of the PEI segments with temperature but a substantial collapse of the PNIPAM on approaching its LCST.

Scattering Experiments. The different hydrodynamic radii obtained in NMR for the copolymers compared to homopolymers are displayed in Figure 2a–c, and corresponding dynamic light scattering (DLS) data for the copolymers is shown in Table 2. Hydrodynamic radii obtained in DLS at temperatures below and above LCST are broadly in agreement with NMR measurements. Reductions in size of ~8 nm for PEI(25)-*g*-PNIPAM(34)₄ and 3 nm for PEI(25)-*g*-PNIPAM(34)_{1.8} are apparent in DLS data from double-distilled water as the polymer solutions are raised above LCST (Table 2). We also observed, although in lower concentrations (~5% of sample), both smaller species (4–6 nm) for PEI(25)-*g*-PNIPAM(34)₄ and PEI(25)-*g*-PNIPAM(34)_{1.8} below LCST, as well as higher radius particles (60–70 nm) above LCST at concentrations above 0.5 wt %. The 4–6 nm species are of the expected dimensions for isolated individual polymer chains, whereas the 60–70 nm particles are in the micellar/aggregate range and of a similar size to those reported previously in phosphate buffered saline solution at pH 7.4.⁴⁴ We would not expect to observe high mass aggregates in PGSE-NMR, but the agreement in size range of the “majority” species (16–24 nm for PEI(25)-*g*-PNIPAM(34)₄, 5–8 nm for PEI(25)-*g*-PNIPAM(34)_{1.8}) in both NMR and DLS experiments nevertheless suggests these are the most important species in solution at this concentration range. However, the differences in the observed radii between the PEI(25)-*g*-PNIPAM(34)₄ and PEI(25)-*g*-PNIPAM(34)_{1.8} pair are rather surprising given the relatively small changes in composition and overall molecular weight.

This behavior implies that these polymers are not simple spherical objects. Small-angle neutron scattering offers the opportunity to probe the size and shape of polymer molecules in solution, and such a study was conducted as a logical extension to the NMR and DLS studies.

SANS. Representative small-angle neutron scattering data (and fits) are presented in Figure 3a for the parent PEI and Figure 3b for the copolymer with higher PNIPAM content (PEI(25)-*g*-PNIPAM(34)₄). The scattering from the highest PNIPAM content copolymers (PEI(25)-*g*-PNIPAM(34)₄) is very different from both the parent PEI and the low PNIPAM content copolymer in that there is a pronounced upturn in intensity at low Q in the high PNIPAM case. Parts a, b, and c of Figure 4

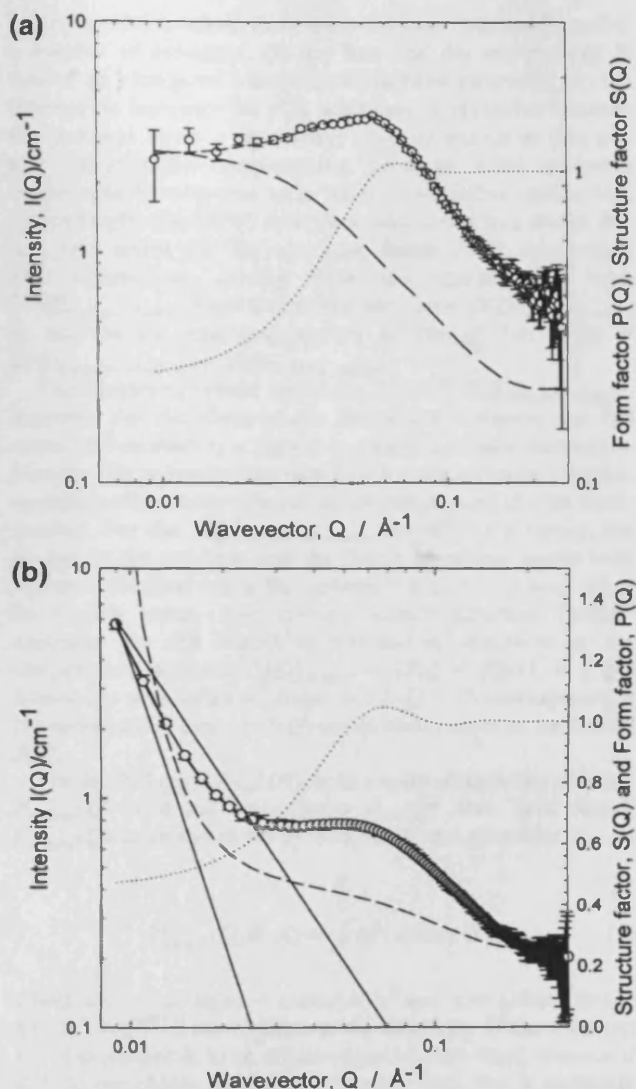


Figure 3. (a) Fit to an ellipsoidal scatterer model to the small angle neutron scattering from PEI 25 K g mol⁻¹ in a 5 wt % aqueous solution at pH 7. The dashed line corresponds to the form factor $P(Q)$ and the dotted line the structure factor $S(Q)$. The ellipsoid for factor fit is parametrized with a radius of 22 Å and an ellipticity of 2. (b) Typical small-angle neutron scattering from PEI(25)-*g*-PNIPAM(18)_{3.4} in D₂O; [polymer] = 4.5 wt %, 308 K. The solid line through the data points corresponds to the fit to a model incorporating a solid ellipsoid form factor $P(Q)$, a Hayter–Penfold structure factor $S(Q)$ and a Q^{-m} power law. The dotted line corresponds to the structure factor $S(Q)$, the dashed line to a rescaled form factor + Q^{-m} , while the two solid lines represent simple Q^{-2} and Q^{-4} behaviors for comparison.

illustrate further how the temperature-dependent scattering changes with molecular characteristics. Specifically, the upturn in the case of PEI(25)-*g*-PNIPAM(34)_x (Figure 4a,b) increases in magnitude with increasing temperature, a trend that is promoted by the higher PNIPAM content (x) but reduced with dilution (data presented in Supporting Information). The emergence of the upturn is also observed in the PNIPAM homopolymer scattering (see inset to Figure 4a). At the highest temperature studied, the PNIPAM homopolymer scattering follows a Q^{-4} dependence, indicating the presence of large solid-like objects, while at the lowest temperature, the scattering may be described by a Gaussian coil model with radius of gyration R_g

= 6.5 (± 0.2) nm. The presence of the upturn in the high PNIPAM content copolymer data suggests that this copolymer retains significant character of the PNIPAM component.

Although less obvious given the respective concentrations studied, the lower PNIPAM content copolymer scattering is also different from the parent branched PEI, but a careful analysis of the absolute intensities is required to extract a meaningful interpretation. The intensity at $Q = 0$ is dependent on the number concentration of scatterers (n_{polymer}), their volume (V_{polymer}), and composition via the respective scattering length densities of the scatterer and the solvent, viz. $I(Q = 0) \propto n_{\text{polymer}} V_{\text{polymer}}^2 (\rho_{\text{scatterer}} - \rho_{\text{solvent}})^2$. In the case of the data for the low-PNIPAM copolymer (PEI(25)-*g*-PNIPAM(18)_{3,4}) in Figure 4c, where the absence of the upturn at low Q permits this analysis, the ratio of the number concentration and composition corrected absolute intensities, i.e.,

$$\frac{\left(\frac{I(Q=0)}{(\rho_{\text{scatterer}} - \rho_{\text{solvent}})^2 n_{\text{polymer}}} \right)_{\text{copolymer}}}{\left(\frac{I(Q=0)}{(\rho_{\text{scatterer}} - \rho_{\text{solvent}})^2 n_{\text{polymer}}} \right)_{\text{PEI}}} \propto \frac{(V_{\text{polymer}}^2)_{\text{copolymer}}}{(V_{\text{polymer}}^2)_{\text{PEI}}}$$

is some 10 \times higher in the copolymer case, suggesting a simple increase in size (i.e., $\times 3$ increase in volume) of the scatterer associated with its higher molecular weight.

The upturn at low Q may have a number of origins, the most probable being either a morphology-dependent contribution arising from (a) the presence of a PNIPAM "corona" around the PEI core, (b) the penetration of the PNIPAM into the PEI core, or (c) an attractive interpolymer interaction as seen in the PNIPAM homopolymer data. A thin shell of PNIPAM "adsorbed" onto the surface of the PEI core would be expected to demonstrate a Q^{-2} dependence, but a simple power law term added to the form factor for the ellipsoidal form factor used to describe the PEI core led to poor fits, especially over the low Q region. Similarly, a model based on PNIPAM chains dispersed throughout the PEI core, forming a homogeneous scatterer of a similar or slightly larger size compared to the PEI core that would follow a Q^{-4} dependence at low Q , also did not yield acceptable fits. Rather, an exponent of $m = -3.1 (\pm 0.2)$ was found to best describe the data, indicating that if this scattering arises from the PNIPAM, it forms a rather ill-defined or fractal aggregate. One might envisage therefore a PEI core with 2–4 PNIPAM moieties forming "blobs", part interspersed with the PEI core, part extended into solution. An elongated shape has therefore been adopted to model the gross morphology of the scatterer.

The visual appearance of the copolymer samples is very instructive when attempting to rationalize the upturn in the SANS data for the high PNIPAM content copolymers; these also show a corresponding clouding behavior with increasing temperature (N.B. no phase separation is observed over the temperature range studied here), whereas there is no change in appearance for the lower PNIPAM copolymer solutions. This suggests that the additional scattering at low Q does not arise due to the PNIPAM moiety, rather the presence of transient aggregates via an attractive interaction. The NMR experiment is less sensitive to the presence of such transient aggregates, and because none was observed over this temperature range, phase separation leading to large aggregates may be discounted. Accordingly, the upturn in low Q is deemed to be due to the presence of a temperature-induced attractive interaction that is dependent on the molecular characteristics of the PNIPAM moiety.

Any model invoked to fit these various data must capture a number of elements: (i) the fact that the morphology is that of an elongated otherwise ill-defined structure, (ii) the interaction between the PEI segments is repulsive because the polymer bears a significant positive charge at this pH, and (iii) at higher temperatures, the form of the scattering varies significantly due to a "sticky" attractive interaction. Accordingly, the SANS data have been fitted to a model that has two terms to the structure factor $S(Q)$ that represent interactions arising from the charged PEI core ($S(Q)_{\text{Hayter-Penfold}}$) and a critical scatter term ($S(Q)_{\text{critical scatter}}$) to address the emerging upturn at low Q , i.e., $S(Q) = S(Q)_{\text{Hayter-Penfold}} + S(Q)_{\text{critical scatter}}$.

The Hayter–Penfold structure factor⁴⁵ $S(Q)_{\text{Hayter-Penfold}}$ accounts for the electrostatic interaction between the PEI cores and embodies a repulsive charged sphere interaction between the polymers incorporating a rescaled mean spherical approximation, with allowance for penetrating charge background. For the $S(Q)_{\text{Hayter-Penfold}}$, the effective radius, the charge on the polymer, and the Debye screening length were allowed to adjust while the volume fraction (ϕ_p) was left at its known value. The critical scatter structure factor³⁶ accounts for the attractive interaction observed as the temperature is raised; $S(Q)_{\text{critical}} = (S(Q = 0))/(1 + \xi^2 Q^2)$ where ξ is a correlation length and $S(Q = 0)$ corresponds to the contribution that this $S(Q)$ component makes to the overall $S(Q)$.

For the PEI core ($P_{\text{PEI}}(Q)$), both a solid ellipsoid form factor $P_{\text{ellipsoid}}(Q)$ or a rod form factor $P_{\text{rod}}(Q)$ have been tested. $P_{\text{ellipsoid}}(Q)$ is parametrized by a radius R and ellipticity X :

$$P_{\text{ellipsoid}}(Q, R, X) = \int_0^{\frac{\pi}{2}} \varphi^2(u) \sin \alpha \, d\alpha \quad (3)$$

where $\varphi(u) = 3(\sin(u) - u \cos(u))/u^3$ and $u = QR[\sin^2(\alpha) - X^2 \cos^2(\alpha)]^{1/2}$. X corresponds to the ellipticity of the scatterer; $X < 1$ corresponds to an oblate ellipsoid (disk-like), whereas if $X > 1$, the ellipse is a prolate (needle-like). For N randomly oriented rods of length L and radius R , $P_{\text{rod}}(Q)$ is given by:

$$P_{\text{rod}}(Q) = N \int_0^{\pi/2} F^2(Q \sin \gamma) d\gamma \quad (4)$$

where

$$F(Q) = (\Delta\rho)^2 V \frac{\sin\left[\frac{1}{2}QL\cos\gamma\right] 2J_1(QR\sin\gamma)}{(1/2)QL\cos\gamma \quad QR\sin\gamma}$$

and J_1 is the first-order Bessel function of the first kind.

Thus, the overall intensity of scattered radiation, $I(Q)$, as a function of the wave vector, Q , is given by:

$$I(Q) = n_p V_p^2 (\rho_{\text{polymer}} - \rho_{\text{solvent}})^2 P_{\text{PEI}}(Q) [S(Q)_{\text{Hayter-Penfold}} + S(Q)_{\text{critical scatter}}] + B_{\text{inc}} \quad (5)$$

where, to recap, n_p and V_p are the number and volume of scatters, respectively ($n_p V_p = \phi_p$ where ϕ_p is the volume fraction of the polymer), and ρ is the scattering length density of the polymer or solvent.

The scattering from PEI 25 K g mol⁻¹ may be described by an (charged) ellipsoid morphology with radius = 22 Å with ellipticity $X = 2$, while a rod-like morphology was found to be equally appropriate at higher pHs.⁴³ Therefore, while both models have been explored, the ellipsoid gives margin-

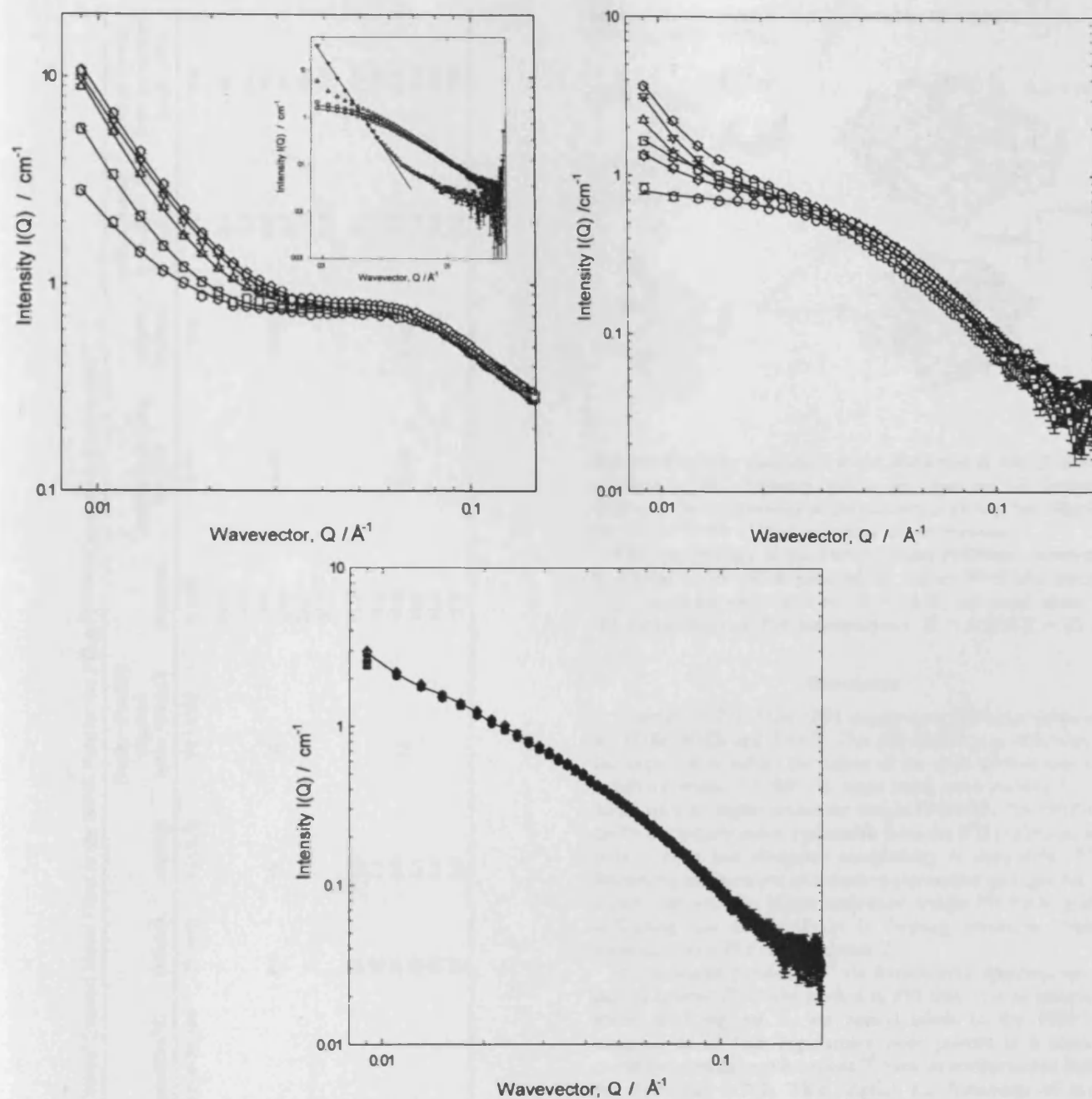


Figure 4. (a) SANS and fits as described in the text for 4.5 wt % PEI(25)-*g*-PNIPAM(34)₄ as a function of temperature: (○) 298 K; (□) 308 K; (Δ) 313 K; (▽) 318 K; (○) 323 K. The inset shows SANS from 2 wt % PNIPAM homopolymer 20 K g mol⁻¹ as a function of temperature: open circles, 298 K; squares, 303 K; upward triangles, 308 K; downward triangles, 313 K. Also shown is a Q^{-4} term (dotted line) and at the lower temperatures, fits to a Gaussian coil morphology ($R_g = 6.3$ nm, 298 K; $R_g = 6.5$ nm, 303 K). (b) SANS and fits as described in the text for 2.5 wt % PEI(25)-*g*-PNIPAM(34)_{1,8} as a function of temperature: (○) 298 K; (◇) 303 K; (□) 308 K; (Δ) 313 K; (▽) 318 K; (○) 323 K. (c) SANS and represent fit as described in the text for 2.5 wt % PEI(25)-*g*-PNIPAM(18)_{3,4} as a function of temperature: (○) 298 K; (□) 308 K; (Δ) 313 K; (▽) 318 K; (○) 323 K.

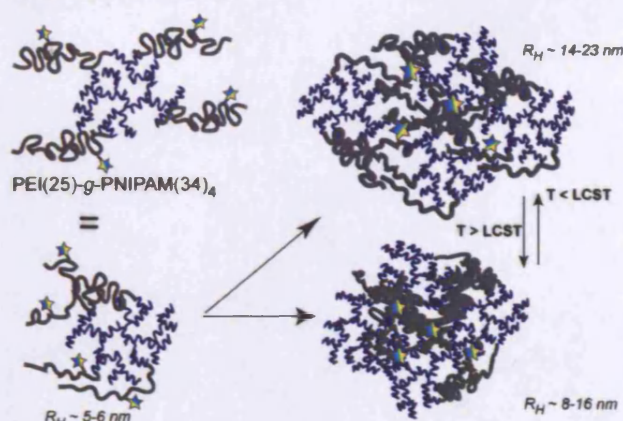
ally better fits and is generally more appropriate given the low degrees of ellipticity observed. Accordingly, only the parameters describing the fits to these data using the solid ellipsoid form factor (equation 3) are presented in Table 3.

For the higher PNIPAM content copolymer (PEI(25)-*g*-PNIPAM(34)₄, Figure 4a), temperature has a pronounced effect on the scattering at low Q , but at higher Q the curves superimpose implying no change in size or shape. The model parameters confirm that the morphology is invariant with temperature, with highly elliptical structures present ($X = 19$) with minor radius of 9 Å. The major radius ~ 170 Å (17 nm) is

in good agreement with the hydrodynamic radius obtained from the NMR study. These fits are at the limit of an ellipsoid morphology, a rod being perhaps more appropriate, but the ellipsoid parameters are presented to facilitate a direct comparison with the other copolymers. The critical scatter term is important at the higher temperatures, with the correlation length being comparable to the dimensions of the scatterer. On diluting this copolymer, the upturn at low Q is much weaker and the correlation length longer, as might be expected. The parameters are not precisely quantified here due to the paucity of data available at low Q and the fact that both the critical scatter term

Table 3. Parameters Describing the Morphology of a "Sticky" Ellipsoid Model Fitted to the SANS Data for the PEI-*g*-PNIPAM Copolymers Studied Here

polymer/concentration	temperature/°C	radius/Å	ellipticity	Hayter-Penfold structure factor radius/Å	charge/e	inverse screening length/Å ⁻¹	volume fraction	critical scatter term $S(Q=0)$ (± 0.1)	critical scatter term correlation length (5%)
PEI(25)- <i>g</i> -PNIPAM(18) _{3,4} $C_{\text{polymer}} = 4.5 \text{ wt } \%$	all temperatures	26 (± 3)	4 (± 0.5)	50 (± 10)	5 (± 2)	0.04	0.045	n/a	n/a
PEI(25)- <i>g</i> -PNIPAM(34) ₄ $C_{\text{polymer}} = 4.5 \text{ wt } \%$	25				24.9			0.5	10
	30				24.0			0.5	10
	35				24.4			0.6	10
	40	8.0	19	50	26.5	0.04	0.045	0.7	30
	45				28.2			1.0	50
PEI(25)- <i>g</i> -PNIPAM(34) ₄ $C_{\text{polymer}} = 2.5 \text{ wt } \%$	50				30.0			2.3	100
	25	22	4.0		15.0			1.1	100
	30	23	4.9		16.2			1.3	100
	35	21	3.6	50	16.3			1.5	300
	40	22	4.1		16.2	0.04	0.025	1.8	300
	45	22	3.8		16.4			7.3	400
	50	21	4.8		16.8			8.2	500

Scheme 2. Association and Conformation Changes of PEI(25)-*g*-PNIPAM(34)₄

and the ellipticity contribute to the scattering at low Q . Subtle changes in the ellipticity would therefore not be detected. However, the morphology of the scatterer is clearly less elliptical ($X = 4$, $R = 24 \text{ Å}$) than at higher concentrations.

The morphology of the lower content PNIPAM copolymer is similar to the dilute case of the higher PNIPAM content copolymer, namely $X = 4$ and $R = 24 \text{ Å}$, and much closer to the morphology of PEI homopolymer, $X = 2$ and $R = 22 \text{ Å}$.

Discussion

A series of PNIPAM-PEI copolymers has been examined by PGSE-NMR and SANS. The self-diffusion coefficients of the copolymers reflect the nature of the graft architecture and relative content of PNIPAM, these being most marked for the series with the higher molecular weight PNIPAM. The PNIPAM grafts are largely indistinguishable from the PEI backbone, and only a gross but elongated morphology is accessible. With increasing temperature, an attractive interaction emerges for the copolymer with the higher molecular weight PNIPAM grafts, indicating that the PNIPAM is forming attractive "blobs" connected to a PEI core, Scheme 2.

It was shown previously⁴⁴ via fluorescence spectroscopy of dansyl-labeled PNIPAM grafted to PEI that, at concentrations above 0.05 mg mL^{-1} , the dansyl labels in the PNIPAM components of both copolymers were present in a reduced mobility/nonpolar environment,⁴⁶ even at temperatures below the PNIPAM LCST. This implies the formation of some structural or associative order, most likely micellar, in these materials, as reported before for PNIPAM copolymers.⁴⁷ The presence of the naphthyl groups on the dansyl label would not in themselves be expected to alter significantly the structural ordering of the copolymers because these were present at $< 1 \text{ mol } \%$ relative to PNIPAM⁴⁴ and thus represented $< 1\%$ by total mass of the copolymers. At lower concentrations, the prior data indicated dual environments for PNIPAM, including both nonpolar and hydrophilic domains below LCST, but hydrophobic (though still hydrated) regions above LCST. However, the magnitude of the self-diffusion coefficients from NMR studies here suggests that no large-scale aggregation of polymers was occurring in these experiments. Dynamic light scattering also indicated the presence of discrete species in the PEI-PNIPAM graft copolymers, without overall aggregation and precipitation from solution above LCST, at least in the concentration ranges and time scales of our experiments. Taken together, the fluorescence data and the results of the PGSE-NMR, DLS, and

SANS experiments are instructive in terms of a mechanistic interpretation of the behavior of the copolymers around the phase transition temperatures of the PNIPAM grafts. One possible mode is the existence of PNIPAM “zone” around the PEI domains below LCST, which then subsequently collapses above LCST inside the PEI regions. The higher relative molar mass of the PNIPAM chains combined with the increased graft density in the PEI(25)-*g*-PNIPAM(34)₄ copolymer would mean the presence of larger hydrophobic domains above LCST and stronger associative forces for this polymer compared to the other two polymers in the study (i.e., PEI(25)-*g*-PNIPAM(34)_{1,8} and PEI(25)-*g*-PNIPAM(18)_{3,4}). The calculated mass percentages of PNIPAM in the polymers PEI(25)-*g*-PNIPAM(34)₄, PEI(25)-*g*-PNIPAM(34)_{1,8}, and PEI(25)-*g*-PNIPAM(18)_{3,4} are 85, 71, and 70%, respectively, suggesting perhaps a threshold proportion of PNIPAM above which associative interactions could dominate above LCST.

An alternative explanation is that these copolymers exist in solution as “interpenetrating” structures in which the PNIPAM domains lie on the inside even below LCST, as these may be more hydrophobic than PEI. In such a case, the collapse of PNIPAM domains above LCST would lead to the enhanced diffusivity observed above LCST in NMR, and this is most apparent for higher molar mass PNIPAM grafts that display the greatest changes in apparent volume. It should be noted that, above LCST, the coil-to-globule transitions and PNIPAM chain collapse are manifest in the PGSE-NMR, the DLS data, and the SANS experiments: the enhanced diffusivity of the chains in the NMR, the reduction in hydrodynamic radii in DLS, and the upturn in the scattering at low *Q* in SANS.

The emergence of stronger attractive interactions above LCST between the PNIPAM components in PEI(25)-*g*-PNIPAM(34)₄ compared to PEI(25)-*g*-PNIPAM(18)_{3,4} copolymers also correlates well with the data from prior AFM studies of these polymers complexed to DNA. The greater tendency of complexes prepared from PEI(25)-*g*-PNIPAM(34)₄ copolymers with DNA to aggregate over time compared to those made using PEI(25)-*g*-PNIPAM(18)_{3,4} is most likely a direct consequence of the reduced colloidal stability arising from the presence of larger hydrophobic surface regions. It should also be noted that closer proximity of polymer chains during an aggregative process would lead to enhanced possibilities for interchain and intrachain H-bonding interactions between PEI amines and amide groups on PNIPAM. The appearance of an attractive interaction between PNIPAM domains above LCST in PEI(25)-*g*-PNIPAM(34)₄ would favor these associative phenomena, giving rise to the more rapid aggregation as observed in AFM.

Finally, the demonstration of conformational and/or associative changes with graft copolymer content and LCST provided by the PGSE-NMR, DLS, and SANS experiments offer a further insight into the gene delivery efficiencies of these materials, as shown in prior transfection studies.³⁴ In both myoblast and fibroblast cell lines, there was higher DNA binding as measured by gel-shift assays for PEI(25)-*g*-PNIPAM(18)_{3,4}, i.e., the copolymer with lower molecular weight PNIPAM grafts when complexes were formed below LCST.³⁴ This suggests that PEI(25)-*g*-PNIPAM(18)_{3,4} was most likely presenting an exposed PEI shell to solution, with the PNIPAM domains insufficient to mask the PEI segments, and indeed, the transfection efficiency of this copolymer in both cell lines was very similar to that of PEI (albeit slightly higher) both below and above LCST. However, we observed previously that the highest overall transfection efficiency was obtained for the copolymer with the higher PNIPAM content when temperature cycles were

carried out around the LCST. The increase in hydrophobic associations above LCST in polymer PEI(25)-*g*-PNIPAM(34)_{1,8} as evidenced by the PGSE-NMR and SANS data suggests that this polymer would have undergone different conformational changes than PEI(25)-*g*-PNIPAM(18)_{3,4} over the temperature cycles. This would most likely have been an initial increase in affinity with DNA above LCST due to a combination of electrostatic and hydrophobic interactions and a reduced affinity below LCST as the PNIPAM hydrophobic interactions were lost. The complexity of the intracellular environment means that other factors (e.g., increased competition for DNA in the complexes by cytoplasmic components) may also have been important in the overall transfection efficiencies. However, the fact that temperature cycles using polymers that did not respond over the temperature ranges did not give rise to temperature-variant transfections suggest these were less significant than the polymer phase transitions. The NMR and SANS data thus provide confirmation that not only can the grafting of PNIPAM to PEI change the solution and associative behavior of the polymer but also support the view that increased transfection efficiency of these copolymers arises from variations in graft density and length of the PNIPAM chains.

Conclusions

Gene delivery vehicles based on novel architecture synthetic polycations are being developed to improve transfection efficiency. Here, we reported the effects of temperature on the size and interaction between copolymers based on a cationic core formed from poly(ethylene imine) (PEI) with differing thermoresponsive poly(*N*-isopropylacrylamide) (PNIPAM) grafts. An analysis of the temperature profile of the self-diffusion coefficients of the copolymer with longer chain PNIPAM grafts showed clear evidence of the collapse of the grafts with increasing temperature, while the scattering data highlighted the emergence of an attractive interpolymer interaction. For the shorter PNIPAM graft copolymer, there was a similar but much smaller collapse of the grafts with temperature, but this did not lead to an attractive interaction being manifest in the scattering. The different temperature behavior of these two copolymers indicates subtle conformational rearrangements that result in various presentations of charged-core and hydrophobic moieties, central to the potential to control nucleic acid binding and cell transfection ability.

Acknowledgment. This work was supported by Cardiff University (N.R.'s Ph.D. studies), and by research grants from the UK Engineering and Physical Science Research Council (EPSRC GR/S25456/01, EP/C013220/1) and Biotechnology and Biological Sciences Research Council (BBSRC BB/C515855/1), and the Science and Technology Facilities Council UK is thanked for provision of neutron beamtime.

Supporting Information Available. The temperature dependent scattering from 2.5 wt % solutions of PEI(25)-*g*-PNIPAM(34)₄ is presented in the Supporting Information to illustrate the fact that the upturn in intensity at low *Q* decreases with concentration, as discussed in the light of the data presented in Figure 4a,b,c. This material is available free of charge via the Internet at <http://pubs.acs.org>.

References and Notes

- (1) Hinrichs, W. L. J.; Schuurmans-Nieuwenbroek, N. M. E.; Van De Wetering, P.; Hennink, W. E. J. *Controlled Release* 1999, 60, 249–259.

- (2) Yokoyama, M. *Drug Discovery Today* **2002**, *7*, 426–432.
- (3) Dincer, S.; Turk, M.; Piskin, E. *Gene Ther.* **2005**, *12*, S139–S145.
- (4) Crassous, J. J.; Ballauff, M.; Drechsler, M.; Schmidt, J.; Talmon, Y. *Langmuir* **2006**, *22*, 2403–2406.
- (5) Tanaka, T. *Phys. Rev. Lett.* **1978**, *40*, 820.
- (6) Hirokawa, Y.; Tanaka, T. *J. Chem. Phys.* **1984**, *81*, 6379–6380.
- (7) Osada, Y.; Okuzaki, H.; Hori, H. *Nature* **1992**, *355*, 242–244.
- (8) Suzuki, A.; Tanaka, T. *Nature* **1990**, *346*, 345–347.
- (9) Tanaka, T.; Fillmore, D.; Sun, S.-T.; Nishio, I.; Swislow, G.; Shah, A. *Phys. Rev. Lett.* **1980**, *45*, 1636.
- (10) Szabo, D.; Szeghy, G.; Zrinyi, M. *Macromolecules* **1998**, *31*, 6541–6548.
- (11) Twaites, B. R.; de las Heras Alarcon, C.; Cunliffe, D.; Lavigne, M.; Pennadam, S.; Smith, J. R.; Gorecki, D. C.; Alexander, C. *J. Controlled Release* **2004**, *97*, 551–566.
- (12) de las Heras Alarcon, C.; Twaites, B.; Cunliffe, D.; Smith, J. R.; Alexander, C. *Int. J. Pharm.* **2005**, *295*, 77–91.
- (13) Yu, T. L.; Lu, W.-C.; Liu, W.-H.; Lin, H.-L.; Chiu, C.-H. *Polymer* **2004**, *45*, 5579–5589.
- (14) Liu, R. C. W.; Cantin, S.; Perrot, F.; Winnik, F. M. *Polym. Adv. Technol.* **2006**, *17*, 798–803.
- (15) Hu, T.; You, Y.; Pan, C.; Wu, C. *J. Phys. Chem. B* **2002**, *106*, 6659–6662.
- (16) Kawasaki, H.; Sasaki, S.; Maeda, H.; Nishinari, K. *Langmuir* **2000**, *16*, 3195–3199.
- (17) Balamurugan, S.; Mendez, S.; Balamurugan, S. S.; O'Brien, M. J., II; Lopez, G. P. *Langmuir* **2003**, *19*, 2545–2549.
- (18) Sun, T.; Wang, G.; Feng, L.; Liu, B.; Ma, Y.; Jiang, L.; Zhu, D. *Angew. Chem., Int. Ed.* **2004**, *43*, 357–360.
- (19) Schmaljohann, D. *Adv. Drug Delivery. Rev.* **2006**, *58*, 1655–1670.
- (20) Baker, A.; Saltik, M.; Lehrmann, H.; Killisch, I.; Mautner, V.; Lamm, G.; Christofori, G.; Gotten, M. *Gene Ther.* **1997**, *4*, 773–782.
- (21) Abdallah, B.; Hassan, A.; Benoist, C.; Goula, D.; Behr, J. P.; Demeneix, B. A. *Hum. Gene Ther.* **1996**, *7*, 1947–1954.
- (22) Kunath, K.; von Harpe, A.; Fischer, D.; Petersen, H. B.; U.; Voigt, K.; Kiessel, T. *J. Controlled Release* **2003**, *89*, 113–125.
- (23) Fischer, D.; Bieber, T.; Li, Y. X.; Elsasser, H. P.; Kissel, T. *Pharm. Res.* **1999**, *16*, 1273–1279.
- (24) Ira, Mely, Y.; Krishnamoorthy, G. *J. Fluoresc.* **2003**, *13*, 339–347.
- (25) Godbey, W. T.; Wu, K. K.; Mikos, A. G. *J. Controlled Release* **1999**, *60*, 149–160.
- (26) Clamme, J. P.; Azoulay, J.; Mely, Y. *Biophys. J.* **2003**, *84*, 1960–1968.
- (27) Ogris, M.; Brunner, S.; Schuller, S.; Kircheis, R.; Wagner, E. *Gene Ther.* **1999**, *6*, 595–605.
- (28) von Harpe, A.; Petersen, H.; Li, Y. X.; Kissel, T. *J. Controlled Release* **2000**, *69*, 309–322.
- (29) Kurisawa, M.; Yokoyama, M.; Okano, T. *J. Controlled Release* **2000**, *69*, 127–137.
- (30) Serres, A.; Baudys, M.; Kim, S. W. *Pharm. Res.* **1996**, *13*, 196–201.
- (31) Ramkissoon-Ganorkar, C.; Liu, F.; Baudys, M.; Kim, S. W. *J. Biomater. Sci., Polym. Ed.* **1999**, *10*, 1149–1161.
- (32) Piskin, E. *Int. J. Pharm.* **2004**, *277*, 105–118.
- (33) Piskin, E.; Dincer, S.; Turk, M. *J. Biomater. Sci., Polym. Ed.* **2004**, *15*, 1181–1202.
- (34) Lavigne, M. D.; Pennadam, S. S.; Ellis, J. S.; Yates, L. L.; Alexander, C.; Gorecki, D. G. *J. Gene Med.* **2007**, *9*, 44–54.
- (35) Twaites, B. R.; Alarcon, C. D. H.; Lavigne, M.; Saulnier, A.; Pennadam, S. S.; Cunliffe, D.; Gorecki, D. C.; Alexander, C. *J. Controlled Release* **2005**, *108*, 472–483.
- (36) Davies, J. A.; Griffiths, P. C. *Macromolecules* **2003**, *36*, 950–952.
- (37) Aubrecht, K. B.; Grubbs, R. B. *J. Polym. Sci., Part A: Polym. Chem.* **2005**, *43*, 5156–5167.
- (38) Yushmanov, P. V.; Furo, I.; Iliopoulos, I. *Macromol. Chem. Phys.* **2006**, *207*, 1972–1979.
- (39) Larsson, A.; Kuckling, D.; Schonhoff, M. *Colloids Surf., A* **2001**, *190*, 185–192.
- (40) Nayak, S.; Lyon, L. A. *Angew. Chem., Int. Ed.* **2005**, *44*, 7686–7708.
- (41) Ohta, H.; Ando, I.; Fujishige, S.; Kubota, K. *J. Polym. Sci., Part B: Polym. Phys.* **1991**, *29*, 963–968.
- (42) Schonhoff, M.; Larsson, A.; Welzel, P. B.; Kuckling, D. *J. Phys. Chem. B* **2002**, *106*, 7800–7808.
- (43) Griffiths, P. C.; A, P.; Fallis, I. A.; Wellappili, C.; Murphy, D. M.; Jenkins, R.; Waters, S. J.; Nilmini, R.; Heenan, R. K.; King, S. M. *J. Colloid Interface Sci.* **2007**, *314*, 460–469.
- (44) Pennadam, S. S.; Ellis, J. S.; Lavigne, M. D.; Gorecki, D. C.; Davies, M. C.; Alexander, C. *Langmuir* **2007**, *23*, 41–49.
- (45) Hayter, J. B.; Penfold, J. *J. Colloid. Polym. Sci.* **1983**, *261*, 1022–1030.
- (46) Capek, I. *Adv. Colloid Interface Sci.* **2002**, *97*, 91–149.
- (47) Poncet-Legrand, C.; Winnik, F. M. *Polym. J. (Tokyo)* **2001**, *33*, 277–283.

BM701096P

